CRCLEME

Cooperative Research Centre for
Landscape Environments
and Mineral Exploration

action
Salinity & Water
AUSTRALIA

Australian Government
Geoscience Australia

OPEN FILE
REPORT
SERIES

Lower Balonne Airborne Geophysical Project

CONSTRAINED INVERSION OF AEM DATA FROM THE LOWER BALONNE AREA, SOUTHERN QUEENSLAND, AUSTRALIA

Richard Lane, Ross Brodie and Andrew Fitzpatrick

CRC LEME OPEN FILE REPORT 163

September 2004

CRC LEME is an unincorporated joint venture between CSIRO-Exploration & Mining, and Land and Water, The Australian National University, Curtin University of Technology, University of Adelaide, Geoscience Australia, Primary Industries and Resources SA, NSW Department of Mineral Resources and Minerals Council of Australia, established and supported under the Australian Government's Cooperative Research Centres Program.

CRC

Australian Government
Geoscience Australia

CRCLEME
Cooperative Research Centre for
Landscape Environments
and Mineral Exploration

Lower Balonne Airborne Geophysical Project

CONSTRAINED INVERSION OF AEM DATA FROM THE LOWER BALONNE AREA, SOUTHERN QUEENSLAND, AUSTRALIA

Richard Lane, Ross Brodie and Andrew Fitzpatrick

CRC LEME OPEN FILE REPORT 163

September 2004

This report was produced for the Lower Balonne Airborne Geophysical Project funded by the National Action Plan for Salinity and Water Quality. The National Action Plan for Salinity and Water quality is a joint initiative between the State and Commonwealth Governments.

© CRC LEME 2004

CRC LEME is an unincorporated joint venture between CSIRO-Exploration & Mining, and Land and Water, The Australian National University, Curtin University of Technology, University of Adelaide, Geoscience Australia, Primary Industries and Resources SA, NSW Department of Mineral Resources and Minerals Council of Australia.

Headquarters: CRC LEME c/o CSIRO Exploration and Mining, PO Box 1130, Bentley WA 6102, Australia

© CRC LEME

This report is one of six CRCLEME Open File Reports contributing to the Lower Balonne Airborne Geophysical Project funded by the National Action Plan for Salinity and Water Quality. The project is providing new knowledge and developing methodologies for improved natural resource management in the Murray Darling Basin area of southern Queensland. This integrated project has a multidisciplinary team with skills in regolith geology, geomorphology, bedrock geology, hydrogeology, geophysics and soil science, working to understand the processes and controls on salinnity in a variable regolith terrain.

Copies of this publication can be obtained from:
The Publications Officer, CRC LEME, c/- CSIRO Exploration & Mining, PO Box 1130, Bentley WA 6102, Australia. Information on other publications in this series may be obtained from the above, or from http://crcleme.org.au
Cataloguing-in-Publication:
Lane, R., Brodie, R. and Fitzpatrick, A.
Constrained inversion of AEM data from the Lower Balonne area, Southern Queensland, Australia.
ISBN
1.
2.
3.
I Lane, R., Brodie, R. and Fitzpatrick, A.
II. Title
CRC LEME Open File Report 163.
ISSN

Address and affiliation of authors:

Richard Lane, Ross Brodie and Andrew Fitzpatrick
CRC LEME
c/o Geoscience Australia
PO Box 378
Canberra, ACT 2601
Australia

© Cooperative Research Centre for Landscape Environments and Mineral Exploration 2004

SUMMARY

Borehole conductivity logs, ground electrical data and ground electromagnetic data indicated that conductivity values of several hundred mS/m would be expected at depths below 100m across the St George AEM Survey area. These observations were at odds with the conductivity predictions delivered by the survey contractor. This reflects the inherent ambiguity in estimation of ground conductivity from AEM data, compounded by incomplete knowledge of the relative geometry between the transmitter loop on a fixed wing aircraft, the receiver coils in a towed bird and the ground. In the absence of the independently measured conductivity values mentioned above, the contractor guided the conductivity predictions towards solutions that had low conductivity values at the depth of investigation of the system, between 100 and 200m in this instance.

With the benefit of the additional borehole and ground conductivity data, an alternate set of conductivity predictions were calculated by CRCLEME using EMFlow, guided in this case towards high conductivity values at depth. In addition to this change, small adjustments were made to the geometry parameters assigned to the system. This improved the match between the borehole conductivity logs and predictions of conductivity for observations near to the boreholes. Despite the improvement, this approach lacked control and did not make full use of the known or "a priori" information now available for the AEM system and the survey area.

The observed data are a combination of ground response and primary field. The latter contains important information about the offset of the receiver coils from the transmitter loop. Knowledge of this offset is important for maximising accuracy in near-surface conductivity predictions. Hence, rather than simply remove the primary field fraction from the observed data and focus on the ground response, an iterative inversion procedure was used to progressively refine estimates of both the receiver offset and ground conductivity. However, there is still a degree of ambiguity between the ground conductivity and receiver coil offset. The constrained inversion procedure was designed to utilise a priori information about the conductivity at depth across the survey area and to invert both X and Z component data simultaneously to reduce this ambiguity.

The inversion procedure and the constraints are described in this report. A list of the revised conductivity products is given in Appendix 1. In brief, the inputs to the inversion were;

- the observed data prior to removal of the primary field, and data uncertainty values,
- layered conductivity model reference values and uncertainties,
- layered conductivity model smoothness reference values and uncertainties,
- transmitter loop to receiver coil horizontal and vertical separation reference values and uncertainties, and
- receiver coil pitch angle reference values and uncertainties.

The outputs were;

- the layered conductivity model,
- transmitter loop to receiver coil horizontal and vertical separation values,
- receiver coil pitch angle, and
- the predicted data.

The quality of the inversion output was assessed through comparison of the borehole conductivity values with conductivity predictions from the closest observation to each borehole. The assessment was carried out using conductivity values transformed to logarithm base 10. It was demonstrated that the conductivity predictions from the constrained inversion more closely matched the borehole conductivity information than either of the two previous sets of predictions. Three different measures were used to describe the quality of the inversion output for each 5m interval between the surface and 120m. The capacity to map the variability in borehole conductivity was measured using a correlation coefficient. This parameter varied from 0.64 to 0.91. The bias in the predictions relative to the borehole conductivity values was assessed using the average misfit between these two quantities. This

parameter was within the range -0.06 to +0.20 decades of conductivity. The magnitude of the differences between borehole conductivity values and the predictions was assessed using the standard deviation of the misfit between these 2 quantities. The standard deviation of the misfit was between 0.09 and 0.28 decades of conductivity.

A "percent data influence" (PDI) parameter was defined based on results for two closely related inversions. PDI profiles as a function of depth were used to arrive at an estimate of the depth of investigation for the survey of 120m.

A comparison of shallow AEM conductivity predictions with EM31 apparent conductivity measurements was carried out in addition to the comparison with borehole conductivity logs. There was a consistent improvement in the statistics used to compare EM31 apparent conductivity observations with each of the 3 generations of 0 to 5m AEM conductivity predictions; from the contractor-supplied EMFlow predictions, the revised EMFlow predictions and finally to the constrained inversion predictions. For the comparison with the latter, the correlation coefficient was ~0.81, misfit mean ~0.18 log10(mS/m) and misfit standard deviation ~0.21 log10(mS/m).

There are fundamental differences in sample volume that limit the degree of correlation that will be observed in any of these comparisons. However, the differences in sample volume can be exploited to obtain the most relevant set of shallow conductivity measurements at different scales of investigation. EM31 or other ground-based devices with a small sampling volume are appropriate for mapping shallow conductivity at paddock to farm scales. AEM measurements with larger sampling volumes provide more comprehensive sampling at sub-catchment to catchment scales.

EM31 apparent conductivity and AEM 0 to 5m conductivity predictions compare more favourably than do borehole 0 to 5m conductivity and AEM 0 to 5m conductivity predictions (e.g., R~0.81 for EM31 and AEM, R~0.64 for boreholes and AEM). This is probably due to a combination of factors such as the smaller sample volume of the borehole measurements, the invasive effects of the drilling process and the vagaries of the smaller number of boreholes (104 boreholes with conductivity logs) compared to the number of EM31 observations.

CONTENTS

1 INTRODUCTION 1
2 GEOLOGY 2
3 BOREHOLE CONDUCTIVITY LOGS 2
4 REVISED EMFlow OUTPUT 5
5 INVERSION METHODOLOGY 8
5.1 Contributions to the AEM measurements 8
5.2 Inversion formulation 10
5.3 Coordinate system conventions 11
5.4 Restoration of primary field removed during initial processing 11
5.5 Primary field calculation for transmitter loop with arbitrary pitch and roll 11
5.6 Forward model calculations 13
5.7 Inversion performance assessment criteria 14
6 DETERMINING THE INVERSION SETTINGS 15
6.1 Geological constraints 15
6.2 Other settings 19
7 ACTIONS TO REDUCE THE ELAPSED TIME FOR INVERSION 23
7.1 Down-sampling of the survey observations 23
7.2 Utilisation of a distributed computing environment 23
8 POST-INVERSION PROCESSING 24
8.1 Levelling 24
8.2 Micro-levelling 25
8.3 Re-sampling of cumulative conductance curves 27
8.4 Gridding 28
8.5 Masking of grids to the survey boundary 29
8.6 Option to rotate X and Z component data 29
9 RESULTS 29
9.1 Performance assessment of “production” inversions 29
9.2 Comparison of shallow AEM conductivity predictions with EM31 35
9.3 Example conductivity section 50
9.4 Example conductivity grids 52
10 RECOMMENDATIONS 55
10.1 Recommended conductivity predictions for the St George survey area 55
10.2 Pre-survey planning 56
10.3 Survey specifications and communication with the survey contractor 56
10.4 Research and development 56
REFERENCES 57

LIST OF FIGURES

Figure 1. Location of the St George AEM survey. 1
Figure 2. Simplified schematic cross-section of the geology for the AEM survey area. 2
Figure 3. Conductivity characteristics of the major geological units obtained from borehole conductivity measurements averaged over 5m intervals. 4
Figure 4. Summary conductivity profiles from borehole conductivity logs averaged over 5 metre intervals. The vertical datum (i.e., elevation=0) is the ground surface for all logs. 4
Figure 5. Summary conductivity profiles from borehole conductivity logs averaged over 5 metre intervals. The vertical datum (i.e., elevation=0) is the top of the Griman Creek Formation. 5
Figure 6. Comparison of average conductivity profiles sampled over 5m vertical intervals. 7
Figure 7. Geometry of the AEM system and the layered conductivity model. 9
Figure 8. Image of average borehole conductivity for the top 15m of fresh Griman Creek Fm. 16
Figure 9. Image of the top of fresh Griman Creek Formation relative to the ground surface. 18
Figure 10. Comparison of average conductivity profiles sampled over 5m vertical intervals. 18
Figure 11. Summary plots of statistical measures used to judge inversion performance. 19
Figure 12. Summary of inverted receiver coil pitch angles as a function of flight number. 21
Figure 13. Profiles of statistics for log10(conductivity) for each line from the NE to the SW of the survey area. 24
Figure 14. A portion of the 0-5m conductivity slice from the SW sector of the survey. 27
Figure 15. Example of cumulative conductance values for the original 12 layers and the re-sampled curve 28
Figure 16. Data misfit summaries for inversion of the borehole subsets. 30
Figure 17. Ground response decay and normalised misfit plots for a single inversion from the borehole subset. 31
Figure 18. Comparison of average conductivity profiles sampled over 5m vertical intervals. 32
Figure 19. Summary plots of statistical measures used to judge inversion performance. 33
Figure 20. Profiles of Percent Data Influence (PDI) derived from inversion of the borehole subset. 34
Figure 21. The locations of the EM31 traverses are shown as black lines. 35
Figure 22. Histograms of (a) EM31 apparent conductivity values, and (b) log10 transformed EM31 apparent conductivity values. 38
Figure 23. Linear regression applied to EM31 observations within 5m of each other. 39
Figure 24. Semi-variograms for log10 transformed EM31 apparent conductivity values outside the Goondoola Basin area. 41
Figure 25. Semi-variograms for EM31 apparent conductivity values (a) Observations from the Goondoola Basin area (b) Observations outside the Goondoola Basin area 42
Figure 26. Scatter plots of log10 (EM31) apparent conductivity against log10 (AEM) conductivity predictions for 0 to 5m depth. 44
Figure 27. Scatter plots of log10(EM31) apparent conductivity against log10(AEM) conductivity predictions for 0 to 5m depth. 45
Figure 28. The location of the EM31 traverse shown in profile form in Figure 29. 46
Figure 29. West to east profiles of EM31 apparent conductivity and AEM 0 to 5m conductivity predictions for the traverse shown in Figure 28. 47
Figure 30. Image of LIN-corrected EM31 apparent conductivity values for the Goondoola Basin subset. 48
Figure 31. Images of AEM 0 to 5m conductivity predictions and EM31 conductivity for the Goondoola Basin area. T 49
Figure 32. Conductivity sections for line 10730. 51
Figure 33. Image of conductivity for 0 to 5m depth below surface. Derived from a grid of manually levelled and micro-levelled constrained inversion conductivity data. 53
Figure 34. Image of conductivity for 30 to 40m depth below surface. Derived from a grid of manually levelled and micro-levelled constrained inversion conductivity data. 54
Figure 35. Image of conductivity for 80 to 120m depth below surface. Derived from a grid of manually levelled and micro-levelled constrained inversion conductivity data. 55

LIST OF TABLES

Table 1. Comparison of halfspace conductivity and apparent conductivity derived with a LIN assumption for an EM39 borehole conductivity instrument. The comparison was carried out using equations provided by McNeil (1986)..... 3

Table 2. Conductivity characteristics of the major geological units obtained from borehole conductivity measurements averaged over 5m intervals. 3

Table 3. Window definitions for the St George TEMPEST data. 14

Table 4. Standard deviation values for TEMPEST high altitude response. 20

Table 5. Layer structure for the inversion models. 22

Table 6. Manual additive level adjustments applied to log10 (conductivity) values. 25

Table 7. De-corrugation settings. 26

Table 8. Micro-levelling settings. 26

Table 9. Settings used for gridding. 29

Table 10. Comparison of halfspace conductivity and apparent conductivity derived with a LIN assumption for an EM31 instrument operated at ground level in vertical dipole mode. 36

Table 11. Table of statistics for a comparison of all EM31 apparent conductivity observations with AEM 0 to 5m conductivity predictions. 43

Table 12. Table of statistics for a comparison of EM31 apparent conductivity values and AEM 0 to 5m conductivity predictions for the traverse shown in Figure 28. 46

APPENDICES

Appendix 1. List of products 61

Appendix 2. Borehole metadata 75

Appendix 3. Plots of borehole conductivity logs and mapped horizons 89

Appendix 4. Plots of borehole conductivity logs and inversion models 103

Appendix 5. Table of summary statistics for 5m depth increments 131

1 INTRODUCTION

An airborne electromagnetic (AEM) survey was flown over an area of approximately 80km by 110km in the vicinity of St George (Figure 1) in south central Queensland in 2001 (Owers et al., 2001). The TEMPEST AEM system as described in Lane et al. (2000) was employed. A total of 28,822 line km of data were acquired on 371 flight lines spread across 3 contiguous blocks. The northeast and southwest blocks were flown with a line spacing of 250m, whilst the central block was flown with a line spacing of 400m. All lines were oriented 138/318 degrees true. Data were supplied for samples at 0.2s intervals, equivalent to an along-line spacing of approximately 13m. Aspects of terrain clearance measurements and DEM generation from this survey have been discussed by Brodie and Lane (2003), whilst Buselli et al. (2003) discuss ground electrical and EM measurements made in support of the AEM survey.

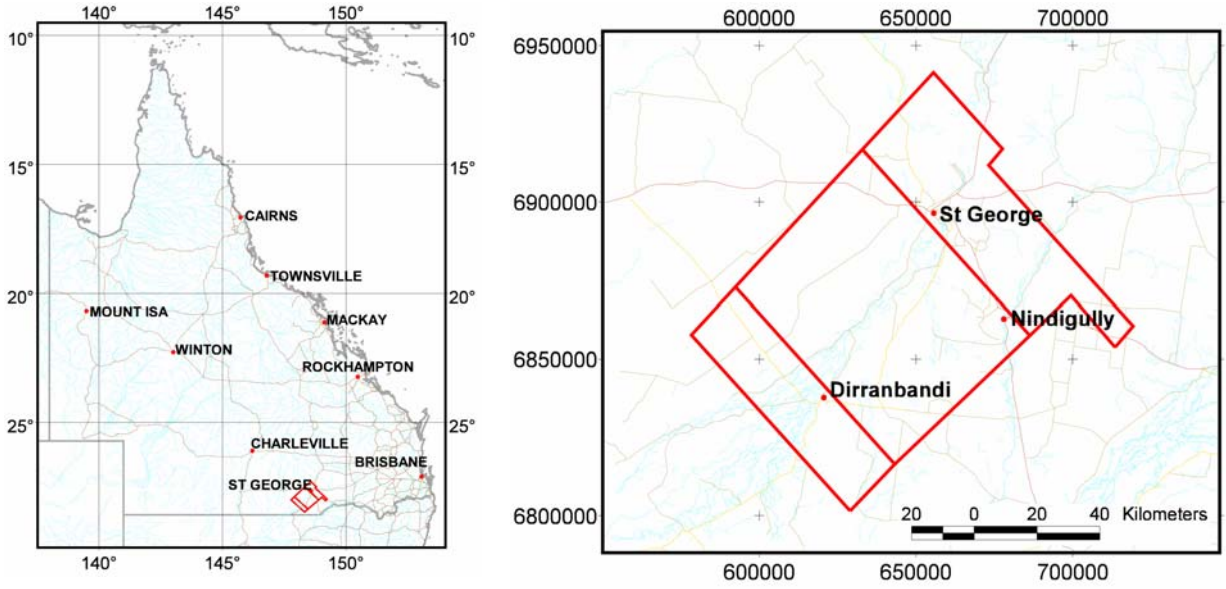

Figure 1. Location of the St George AEM survey. Unless otherwise stated, coordinates in this report are given for MGA55 projection and GDA94 datum.

The contractor-supplied survey data included 2 forms of conductivity predictions; Conductivity Depth Images (CDI) derived using program EMFlow (Macnae et al., 1998) and three-layer Layered Earth Inversions (LEI) produced with a program described by Sattel (1998).

Following delivery of the survey data, a total of 104 boreholes were logged with an inductive conductivity tool. A preliminary comparison of the CDI and LEI products with borehole conductivity logs showed a reasonable correspondence. However, certain characteristics of the CDI and LEI products were noted;

- The CDI and LEI products were based solely on the X component data. Independent Z component data were not utilised.
- Both the CDI and LEI conductivity predictions had a tendency towards low conductivity values at and below the depth of investigation of the AEM system, estimated to be 100 to 200m below surface in this instance.
- The 3-layer LEI structure was unable to accommodate the gradational vertical conductivity variations present in the borehole conductivity logs.
- The CDI output was restricted to 20 discrete conductivity values.

- EMFlow allows the user to apply a constant vertical offset to the supplied transmitter loop terrain clearance measurements. A positive offset increases the terrain clearance for the transmitter loop. This could be used to correct for an offset between the sensor used for the terrain clearance measurements and the transmitter loop, or to make an empirical adjustment to the conductivity profile with respect to ground level. In this instance, a transmitter loop terrain clearance vertical offset of +8m was used during the CDI processing. It was unclear whether this had produced the optimal near-surface conductivity predictions.

With the aid of conductivity and lithological logs of boreholes within the survey area, there was potential to design constraints that could be used to guide the conversion from AEM response to conductivity and to quantify any improvement that could be made to the predictions.

2 GEOLOGY

A simplified geological cross-section is shown in Figure 2. More detailed geological information for the survey area can be found in Graham (1972), Reiser (1971), Senior (1971) and Senior (1972). Quaternary sediments of variable thickness are present above the Cretaceous Griman Creek Formation. A variable thickness of the upper part of the Griman Creek Formation is weathered. The Griman Creek Formation is present at depth across the entire survey area, and extends below the depth of investigation of the AEM system.

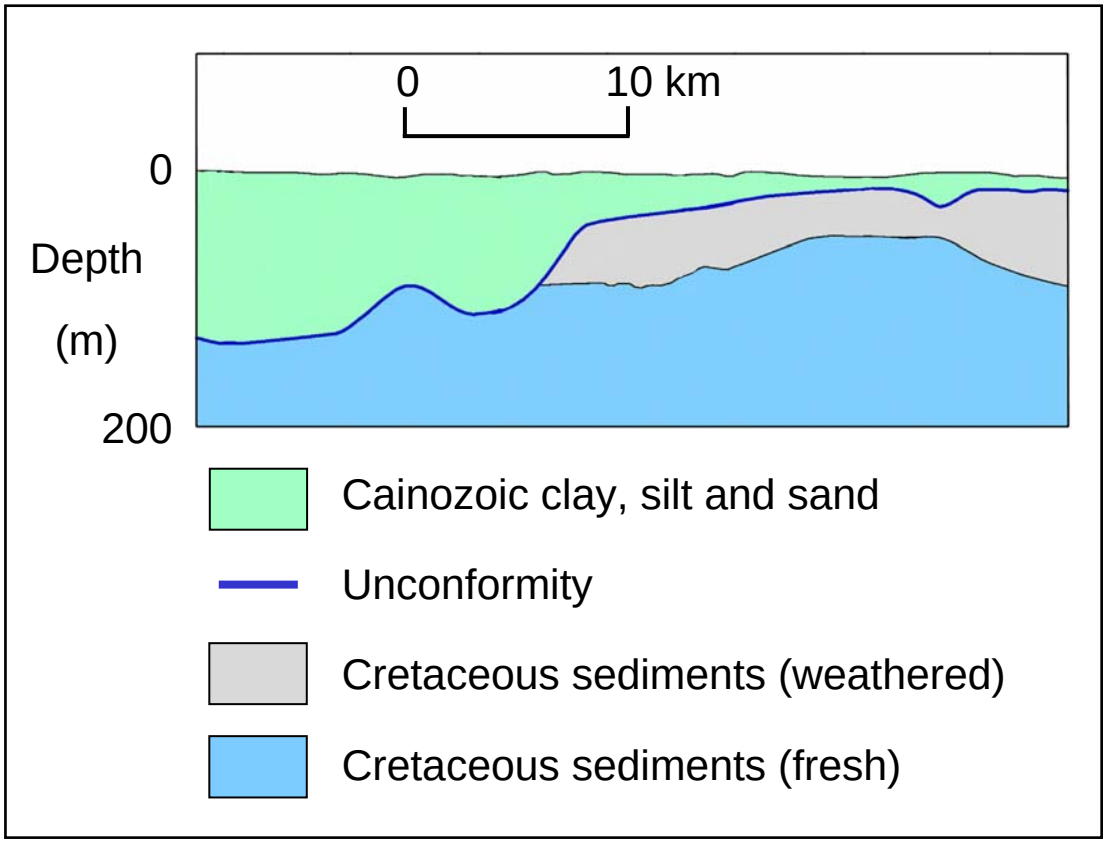

Figure 2. Simplified schematic cross-section of the geology for the AEM survey area.

3 BOREHOLE CONDUCTIVITY LOGS

The Bureau of Rural Sciences and the Queensland Department of Natural Resources and Mines obtained borehole conductivity logs for 104 holes ranging in depth from a few metres to 180m. These data were supplied in digital form for samples taken at 5cm intervals. Details of the boreholes are summarised in Appendix 2. It was assumed that appropriate calibration procedures and corrections for the low induction number (LIN) approximation had been used. The magnitude of the errors if the latter

corrections are not applied can be gauged from Table 1 which shows the difference between true halfspace conductivity and apparent conductivity derived with a LIN approximation for an EM39 borehole conductivity instrument. For conductivity values between 1 and 1000mS/m, the errors range from zero to approximately 13%. The apparent conductivity values would always under-estimate the true conductivity. The magnitude of the differences would vary with the type of instrument used since the degree of approximation depends on the coil geometry, coil spacing and operating frequency.

Table 1. Comparison of halfspace conductivity and apparent conductivity derived with a LIN assumption for an EM39 borehole conductivity instrument. The comparison was carried out using equations provided by McNeil (1986).

Halfspace conductivity (mS/m)	Apparent conductivity with LIN approximation (mS/m)
1	1
2	2
5	5
10	10
20	20
50	49
100	96
200	188
300	279
400	367
500	454
600	539
700	624
800	707
900	789
1000	870
1120	966
1200	1029
1500	1262
2000	1634

The majority of the boreholes logged with a conductivity tool were also lithologically logged. Conductivity characteristics of the 3 major units were obtained by separating out portions of the conductivity logs according to mapped lithology. Prior to analysis, the borehole conductivity values were averaged over 5m intervals then transformed to logarithm base 10. The results of the analysis are presented in Table 2 and Figure 3.

Table 2. Conductivity characteristics of the major geological units obtained from borehole conductivity measurements averaged over 5m intervals.

	Minimum (mS/m)	Median (mS/m)	Maximum (mS/m)	Mean - standard deviation (mS/m)	Mean (mS/m)	Mean + standard deviation (mS/m)	Standard deviation (log10(mS/m))	Number of samples
Quaternary	24	126	749	63	126	255	0.305	167
Griman Creek Formation (weathered)	47	352	881	178	352	696	0.296	166
Griman Creek Formation (fresh)	148	384	785	277	384	532	0.142	107

The conductivity values for Quaternary sediments are generally lower by a factor of 3 than the conductivity values for the Griman Creek Formation. The averages of the conductivity values for weathered and fresh Griman Creek Formation are similar, but the weathered Griman Creek Formation displays considerably greater variability.

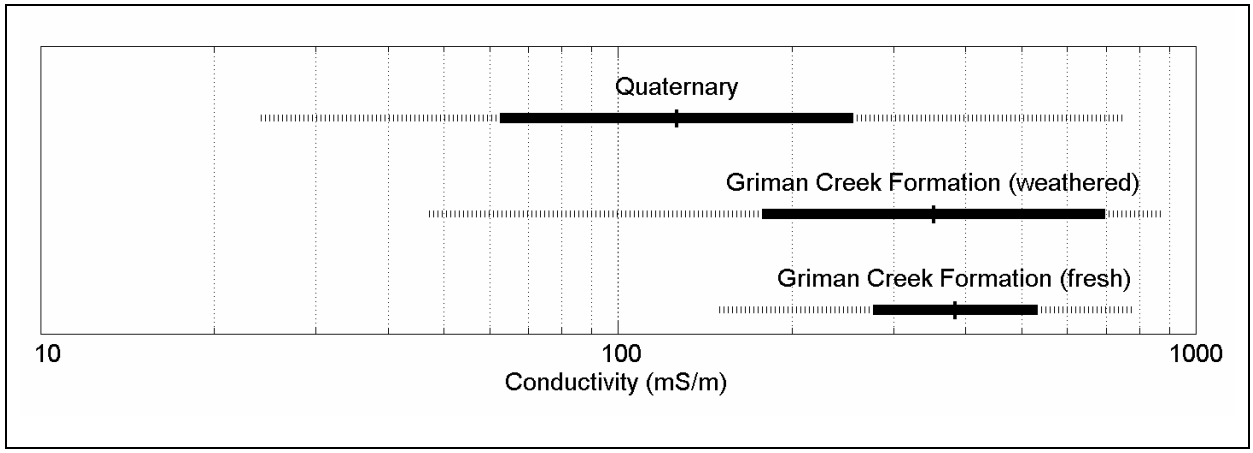

Figure 3. Conductivity characteristics of the major geological units obtained from borehole conductivity measurements averaged over 5m intervals. The mean value is indicated by a short vertical line. The mean +/- 1 standard deviation is indicated by the solid horizontal line. The extreme limits of the values for each category are indicated by the extent of the dashed lines.

Summary profiles for borehole conductivity as a function of depth below surface are given in Figure 4. There is a general increase in conductivity with depth, reflecting the progression from Quaternary sediments to the more conductive Griman Creek Formation. There is a decrease in the variability, as measured by the standard deviation, below 100m as the proportion of boreholes sampling fresh Griman Creek Formation increases.

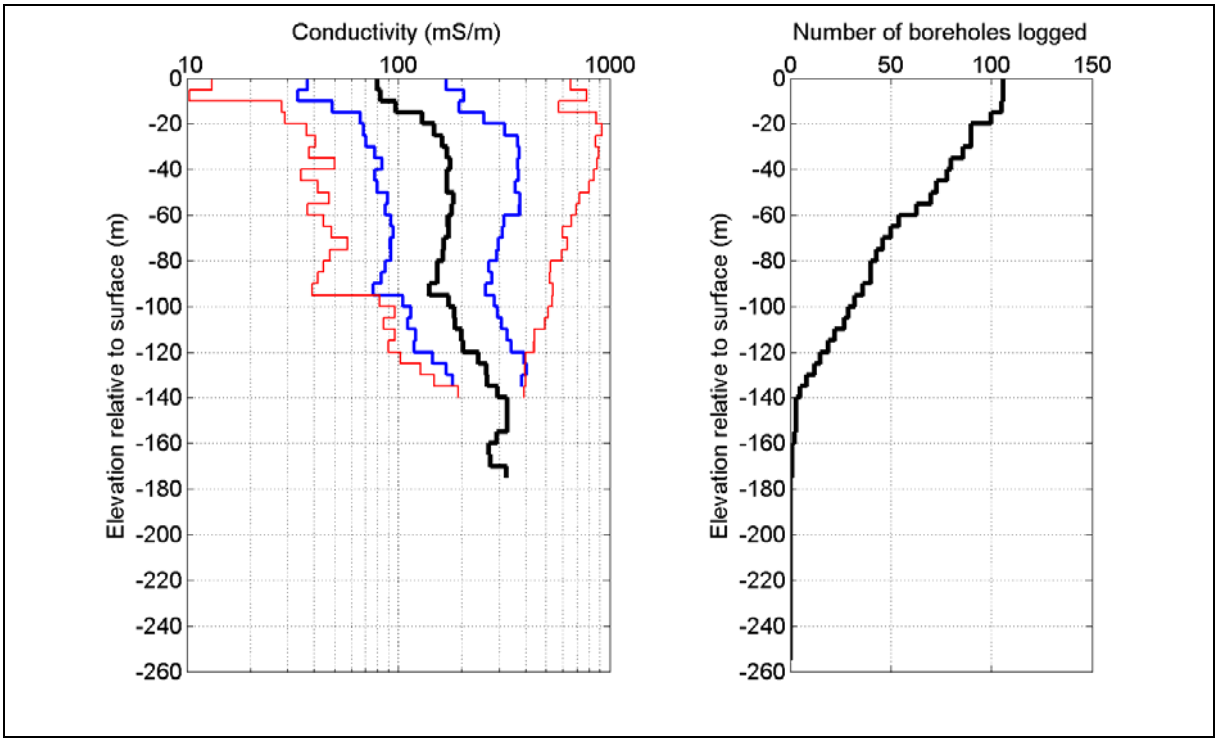

Figure 4. Summary conductivity profiles from borehole conductivity logs averaged over 5 metre intervals. The vertical datum (i.e., elevation=0) is the ground surface for all logs. The thick black line in the conductivity panel is the average (in log10 space) of all available interval conductivity values. The blue lines are the average +/- the standard deviation, whilst the red lines indicate the limits of the values within each interval. The right hand panel shows the number of boreholes used at each depth interval.

Prior to generation of the summary profiles shown in Figure 5, the vertical datum for each borehole conductivity log was changed from the elevation of the ground surface to the top of the Griman Creek Formation. Hence, elevations greater than zero reflect Quaternary sediments. These materials have conductivity values generally between 50 and 150mS/m. There is a "bulge" in the average conductivity profile within the weathered Griman Creek Formation, corresponding in shape to a Type B profile as described by Buselli and Williamson (1996). The bulge has a peak in average conductivity of ~500mS/m 40m below the top of the formation. Below the bulge, there is a gradual decrease of conductivity that equates to a rate of approximately -0.002 decades per metre.

For the purposes of testing different parameter settings for the constrained inversion, a subset of the AEM observations was formed by taking the closest observation to each of the 104 boreholes for which there was a borehole conductivity log. This was referred to as the "borehole subset" of the AEM data.

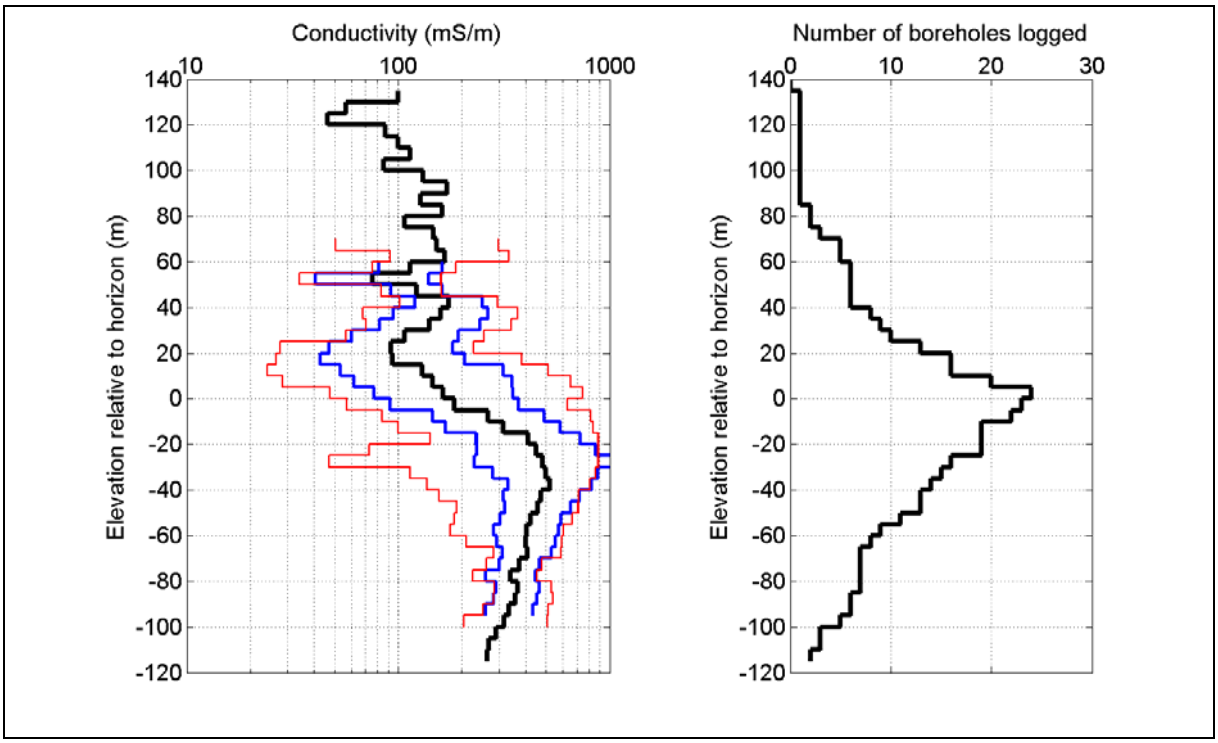

Figure 5. Summary conductivity profiles from borehole conductivity logs averaged over 5 metre intervals. The vertical datum (i.e., elevation=0) is the top of the Griman Creek Formation. The thick black line in the conductivity panel is the average (in log10 space) of all available interval conductivity values. The blue lines are the average +/- the standard deviation, whilst the red lines indicate the limits of the values within each interval. The right hand panel shows the number of boreholes used at each depth interval.

4 REVISED EMFLOW OUTPUT

The CDI conductivity values supplied by the survey contractor, Fugro Airborne Surveys, were produced with version 4.00 of EMFlow. The input to EMFlow was X component data that had been subject to a standard form of primary field removal (Lane et al., 2000), and had been corrected, in an approximate manner, to the response for a standard geometry (Green, 1998). The nominal horizontal and vertical transmitter-loop to receiver-coil separation values for this survey were 122m and 41m, respectively, whilst the nominal transmitter loop terrain clearance was 120m (Owers et al., 2001). The nominal transmitter loop moment orientation was vertical. In the absence of direct observations, the receiver coil assembly was assumed to be perfectly aligned with the flight line frame of reference at all times. These corrections utilised measured transmitter loop pitch and roll orientation values as well as measured transmitter loop terrain clearance values. The initial horizontal and vertical transmitter-loop to receiver-coil separation values were derived from the primary field estimates.

Without access to any ground or borehole conductivity data that would have indicated that material with elevated conductivity values was present at depth, the primary field removal was carried out with a standard bias towards resistive conditions at depth. This involves forcing the late time ground response component of the total response to be as small as possible whilst being consistent with the characteristics of a response from a layered model. A trend towards resistive values at depth in the supplied CDI conductivity values is at odds with the average of all of the available borehole conductivity logs (compare the black and green lines in Figure 6).

EMFlow has two important processing stages; decomposition of the supplied arbitrary waveform data into a primary field term and a series of exponential basis function terms (from which step response can be inferred), followed by transformation of step response to conductivity-depth-image values. The allowance for a primary field term is not shown in Macnae et al. (1998), but would contribute an additional column to the matrix on the right hand side of Equation 13 in Macnae et al. (1998) and an additional amplitude term to the column vector;

$$\mathbf{D} = \boldsymbol{\beta} \cdot \mathbf{A} \qquad \text{(Equation 1)}$$

$$\mathbf{D} = \begin{bmatrix} D(t_1) \\ . \\ . \\ . \\ D(t_n) \end{bmatrix} \qquad \text{(Equation 2)}$$

$$\boldsymbol{\beta} = \begin{bmatrix} \beta(t_1,\tau_1) & . & \beta(t_1,\tau_m) & P(t_1) \\ . & . & . & . \\ . & . & . & . \\ . & . & . & . \\ \beta(t_n,\tau_1) & . & \beta(t_n,\tau_m) & P(t_n) \end{bmatrix} \qquad \text{(Equation 3)}$$

$$\mathbf{A} = \begin{bmatrix} A_1 \\ . \\ . \\ A_m \\ A_{pf} \end{bmatrix} \qquad \text{(Equation 4)}$$

where D are the data measured at times t_1 to t_n, β are the basis functions for τ_1 to τ_m, P is the primary field term, and A are the amplitudes of the exponential basis function terms 1 to m plus the primary field term.

Model and data weights are generally used to control the influence of the various terms;

$$\mathbf{W}_d \cdot \mathbf{W}_b \cdot \mathbf{D} = \mathbf{W}_d \cdot \mathbf{W}_b \cdot \boldsymbol{\beta} \cdot \mathbf{A} \qquad \text{(Equation 5)}$$

where $\mathbf{W}_d$ is a data weighting matrix and $\mathbf{W}_b$ is a basis function weighting matrix.

The data weights are available to be set by the user of EMFlow, but the model weights are not. This makes it difficult for the user to control the primary field adjustment process. However, it has been noted that the amount of primary field that is removed is generally as small an amount as is possible. Thus, even if a large amount of primary field is included in the input data, it will not necessarily all be removed. This results in the late time ground response portion of the total response being as large as possible whilst being consistent with the sums of exponentials ground response model. This is consistent with the response when conductive material is present at depth.

Revised EMFlow CDI conductivity values were produced by CRC LEME (the red line in Figure 6). These were again based solely on X component data. In contrast to the survey contractor, CRC LEME had access to borehole conductivity logs that indicated conductivity values in the range 150 to 600mS/m at depths below 100m. Consequently, a bias towards conductivity values at depth was introduced. This was achieved by adding back some of the response removed by the survey contractor during the primary field removal stage of processing. Assuming perfect alignment of the receiver coil assembly with the flight line frame of reference, vertical transmitter loop moment orientation, and the nominal transmitter loop and receiver coil geometry values given previously, the X and Z component inductive limit values for this geometry are 10.5fT and 9.3fT, respectively. These values represent the upper limit in response. Use of a repetitive waveform reduces the true inductive limit. A DC shift corresponding to an error in primary field estimate can be applied to the data, in the absence of direct observation of the system geometry, provided the inductive limit is not exceeded. The effect of different positive shifts on the derived conductivity estimates was evaluated, and it was found that the weighting used by EMFlow would produce very similar conductivity values for shifts applied to the X component data of 0.1 through to 1.0fT. The effect of this adjustment is evident in Figure 6 where the "EMFlow (LEME)" curve heads towards increasing conductivity at depth.

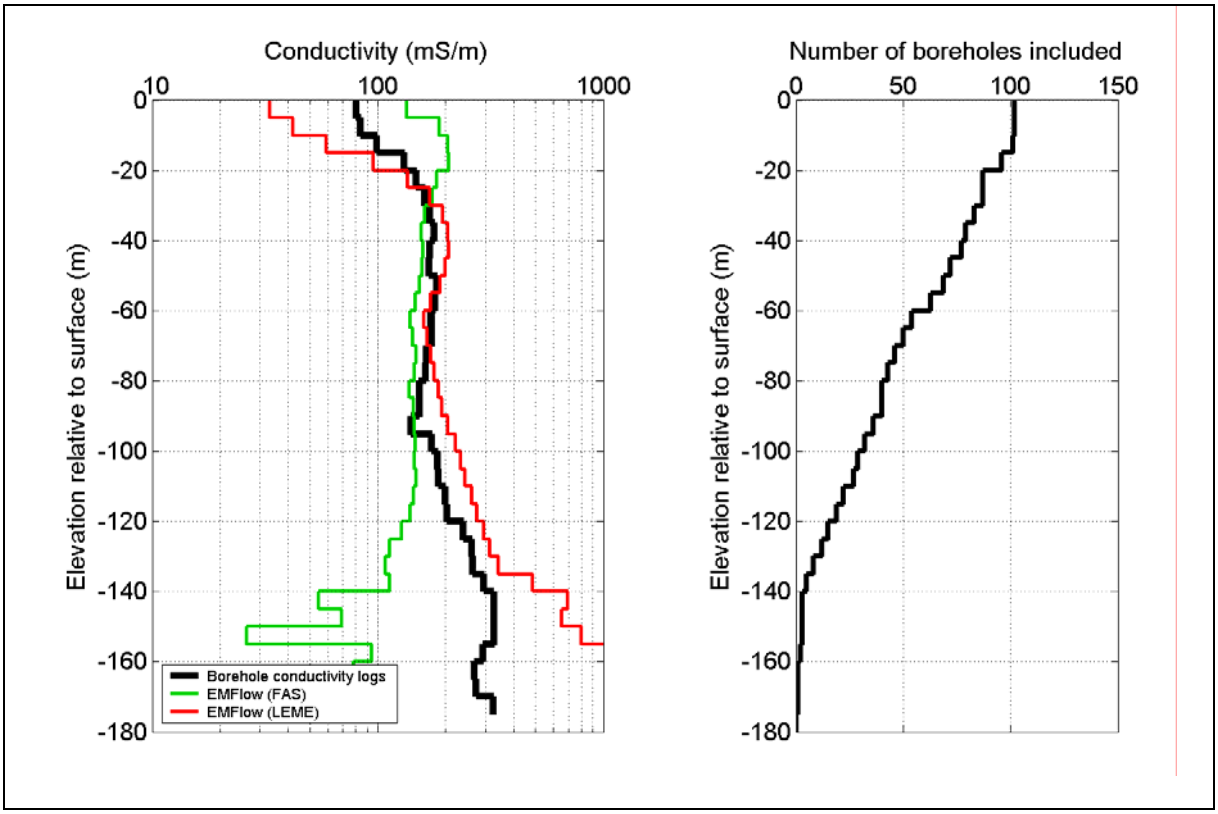

Figure 6. Comparison of average conductivity profiles sampled over 5m vertical intervals. The same intervals used to form the average borehole conductivity profile (black line) were extracted from the different models; EMFlow CDI values as delivered by the survey contractor (green line) and EMFlow CDI values as calculated by CRC LEME with modifications to the primary field and transmitter loop vertical offset (red line). The number of boreholes contributing to the average values at different depths is shown in the right-hand panel.

A +8m vertical transmitter loop offset was introduced by the survey contractor as an empirical calibration setting based on AEM and borehole conductivity comparisons during a number of previous surveys carried out with a different aircraft to that used at St George. CRC LEME obtained a better alignment between the peak in the average borehole conductivity trace between depths of 30 and 60m and the "EMFlow (LEME)" conductivity values by resetting this offset to zero. Although not evident in Figure 6, the revised EMFlow conductivity values also benefited from an increase in the number of discrete conductivity values from 20 available in version 4.00 to 250 available in version 5.22 that was used by CRC LEME for the re-processing.

The revised conductivity values produced using EMFlow demonstrate that it is possible with EMFlow to introduce some form of a priori information concerning the nature of the conductivity at depth. However, the EMFlow interface does not allow this to be done in a controlled fashion. For this reason, continuing effort was directed towards an in-house constrained inversion solution.

5 INVERSION METHODOLOGY

5.1 Contributions to the AEM measurements

The TEMPEST AEM system measures a linear combination of primary field response and ground response (Lane et al., 2000). Smith (2001a) presented this as;

$$T(t_i) = P(t_i) + G(t_i) \qquad \text{(Equation 6)}$$

where T is the total measured response at time t_i, P is the primary field contribution and G is the ground response contribution.

The primary field response is a function of the measurement system transfer function, the transmitter loop magnetic field moment waveform, and the transmitter loop to receiver coil geometry. The TEMPEST measurement system transfer function is deduced from measurements of the transmitter loop current and received waveform taken at high altitude, in the absence of ground response. The transmitter loop magnetic field moment waveform is known because the current waveform is monitored continuously and the area and number of turns of the transmitter loop is known. The primary field cannot, however, be accurately predicted because elements of the transmitter loop to receiver coil geometry are not measured. The full system geometry is shown schematically in Figure 7. Two of the three angles that define the orientation of the transmitter loop moment vector, $\mathbf{M_t}$, are measured (i.e., pitch and roll angles, but not the yaw angle). The transmitter loop to receiver coil separation vector, **r**, is not measured in any way. The number of turns, area of each turn and amplifier gain of each receiver coil is known, thus the amplitude of the receiver coil waveform is sufficiently calibrated. However, there are no measurements available for the attitude of the receiver coil assembly. It is usual to assume that this assembly is aligned such that the axis of the X component coil is horizontal in the direction of the flight line, the axis of the Y component is horizontal perpendicular to the direction of the flight line and the axis of the Z component is vertical (i.e., perfectly aligned with the flight line frame of reference).

The ground response is a function of all of the factors that influence the primary field together with the transmitter loop to ground geometry, the receiver coil to ground geometry, and the conductivity structure of the ground. The transmitter loop to ground geometry, h_t, is measured with an altimeter. The receiver coil to ground geometry depends on the transmitter loop to receiver coil separation, **r**, which is not known.

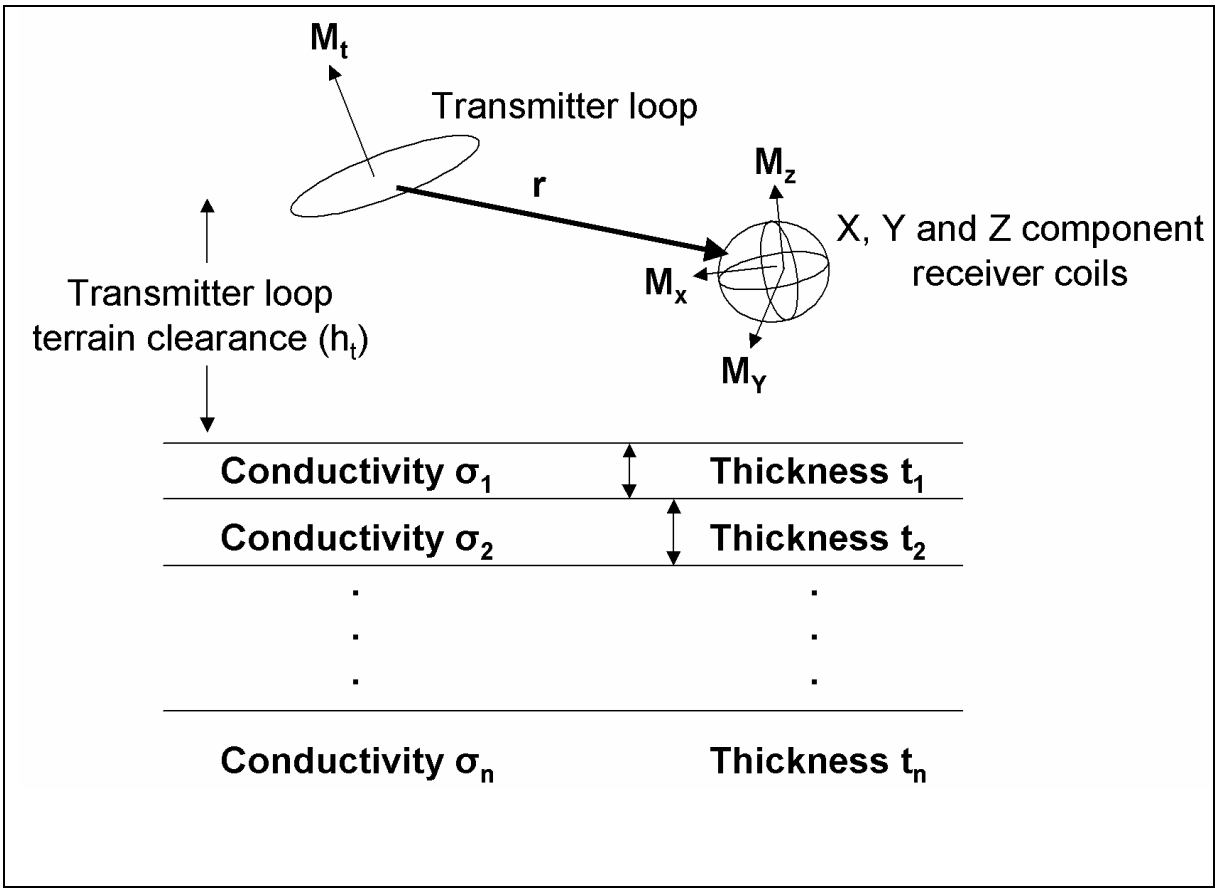

Figure 7. Geometry of the AEM system and the layered conductivity model. In all instances, the thickness of the bottom layer is set to a very large value, thus approximating a halfspace.

Certain aspects of the TEMPEST data processing simplify the simultaneous modelling of ground conductivity and primary field. De-convolution of the system transfer function and the transmitter loop current waveform compensates for the non-ideal nature of the measurement system and for any variations in shape and amplitude of the transmitter loop moment from one observation to another. This means that in modelling applications, the amplitude and shape of the transmitter loop waveform is known accurately and is constant from one observation to the next and indeed from one survey to the next. However, the primary field measured at the receiver coil location is still unknown since it is a function of the transmitter loop to receiver coil separation and the attitude of the transmitter loop and receiver coils. Using the high altitude waveform, R, as a reference, and noting that transmitter loop waveform shape and amplitude variations have been compensated for during TEMPEST data processing, the primary field can be described by;

$$P(t_i) = \alpha_p R(t_i) \qquad \text{(Equation 7)}$$

where R is the reference waveform and α_p is a coupling factor that is solely a function of geometry. Without de-convolution, R would not only be a function of delay time, t_i, but would be a function of observation. This could be managed, but would be cumbersome.

Smith (2001a) showed that the ground response measured by a system such as TEMPEST was composed of variable proportions of a "time domain in-phase" component that has the same shape as the primary field, and hence the reference waveform, and a "time domain quadrature" component that is orthogonal to the primary field;

$$G(t_i) = \alpha_g R(t_i) + Q(t_i) \qquad \text{(Equation 8)}$$

where α_g is a scaling factor that relates the ground response time domain in-phase component to the reference waveform and Q is the time domain quadrature component.

The presence of the time domain in-phase component of the ground response means that the primary field cannot be removed from the measured response without considering the nature of the ground response. Primary field removal thus entails interpretation of the ground response, or in other words, it is necessary to solve for ground response and primary field components simultaneously rather than sequentially;

$$T(t_i) = (\alpha_p + \alpha_g)R(t_i) + Q(t_i) \qquad \text{(Equation 9)}$$

Coggon (pers. comm., 2000) and Sattel (pers. comm., 2000) recognised the need to invert simultaneously for primary field and ground response contributions to the measured response. They used X and Z component data to reduce the ambiguity in the response, and found it necessary to use a non-zero receiver coil assembly pitch to be able to fit both the X and Z component response at any observation to a single layered conductivity model. These conclusions were also reached by one of the authors (Brodie) on a study of TEMPEST data in 2002.

The ambiguity between the ground response and primary field contributions to the measured response is increased in areas with elevated conductivity that extends beyond the depth of investigation at late time. Some form of a priori information or external constraint is required to produce a stable, accurate solution to the separation of the two quantities.

5.2 Inversion formulation

The formats for the inversion input and output files are described in Appendix 1, together with the settings passed to the inversion program through a control file.

The algorithm inverts the total observed noise-weighted X and Z component response values and layer conductivity smoothness values to a model that consists of layer conductivity parameters, the transmitter loop to receiver coil separation values, and the receiver coil pitch angle, subject to a priori estimates for the model parameters values and errors. The algorithm follows the expression given in Equation 9.11[1] of Menke (1984).

The geometry and data elements to be considered in a layered conductivity model inversion for the TEMPEST system are given in Figure 7. The following elements were not included in the inversion inputs or outputs;

- Y component data (not supplied),
- transmitter loop yaw angle (not supplied, insufficient information available to solve for this parameter),
- receiver coil yaw angle (not supplied, insufficient information available to solve for this parameter),
- receiver coil roll angle (not supplied, insufficient information available to solve for this parameter, could be included as an inversion model parameter if Y component data were supplied) and
- transmitter loop to receiver coil transverse horizontal offset, DY (not supplied, insufficient information available to solve for this parameter, could be included as an inversion model parameter if Y component data were supplied).

A multi-layer inversion model with the same fixed thickness values was used for each observation. All operations involving conductivity were carried out on logarithm to the base 10 of the conductivity values. Smoothness constraints for conductivity values of each of the internal layers were defined as;

---

[1] Note the equation in Menke (1984) should not contain the second transpose operator in the expression $G_n^T [\mathrm{cov}\, d]^{-1} G_n^T$.

$$S_i = -C_{i-1} + 2C_i - C_{i+1} \qquad \textit{for } i = 2,n\text{-}1 \qquad \text{(Equation 10)}$$

where S is the smoothness value, C is a layer conductivity value (log10), *i* is the layer number and *n* is the total number of layers. Note that smoothness is only defined for the internal layers, and that it does not take into account the layer thickness values.

Each input data value had an associated uncertainty standard deviation. Each inversion model parameter had a start value, reference value and an uncertainty standard deviation. For simplicity, the start and reference values were the same.

Although there was provision for data and model covariances, all were assumed to be independent (i.e., all elements away from the leading diagonals of the data and model covariance matrices were zero).

5.3 Coordinate system conventions

The inversion program utilises a right-handed flight line frame of reference such that the X-axis is positive in the flight line direction, the Y-axis is positive in the left wing direction and the Z-axis is positive vertically upwards. The origin of the coordinate system is at the centre of the transmitter loop. Roll is a rotation about the X-Axis that would bring the left wing up. Pitch is a rotation about the Y-Axis that would take the nose down. Yaw is a rotation about the Z-axis that would take the nose to the left.

The TEMPEST AEM system geometry has 10 degrees of freedom (Figure 7). The orientation of the transmitter loop moment away from the standard Z axis direction can be described in terms of sequentially applied pitch, tx_p, roll , tx_r, and yaw, tx_y, rotations. The receiver coils are assumed to form a combined unit with a common centre point such that the X, Y and Z coils have axes that are mutually perpendicular. The attitude of the receiver coil unit away from the standard orientation aligned with the flight line frame of reference can be described in terms of sequentially applied pitch, rx_p, roll, rx_r and yaw, rx_y , rotations. The receiver coil unit is offset from the centre of the transmitter loop by a vector **r** that can be decomposed into offsets in the X, Y and Z axis directions (dx,dy,dz). The centre of the transmitter loop is located at height h_t above the ground surface.

The supplied TEMPEST data differ from the above conventions in several ways. The supplied pitch values were multiplied by –1 to account for a difference in coordinate systems. Similarly, the Z component data were multiplied by –1 prior to inversion. Assuming that the bird is always behind and below the aircraft, the dx and dz values were required to be negative.

5.4 Restoration of primary field removed during initial processing

The X and Z component data supplied by the survey contractor are an estimate of the true ground response rather than the total measured response required as an input to the inversion. To obtain the total measured response, it was necessary to add back the estimate of the primary field that had been removed by the survey contractor. These amounts were not available directly, but could be recovered from the supplied horizontal and vertical transmitter loop to receiver coil separation values. The offsets were calculated assuming that the X and Z component primary field values arise from magnetic field coupling between a transmitter loop that has a 100% duty cycle, a unit peak-to-peak moment, and the observed transmitter loop pitch and roll orientation and receiver magnetic field sensors that are perfectly aligned with a flight line frame of reference (i.e., X component axis horizontal in the direction of the flight line, Z component axis vertical).

5.5 Primary field calculation for transmitter loop with arbitrary pitch and roll

Given the size of the transmitter loop and the separation of the transmitter loop from the receiver coils, the transmitter loop primary magnetic field, $\mathbf{B}_P$, at the receiver coils can be approximated by that of a magnetic dipole source. An expression for this field can be found in King and Macnae (2001).

$$\mathbf{B}_P = \frac{\mu_0}{4\pi|\mathbf{r}|^3}\left[3(\mathbf{M}_t \bullet \hat{\mathbf{r}})\hat{\mathbf{r}} - \mathbf{M}_t\right] \qquad \text{(Equation 11)}$$

The orientation of the transmitter loop moment[2], $\mathbf{M}_t$, given arbitrary pitch and roll attitude was calculated using sequential application of a general expression for anticlockwise rotation by an angle θ of a vector (X,Y,Z) about an axis defined by a unit vector (x,y,z), giving rise to a new vector (X',Y',Z').

$$\begin{pmatrix} X' \\ Y' \\ Z' \end{pmatrix} = \begin{pmatrix} x^2 + (1-x^2)\cos\theta & xy(1-\cos\theta) - z\sin\theta & xz(1-\cos\theta) + y\sin\theta \\ xy(1-\cos\theta) + z\sin\theta & y^2 + (1-y^2)\cos\theta & yz(1-\cos\theta) - x\sin\theta \\ xz(1-\cos\theta) - y\sin\theta & yz(1-\cos\theta) + x\sin\theta & z^2 + (1-z^2)\cos\theta \end{pmatrix} \begin{pmatrix} X \\ Y \\ Z \end{pmatrix}$$

(Equation 12)

It was assumed that the vertical gyroscope used to measure the orientation of the transmitter loop provides pitch and roll attitude values in the flight line frame of reference. The order of sequential rotations in 3-dimensions is important, but the order used by the vertical gyroscope was not known. It was thus arbitrarily assumed that the order was pitch followed by roll. For pitch, rotation of the initial vertical transmitter loop moment takes place around the y-axis.

$$(X,Y,Z) = (0,0,1) \qquad \text{(Equation 13)}$$

$$(x,y,z) = (0,1,0) \qquad \text{(Equation 14)}$$

The result is a modified transmitter loop moment vector, (X',Y',Z'). For the subsequent roll attitude modification, rotation takes place about the x-axis to produce a further modified transmitter loop moment vector, (X'',Y'',Z'').

$$(x,y,z) = (1,0,0) \qquad \text{(Equation 15)}$$

For consistency with the computations of the secondary (ground) response, the coordinate system was changed such that horizontal component of the primary field was aligned with the y-axis. This was achieved by rotation about a vertical axis by angle Φ,

$$\Phi = \frac{\pi}{2} - a\tan 2\left(\frac{Y''}{X''}\right) \qquad \text{(Equation 16)}$$

where the transmitter loop moment following pitch and roll rotations is (X'',Y'',Z'') and *atan2* is a four-quadrant inverse tangent function[3]. The same rotation was applied to the receiver coil offset from the transmitter loop (dx,dy,dz), resulting in an offset of (dx_r,dy_r,dz_r).

The vector form of the dipole primary field expression can be broken down into the contribution to each Cartesian component from vertical and horizontal sources (Wait, 1982). The expressions for the primary field $(B^V_{XP},B^V_{YP},B^V_{ZP})$ due to the vertical component of the transmitter loop moment, m^V, for a transmitter loop at location (0,0,0) and a receiver located at (dx,dy,dz) are given in Equation 20, Equation 21 and Equation 22. The corresponding expressions for the primary field $(B^H_{XP},B^H_{YP},B^H_{ZP})$ due to the y-axis directed horizontal component of the transmitter loop moment, m^H, for a transmitter loop at location (0,0,0) and a receiver located at (dx,dy,dz) are given in Equation 23, Equation 24 and Equation 25.

---

[2] TEMPEST data are processed to produce square-wave B-field response normalised to unit area and unit peak-to-peak current. Thus, the normalisation results in unit transmitter loop moment where moment is the product of turns by area by current (Lane et al., 2000).

[3] For a definition of atan2, see for example http://www.netlib.org/fdlibm/e_atan2.c .

$$C^V = \frac{\mu_0 m^V}{4\pi} = Z'' \quad \text{(Equation 17)}$$

$$C^H = \frac{\mu_0 m^H}{4\pi} = \sqrt{\left((X'')^2 + (Y'')^2\right)} \quad \text{(Equation 18)}$$

$$R = \sqrt{\left(dx_r{}^2 + dy_r{}^2 + dz_r{}^2\right)} \quad \text{(Equation 19)}$$

$$B^V_{XP} = \frac{3C^V dx_r \cdot dz_r}{R^5} \quad \text{(Equation 20)}$$

$$B^V_{YP} = \frac{3C^V dy_r \cdot dz_r}{R^5} \quad \text{(Equation 21)}$$

$$B^V_{ZP} = \frac{3C^V dz_r{}^2}{R^5} - \frac{C^V}{R^3} \quad \text{(Equation 22)}$$

$$B^H_{XP} = \frac{3C^H dx_r \cdot dy_r}{R^5} \quad \text{(Equation 23)}$$

$$B^V_{ZP} = \frac{3C^H dy_r{}^2}{R^5} - \frac{C^H}{R^3} \quad \text{(Equation 24)}$$

$$B^H_{ZP} = \frac{3C^H dy_r \cdot dz_r}{R^5} \quad \text{(Equation 25)}$$

Finally, the contributions to the primary field from the vertical and horizontal components of the transmitter loop moment were summed and rotated back to the original frame of reference through a rotation about a vertical axis by an amount -Φ.

5.6 Forward model calculations

Details of the TEMPEST AEM System and the data processing sequence used by the survey contractor can be found in Lane et al. (2000). The data processing sequence can be summarised as:

- Sferic filtering.
- Stacking.
- Deconvolution of the system transfer function and normalisation for the receiver coil effective area, transmitter loop current, transmitter loop turns and transmitter loop area.
- Convolution of the resultant impulse response with a square waveform.
- Windowing.
- Primary field removal.

Although the system transmits a 50% duty cycle, approximately square transmitter loop current waveform, and receives the response as a voltage time series, final data are presented as equivalent B-field square-wave response for a perfect 100% duty cycle periodic waveform with unit current steps.

The processed data relate to a system with periodic transmitter loop waveform at a base frequency of 25 Hz. A full waveform consists of 3000 samples at 13.333 microsecond intervals (i.e. 75 kHz sample rate). The first sample is assigned a time of 6.666 microseconds after time zero. The first 1500 samples have a current of +0.5 A, the second 1500 samples have a current of –0.5 A (i.e. 100% duty cycle square waveform with steps of 1 A). The transmitter loop has a single turn enclosing an area of 1 m^2.

Horizontal in-line (X) and vertical (Z) components of the received magnetic field response were supplied. Output window definitions are given in Table 3.

Table 3. Window definitions for the St George TEMPEST data.

Window	Start_time (ms)	End_time (ms)	Width (samples)
1	0.00667	0.02000	2
2	0.03333	0.04667	2
3	0.06000	0.07333	2
4	0.08667	0.12667	4
5	0.14000	0.20667	6
6	0.22000	0.34000	10
7	0.35333	0.55333	16
8	0.56667	0.87333	24
9	0.88667	1.35333	36
10	1.36667	2.10000	56
11	2.11333	3.27333	88
12	3.28667	5.11333	138
13	5.12667	7.99333	216
14	8.00667	12.39333	330
15	12.40667	19.99333	570

Forward modelling of layered conductivity models to produce ground response for the TEMPEST system was performed with an in-house program. The code is based on the formulation of Wait (1982) for the frequency domain response of vertical and horizontal magnetic dipole sources over a horizontally layered medium. Evaluation of the Hankel transforms was achieved via the filter coefficients derived by Guptasarma and Singh (1997).

The time domain waveform described above was transformed to the frequency domain via fast fourier transform (FFT). The secondary B field was calculated for 5 (logarithmically equi-spaced) frequencies per decade between 10Hz and 100,000Hz. The inphase and quadrature parts of each component were then individually splined to obtain 3000 linearly spaced frequencies at the same frequencies as the nodes of the transformed waveform. Complex multiplication followed by inverse FFT of the 3000 samples of transformed waveform and the B field, yielded the B field transient response. The transient was then windowed into the 15 windows by averaging those samples that fell within each window.

5.7 Inversion performance assessment criteria

Inversion performance was assessed through analysis of the misfit between observed and predicted data and by comparison of the inversion models with borehole conductivity logs.

Data misfit

The differences between observed and calculated data were analysed using decay plots that superimposed observed and calculated data, plots of a "normalised misfit" function, φ, and through histograms of a "data misfit" function, χ;

$$\varphi_i = \left(\frac{(y_i - x_i)}{\sigma_i} \right) \qquad \text{(Equation 26)}$$

where y_i are the predicted data, x_i are the observed data, σ_i are the data uncertainty standard deviation values, and

$$\chi = \sqrt{\sum_{i=1}^{N}\left(\frac{(y_i - x_i)}{\sigma_i}\right)^2} \qquad \text{(Equation 27)}$$

where N is the number of data (30 in this instance, excluding the smoothness constraints).

Model characteristics

The effectiveness of various inversion settings was assessed through inversion of the borehole subset and comparison of the conductivity predictions with borehole conductivity logs.

Qualitative comparisons were made between the conductivity predictions and borehole conductivity logs using plots such as those presented in Appendix 4.

Quantitative statistical comparisons were made using average conductivity values for 5m depth increments transformed to logarithm base 10. The conductivity predictions were cross-referenced to the available borehole log measurements to ensure that only those predictions where a corresponding conductivity log value was present were used in the procedure.

Three statistical measures were used to quantify the performance of conductivity predictions. A correlation coefficient (R) was derived for each 5m depth increment. The quantity R^2 describes the proportion of the variance for the log10 borehole conductivity values that can be accounted for by the log10 conductivity predictions. "Misfit mean" (MM) and "misfit standard deviation" (MSD) statistics were also calculated for each 5m depth increment (Brodie et al., 2002);

$$MM = \frac{\sum_{i=1}^{N}(y_i - x_i)}{N} \qquad \text{(Equation 28)}$$

$$\mathrm{MSD} = \sqrt{\left(\frac{\sum_{i=1}^{N}\{(y_i - x_i) - \mathrm{MM}\}^2}{N-1}\right)} \qquad \text{(Equation 29)}$$

where x_i are log10(borehole conductivity) values, y_i are log10(conductivity predictions), N is the number of observations and the subscript i signifies the i^{th} prediction or observation.

6 DETERMINING THE INVERSION SETTINGS

Prior to inversion of the complete survey data set, staged trials were carried out. Some of these trials involved custom subsets of the data, chosen to allow specific aspects of the inversion settings to be investigated.

The majority of the trials were carried out on the "borehole subset", the set of closest observations to the 104 boreholes for which conductivity logs were available. When acceptable settings had been determined, inversions of observations along a single complete flight line were carried out to review the inversion models in section view. Finally, inversions of a highly down-sampled version of the entire survey were carried out to check the spatial coherency of the inversion models. When all of these stages had been completed successfully, inversion of the complete survey commenced.

6.1 Geological constraints

Borehole lithological logs and conductivity logs were reviewed to determine if there were any associations between lithology and conductivity that could be exploited as inversion constraints,

specifically to define the reference conductivity values and the conductivity uncertainty standard deviation values. With the major objective of the AEM survey being to return independent information about the near-surface conductivity distribution, the logical focus of attention for finding suitable constraints was at depth.

The conductivity properties of the three major units have been discussed previously. It was noted that fresh Griman Creek Formation was present at depth across the entire survey area, and that this unit had the lowest variability in conductivity. It was suggested that reference conductivity values derived from borehole conductivity logs for fresh Griman Creek Formation could be used as a constraint. In one scenario, this could be applied as a "strong" constraint that would virtually fix the conductivity to these reference values at depths below which the fresh Griman Creek Formation would be expected to be present. In an alternate scenario, a "weak" constraint that would only slightly favour reference conductivity values would be applied at all depths.

Conductivity of fresh Griman Creek Formation

There were only 11 borehole conductivity logs that included measurements for a significant amount of fresh Griman Creek Formation (i.e., at least 15m). An image of a grid of the average conductivity for the top 15m of fresh Griman Creek Formation is shown in Figure 8. It was unclear whether (1) a spatially varying reference conductivity value for "fresh" Griman Creek Formation as shown in Figure 8 could be supported or (2) whether the average of the 11 values should be used everywhere.

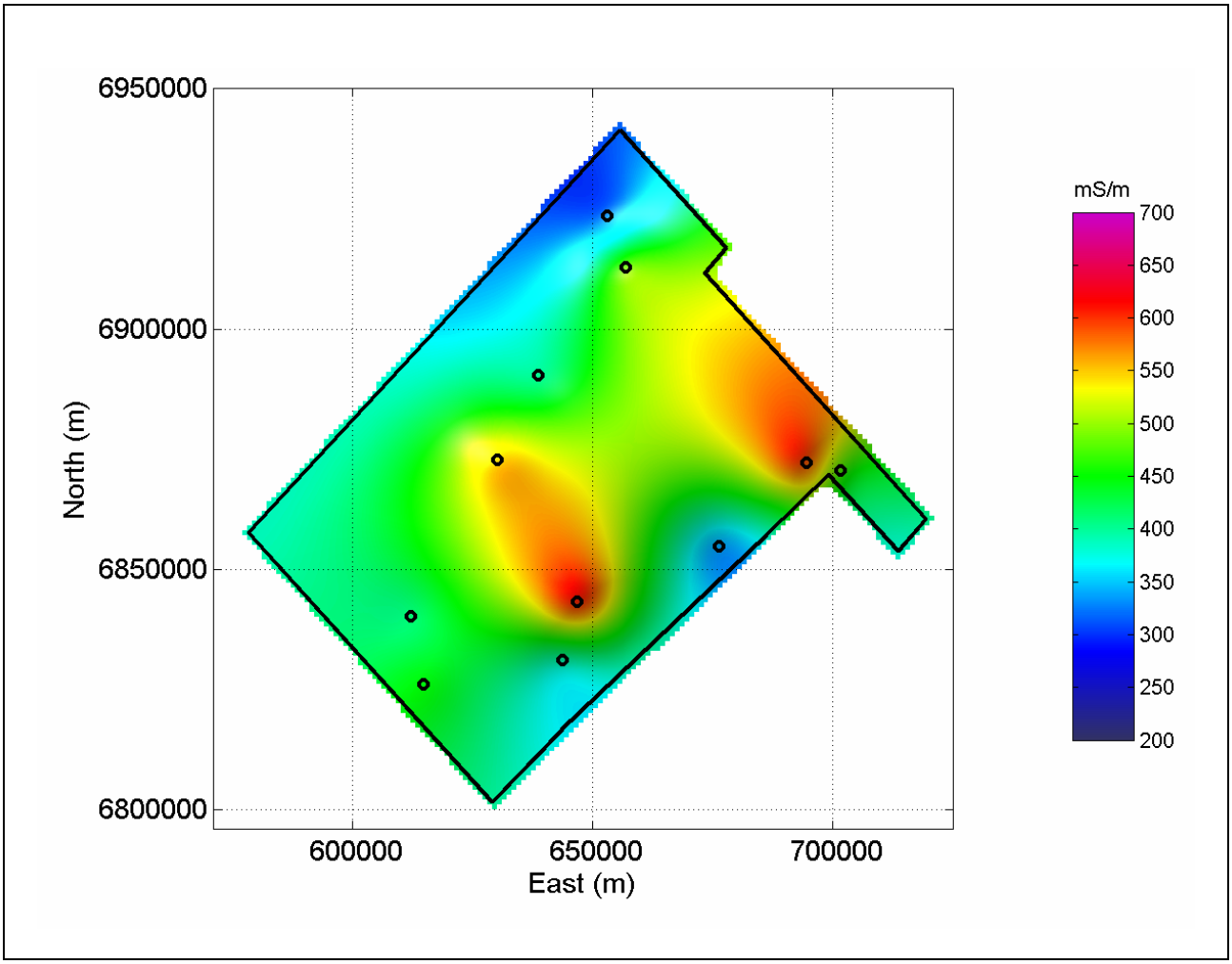

Figure 8. Image of average borehole conductivity for the top 15m of fresh Griman Creek Formation. The locations of boreholes used to construct this surface are shown as black circles.

A "leave-one-out" cross validation test was used to decide which of these two options to use. For each of the two available options, 11 experiments were carried out. In each experiment, one of the

observations was left out and the remaining observations were used to predict the value of the excluded observation. The estimate of the standard deviation of the error for each option was determined as the standard deviation of the differences between the predictions and the actual value of the excluded observation. In the case of the spatially variable conductivity model, the experiment involved production of a grid of conductivity values using 10 of the 11 samples, and extraction of the grid value at the location of the excluded observation. For the single value conductivity model, the predicted value for the excluded observation was the average of the other 10 conductivity values. All calculations were performed on conductivity values transformed to logarithm base 10.

The estimated standard deviation of errors for the spatially varying reference conductivity option was 0.190 decades of conductivity, whilst the estimate for the single value reference conductivity option was 0.135 decades of conductivity. It was concluded that the spatially varying option could not be supported, and that it would be better to use the same reference conductivity value for all locations. The mean of the 11 conductivity values calculated using logarithms to base 10 was 2.65 log10 (mS/m) or 447mS/m. It was previously noted that conductivity within fresh Griman Creek Formation appeared to decrease slowly with depth. Hence, the conductivity chosen as representative of the conductivity at depth across the entire survey area was 0.2 decades lower than the average value, or a value of 282mS/m.

Depth to fresh Griman Creek Formation

There were many more boreholes (106) in which the transition from weathered to fresh Griman Creek Formation had been noted than there were boreholes with conductivity logs extending for 15m into fresh Griman Creek Formation (11). There was little question that a grid portraying the spatial variability of the depth to fresh Griman Creek Formation (Figure 9) would be a better predictor of the depth to this horizon than a single fixed value for this depth corresponding to the average of all available depths.

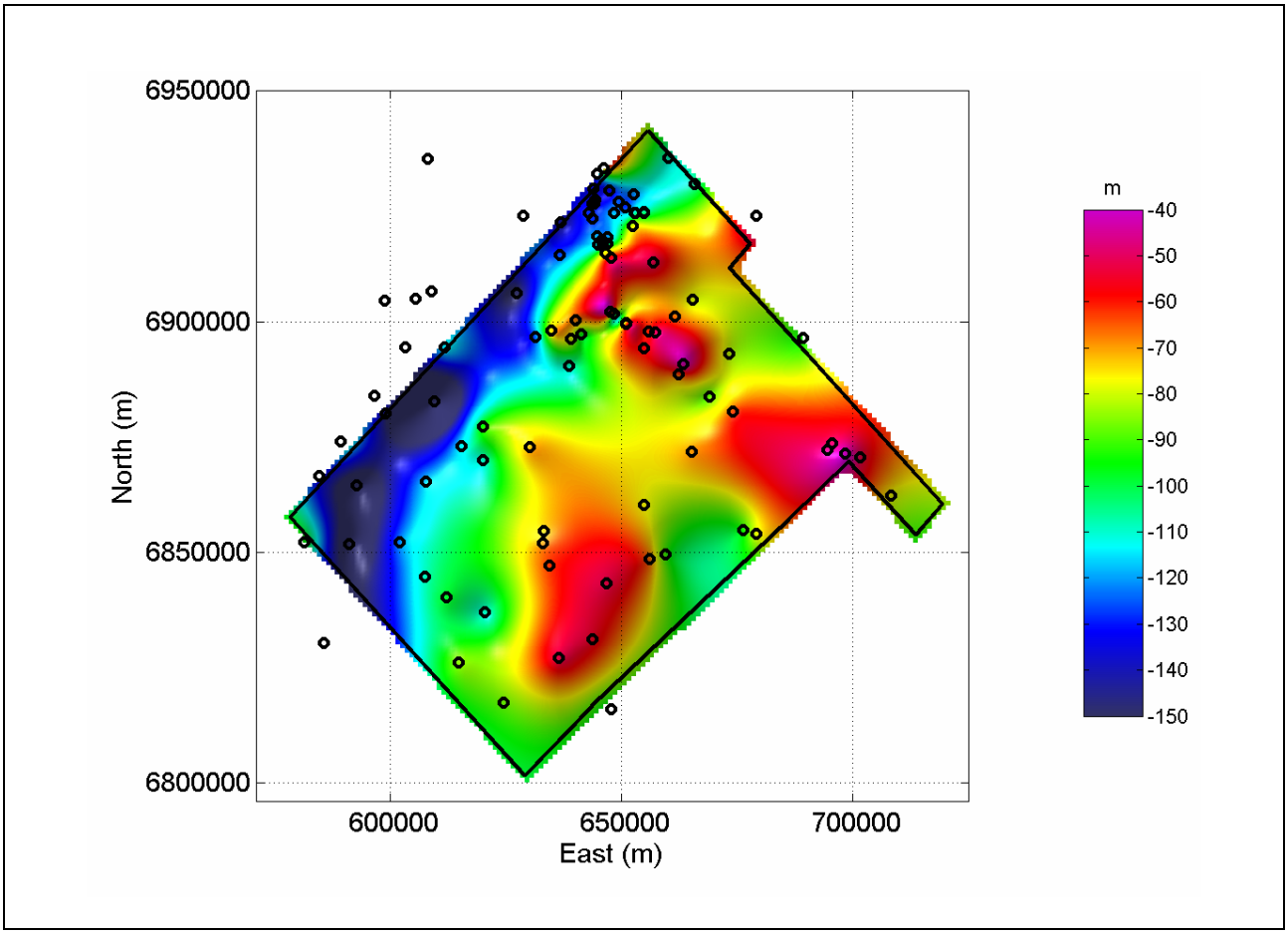

Figure 9. Image of the top of fresh Griman Creek Formation relative to the ground surface. The locations of boreholes used to construct this surface are shown as black circles.

To allow for the use of discrete layers during the inversion procedure, the reference conductivity was fixed for all layers at depths starting from 40m below the value of the depth to fresh Griman Creek Formation extracted from the grid shown in Figure 9.

Trials involving geological constraint options

Two different options for geological constraints have been defined;

1. A "strong" constraint that would virtually fix the conductivity to the reference value at depths below which the fresh Griman Creek Formation would be expected to be present.
2. A "weak" constraint that would only slightly favour the reference conductivity but would be applied equally at all depths.

The performance of these two options was assessed through trials on the borehole subset. The results are summarised in Figure 10 and Figure 11. The differences were quite marginal, particularly in the top 80m where most attention was focussed. It was concluded that the second option would be used since this was the simpler and more general of the two options.

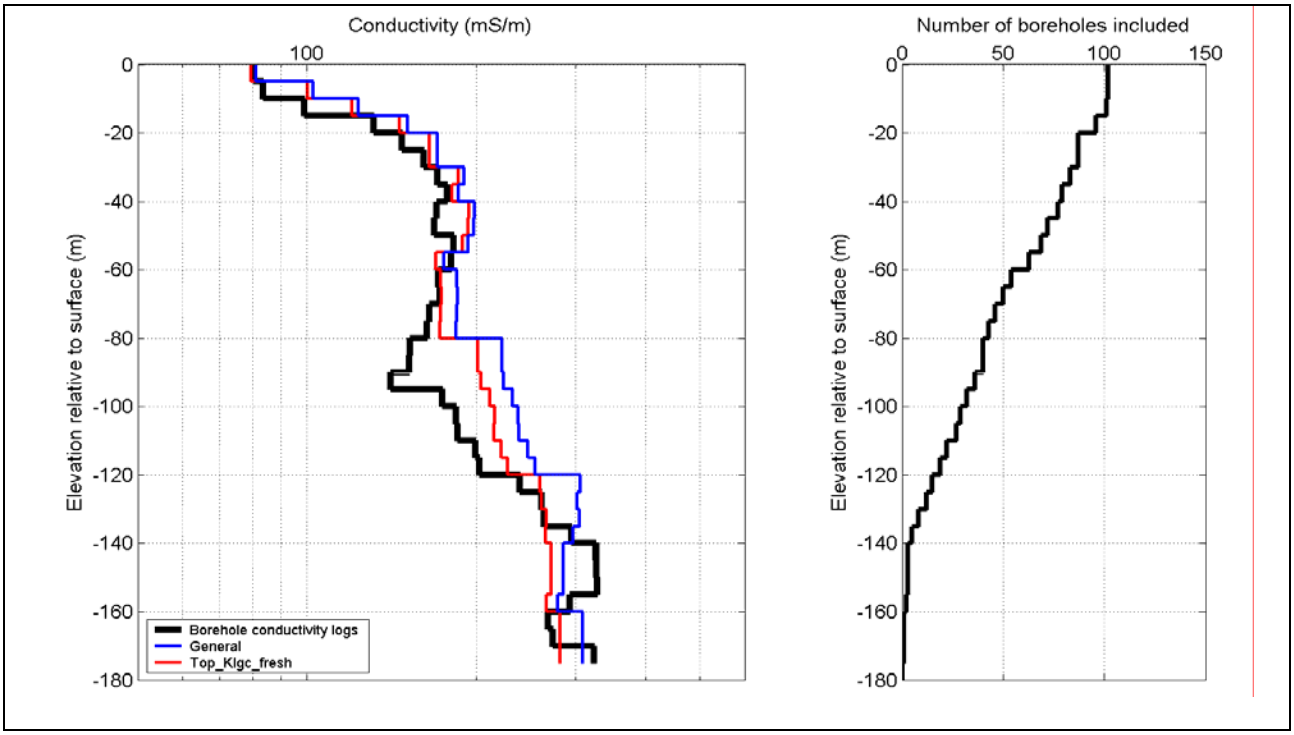

Figure 10. Comparison of average conductivity profiles sampled over 5m vertical intervals. The same intervals used to form the average borehole conductivity profile (black line) were extracted from the different models; inversion models employing a very loose constraint towards a reference conductivity value at all levels (blue line labelled "General") and inversion models with conductivity fixed at the reference value below the interpreted top of fresh Griman Creek Formation (red line labelled "Top_Klgc_fresh").

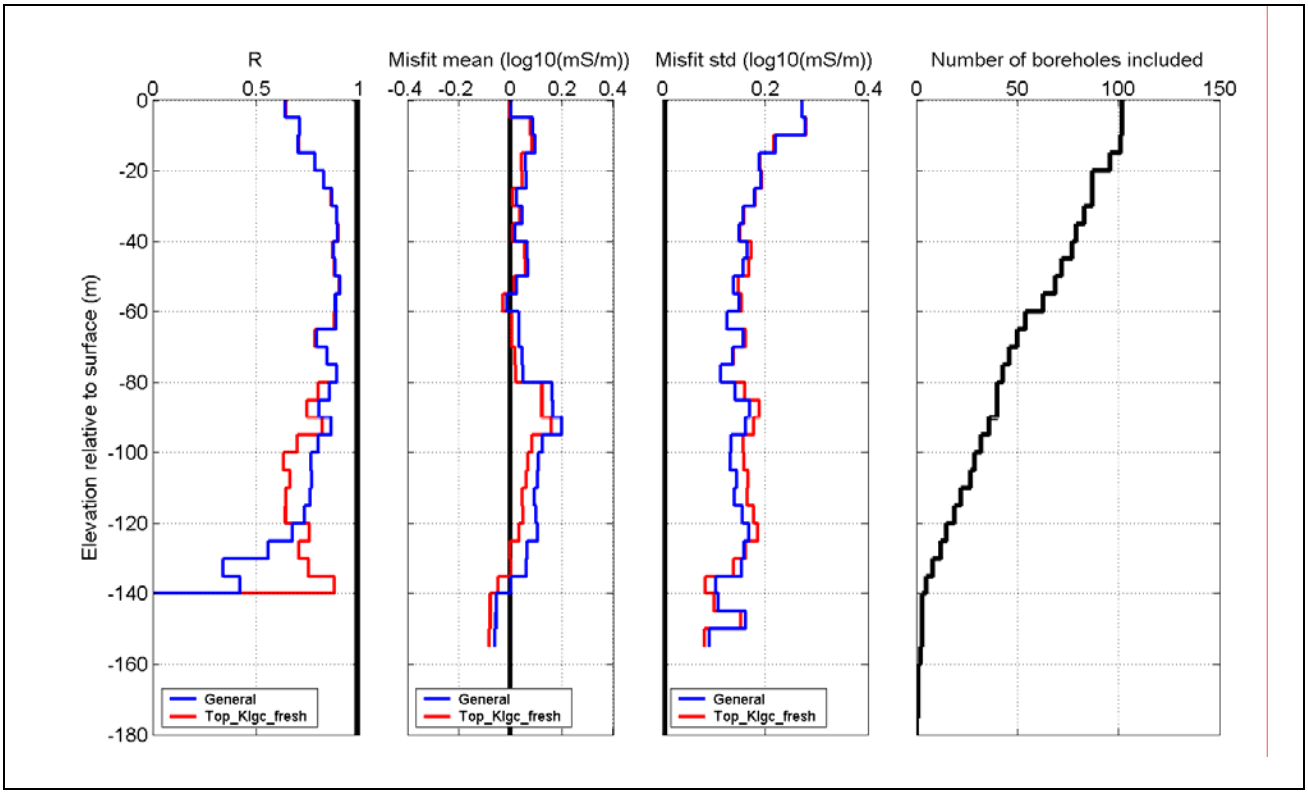

Figure 11. Summary plots of statistical measures used to judge inversion performance. Results for inversion models employing a very loose constraint towards a reference conductivity value at all levels are shown with a blue line and those for inversion models with conductivity fixed at the reference value below the interpreted top of fresh Griman Creek Formation are shown with a red line.

6.2 Other settings

AEM data

Use of both X and Z component data in the inversions was an important improvement over the previous generation of conductivity predictions for this survey. This allowed transmitter loop to receiver coil horizontal and vertical separation values to be included, along with the receiver coil pitch angle as inversion model parameters. The data were not transformed to logarithm base 10 at any stage within the inversion.

Uncertainty for data values

Uncertainty standard deviation values for the data were based on analysis of data acquired at high altitude and for survey altitude repeat lines. The method of analysis was that of Green and Lane (2003). The analyses included repeat line data from the St George survey itself. The noise model defines the total noise standard deviation as;

$$E_t(i) = \sqrt{\left(E_a(i)^2 + E_m(i)^2\right)} = \sqrt{\left(E_a(i)^2 + (m \cdot G(i))^2\right)} \qquad \text{(Equation 30)}$$

where E_t is the total uncertainty standard deviation, E_a is the additive uncertainty standard deviation, E_m is the multiplicative standard deviation, m is the multiplicative error factor, G is the ground response, and i refers to the i^{th} datum. The standard deviation values for high altitude data are given in Table 4. In the noise model, these are taken as the level of additive noise that is independent of the ground response amplitude. Multiplicative noise levels used for the inversions were 1.4% of the ground response for the X component and 1.3% of the ground response for the Z component. The fraction of the total response attributed to the ground response was a variable throughout the inversion so an initial estimate of the ground response was made for the purposes of estimating the multiplicative noise levels. The ground response as supplied by the survey contractor was used for

estimating the multiplicative data errors. These noise estimates were then held constant during the inversion.

Table 4. Standard deviation values for TEMPEST high altitude response.

Window Number	X component standard deviation (fT)	Z component standard deviation (fT)
1	0.021	0.014
2	0.019	0.010
3	0.018	0.009
4	0.017	0.009
5	0.016	0.008
6	0.015	0.008
7	0.014	0.008
8	0.013	0.007
9	0.013	0.008
10	0.016	0.009
11	0.021	0.009
12	0.014	0.007
13	0.012	0.006
14	0.009	0.004
15	0.009	0.005

Uncertainty for conductivity smoothness constraints

Uncertainty standard deviation values for the conductivity smoothness constraints were chosen following trials involving the borehole subset. Small values of the standard deviation resulted in very smooth conductivity models. In extreme cases, smoothness did not allow adequate fitting of the data to occur. Conversely, large standard deviation values resulted in some irregularities in the individual layer conductivities that did not improve the fit to the borehole conductivity logs. A value of 0.1 decades of conductivity was used.

Transmitter loop terrain clearance

The predicted conductivity of the near-surface (i.e., 0 to 5m depth range) is extremely sensitive to this parameter, hence this parameter was not allowed to vary in the inversion. It was assumed that the supplied values had been precisely measured, but possibly mis-calibrated. An offset of –1m (i.e., 1m closer to the ground) was chosen to optimise the visual match between the average predicted near-surface conductivity and the average of the borehole conductivity logs.

Transmitter loop pitch and roll angles

These angles were assumed to be accurately measured. The yaw angle was assumed to be zero.

Transmitter loop to receiver coil separation

The primary field strength is directly related to this separation. The secondary response is also related through the coupling of the receiver coils to the currents induced in the ground. The separation vector is broken down into dx, dy, and dz components parallel to the X, Y and Z axes of the flight line frame of reference respectively. If a single data component were used, there would have been considerable ambiguity in the values of these parameters, and it would have been sufficient to allow just one to vary to allow the primary field component of the measured response to vary. With the use of both X and Z component data, dx and dz were solved parameters in the inversion model.

Uncertainty for dx and dz values

Uncertainty standard deviation values of 2m were selected based on the distribution of values in the data supplied by the survey contractor. Similar standard deviation values were observed by Smith (2001b). These are not strictly uncertainty standard deviations for individual determinations of dx and dz, but standard deviations for large populations of these parameters. These values were evaluated through trials involving the borehole subset. Evidence that the chosen values were too large included excessive variability in the conductivity values at depth, whilst evidence that the chosen values were too small included the failure of the inversion to fit the data to the expected noise levels.

Receiver coil pitch

The data could only be fit to within the measured noise levels through introduction of a non-zero receiver coil pitch angle. Trials indicated that the inversion was stable and returned sensible pitch angles (i.e., between zero and minus 10 degrees) if this parameter was included as a variable inversion model parameter.

Figure 12 shows statistics for the receiver coil pitch angles returned during inversion of a highly down-sampled version of the entire survey. The flights are in order within each of the 3 sub-blocks of the survey. There were approximately 20 to 80 inversions per flight.

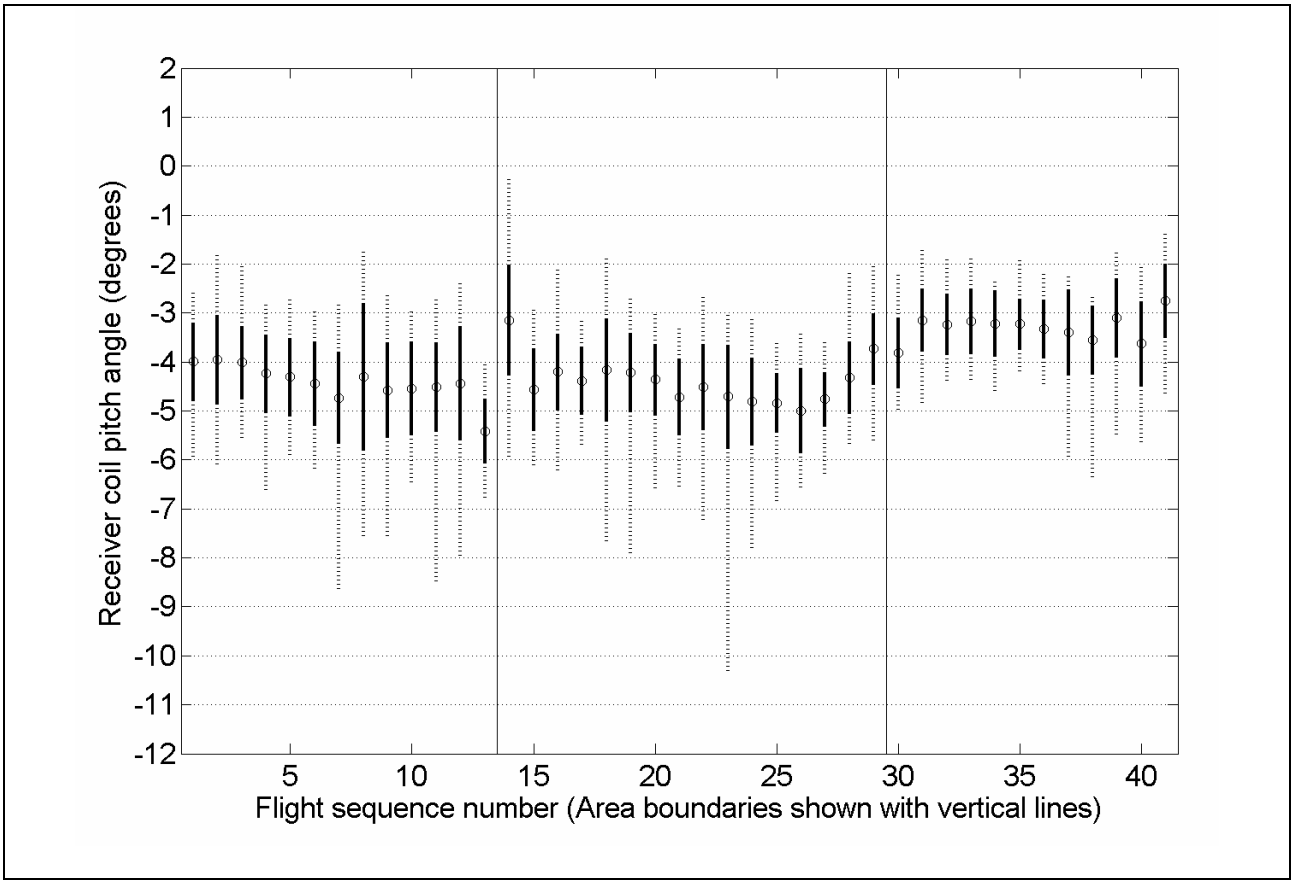

Figure 12. Summary of inverted receiver coil pitch angles as a function of flight number. The thin solid lines extending across the entire graph separate the flights into groups by survey sub-block. For each flight, the circle is plotted at the mean value, the thick vertical line represents +/- one standard deviation about the mean, and the dashed line extend to the minimum and maximum values.

The restricted range of returned pitch angles indicates that the inclusion of the receiver coil pitch angle was quite stable. There were some small systematic variations across the survey, but if a single fixed value had to be chosen for all flights, a value of -4 degrees would be within 1 standard deviation of the "optimum" value for almost all data. However, this restriction was not necessary, and receiver coil pitch angle was included as a variable inversion model parameter.

It would not be sensible to invert for the receiver coil roll angle without Y component data, so this angle was assumed to be zero. The receiver coil yaw angle was also assumed to be zero.

Uncertainty for receiver pitch angle

Trials on down-sampled data from the entire survey indicated that a standard deviation of 2 degrees allowed the expected data misfits to be achieved.

Layer thickness parameters

Layer thickness values were fixed to simplify manipulation of the output (e.g., depth slices). Thickness values were chosen such that;

- the number of layers was kept to a minimum, since the time for each inversion increases with each additional layer,
- there were enough layers to accommodate the observed response (i.e., 1-5 significant inflections in the conductivity profile with respect to depth),
- each layer was thinner than the expected resolution at the depth of the layer, and
- the cumulative conductance curve with respect to depth would be adequately defined, allowing a smooth conductivity profile to be obtained post-inversion through re-sampling of this curve.

A 12–layer inversion model (Table 5) with the same fixed thickness values was used for each observation.

Table 5. Layer structure for the inversion models.

Layer number	1	2	3	4	5	6	7	8	9	10	11	12
Thickness (m)	5	5	5	5	10	10	20	20	40	40	40	∞
Depth to base (m)	5	10	15	20	30	40	60	80	120	160	200	∞

Reference conductivity values

The reference conductivity values and the conductivity standard deviation values were the most contentious settings in the inversion. The reference values were obtained through analysis of borehole conductivity logs in combination with picks of the "top of fresh Griman Creek Formation". The average conductivity of the first 15m of fresh Griman Creek Formation in 11 boreholes was used as a uniform reference conductivity for layers and all observations. The mean was adjusted downwards by 0.2 decades based on the observation of slowly decreasing conductivity with depth (at a rate of approximately 0.002 decades per metre).

Use of the average borehole conductivity trace as a reference model was considered. This would have made it much more difficult to see whether the reference model or the data was driving the conductivity values. However, it would have meant that the reference model was a better estimate of the expected conductivity profile for each observation. It was thought that the most important aspect of the reference model was to get approximately the correct reference conductivity model value at depth so that the ambiguity between primary field and ground response could be resolved.

Uncertainty for layer conductivity parameters

Trials involving the borehole subset confirmed that both the absolute values and the relative magnitude of the uncertainty standard deviation values from one layer to the next were important to the inversion outcome. Use of a strong constraint (i.e., layer conductivity held closely to the reference value through a small uncertainty standard deviation) that was based on the interpreted top of fresh

Griman Creek Formation was considered as an option but rejected. A uniform value of 0.1 decades of conductivity was applied to all conductivity parameters.

Initial values for inversion model parameters

The initial values for all inversion model parameters were set to the supplied reference values. It was hoped that this would place the inversion sufficiently close to the global minimum in the data objective function that the inversion outcome would be reasonably independent of the chosen initial values.

Termination criteria

Termination criteria were passed to the inversion program through the control file (Appendix 1). The maximum number of iterations, 20, was based on observed convergence rates. The minimum data objective, 5, is the approximate expected value for the data misfit (see Equation 14). Note that the smoothness values are considered to be data in this inversion formulation but that they account for only a relatively small fraction of the data objective function. A smaller value would equate to over-fitting (i.e., fitting the noise). The minimum data misfit improvement for each iteration, 0.5%, was based on a visual assessment of the significance of the observed changes to the model during trial inversions.

The program contains another defacto termination criterion. If the new parameter values for the current iteration would result in a data misfit that was larger than the data misfit at the end of the previous iteration, the parameter change is halved. If the parameter change was halved 5 times in a single iteration, the inversion was terminated.

7 ACTIONS TO REDUCE THE ELAPSED TIME FOR INVERSION

7.1 Down-sampling of the survey observations

The full survey is composed of 2,157,377 individual observations with 0.2s or approximately 13m spacing between observations. To reduce the computing requirement, every 5th observation was inverted, or a total of 431,674 observations. This equates to an along-line interval of 1 second or approximately 70m. Given that (1) the delivered data have been stacked with a cosine-shaped filter of length 3 seconds, and (2) the principal products upon which interpretation will be based are grids with 80m cell size, the down sampling was not considered to have compromised the resolution of the conductivity products.

7.2 Utilisation of a distributed computing environment

Each inversion took between 10 and 50 seconds depending on the speed of the computer used for the inversion and the number of iterations required to achieve a satisfactory solution. The complete job of 431,674 inversions thus amounted to between 50 and 250 computer days of processing.

An in-house program was used to run the inversions as a distributed application on the Geoscience Australia PC network, making use of under-utilised standard desktop computers. Individual users started a program that requested work from a master computer. The master computer sent out input data for 60 inversions upon each request. The inversions ran as a low priority task. Upon completion of each batch of 60 inversions, the slave computers sent the output back to the master computer and requested further work. At one stage there were 135 computers performing inversions. The job was completed in 3 days, representing an improvement over what could be achieved with a single computer by roughly a factor of one hundred.

8 POST-INVERSION PROCESSING

8.1 Levelling

Some minor level changes were noted in grids of the inverted conductivity values. The source of these problems is not known. Following is an outline of the procedure used to level these data.

- The output ASCII file from the inversion was imported into a Geosoft database.
- The 12 layer conductivities were transformed to logarithm base 10.
- The log10 conductivity data for each layer were gridded with a cell size of 80m using Oasis Montaj. The grid of conductivity for 0 to 5m depth was assessed to have the most obvious levelling errors. Several anomalous lines and one entire flight were selected for manual levelling.
- The mean and standard deviation of conductivity values for each flight line and layer were calculated using values transformed to logarithm base 10. As an example, the profiles of these statistics for the uppermost layer are shown in Figure 13. Spikes in the mean were used to manually identify lines that required levelling. An entire flight with line sequence numbers from 354 onwards was deemed to require levelling (Figure 13 (a)). The jump in level around line sequence number 25 is an effect related to a change in the line length in the northern corner rather than to a levelling problem. The absence of obvious busts in the profile of line standard deviation values (Figure 13 (b)) suggested that multiplicative corrections to the log10(conductivity) could not be justified.

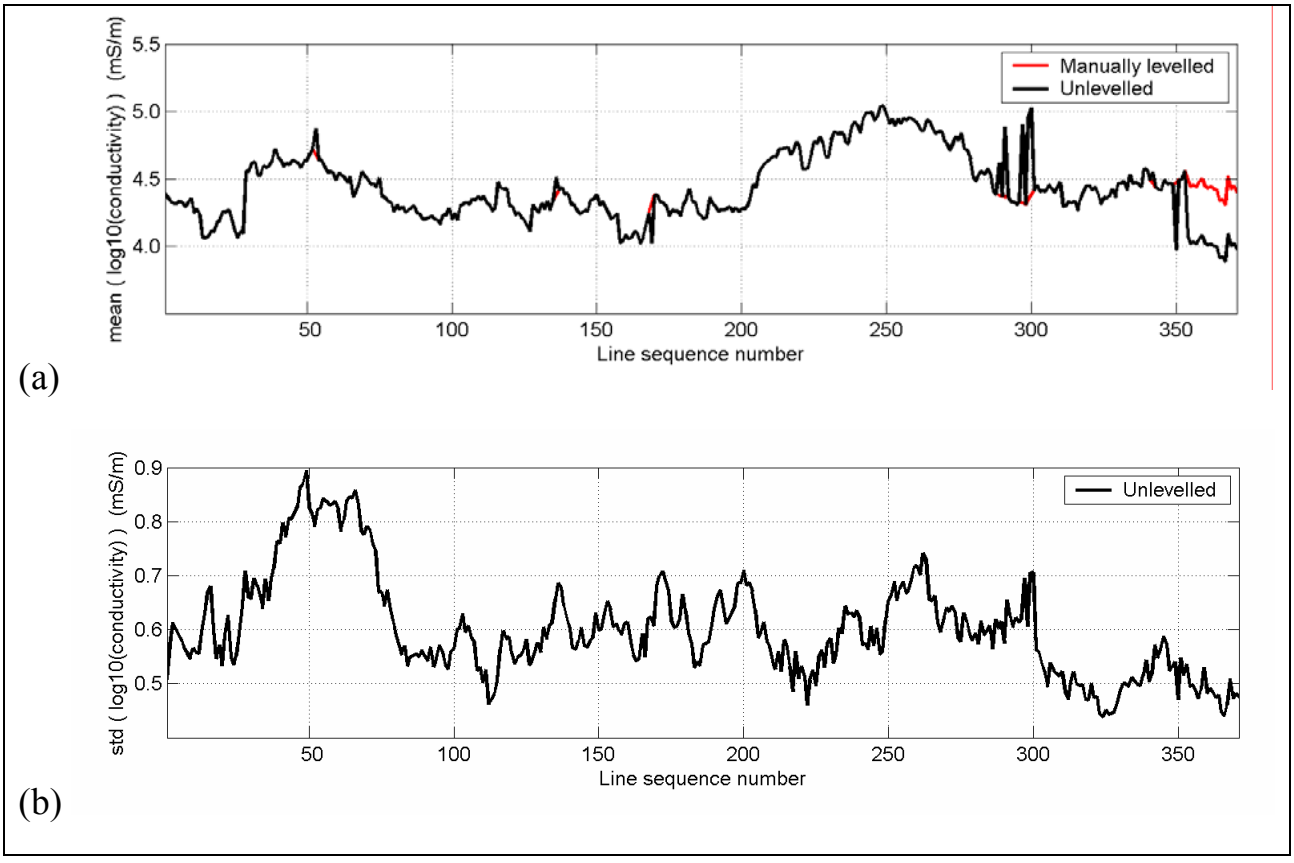

Figure 13. Profiles of statistics for log10(conductivity) for each line from the NE to the SW of the survey area. (a) Mean, prior to and after levelling. (b) Standard deviation, which was unaffected by the constant level adjustments made to the lines during levelling.

- The adjusted log10 (conductivity)line means were determined by linear interpolation from valid line average values on either side of the lines to be levelled. The constant correction to be applied to the block of lines on the SW margin of the survey was determined manually such that the block followed smoothly from the adjacent lines. The corrections are given in Table 6.

Table 6. Manual additive level adjustments applied to log10 (conductivity) values.

Line	Layer number											
Number	1	2	3	4	5	6	7	8	9	10	11	12
10530	-0.193	-0.130	-0.077	-0.039	-0.015	-0.001	0.006	0.007	0.005	0.000	-0.009	-0.022
20010	-0.133	-0.093	-0.060	-0.039	-0.027	-0.021	-0.017	-0.012	-0.005	0.004	0.015	0.030
20340	0.290	0.205	0.134	0.082	0.044	0.022	0.018	0.015	0.010	0.004	0.002	0.001
30031	-0.239	-0.168	-0.108	-0.061	-0.025	0.001	0.009	0.010	0.014	0.016	0.016	0.016
30051	-0.518	-0.358	-0.229	-0.135	-0.066	-0.017	0.002	0.009	0.016	0.022	0.028	0.036
30111	-0.581	-0.392	-0.241	-0.133	-0.058	-0.011	0.005	0.014	0.031	0.048	0.056	0.063
30131	-0.612	-0.427	-0.276	-0.162	-0.077	-0.014	0.017	0.030	0.042	0.051	0.052	0.055
30141	-0.648	-0.443	-0.276	-0.153	-0.065	-0.006	0.017	0.024	0.032	0.041	0.049	0.063
30560	-0.090	-0.057	-0.030	-0.011	0.002	0.006	0.006	0.005	0.008	0.012	0.016	0.019
30641	0.499	0.395	0.298	0.202	0.102	0.016	-0.015	-0.026	-0.048	-0.060	-0.052	-0.036
30680	0.423	0.307	0.204	0.125	0.074	0.053	0.060	0.048	0.014	-0.017	-0.032	-0.041
30690	0.423	0.307	0.204	0.125	0.074	0.053	0.060	0.048	0.014	-0.017	-0.032	-0.041
30700	0.423	0.307	0.204	0.125	0.074	0.053	0.060	0.048	0.014	-0.017	-0.032	-0.041
30710	0.423	0.307	0.204	0.125	0.074	0.053	0.060	0.048	0.014	-0.017	-0.032	-0.041
30720	0.423	0.307	0.204	0.125	0.074	0.053	0.060	0.048	0.014	-0.017	-0.032	-0.041
30730	0.423	0.307	0.204	0.125	0.074	0.053	0.060	0.048	0.014	-0.017	-0.032	-0.041
30740	0.423	0.307	0.204	0.125	0.074	0.053	0.060	0.048	0.014	-0.017	-0.032	-0.041
30750	0.423	0.307	0.204	0.125	0.074	0.053	0.060	0.048	0.014	-0.017	-0.032	-0.041
30760	0.423	0.307	0.204	0.125	0.074	0.053	0.060	0.048	0.014	-0.017	-0.032	-0.041
30770	0.423	0.307	0.204	0.125	0.074	0.053	0.060	0.048	0.014	-0.017	-0.032	-0.041
30780	0.423	0.307	0.204	0.125	0.074	0.053	0.060	0.048	0.014	-0.017	-0.032	-0.041
30790	0.423	0.307	0.204	0.125	0.074	0.053	0.060	0.048	0.014	-0.017	-0.032	-0.041
30800	0.423	0.307	0.204	0.125	0.074	0.053	0.060	0.048	0.014	-0.017	-0.032	-0.041
30810	0.423	0.307	0.204	0.125	0.074	0.053	0.060	0.048	0.014	-0.017	-0.032	-0.041
30820	0.423	0.307	0.204	0.125	0.074	0.053	0.060	0.048	0.014	-0.017	-0.032	-0.041
30830	0.423	0.307	0.204	0.125	0.074	0.053	0.060	0.048	0.014	-0.017	-0.032	-0.041
30841	0.423	0.307	0.204	0.125	0.074	0.053	0.060	0.048	0.014	-0.017	-0.032	-0.041
30850	0.423	0.307	0.204	0.125	0.074	0.053	0.060	0.048	0.014	-0.017	-0.032	-0.041

8.2 Micro-levelling

Since the three sub-blocks of the St George survey have different line spacings, data for each sub-block were gridded separately prior to de-corrugation filtering. The de-corrugation tool within Intrepid requires grids to be orientated north-south or east-west, hence the log10(conductivity) data were re-gridded with a rotation of 138 degrees applied. A number of trials were carried out to determine suitable settings for the filtering. In each case, the results were visualised using ERMapper. The final settings for the de-corrugation filter are given in Table 7.

Table 7. De-corrugation settings.

Filter	High Pass	Naudy Filter
	Low Pass	Smoothed Fuller
Extrapolator	High Pass	Mirror
	Low Pass	Flipped mirror
Minimum streak length		10000 m
Streak width	Sub-block A	750m
	Sub-block B	1200m
	Sub-block C	750m
Minimum adjustment		-1
Maximum adjustment		1

The de-corrugation corrections were applied to the manually levelled point located data using the Intrepid micro-levelling tool. The micro-levelling settings are given in Table 8.

Table 8. Micro-levelling settings.

Secondary filter along line correction	10000
Nominal strike	138
Minimum adjustment	-1
Maximum adjustment	1

Images of 0 to 5m conductivity for a subset of the survey area are presented in Figure 14 to demonstrate the changes brought about by levelling and micro-levelling. The area used as an example was by far the worst affected portion of the survey. Both the manually levelled and manually levelled plus micro-levelled data are supplied in point located and grid format (Appendix 1).

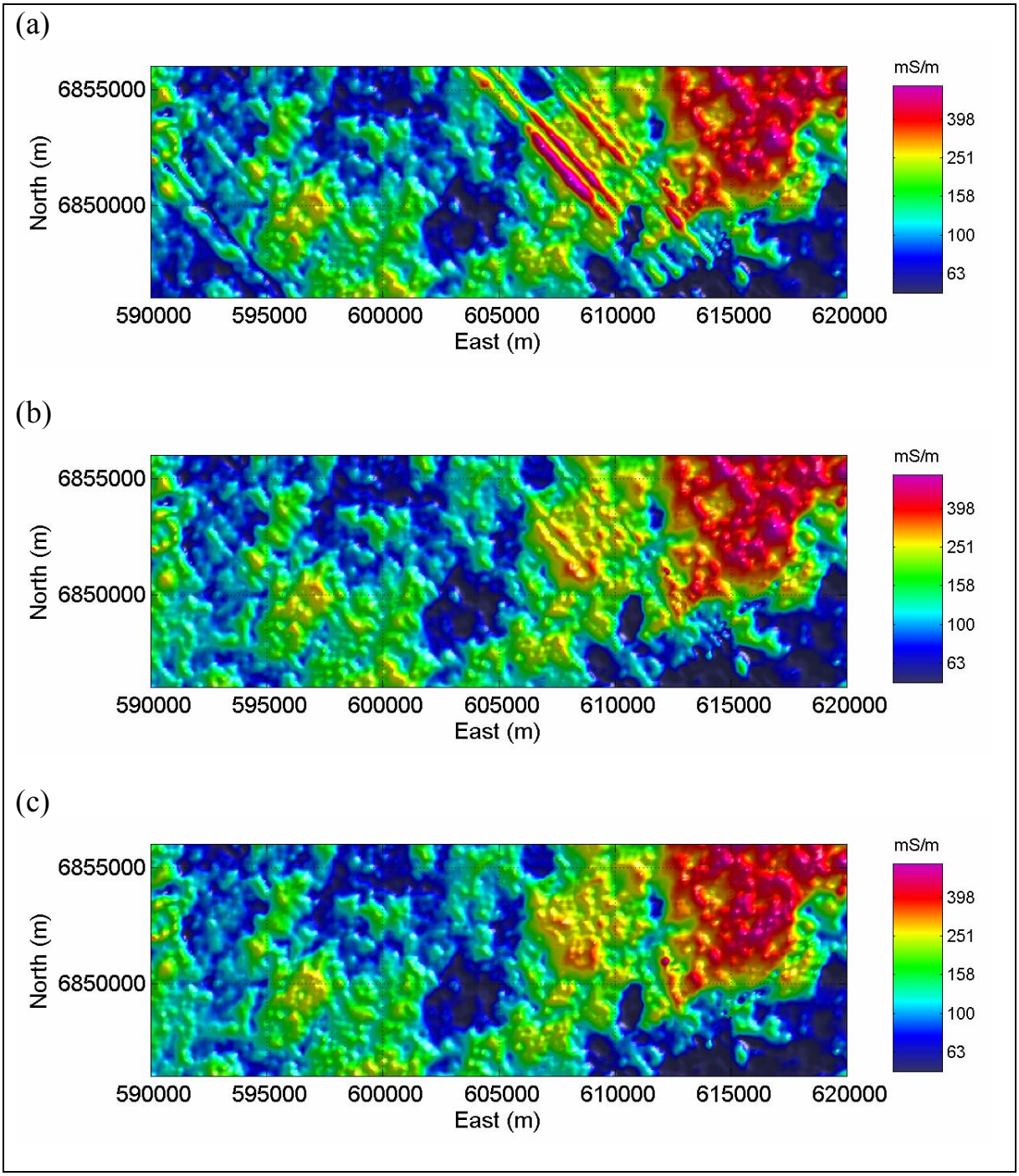

Figure 14. A portion of the 0-5m conductivity slice from the SW sector of the survey. (a) Unlevelled data. (b) Manually levelled data. (c) Manually levelled and micro-levelled data. Note that the flight lines are oriented at 138/318 degrees.

8.3 Re-sampling of cumulative conductance curves

The inverted conductivity models had layers with discrete boundaries and uniform conductivity within each layer. The use of discrete boundaries is somewhat at odds with the use of a smoothness constraint. Since the processing time increases with the number of layers, the number of layers and the thickness values were chosen carefully. The thickness values of these layers were chosen such that the shape of the cumulative conductance (conductivity times thickness) versus depth curve was adequately defined. This condition was satisfied by making the layers thinner than the vertical resolution of the

AEM system. This resolution diminishes with depth, allowing the use of layers of increasing thickness with increasing depth.

The cumulative conductance values for the base of the layers are plotted with symbols on the left panel of Figure 15. It is possible to fit a smooth curve to these points and to resample this curve at finer depth increments. This does not change the resolution of the output, but enables a smooth trace of conductivity as a function of depth to be obtained. The original 12-layer model is shown with a black line on the right panel of Figure 15 (a). The re-sampled model, with constant 5m depth increments in this instance, is shown as the blue line. The re-sampled model is identical to the original model for the first 4 layers, but thereafter is a smoother, less blocky model. Given the method used to generate the re-sampled model, the new model would be expected to have a very similar response to that of the inversion model.

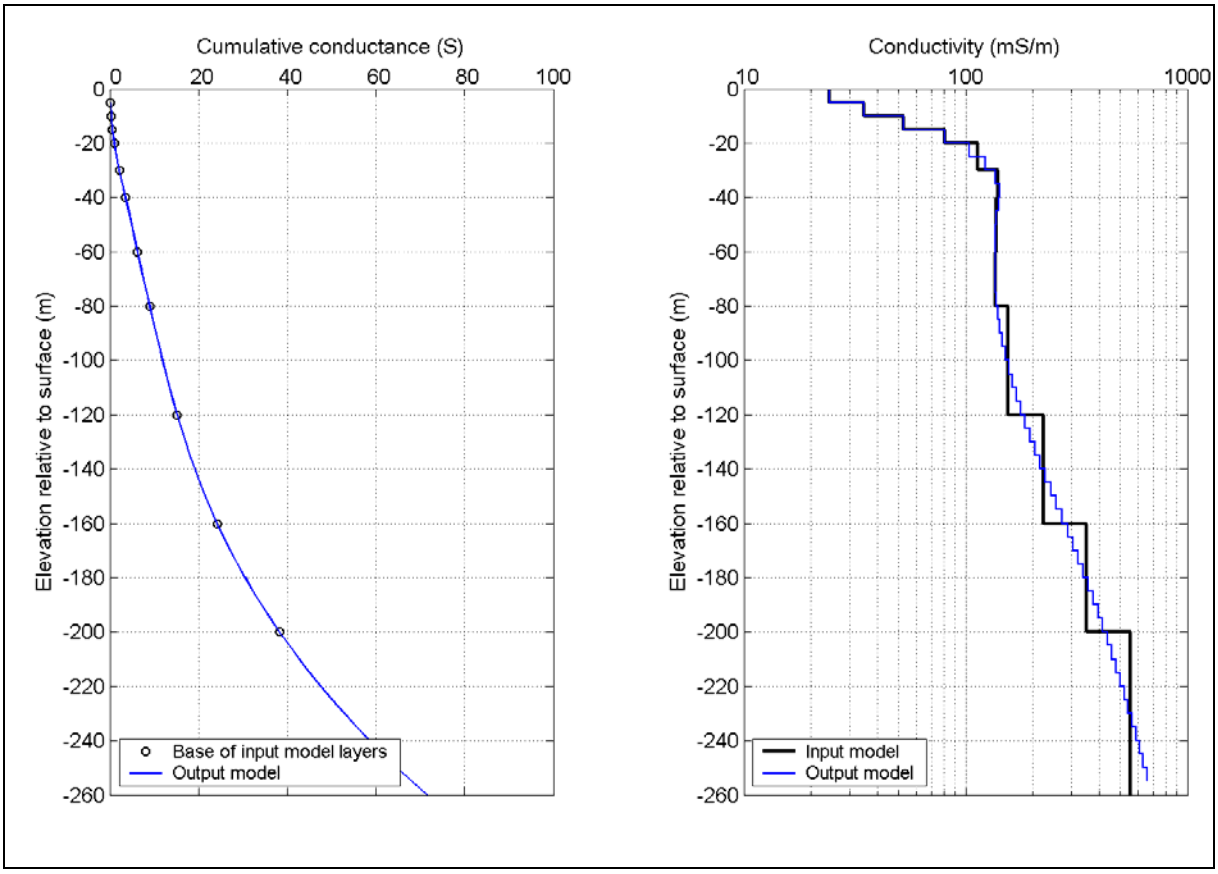

Figure 15. Example of cumulative conductance values for the original 12 layers (shown with symbols on the left-hand panel) and the re-sampled curve (blue line on the left-hand panel). The original and re-sampled models are shown in the right-hand panel.

8.4 Gridding

Grids with an 80-metre cell size were created within Oasis Montaj using a minimum curvature algorithm (RANGRID). The inputs to gridding were log10(conductivity) values. Lines 20010, 21500 and 21510 from sub-block 2 that overlapped data in sub-blocks 1 and 3 were excluded from the input data. Grids were assigned an MGA55 projection and GDA94 datum. Settings used during gridding are given in Table 9.

Table 9. Settings used for gridding.

Grid Cell Size	+8.00000e+001	
Grid Origin (X0,Y0)	+5.78080e+005	+6.80104e+006
Grid Size (DX,DY)	+1.42080e+005	+1.40800e+005
Grid Dimensions (NX,NY)	1777	1761
Clip Boundary Areas	1	
Z column selector	N/A	
Log option	0	
Minimum Z for log	1	
De-sample Fact1	1	
Blanking Radius	+4.72850e+002	
Maximum Search Radius	+5.12000e+003	
Order of Weighting Function	2	
Weighting Slope	0	
Tolerance Limit in Iteration	+1.39974e-003	
Points Passed Tolerance Limit (%)	+9.90000e+001	
Maximum Iteration Times	100	
Internal Tension Parameter	0	
Coarse Grid Fact	16	

8.5 Masking of grids to the survey boundary

Grids were masked back to the survey boundary to avoid misrepresentation through extrapolation beyond the limits of the data.

8.6 Option to rotate X and Z component data

Having solved for the pitch angle of the receiver coil unit, it would be possible to rotate the input and output X and Z component data into the flight line frame of reference. In this state, the data might be used as input data to other conductivity prediction schemes that did not allow for data in directions away from the axes of the flight line frame of reference. This procedure was not applied at this time and is noted here for reference only.

For a receiver coil pitch angle of r_p;

$$X' = X\cos(r_p) + Z\sin(r_p) \quad \text{(Equation 31)}$$

$$Z' = -X\sin(r_p) + Z\cos(r_p) \quad \text{(Equation 32)}$$

where X and Z are the window amplitudes in the orientation of the receiver coil unit and X' and Z' are the amplitudes in the flight line frame of reference.

9 RESULTS

9.1 Performance assessment of "production" inversions

Data misfit

Given a suitable model structure and reasonable estimates of the data uncertainties, it would be expected that the inversion would be able to able to produce χ values of $\sqrt{(N)} = \sqrt{(30)} \approx 5.5$ or less, where N is the number of data values. Using a fixed value for the receiver coil pitch of zero in trials involving the borehole subset, this expectation was not met. Figure 16 (a) shows that the average χ value was around 12 in this case. Figure 16 (b) shows that when the receiver coil pitch angle was included in the inversion as a variable model parameter, χ values around 5 could be achieved. Note

that a χ value of 5 was one of the termination criteria in both of these trials. The box plots summarising the normalised misfit values for each of the 15 X and 15 Z component windows show that the φ values have very significant systematic departures from the expected distribution (lower 2 panels of Figure 16 (a)) when the receiver coil pitch angle was fixed at zero. In contrast, the results for the trial where the pitch angle was included as a variable inversion model parameter are more in line with the expectation of the majority of the normalised misfit values lying within a range of +/-1 for each window of each component (lower 2 panels of Figure 16 (b)).

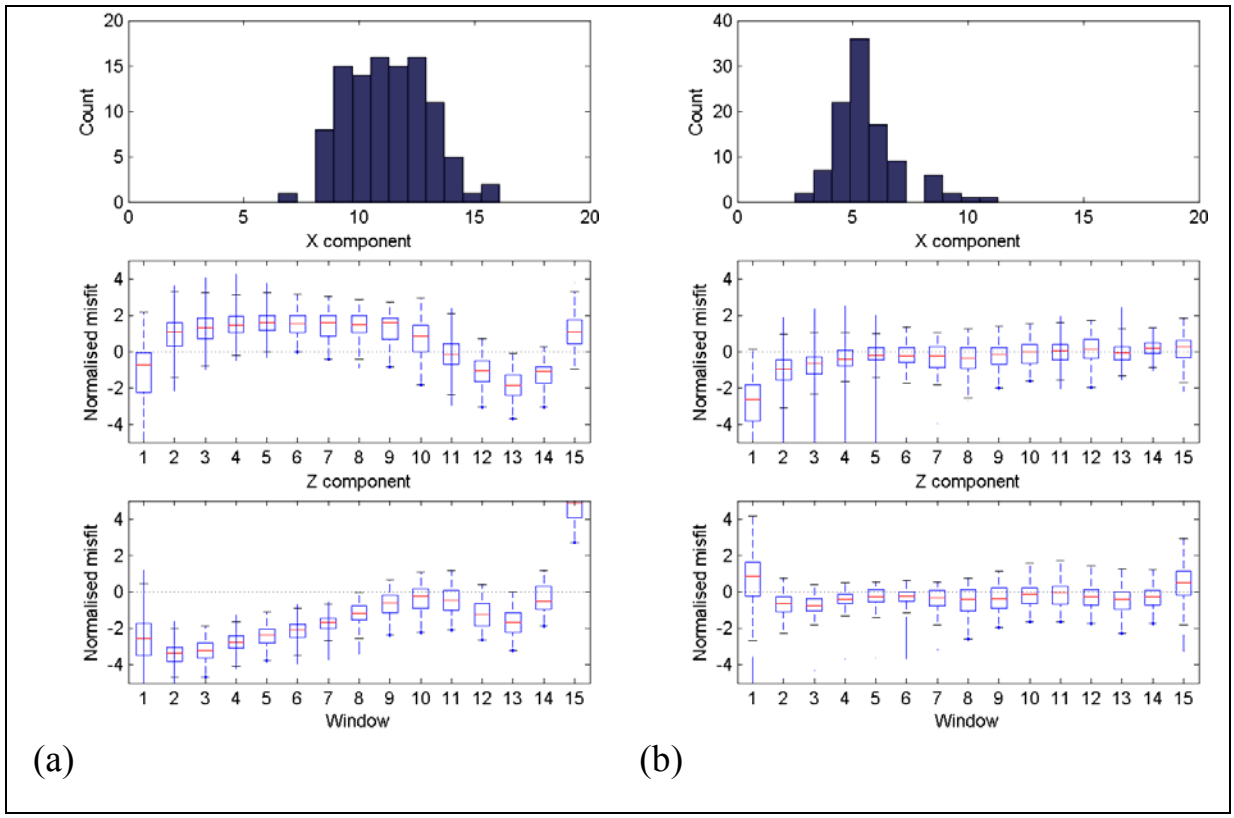

Figure 16. Data misfit summaries for inversion of the borehole subsets. (a) Inversions with the receiver coil pitch angle fixed at zero. (b) Inversions with the receiver coil pitch angle included as a variable model parameter. The top panel is a histogram of the χ data misfit. The middle panel is a box plot that summarises the spread of normalised misfit values for each of the 15 X component windows, whilst the bottom panel is a box plot for the 15 Z component normalised misfit values.

Figure 17 shows typical ground response decay curves and normalised misfit curves for a single inversion from the borehole subset. The small size of the data uncertainties compared to the dynamic range of the decays makes it difficult to observe the difference between the observed and fitted data in the decay plots. These differences are much clearer in the normalised misfit plots. When the receiver coil pitch angle was fixed at zero (Figure 17 (a)), the normalised misfits are substantially larger than would be expected. The normalised misfits are closer to the expected values in the case where the receiver coil pitch angle was included as a variable inversion model parameter (Figure 17 (b)).

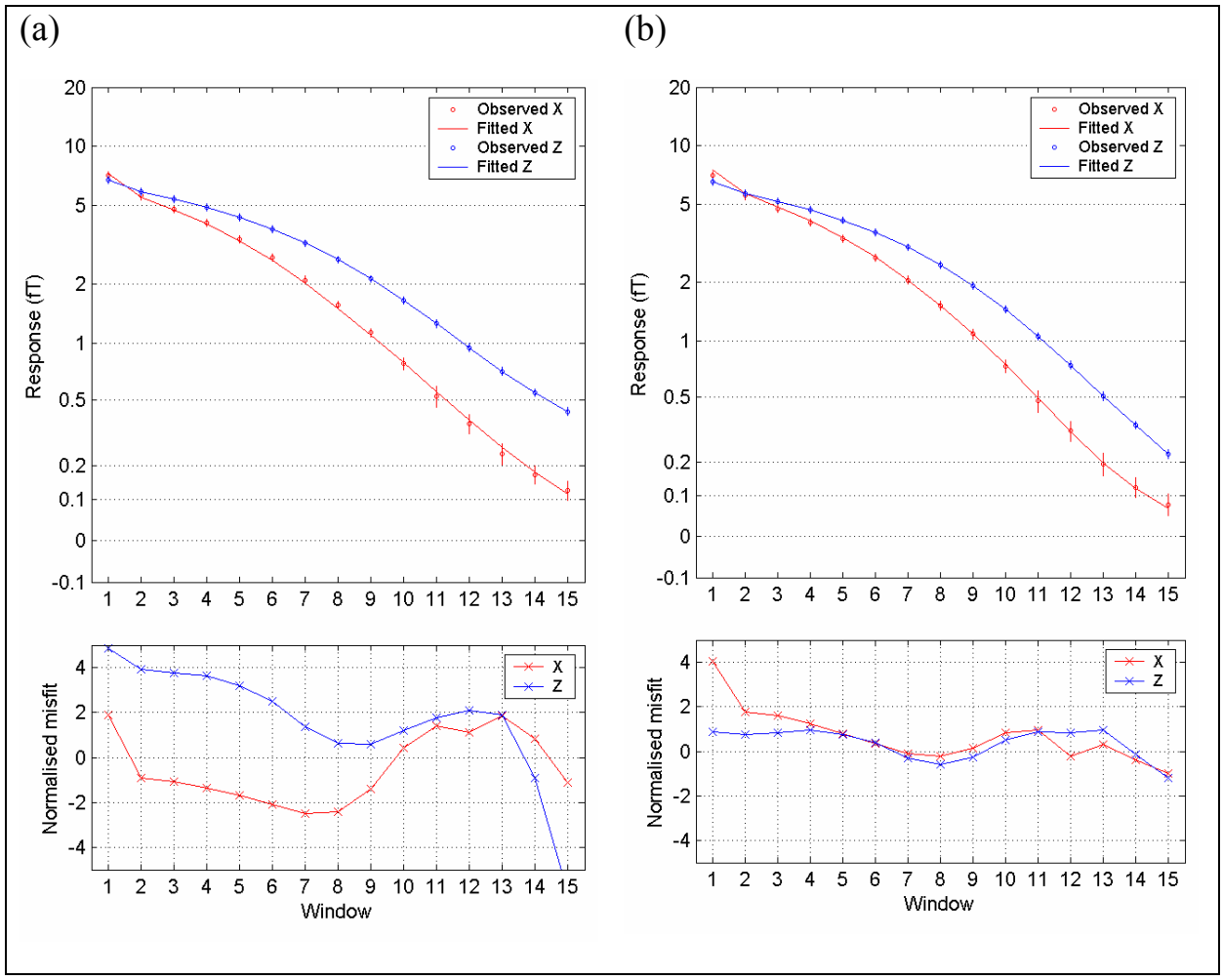

Figure 17. Ground response decay and normalised misfit plots for a single inversion from the borehole subset. (a) Inverted with the receiver coil pitch angle fixed at zero. (b) Inverted with the receiver coil pitch angle included as a variable model parameter. The top panel shows the observed and fitted ground response decay curves for X and Z component data. The vertical error bars have a length equal to plus and minus 3 times the estimated data uncertainty standard deviation. The bottom panel shows the normalised misfit values for the inversion.

Model characteristics

Before utilising the borehole conductivity logs as information against which to judge the outcome, it is worth reviewing the degree of independence of this information from the a priori constraints used in the inversion. The conductivity logs were the source of 11 values of the conductivity of the fresh Griman Creek Formation used to derive the reference conductivity. This would be expected to influence the correlation between borehole conductivity logs and the conductivity predictions from the inversion models at depth where fresh Griman Creek Formation is present. The question of the influence of the a priori constraints on the inversion model is discussed further in Section 10.1.3.

A comparison between the average borehole conductivity trace and conductivity traces for three different conductivity prediction schemes is shown in Figure 18. The desirable behaviour for each of the conductivity prediction schemes is for the average to be as close as possible to the average trace of the conductivity logs. The constrained inversion is clearly superior in the top 20m, and more or less on a par with the FAS and LEME EMFlow results between 20 and 80m depth. The strong performance of the constrained inversion below 140m is a result of the gentle persuasion that this method employs towards the reference value of 282mS/m.

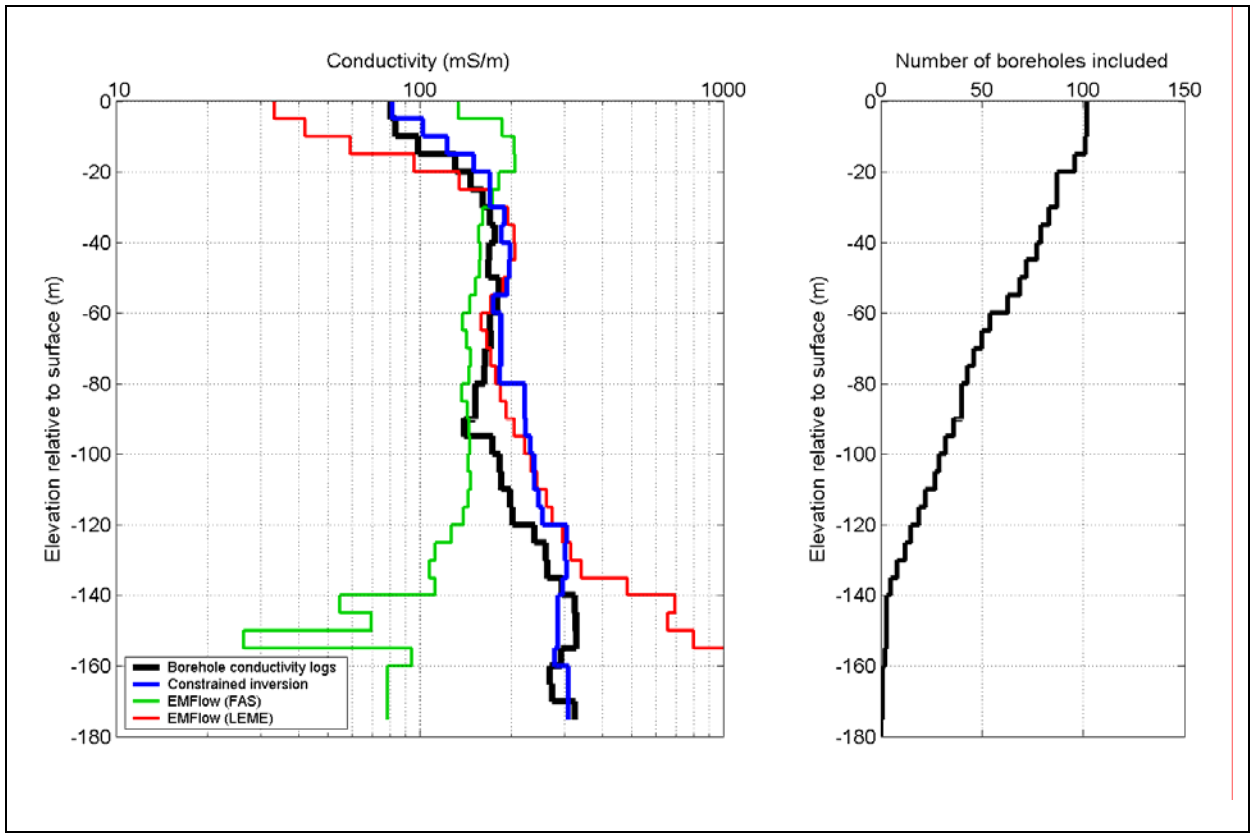

Figure 18. Comparison of average conductivity profiles sampled over 5m vertical intervals. The same intervals used to form the average borehole conductivity profile (black line) were extracted from the different models; constrained inversion models (blue line), EMFlow CDI values as delivered by the survey contractor (green line) and EMFlow CDI values as calculated by CRC LEME with modifications to the primary field and transmitter loop vertical offset (red line). The number of boreholes contributing to the average values at different depths is shown in the right-hand panel.

The results of the statistical calculations for the conductivity predictions from the constrained inversion as well as the two generations of EMFlow conductivity predictions are summarised in Figure 19. Correlation coefficients are an indicator of the degree to which the conductivity predictions can account for the variability observed in the borehole logs. The desirable behaviour is to have the correlation coefficient as close to 1 as possible. The constrained inversion has correlation coefficient values closer to 1 than the other two forms of conductivity predictions at all depths (panel 1 of Figure 19). When the number of samples becomes small, estimation of the correlation coefficient becomes unstable. This is observed below 120m.

The second panel of Figure 19 shows values of the misfit mean. The plot is in units of decades of conductivity since the analysis was done on log10 transformed conductivity values. The desirable behaviour is to have zero positive or negative bias (i.e., zero under or over estimation of conductivity relative to the borehole conductivity logs). The constrained inversion results are equal to or superior to the other conductivity predictions down to 80m. They are very clearly the best of the three sets of conductivity predictions in the top 20m.

The third panel of Figure 19 shows values of the misfit standard deviation. This is a measure of the spread of values about the average difference between the conductivity logs and the predictions. It would be desirable to have the least spread. The constrained inversion is equal to or superior to the other two sets of conductivity predictions at all depths.

The fourth panel indicates how many boreholes contributed to the analysis at each of the 5m depth increments.

In conclusion, the statistical values shown in the first 3 panels of Figure 19 can be used to quantify the quality of the predictions from the constrained inversion in relation to conductivity measured in a borehole in close proximity (<250m) of an AEM observation. For example, for the depth interval of 15 to 20m, the predictions from the constrained inversion would be expected to show;

- a correlation coefficient of ~0.8,
- an average that is biased by +0.08 decades (i.e., overestimation by a factor of 10.^0.08 or a factor of ~1.2), and
- a standard deviation about this average of just less than 0.2 decades.

This level of performance represents an improvement over the previous conductivity predictions (i.e., both the contractor supplied EMFlow values and the re-processed LEME EMFlow values).

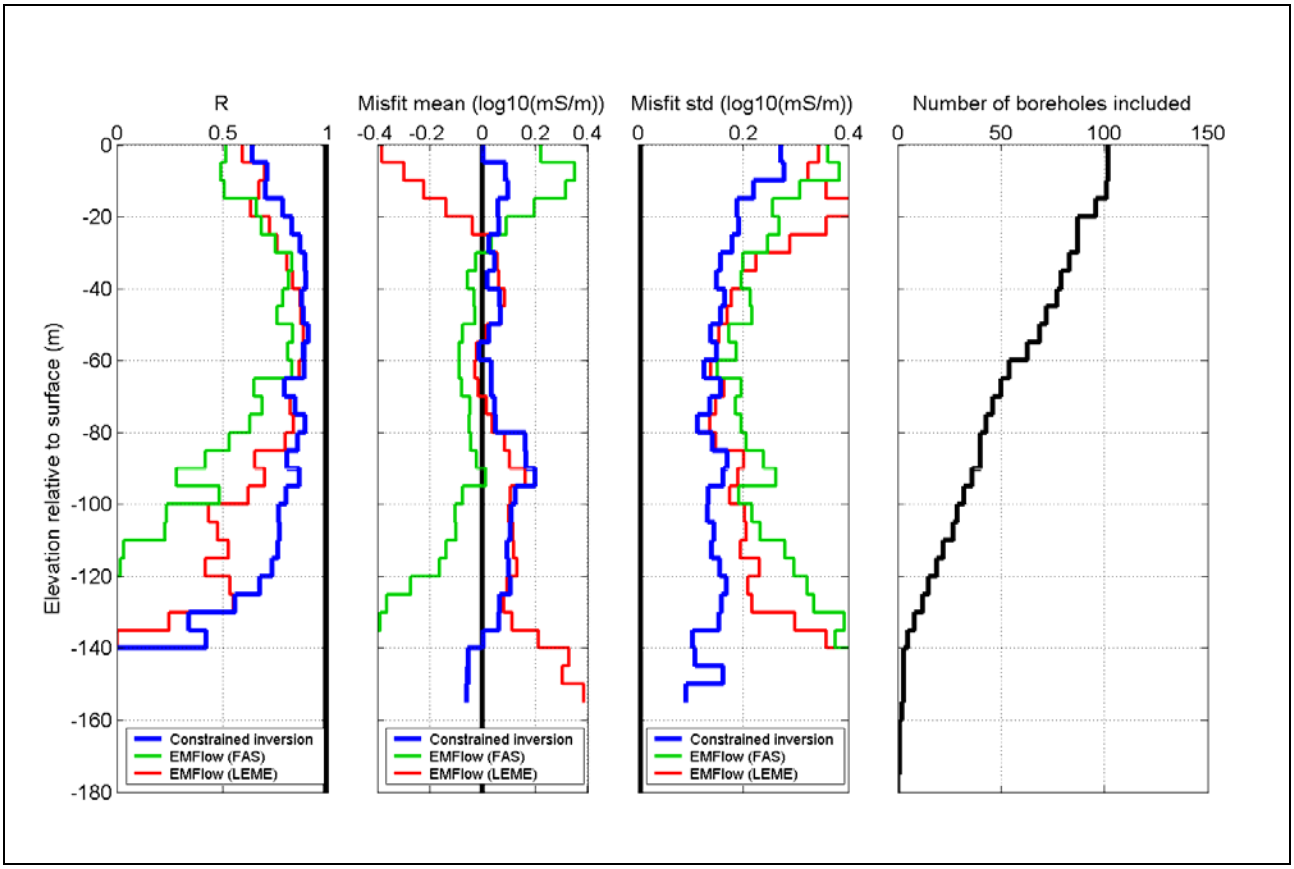

Figure 19. Summary plots of statistical measures used to judge inversion performance. Results for the constrained inversion models are shown with a blue line, those for EMFlow CDI values as delivered by the survey contractor with a green line and those for EMFlow CDI values as calculated by CRC LEME with modifications to the primary field and transmitter loop vertical offset in a red line.

Percent data influence (PDI)

One of the difficulties with inversion processing is to determine and communicate information concerning the relative contributions of the data and the a priori constraints to the parameters of the inversion model. Oldenburg and Li (1999) tackled this problem in the context of DC resistivity and induced polarisation inversion by performing 2 inversions with different reference or a priori values for each model parameter. A depth-of-investigation (DOI) parameter was defined as the ratio of the difference in each model parameter to the difference in the reference values for that parameter between the 2 inversions. In this report, an alternate parameter, the percent data influence (PDI), is defined as;

$$PDI_i = 100\left(1 - \frac{(m_{1i} - m_{2i})}{(m_{1ri} - m_{2ri})}\right) = 100(1 - DOI) \qquad \text{(Equation 33)}$$

where m_{1i} and m_{2i} are the ith model parameters for the 1st and 2nd inversions, and m_{1ri} and m_{2ri} are the ith reference values for the 1st and 2nd inversions.

The PDI is 100% when the inversion output is unchanged in response to a change in the reference value. This would indicate that the data were the dominant influence on the inversion output. In contrast, a PDI of 0% occurs when the inversion output changes in exactly the same amount as the change in the reference value. Depth-of-investigation might be defined as the depth below which the PDI falls below a user-defined threshold.

PDI calculations were performed for the borehole subset using two pairs of reference conductivity, both involving the reference value of 282mS/m; 230mS/m and 282mS/m, and 282mS/m and 350mS/m. The resultant PDI profiles (Figure 20) show a decrease in both cases from close to 100% near-surface to approximately zero at 200m depth below surface. PDI values below 0% and above 100% are an indication of the complexity of the relationships between reference values and final model values for the inversion. It can be noted that there is a greater variability in the response to a change in the reference conductivity for the top 40m.

Use of a PDI value of 50% as a threshold would correspond to the depth where the inversion output is determined equally by the choice of a priori reference conductivity and the observed data. This threshold would lead to an estimate for the average depth of investigation of 120m depth below surface for this survey.

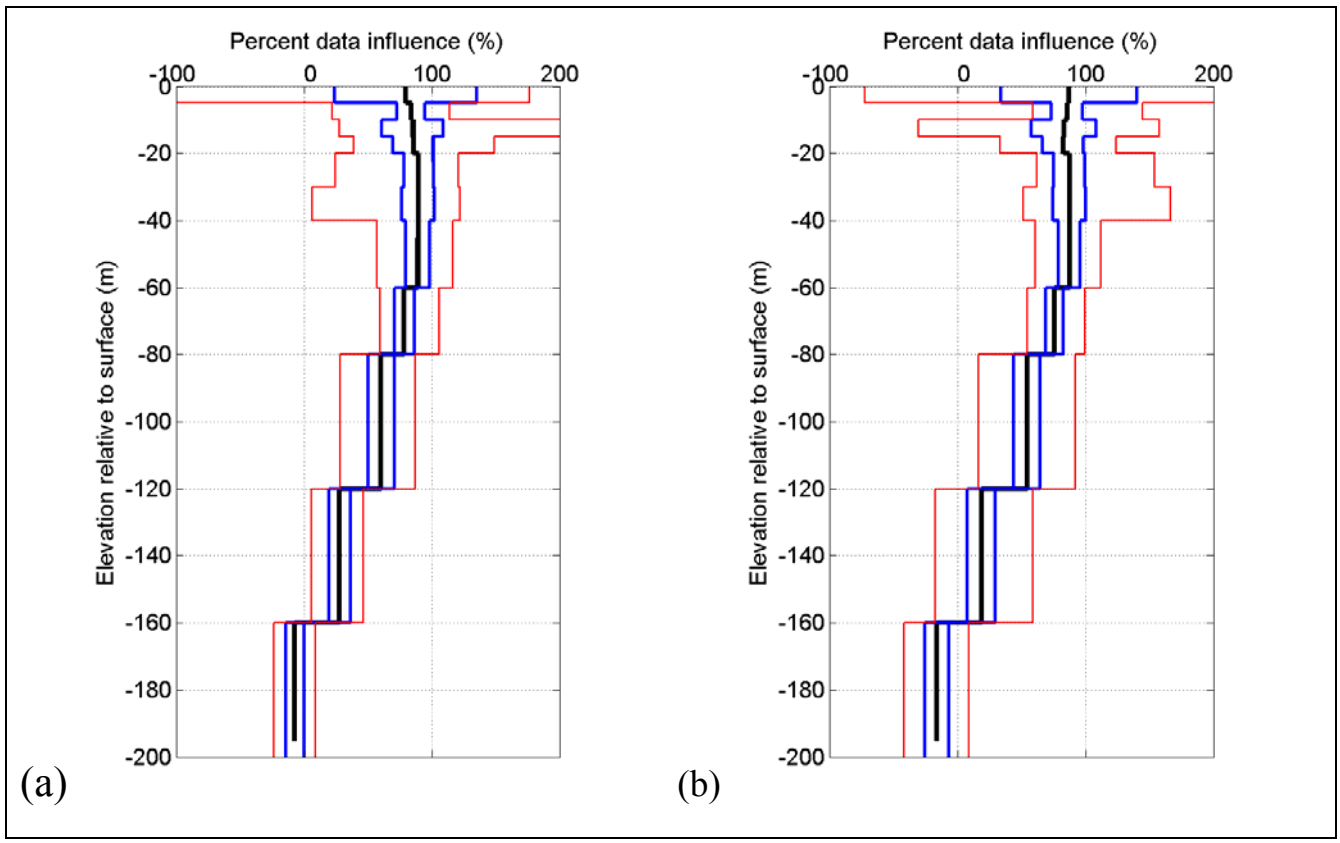

Figure 20. Profiles of Percent Data Influence (PDI) derived from inversion of the borehole subset for (a) reference conductivity values of 230mS/m and 282mS/m, and (b) reference conductivity values of 282mS/m and 350mS/m. The thick black line is the average (in log10 space). The blue lines are the average +/- the standard deviation, whilst the red lines indicate the limits of the values within each interval.

9.2 Comparison of shallow AEM conductivity predictions with EM31

EM31 data were not used to provide constraints or to make decisions on the settings to use in the inversions. However, EM31 data are used extensively at paddock to farm scales to quantify the conductivity of the top few metres. It was thus useful to compare the shallow AEM conductivity predictions (i.e., 0 to 5m depth) with available EM31 data. This would be expected to provide some guidance to the interpretation of the shallow AEM conductivity predictions.

Approximately 60,000 EM31 observations spaced at 12m intervals (Figure 21) were acquired as part of investigations into the salinisation of the Goondoola Basin (~699000mE 6873000mN) and to assist in the evaluation of the St George AEM Survey (Wilkinson, 2003). The large number of EM31 observations can be compared with the 104 boreholes for which there were borehole conductivity logs. For characterisation of shallow sub-surface conductivity, EM31 measurements have the advantage over borehole conductivity measurements of being non-invasive. They are thought to be more representative of the shallow conductivity than the upper parts of borehole conductivity logs.

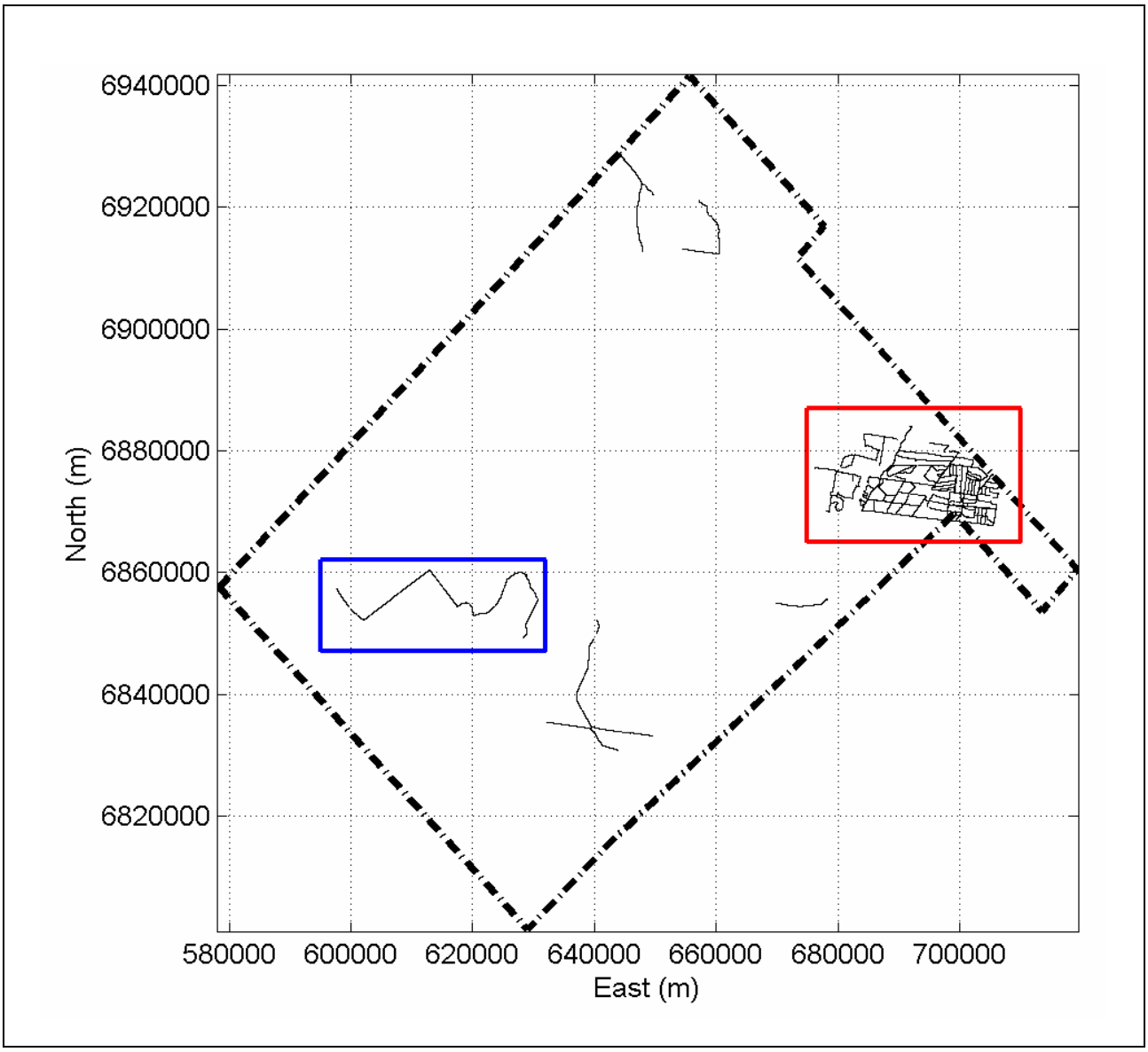

Figure 21. The locations of the EM31 traverses are shown as black lines. The outline of the St George AEM survey is shown as a dashed dot line. The location of the "Goondoola Basin" subset is shown in red. The location of the traverse featured in Figure 27 is shown with a blue outline.

Correction for Low Induction Number (LIN) approximation

The EM31 data were acquired in the vertical dipole mode. The instrument uses a Low Induction Number (LIN) approximation to derive apparent conductivity values (McNeil, 1980). As shown by Reid and Howlett (2001), this approximation can lead to significant underestimation of the true apparent conductivity in regions with elevated conductivity such as St George. The degree of underestimation can be gauged from Table 10 that compares halfspace conductivity and apparent conductivity derived with a LIN assumption for an EM31 instrument operated at ground level. Note that apparent conductivity based on a LIN approximation reaches a maximum of 316mS/m for a true halfspace conductivity of around 1120mS/m[*]. For higher halfspace conductivity values, the apparent conductivity based on a LIN approximation actually diminishes. This "roll-over" behaviour introduces ambiguity into the interpretation of high apparent conductivity values based on a LIN approximation.

Table 10. Comparison of halfspace conductivity and apparent conductivity derived with a LIN assumption for an EM31 instrument operated at ground level in vertical dipole mode.

Halfspace conductivity (mS/m)	Apparent conductivity with LIN approximation (mS/m)
1	1
2	2
5	5
10	9
20	18
50	41
100	76
200	133
300	178
400	215
500	244
600	267
700	285
800	299
900	308
1000	313
1120	316
1200	315
1500	297
2000	227

A non-linear inversion routine was used to correct for the LIN approximation prior to all analyses of the EM31 data. The forward model algorithm was based on equations given in the Appendix of McNeil (1980) for an EM31 instrument operating in vertical dipole mode at ground level. For each observed EM31 LIN apparent conductivity value, the routine found a halfspace conductivity value that would minimise the squared difference between the log10 transformed observed EM31 LIN apparent

[*] When operated at a height of 1m above the ground surface, the maximum reading of the EM31 instrument is around 410mS/m at a true halfspace conductivity of approximately 2500mS/m. The presence of EM31 readings greater that 316mS/m, the theoretical maximum for ground level measurements, may indicate that the measurements were made at some distance above the ground surface. This may also explain the need to scale the shallow AEM conductivity predictions when making comparisons with EM31 apparent conductivity values (LIN corrected assuming measurements taken at ground level) shown in Figure 29 (J. Reid, personal communication, 2004).

conductivity value and the log10 transformed EM31 LIN apparent conductivity value that would be predicted for the relevant true halfspace conductivity. If the inversion was unable to reproduce the observed EM31 LIN apparent conductivity value to within 2% (i.e., a squared misfit between log10 transformed conductivity values of $(0.02)^2$), the output was set to undefined. This situation occurred in 37 instances when the EM31 LIN apparent conductivity significantly exceeded the theoretical maximum apparent conductivity that can be obtained with the LIN approximation. Taking into account the tolerance allowed in the misfit, this threshold corresponds to rejection of observed values exceeding ~330mS/m.

Sampling of AEM predictions

AEM shallow conductivity predictions corresponding in location to the EM31 observations were obtained through bilinear interpolation of gridded 0 to 5m constrained inversion conductivity predictions. With line spacing of 250 or 400m for the AEM data, the closest actual AEM observation could be up to 200m from an EM31 observation. The typical distance from an EM31 observation to the nearest AEM observation would be ¼ of the line spacing or 60 to 100m.

Spatial filtering of EM31 data

To simulate the much larger sampling volume of AEM measurements, cosine weighted filters of various lengths were applied in some circumstances along traverses of EM31 data. Prior to filtering, the supplied EM31 data were separated into distinct traverses to avoid filtering across the spatial gaps between the ends of different traverses. The start and end of different traverses, within the supplied located data file, were identified using a threshold of >500m for the distance between adjacent points. Any use of filtering on the EM31 data is clearly indicated in the text.

Analysis of log10 values or linear values?

The histogram in Figure 22 (a) shows that the EM31 apparent conductivity values form a skewed distribution. The application of a log10 transformation reveals that the EM31 data are a combination of two lognormal populations (Figure 22 (b)). Visual inspection of the EM31 data suggests that the population with mean around 300mS/m (i.e., $(10)^{2.5}$) corresponds to the measurements sampling the elevated conductivity in the Goondoola Basin. The population with mean around 100mS/m is more typical of the near-surface conductivity in the St George AEM survey area. This is consistent with the conductivity of Quaternary sediments observed in borehole conductivity logs.

A lognormal distribution of conductivity values is generally observed when dealing with conductivity data, so a log10 transformation is applied to these data prior to any statistical analysis. This was the case throughout the work reported here. This transformation pre-conditions the data for any procedure that assumes that a normal distribution is present.

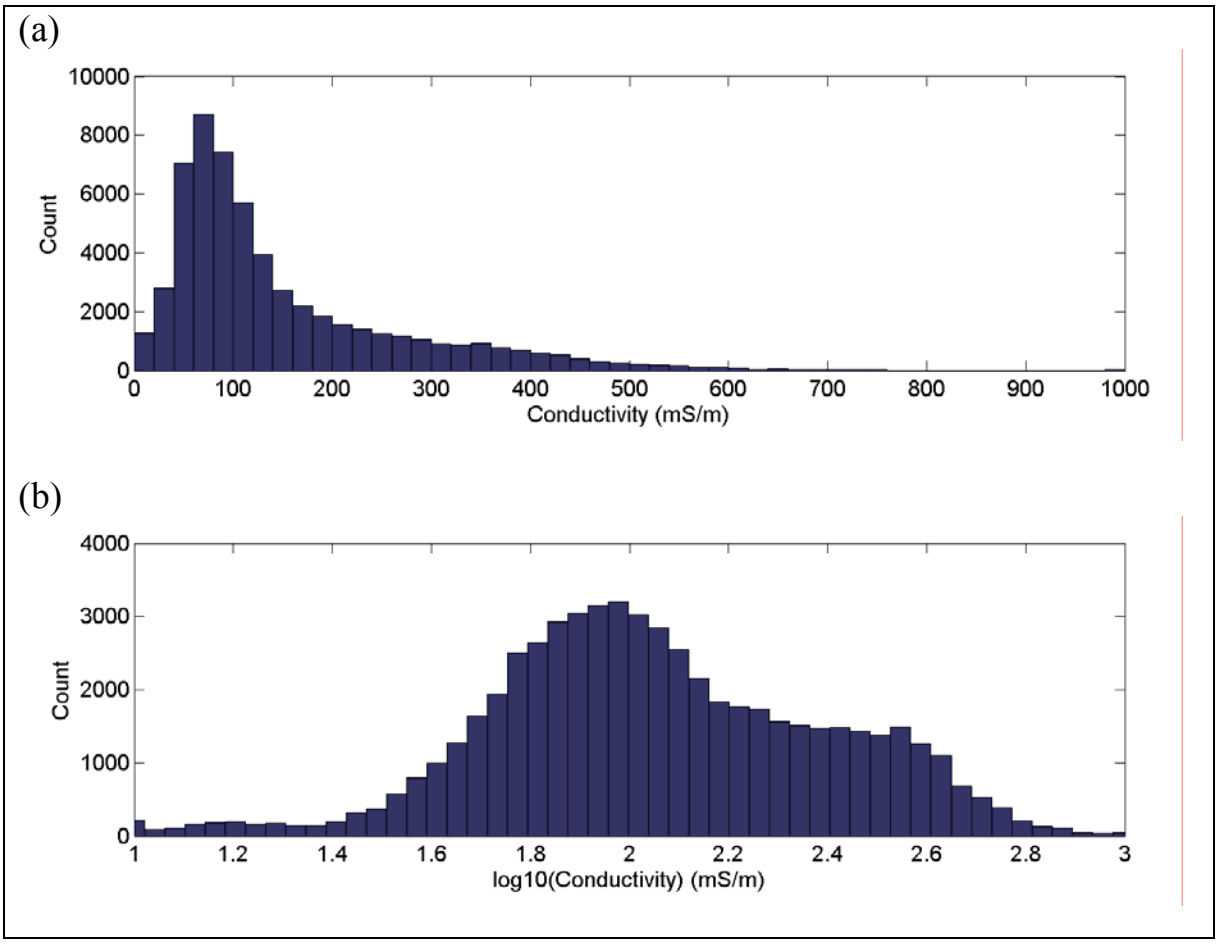

Figure 22. Histograms of (a) EM31 apparent conductivity values, and (b) log10 transformed EM31 apparent conductivity values.

An example of an application that requires some degree of normality for the input data is linear regression. An example is given in Figure 23 where pairs of EM31 apparent conductivity values for observations from different traverses that were within 5m of each other are compared. Linear regression is underpinned by 5 assumptions (Helsel and Hirsch, 2002);

1. The two quantities are linearly related.
2. The data used in the regression are representative of the relationship.
3. The variance of the residuals does not depend on the magnitude of either of the quantities.
4. The residuals are independent.
5. The residuals are normally distributed.

Prior to log10 transformation, assumption 3 is violated in that the variance of the residuals for high conductivity values is much higher than that for low conductivity values. This is indicated by the increasing spread of residuals about the line of best fit in Figure 23 (a) with increasing conductivity. This would mean that the regression relationship would be biased towards fitting of values with high conductivity. In contrast, following log10 transformation, the residuals have relatively equal variance or scatter about the regression line as a function of log10(conductivity).

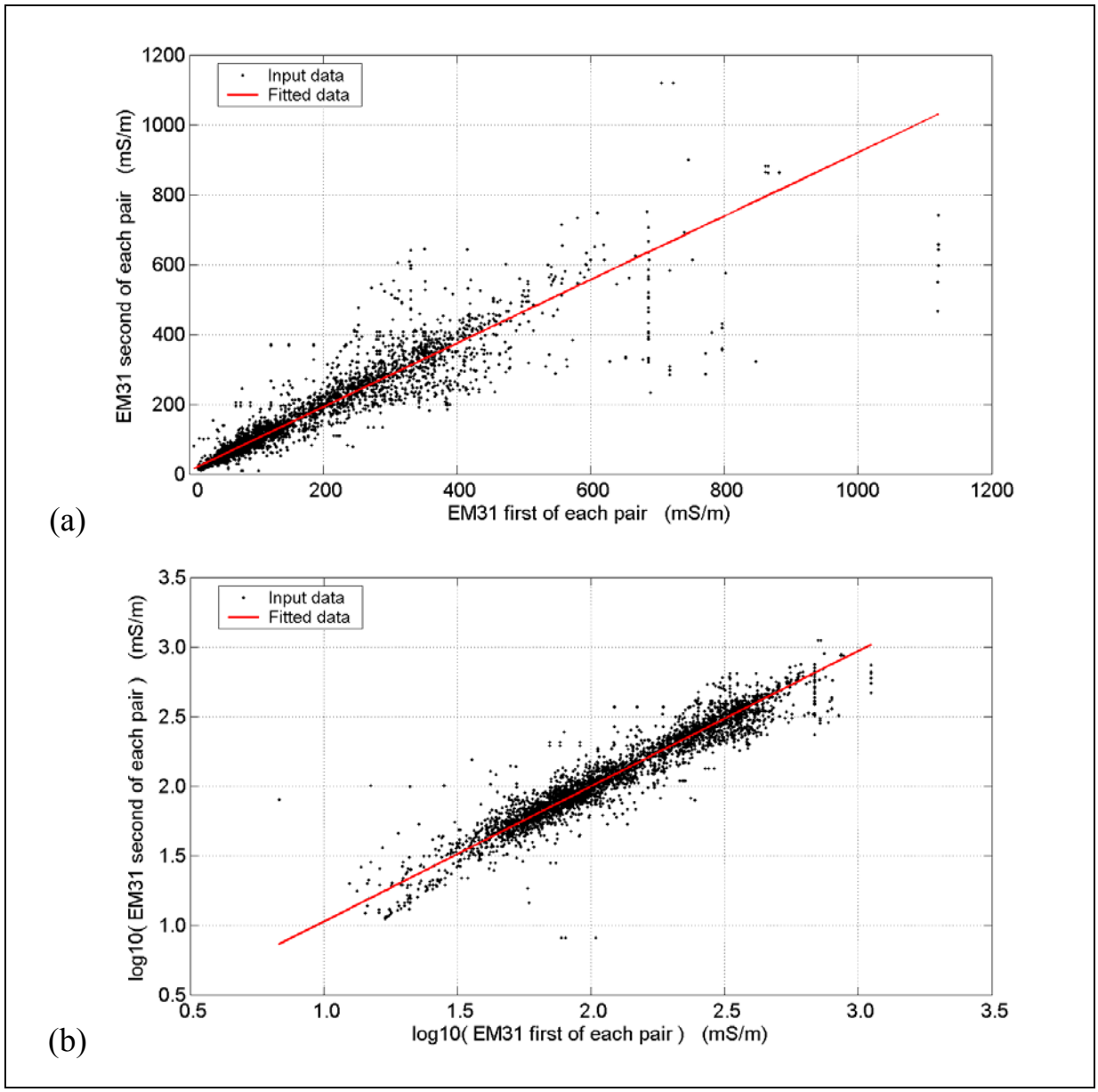

Figure 23. Linear regression applied to EM31 observations within 5m of each other. (a) Applied to EM31 apparent conductivity values, and (b) applied to log10 transformed EM31 apparent conductivity values.

Log10 transformation of conductivity prior to processing and analysis has the additional benefit of ensuring positivity when the transformed values are restored through exponentiation.

Semi-variograms

Any comparison of different conductivity measurements needs to consider the issues that arise if the samples are not exactly co-located and if the measurements reflect substantially different sample volumes. In geostatistical literature, the sample volume is termed the "support" of a sample. Both of the above issues relate to spatial variability in the underlying physical property distribution.

The sample volume or volume of investigation for AEM measurements is not easily defined. The volume depends on the conductivity structure of the ground, the transmitter loop moment waveform, the receiver characteristics, the geometry of the system, and system noise levels. The horizontal extent of the sample volume is characterised to a degree by the 'footprint'. Liu and Becker (1990) defined this as "the side length of a square surface, centred directly below the transmitter coil that contains the induced currents, which account for 90% of the observed secondary magnetic field". The calculation is generally performed with a perfectly conducting ground. This provides the minimum horizontal length

scale; for finite conductivity values, the footprint would be larger. The depth extent of the sample volume is often characterised by the volumetric skin depth which Beamish (2004) defined as the volume bounded by the surface upon which the modulus of the total induced electric field has decayed to 1/e of the maximum electric field located on the surface of the ground.

The (minimum) footprint of a TEMPEST system with geometry similar to that present during this survey (i.e., transmitter loop terrain clearance of 120m, transmitter loop to receiver coil horizontal separation of 120m and transmitter loop to receiver coil vertical separation of 33m) was calculated using the definition of Liu and Becker (1990) and magnetic field method of King and Macnae (2001). The footprint was approximately 150m for the X component and approximately 350m for the Z component. Since the constrained inversion involved both components, the (minimum) footprint was taken as 350m.

Borehole conductivity measurements averaged over 5m intervals involve a sample volume of approximately $15m^3$ (i.e., a cylinder with 1m radius and 5m depth). EM31 observations have a sample volume of approximately $150m^3$ (i.e., a cylinder with 3m radius and 6m depth). Each AEM conductivity prediction for the 0 to 5m depth range involves a sample volume of approximately $1{,}000{,}000m^3$ (i.e., a box with dimensions 5m by 350m by 560m, or depth by footprint by footprint plus along-line processing distance). These three measurement types thus sample volumes that are different by a ratio of 1 : 10 : 65,000.

How will EM31 samples ($\sim 150m^3$) compare with the AEM 0 to 5m conductivity predictions ($\sim 1{,}000{,}000m^3$)? The AEM conductivity predictions would be expected to show greatly reduced variability. Beyond that generalisation, any actual comparison will depend on the spatial variability of conductivity. This variability will be different from one area to another, but might be expected to be similar in comparable geological environments.

Semi-variogram plots are a geostatistical tool for quantifying spatial variability (e.g., Goovaerts, 1997). These plots show the variance of pairs of data as a function of the separation between the two data points. The variance is a combination of measurement uncertainty and the true spatial variability. In general, closely spaced pairs of observations would be expected to be more alike than widely spaced pairs of observations. Hence, semi-variograms tend to show an increase in variability as a function of the spacing between pairs of observations or "lag". Distributions that exhibit smooth, broad trends have semi-variograms that rise slowly to the maximum variance. Distributions that vary rapidly with position rise quickly to the maximum variance. The lag or sample separation at which the variance reaches a plateau is called the "range", and is a characteristic measure of the spatial variability, together with the "sill" or value of the variance at the range. Regional trends and spatial periodicity produce effects that can complicate semi-variogram interpretation beyond the simple characteristics described above.

The semi-variograms in Figure 24 illustrate the support effect. The variance of pairs of EM31 samples rises more rapidly and to a higher value as a function of separation than the AEM 0 to 5m conductivity predictions due to the smaller support size of the EM31 values. Any cross-plot between EM31 and AEM measurements would thus show a degree of scatter that reflects differences in responsiveness to short range variability in conductivity.

The application of a cosine-shaped spatial averaging filter to the EM31 values along each traverse can simulate the impact of the larger support size of AEM values. A filter length of 71 observations or approximately 900m was required to match the short-range variability of EM31 and AEM values (Figure 24). This filter length is a function of the spatial variability of shallow conductivity, the relative sample volumes, the footprint of the AEM system (~350m), the along-line processing functions applied to the AEM observations (~210m) and the line spacing for the AEM observations (250 to 400m).

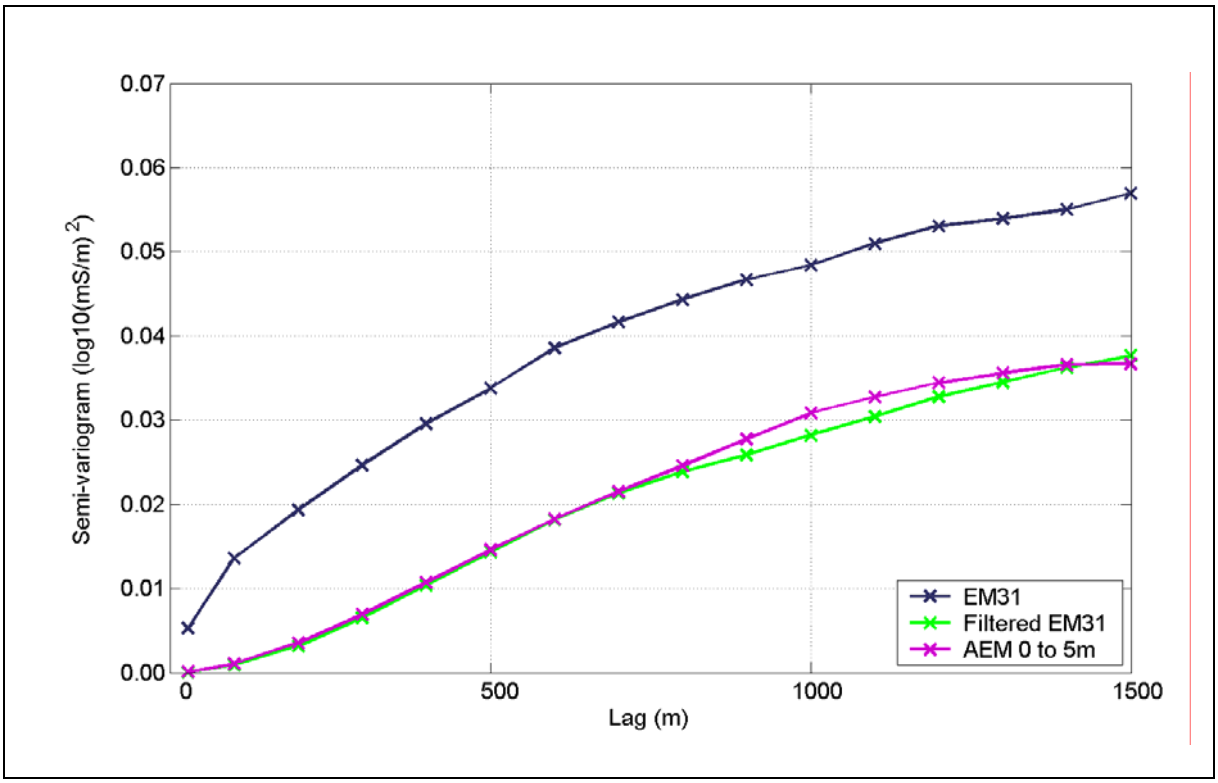

Figure 24. Semi-variograms for log10 transformed EM31 apparent conductivity values outside the Goondoola Basin area. The semi-variogram for the observed EM31 apparent conductivity values is shown on blue. The semi-variogram for the constrained inversion AEM 0 to 5m conductivity predictions at these locations is shown in magenta. The semi-variogram for the spatially filtered EM31 apparent conductivity values is shown in green.

Distinct differences in the spatial variability in the Goondoola Basin area compared to elsewhere were noted during exploratory analysis of the EM31 apparent conductivity data. Accordingly, the EM31 observations were divided into two subsets prior to calculating semi-variograms (Figure 25). To assist in the characterisation of the variability, the observed semi-variograms were modelled. It was necessary to use pairs of models to fit the observations for either subset. The semi-variograms for the individual models can be added together under the assumption that the observations arise from a linear combination of independent random function (Goovaerts, 1997 – Section 4.2.3). Such 'nested' models are not uncommon.

The semi-variogram for observations in the Goondoola Basin area shows a sharp rise at spacings less than 1km (exponential model with zero nugget, 0.025log10(mS/m)^2 sill and 900m range) together with a long-range trend that reflects the presence of the broad conductivity high (spherical model with zero nugget, 0.12log10(mS/m)^2 sill and 20,000m range). The semi-variogram for the observations outside the Goondoola Basin area shows a similar sharp rise at spacings up to 2km (exponential model with zero nugget, 0.07log10(mS/m)^2 sill and 2500m range), but only a subtle, low amplitude long-range trend at larger spacings (spherical model with zero nugget, 0.03log10(mS/m)^2 sill and 10,000m range). The slight downward inflection at 6km spacing in the observed semi-variogram for observations outside the Goondoola Basin (Figure 25(b)) might represent a 'hole' effect (i.e., an indication of repeated structure). However, there is a coincident change in the number of distinct pairs available for the semi-variogram calculation at this spacing that suggests that this might be a minor artefact of the spatial distribution of the observations.

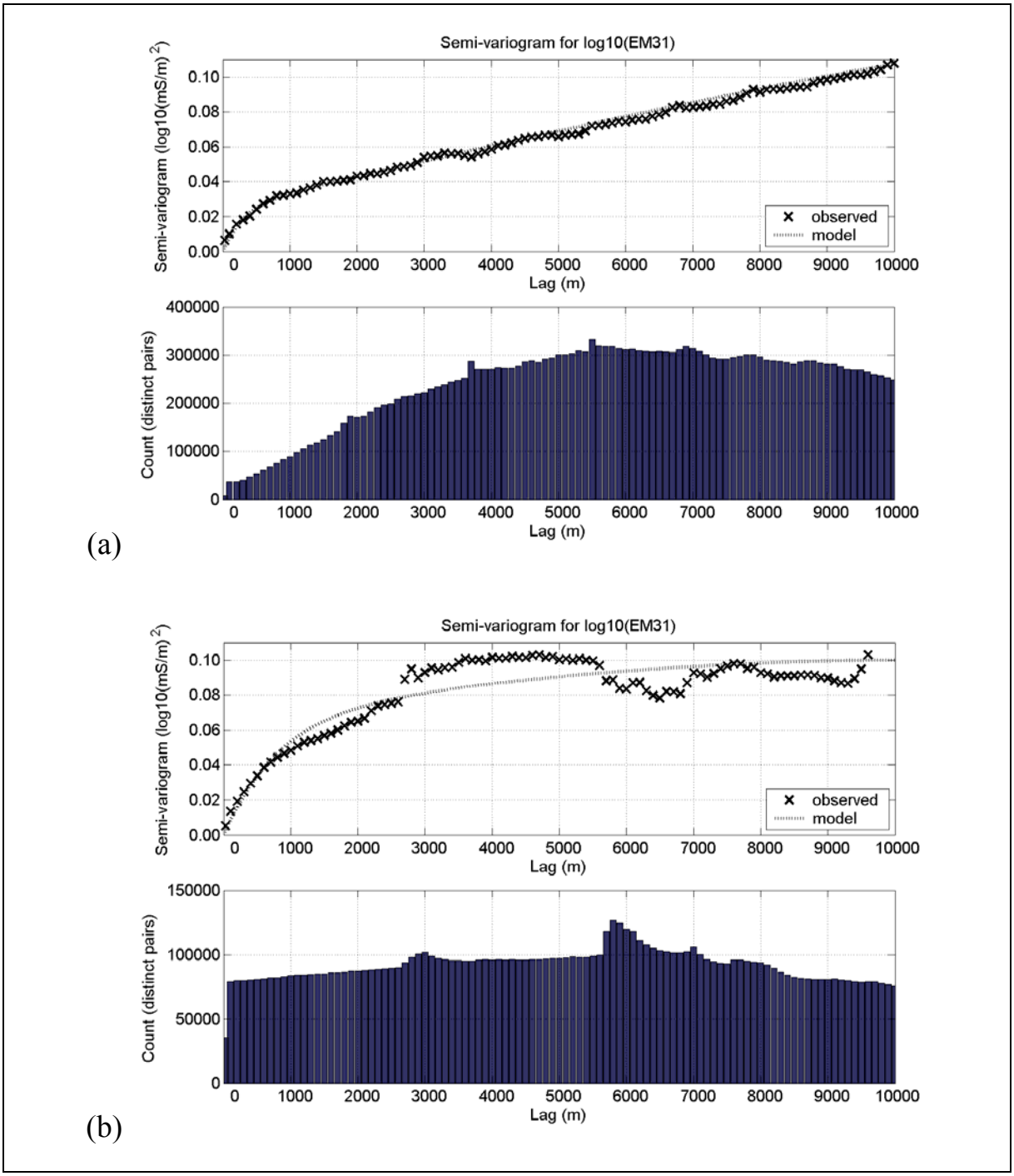

Figure 25. Semi-variograms for EM31 apparent conductivity values (a) Observations from the Goondoola Basin area and the combined result of an exponential model with zero nugget, 0.025log10(mS/m)^2 sill and 900m range and spherical model with zero nugget, 0.12log10(mS/m)^2 sill and 20,000m range. (b) Observations outside the Goondoola Basin area and the combined result of an exponential model with zero nugget, 0.07log10(mS/m)^2 sill and 2500m range and spherical model with zero nugget, 0.03log10(mS/m)^2 sill and 10,000m range.

Statistical analysis

The relationship between EM31 apparent conductivity values and AEM 0 to 5m conductivity predictions was investigated through scatter plots, linear regression and calculation of MM and MSD statistics (Figure 26 and Table 11).

The impact of the restricted range of conductivity values (40 to 1000mS/m) used in the contractor-supplied EMFlow predictions is evident as truncation at high and low conductivity levels in Figure 26 (a). This reduces the degree of correlation that was achieved with EM31 apparent conductivity.

An improvement in correlation with EM31 apparent conductivity is noted for the revised EMFlow predictions. The scatter plot (Figure 26 (b)) shows, however, a distinct curvature between log transformed EM31 apparent conductivity and AEM conductivity predictions and hence a departure from a simple linear relationship.

The constrained inversion conductivity predictions show a further improvement in the correlation with EM31 apparent conductivity (Figure 26 (c)). A slight departure from linearity is noted at low conductivity values.

A significant contribution to the scatter away from the regression line in each case is due to the difference in sample volume between the two measurement types. A cosine-shaped spatial averaging filter of length 71 observations (~900m) was applied to the EM31 values along each traverse to simulate the effects of the AEM system footprint, along-line processing functions and line spacing on the sample volume of the AEM values used in the comparison. When the statistical analysis was repeated, there was an improvement in all of the measures used to compare the modified EM31 apparent conductivity values and the AEM conductivity predictions (Table 11 and Figure 27).

Of all the pairings, the filtered EM31 apparent conductivity values and constrained inversion predictions demonstrate the best overall match, although the misfit mean is marginally better for the revised EMFlow conductivity predictions. It is notable that EM31 apparent conductivity values and AEM 0 to 5m conductivity predictions compare more favourably that do borehole 0 to 5m interval conductivity values and AEM 0 to 5m conductivity predictions (Table 11).

Table 11. Table of statistics for a comparison of all EM31 apparent conductivity observations with AEM 0 to 5m conductivity predictions. All comparisons were made using log10 transformed conductivity values. Desirable characteristics for a close match between the abscissa and ordinate quantities would be a correlation coefficient, "R", close to 1, "slope" close to 1, "intercept" close to zero, misfit mean, "MM", close to zero, and misfit standard deviation, "MSD", close to zero. The last row of the table presents the same statistics for the comparison of borehole conductivity observations averaged over 0 to 5m depth with AEM 0 to 5m conductivity predictions.

Abscissa	**Ordinate**	**R**	**Slope**	**Intercept** log10(mS/m)	**MM** log10(mS/m)	**MSD** log10(mS/m)	**N**
EM31	EMFlow FAS	0.57	1.025	0.536	0.588	0.322	57951
Filtered EM31	EMFlow FAS	0.59	1.140	0.285	0.573	0.303	57951
EM31	EMFlow LEME	0.70	0.812	0.317	-0.068	0.252	57951
Filtered EM31	EMFlow LEME	0.73	0.894	0.136	-0.083	0.227	57951
EM31	Constrained inversion	0.81	0.924	0.341	0.185	0.208	57951
Filtered EM31	Constrained inversion	0.84	1.000	0.171	0.171	0.183	57951
Borehole	Constrained inversion	0.64	0.858	0.274	-0.005	0.272	102

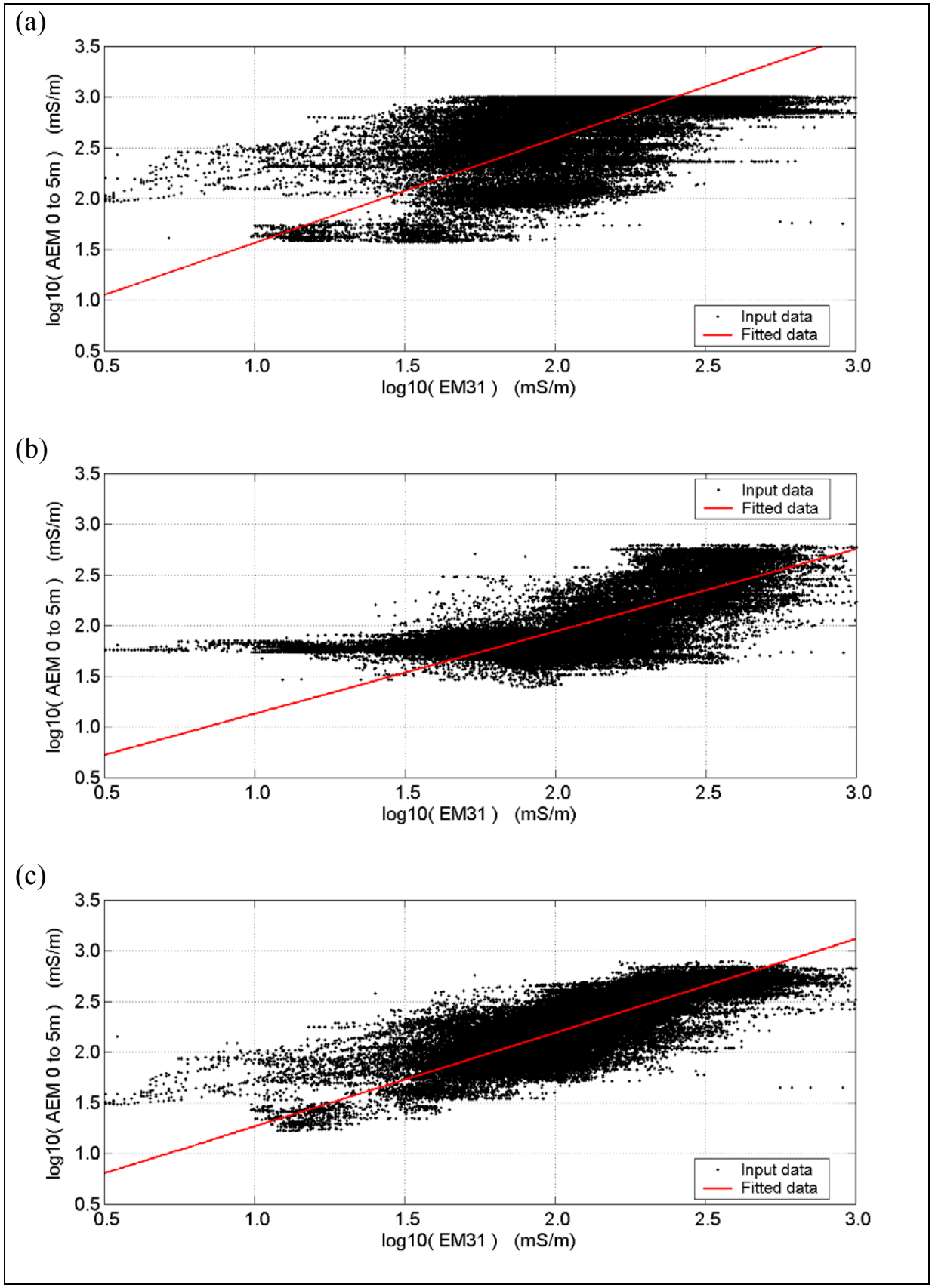

Figure 26. Scatter plots of log10 (EM31) apparent conductivity against log10 (AEM) conductivity predictions for 0 to 5m depth. The red line is the line of best fit through the points. (a) Contractor supplied EMFlow predictions. (b) Revised EMFlow predictions. (c) Constrained inversion predictions.

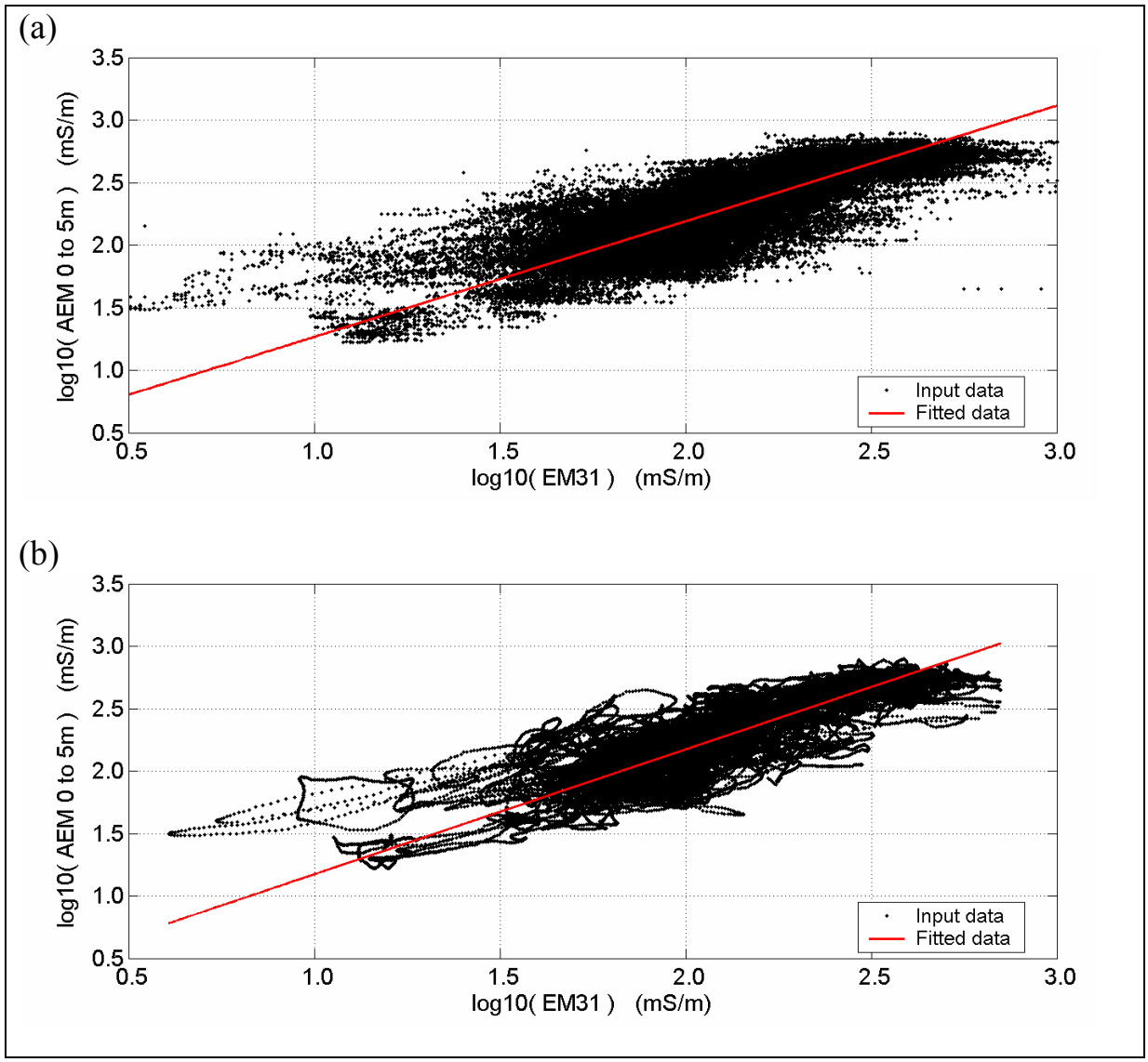

Figure 27. Scatter plots of log10(EM31) apparent conductivity against log10(AEM) conductivity predictions for 0 to 5m depth. The red line is the line of best fit through the points. (a) Constrained inversion predictions and EM31 conductivity values. (b) Constrained inversion predictions and filtered EM31 conductivity values.

A similar statistical analysis was carried out for the subset of EM31 and AEM data along the traverse shown in Figure 28 (see Table 12). There are minor differences as would be expected in the statistics for the entire dataset (Table 11) compared to those for a subset of the dataset (Table 12).

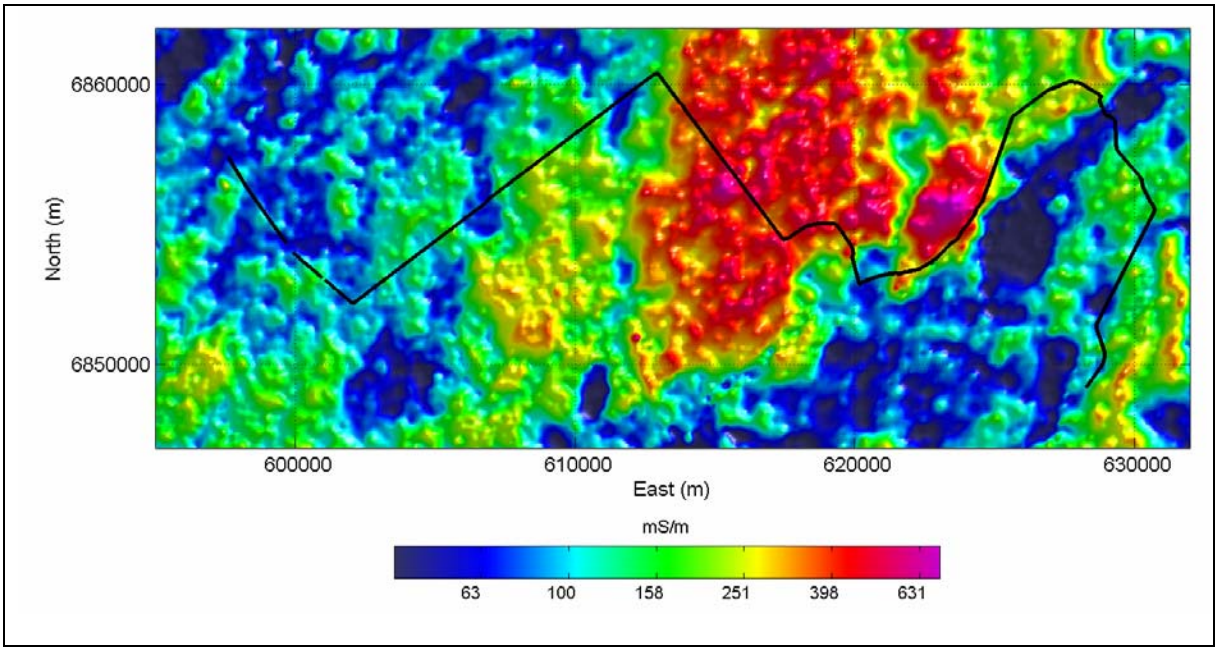

Figure 28. The location of the EM31 traverse shown in profile form in Figure 29. The background image is derived from a grid of constrained inversion AEM conductivity predictions for 0 to 5m depth.

Table 12. Table of statistics for a comparison of EM31 apparent conductivity values and AEM 0 to 5m conductivity predictions for the traverse shown in Figure 28. All comparisons were made using log10 transformed conductivity values.

Abscissa	**Ordinate**	**R**	**Slope**	**Intercept** log10(mS/m)	**MM** log10(mS/m)	**MSD** log10(mS/m)	**N**
EM31	EMFlow FAS	0.22	0.220	1.939	0.411	0.277	4456
Filtered EM31	EMFlow FAS	0.20	0.274	1.827	0.395	0.254	4456
EM31	EMFlow LEME	0.69	1.165	-0.291	0.031	0.218	4456
Filtered EM31	EMFlow LEME	0.76	1.374	-0.722	0.015	0.189	4456
EM31	Constrained inversion	0.78	1.057	0.148	0.259	0.179	4456
Filtered EM31	Constrained inversion	0.83	1.241	-0.233	0.243	0.152	4456

A comparison between EM31 apparent conductivity values and AEM 0 to 5m conductivity predictions is presented in profile form (Figure 29) for the traverse shown Figure 28. A reduction in spatial variability brought about by spatial filtering of the EM31 data is evident in the increased smoothness between the cyan and blue curves. An improvement in correlation between the two generations of EMFlow AEM conductivity predictions and the EM31 apparent conductivity values can be seen from the profiles in Figure 29 (a) and (b). However, the revised EMFlow conductivity predictions have very poor correlation with EM31 apparent conductivity values less than 100mS/m. This characteristics gives rise to the horizontal streak across the scatter plot of Figure 26 (b) for AEM conductivity prediction levels around 60mS/m (i.e., $(10)^{1.6}$). A significant improvement in this aspect can be seen for the constrained inversion AEM conductivity predictions in Figure 29 (c).

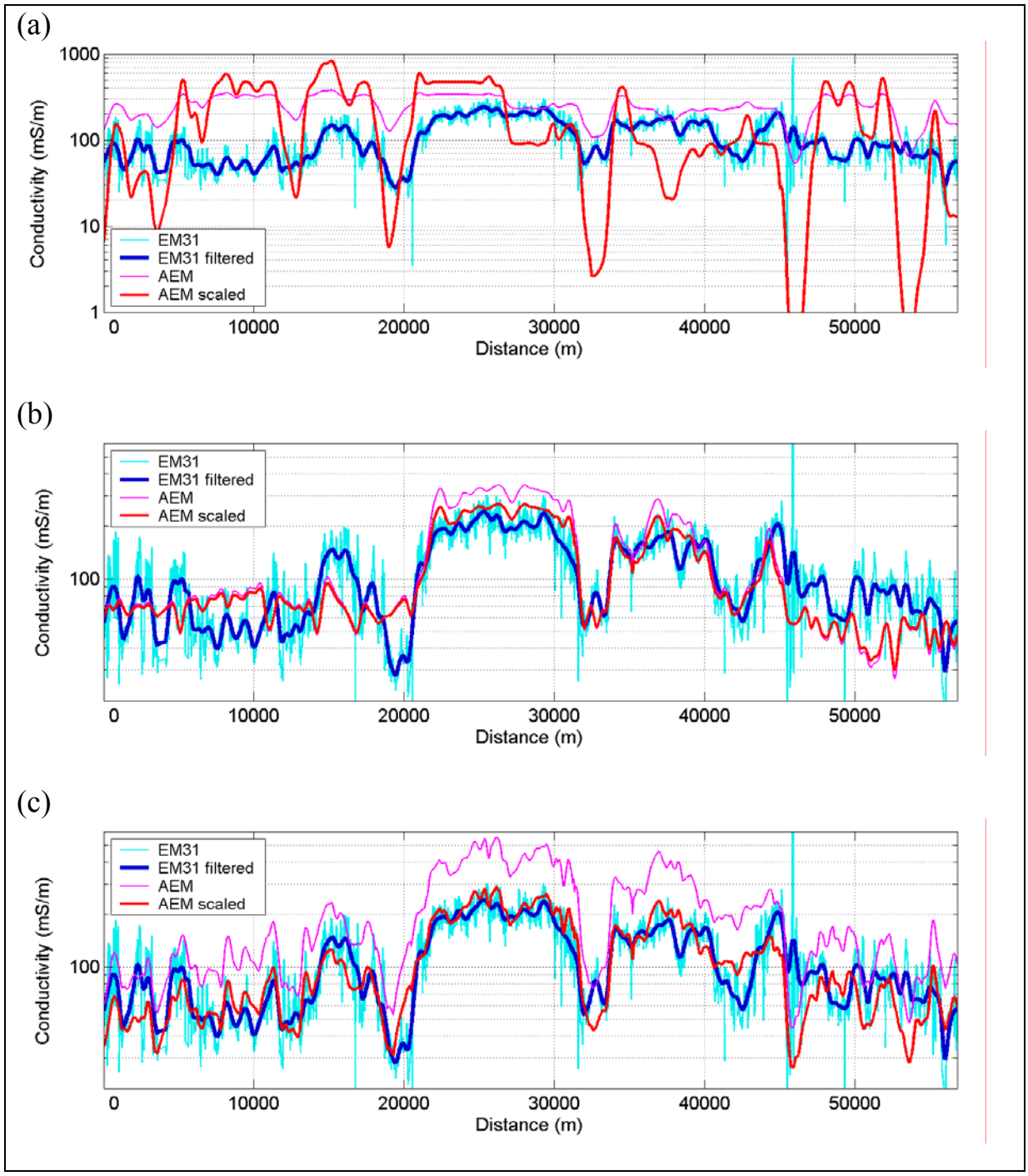

Figure 29. West to east profiles of EM31 apparent conductivity and AEM 0 to 5m conductivity predictions for the traverse shown in Figure 28. The LIN-corrected EM31 apparent conductivity profiles are shown with a thin cyan line. The filtered profiles are shown with a thick blue line. The AEM conductivity predictions are shown with a thin magenta line. The AEM conductivity predictions scaled and level shifted by the slope and intercept linear regression parameters for the appropriate AEM conductivity predictions and the filtered EM31 data from Table 12 are shown with a thick red line. (a) Contractor-supplied EMFlow predictions. (b) Revised EMFlow predictions. (c) Constrained inversion predictions.

Images of EM31 apparent conductivity and AEM 0 to 5m conductivity predictions for the Goondoola Basin area are shown in Figure 30 and Figure 31. The dominant feature of the EM31 apparent conductivity image is a large conductivity high approximately 8km in diameter associated with the Goondoola Basin.

Wilkinson (2003) noted that the contractor-supplied EMFlow conductivity predictions showed a "donut" pattern with a ring of elevated conductivity values surrounding the basin, but a relative drop in conductivity from the values for this ring to the values observed over the basin itself (Figure 31(a)).

This discrepancy was absent from the revised EMFlow conductivity predictions (Figure 31(b)). However, there is a lack of discrimination in conductivity predictions below 100mS/m that is evident as a flat background away from the Goondoola Basin.

An improvement in this aspect of the conductivity predictions in evident in the image for the constrained inversion predictions in Figure 31(c). Upon close examination, there are in fact some reversals in relative magnitude between Figure 31(b) and Figure 31(c) at mid to low conductivity levels (e.g., around 681000mE 6875000mN, 695000mE 6882000mN, etc). Although these locations are not well covered by the EM31 readings, it appears that the EM31 and constrained inversion results are in agreement, suggesting that the revised EMFlow results in these locations are some form of processing artifact.

A wealth of spatial patterns that are important for the identification and delineation of regolith features can be seen in Figure 31(c). These patterns are less evident in Figure 30 due to the irregular generally broader spacing between traverses in comparison with the AEM flight path that had lines spaced at regular 250 or 400m intervals.

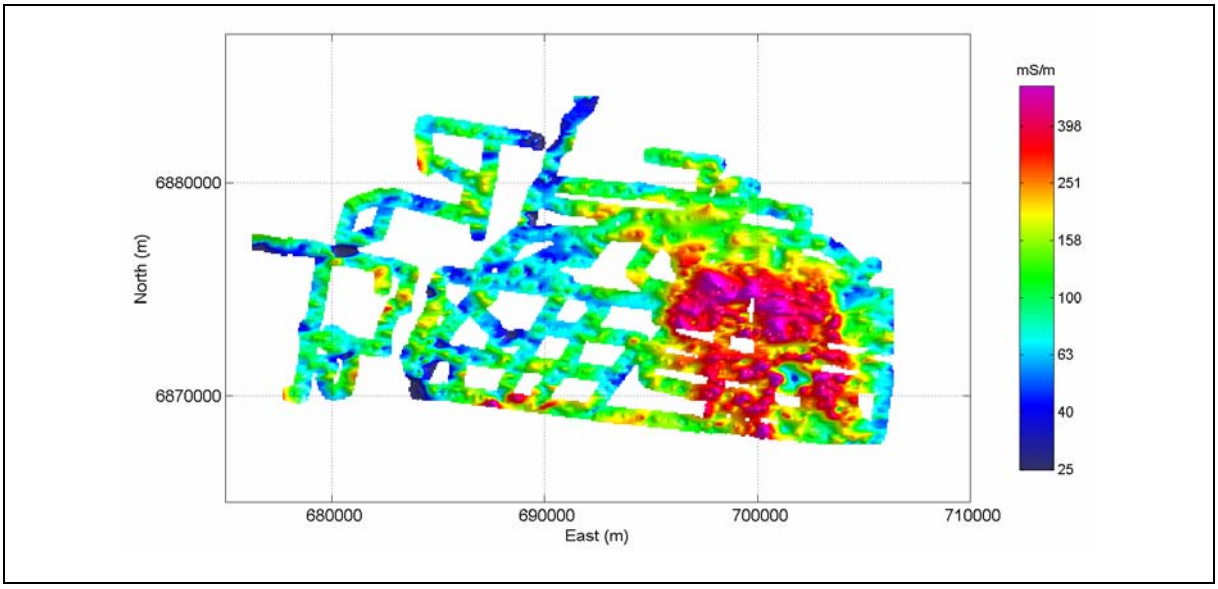

Figure 30. Image of LIN-corrected EM31 apparent conductivity values for the Goondoola Basin subset.

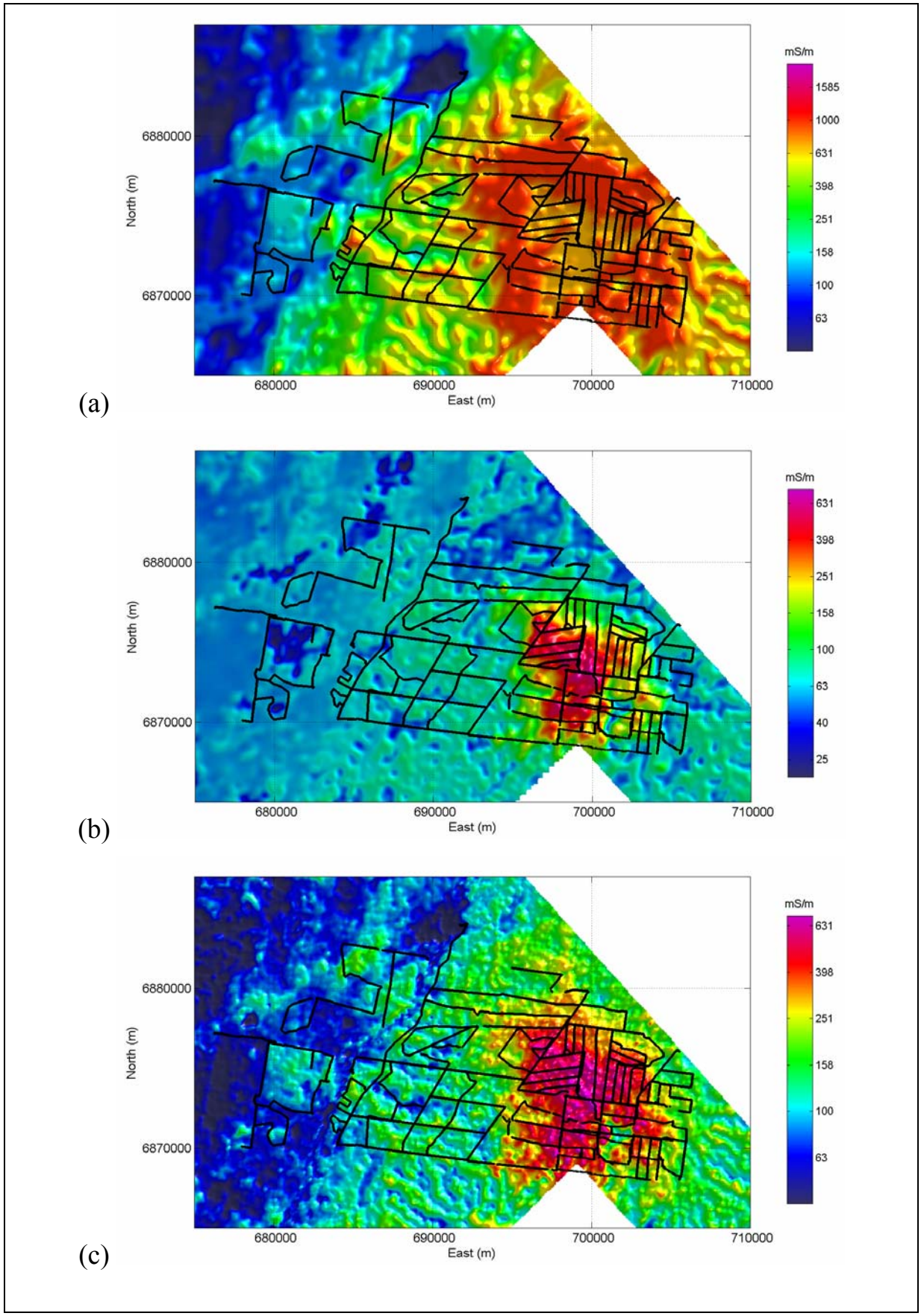

Figure 31. Images of AEM 0 to 5m conductivity predictions for the Goondoola Basin area. The locations of the EM31 traverses are shown as black lines. (a) Contractor supplied EMFlow predictions. (b) Revised EMFlow predictions. (c) Constrained inversion predictions. Colour scaling is logarithmic in all cases, but the limits were adjusted in each case to achieve the best visual match to the EM31 apparent conductivity image in Figure 30.

9.3 Example conductivity section

The conductivity (para-)section for line 10730, passing close to St George, is shown as an example of the appearance of the inversion output in section view (Figure 32). It should be noted that the sections were compiled by stitching together inversion results for each observation, and are not the result of 2D inversion.

The basic section showing the 12 layers of the inversion model is shown in Figure 32 (a). There were 1215 individual inversions along this line. The layer boundaries can be distracting when viewed in a section. The section in Figure 32 (b) shows the model re-sampled at constant 5m depth increments. The original 12 layers are no longer evident.

Once the conductivity values form a virtual continuum, it is easier to filter the sections without simply smearing out the layer boundaries. In this example, a very short horizontal filter (a 7-observation horizontal median filter followed by a 7-observation horizontal gaussian-smoothing filter) has been used to reduce the visual impact of small observation-to-observation instabilities in the inversion (Figure 32 (c)). Of course, these short-range variations could be real, and very important. Consequently, filtered products should always be used in conjunction with the original, least processed output.

Heavier filtering (a 21-observation horizontal median filter followed by a 21-observation horizontal gaussian-smoothing filter) can be applied if a more generalised section is desired (Figure 32 (d)). The data misfit is also shown at the bottom of Figure 32 (d).

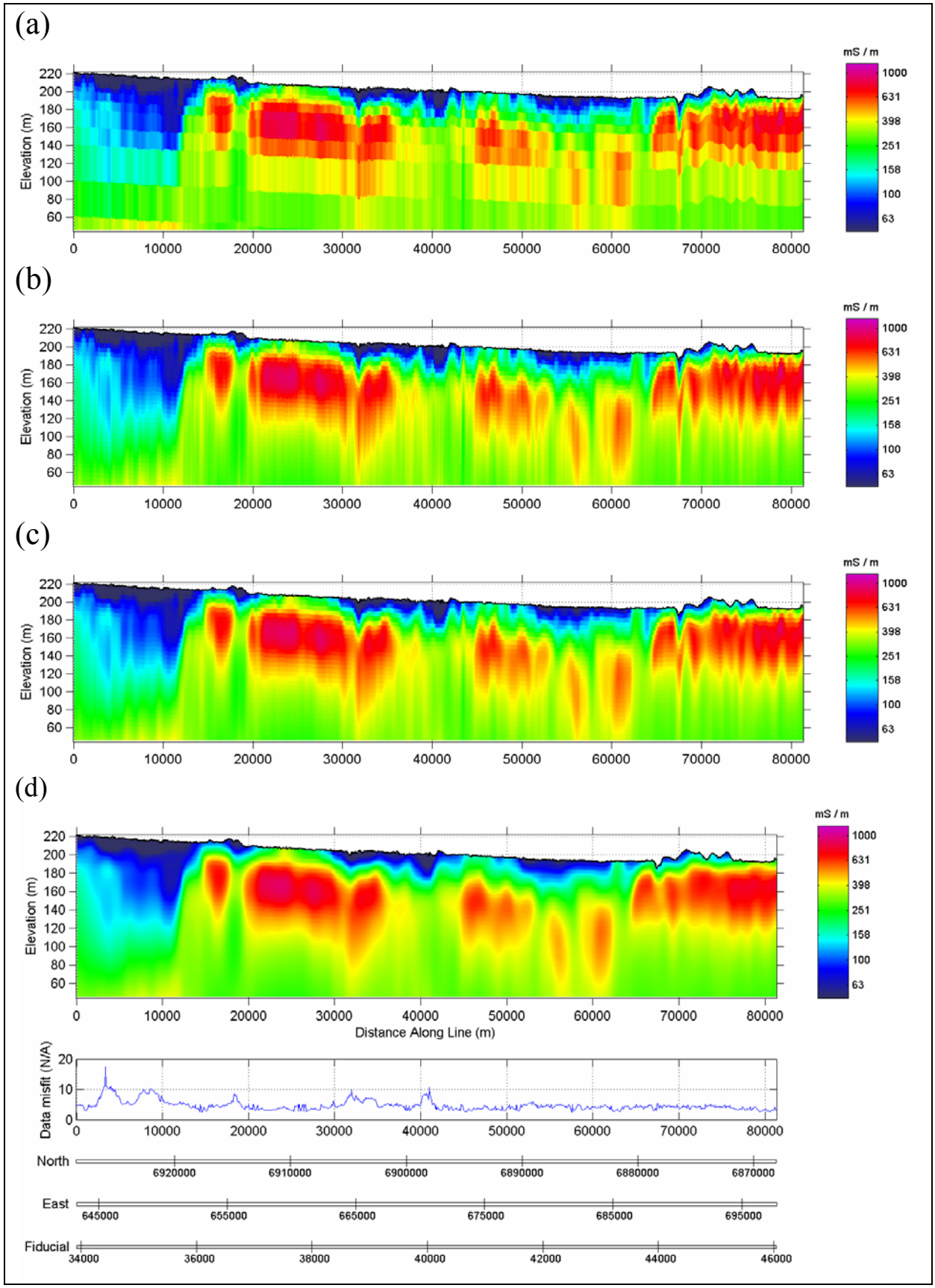

Figure 32. Conductivity sections for line 10730. (a) 12-layer inversion output. (b) Inversion output re-sampled at constant 5m increments. (c) Lightly filtered version of the re-sampled section. (d) More heavily filtered version of the re-sampled section. See section 9.3 for an explanation of the filtering applied in (c) and (d).

9.4 Example conductivity grids

Examples of images of the final conductivity data for depth slices 0 to 5m, 30 to 40m and 80 to 120m are included as Figure 33, Figure 34 and Figure 35 respectively.

The St George AEM Survey was flown as part of a State and Commonwealth government funded multi-disciplinary study of the Lower Balonne area in southern Queensland, involving collaboration between the Cooperative Research Centre for Landscape Environments and Mineral Exploration (CRC LEME), the Queensland Department of Natural Resources and Mines and the Bureau of Rural Sciences. The conductivity predictions from constrained inversion were used to provide context for direct observations of the sub-surface provided by scatter drillholes. The conductivity predictions substantially improved the definition and knowledge of the sub-surface geometry of the various units. The integrated interpretations and implications for land management are presented in other reports associated with the study, but Clarke et al. (2004) and Kernich and Pain (2004) summarise some of the main geological observations.

The elevated conductivity values evident at 80 to 120m depth (Figure 35) covering the south-east two thirds of the survey area reflect the presence of fresh and weathered Cretaceous marine sediments of the Surat Basin. The resistive material along the north-west margin of the survey is associated with Quaternary alluvial material filling the fault-bounded Dirranbandi Trough. The relatively abrupt boundary between the Cretaceous and Quaternary sediments marks the position of the bounding fault. A palaeovalley, incised into the Cretaceous sediments and feeding northwest into the Dirranbandi Trough (~630000mE 6895000mN) is evident as a sinuous to dendritic resistive feature.

At 30 to 40m depth (Figure 34), the extent of (conductive) weathered Cretaceous sediments is substantially more restricted. Resistive Quaternary sediments deposited by the palaeo-Moonie and palaeo-Balonne Rivers cover more than half of the survey area.

The present-day Balonne River runs through the centre of the survey area (~655000mE 6930000mN, 640000mE 6870000mN, to 600000mE 6835000mN). Anastomosing resistive alluvial deposits are associated with the river system are evident at shallow depth (Figure 33). The relict Maranoa Fan covers the majority of the north-west third of the survey area. Although patchy, conductivity is observed to generally rise slightly towards the south-east margin of the fan. Conductivity is particularly elevated around ~620000mE 6860000mN. The other prominent conductivity high at shallow depth is associated with the Goondoola Basin (~700000mE 6872000mN). This feature is surrounded by weathered Cretaceous material with elevated conductivity. Such material is also present around 640000mE 6840000mN and 670000mE 6910000mN.

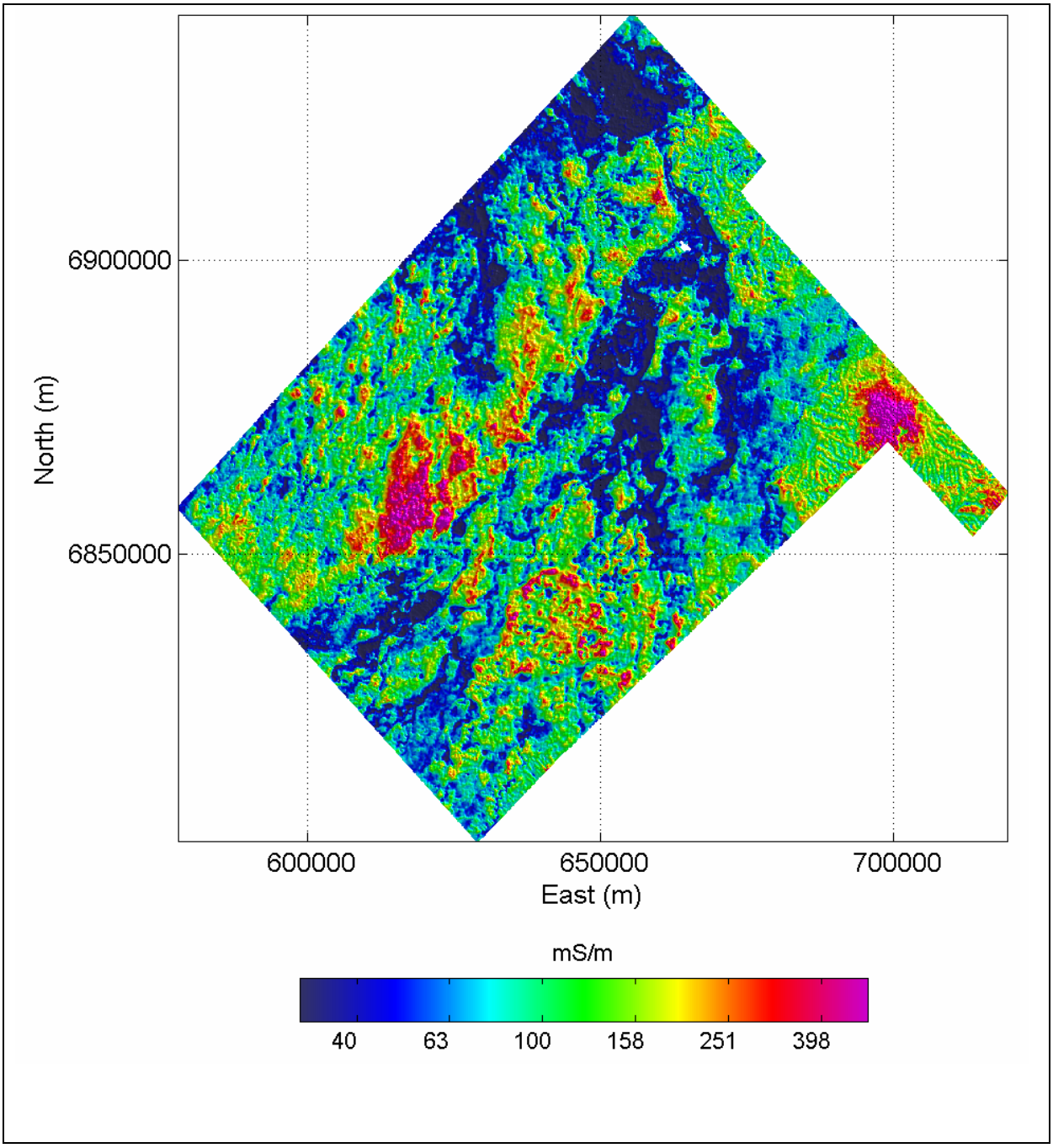

Figure 33. Image of conductivity for 0 to 5m depth below surface. Derived from a grid of manually levelled and micro-levelled constrained inversion conductivity data. A logarithmic colour stretch has been applied to the gridded data between limits of 30 and 500mS/m. Note that different colour scaling limits have been applied in Figure 33, Figure 34 Figure 35. This was done to optimise the interpretation of spatial patterns in the conductivity data for each depth slice. To facilitate interpretation of the change in conductivity with depth, it would be recommended that the same colour scaling be applied to each depth slice.

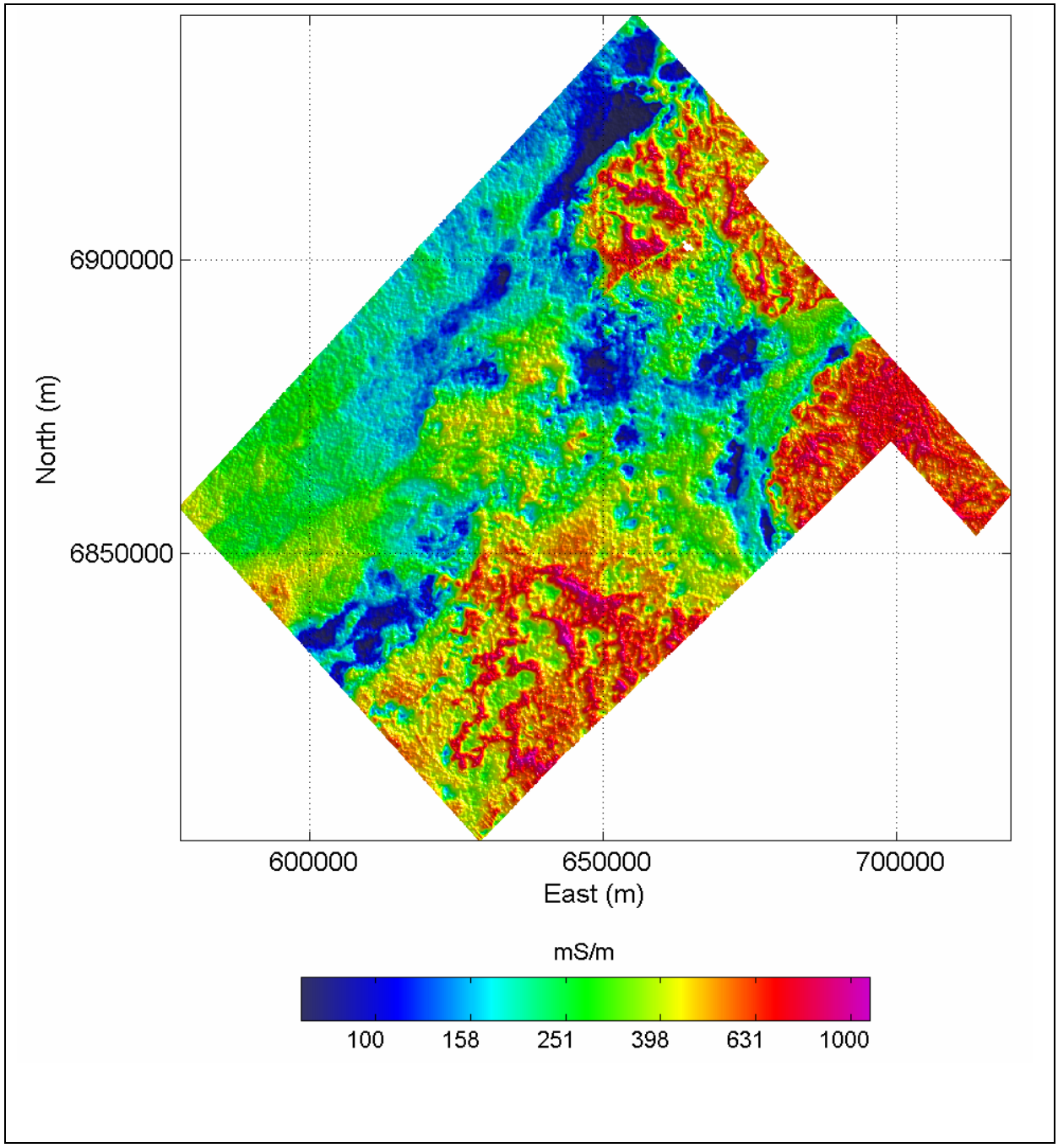

Figure 34. Image of conductivity for 30 to 40m depth below surface. Derived from a grid of manually levelled and micro-levelled constrained inversion conductivity data. A logarithmic colour stretch has been applied to the gridded data between limits of 70 and 1100mS/m. Note that different colour scaling limits have been applied in Figure 33, Figure 34 Figure 35. This was done to optimise the interpretation of spatial patterns in the conductivity data for each depth slice. To facilitate interpretation of the change in conductivity with depth, it would be recommended that the same colour scaling be applied to each depth slice.

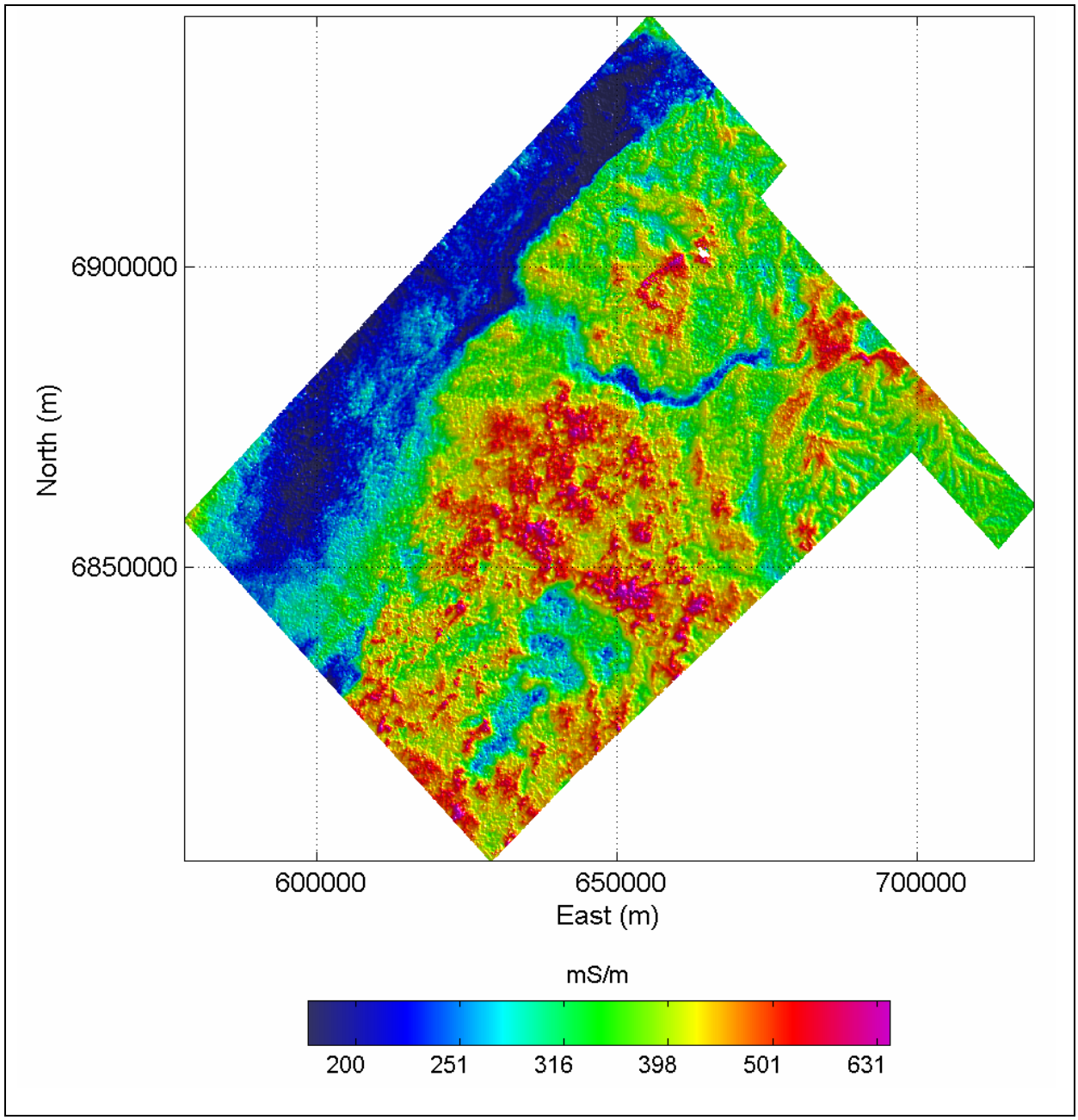

Figure 35. Image of conductivity for 80 to 120m depth below surface. Derived from a grid of manually levelled and micro-levelled constrained inversion conductivity data. A logarithmic colour stretch has been applied to the gridded data between limits of 180 and 650mS/m. Note that different colour scaling limits have been applied in Figure 33, Figure 34 Figure 35. This was done to optimise the interpretation of spatial patterns in the conductivity data for each depth slice. To facilitate interpretation of the change in conductivity with depth, it would be recommended that the same colour scaling be applied to each depth slice.

10 RECOMMENDATIONS

Survey-specific and more general recommendations have been drawn from the work carried out to re-process the St George AEM data.

10.1 Recommended conductivity predictions for the St George survey area

(a) It is recommended that the conductivity predictions reported herein be used in preference to either those supplied by the survey contractor or the revised EMFlow conductivity predictions produced by CRC LEME.

10.2 Pre-survey planning

(b) All relevant boreholes within the proposed survey area should be logged for lithology by geoscientists with regolith training as part of the pre-survey planning process.
(c) The conductivity structure of the survey area should be investigated through logging of selected boreholes as part of the pre-survey planning process.
(d) Appropriate borehole conductivity calibration procedures should be adhered to and recorded.
(e) Location and other metadata for the boreholes in the survey area should be managed carefully.
(f) Provision of resources for drilling and logging of additional boreholes needs to be included in the survey budget. These bores would be drilled following initial review of the AEM survey data to resolve ambiguities in interpretation.

10.3 Survey specifications and communication with the survey contractor

(g) Information on the survey objectives and the conductivity structure of the survey area should be communicated to the survey contractor so that decisions made during processing will result in the optimum data output.
(h) Acquisition of tie lines would be recommended to aid levelling of AEM data and derived quantities.
(i) Acquisition of full component data (i.e., X, Y and Z component) would be recommended if using a system with TEMPEST-style transmitter loop and receiver coil geometry.
(j) Window amplitude data prior to primary field removal should be included in the data products supplied by the survey contractor.

10.4 Research and development

(k) Research and development into methods to improve measurement of AEM system geometry should be supported to improve the quality of near-surface conductivity predictions.
(l) Constraint schemes for areas with variable conductivity at depth should be developed and tested.

ACKNOWLEDGMENTS

This work was supported by the Cooperative Research Centre for Landscape Environments and Mineral Exploration (CRC LEME) as part of the Nation Action Plan for Salinity and Water Quality supported by State and Commonwealth governments. The authors would like to acknowledge the contribution made by numerous personnel from CRC LEME, the Queensland Department of Natural Resources and Mines and the Bureau of Rural Sciences.

The authors would also like to thank James Read for his review and constructive suggestions that have improved the report.

This report is published with the permission of the Chief Executive Officers of CRC LEME and Geoscience Australia.

REFERENCES

Beamish, D., 2004, Airborne EM skin depths: Geophysical prospecting, 52, 439-449.

Brodie, R., Lane, R., and Gibson, D., 2002, Comparison of AEM and borehole conductivity data, Gilmore Project: Unpublished report for CRC LEME.

Brodie, R., and Lane, R., 2003, The importance of accurate altimetry in AEM surveys for land management; Exploration Geophysics, 34, 77-81.

Buselli, G., Hunter, D., Munday, T., and Wilkinson, K., 2003, Ground-based geophysical measurements prior to AEM surveys over salinity-affected agricultural areas: Submitted to Exploration Geophysics.

Buselli, G., and Williamson, D.R., 1996, Modeling of broadband airborne electromagnetic responses from saline environments: Geophysics, 61, 1624-1632.

Clarke, J.D.A., Lawrie, K., Riesz, A., Fitzpatrick, A., and Macphail, M., 2004, Comparatively rapid fluvial landscape evolution, Lower Balonne region, southern Queensland: Conference Program, Australian and New Zealand Geomorphology Group 11th Conference, Mount Buffalo, Australia, February 15-20, 2004, ANZGG Occasional Paper No.3, p14.

Coggon, 2000, Personal communication concerning the processing of TEMPEST data from the North Lake Carey Survey flown over the Wallaby deposit in 1999.

Goovaerts, P., 1997, Geostatistics for Natural Resources Evaluation: Oxford University Press, New York, 483p.

Graham, B., 1972, Dirranbandi, Queensland, Sheet SG/55−3, 1:250,000 Geological Series Explanatory Notes: Bureau of Mineral Resources, Geology and Geophysics, Canberra.

Green, A., 1998, Altitude correction of time domain AEM data for image display and geological mapping, using the Apparent Dipole Depth (ADD) method: Exploration Geophysics, 29, 87-91.

Green, A., and Lane, R., 2003, Estimating noise levels in AEM data: Extended abstract, ASEG, Conference, Adelaide, Australia, February 2003.

Guptasarma, D., and Singh, B., 1997, New digital linear filters for Hankel J_0 and J_1 transforms, Geophysical Prospecting, 45, 745-762.

Helsel, D.R., and Hirsch, R.M., 2002, Statistical methods in water resources: USGS Techniques in Water-Resources Investigations, Book 4, Chapter A3. (see http://water.usgs.gov/pubs/twri/twri4a3/)

Kernich, A.L. and Pain, C., 2004, Regolith landforms and salt in the Lower Balonne area, southern Queensland: Conference Program, Australian and New Zealand Geomorphology Group 11th Conference, Mount Buffalo, Australia, February 15-20, 2004, ANZGG Occasional Paper No.3, p41.

King, A., and Macnae, J.C., 2001, Modeling of the EM inductive-limit surface currents: Geophysics, 66, 476-481.

Liu, G. and Becker, B., 1990, Two-dimensional mapping of sea-ice keels with airborne electromagnetics: Geophysics, 55, 239-248.

Lane, R., Green, A., Golding, C., Owers, M., Pik, P., Plunkett, C., Sattel, D., and Thorn, B., 2000, An example of 3D conductivity mapping using the TEMPEST airborne electromagnetic system: Exploration Geophysics, 31, 162-172.

Macnae, J.C., King, A., Stolz, N., Osmakoff, A., Blaha, A., 1998, Fast AEM data processing and inversion: Exploration Geophysics, 29, 163-169.

McNeill, J.D., 1980, Electromagnetic terrain conductivity measurement at low induction numbers: Geonics Ltd. Technical Note TN-6.

McNeill, J.D., 1986, Geonics EM39 borehole conductivity meter - theory of operation: Geonics Ltd. Technical Note TN-20.

Menke, W., 1984, Geophysical data analysis: discrete inverse theory: Academic Press.

Oldenburg, D.W., and Li, Y., 1999, Estimating depth of investigation in dc resistivity and IP surveys: Geophysics, 64, 403-416.

Owers, M., Chambers, P., and Sattel, D., 2001, Acquisition and processing report, St George TEMPEST Survey; Fugro Airborne Survey report to the Bureau of Rural Sciences for Job 902.

Reid, J.E., and Howlett, A., 2001, Application of the EM-31 terrain conductivity meter in highly-conductive regimes: Exploration Geophysics, 32, 219-224.

Reiser, R.F., 1971, Surat, Queensland, Sheet SG/55−16, 1:250,000 Geological Series Explanatory Notes: Bureau of Mineral Resources, Geology and Geophysics, Canberra.

Sattel, D., 1998, Conductivity information in three dimensions: Exploration Geophysics, 29, 157-162.

Sattel, D., 2000, Personal communication concerning the processing of TEMPEST data from Fugro Airborne Surveys Job 1429.

Senior, B.R., 1971, Homeboin, Queensland, Sheet SG/55−5, 1:250,000 Geological Series Explanatory Notes: Bureau of Mineral Resources, Geology and Geophysics, Canberra.

Senior, D., 1972, St George, Queensland, Sheet SG/55−4, 1:250,000 Geological Series Explanatory Notes: Bureau of Mineral Resources, Geology and Geophysics, Canberra.

Smith, R., 2001a, On removing the primary field from fixed-wing time-domain airborne electromagnetic data: some consequences for quantitative modelling, estimating bird position and detecting perfect conductors: Geophysical Prospecting, 49, 405-416.

Smith, R.S., 2001b, Tracking the transmitting-receiving offset in fixed-wing transient EM systems: methodology and application: Exploration Geophysics, 32, 14-19.

Wait, J.R., 1982, Geo-electromagnetism: Academic Press.

Wilkinson, K., 2003, Investigation into the salinisation of Goondoola Basin, southern Queensland: Unpublished Masters Thesis, School of Civil and Environmental Engineering, The University of New South Wales.

Appendix 1. List of products

Point located data

1) Inversion input file.
2) Inversion output file.
3) Inversion output file with levelling corrections.
4) Inversion output file with levelling and micro-levelling corrections.
5) Re-sampled cumulative conductance data derived from (4),
   at constant 5m depth increments from 0-5m to 195-205m.
6) Re-sampled conductivity data derived from (4),
   at constant 5m depth increments from 0-5m to 195-205m.

Grid data

7) Grids of conductivity for each of the 12 layers in (2) (i.e., before levelling and micro-levelling) (80m grid cell size as per the original contractor delivered grids).
8) Grids of conductivity for each of the 12 layers in (3).
9) Grids of conductivity for each of the 12 layers in (4).
10) Grids of cumulative conductance for the first 40 layers in (5).
11) Grids of conductivity for each of the 41 layers in (6).

Report

12) "Constrained inversion of AEM data from St George, Queensland, Australia"

Additional items

13) A copy of the original FAS acquisition and processing report.
14) A copy of the original (laser upgraded) DEM grid.
15) A copy of the original TMI grid and 1VD of TMI grid from the AEM survey.

Header for inversion input file

```
Header for file: Inversion_input_file_st_george_sub5.asc
(Inversion input file)

(column 1)      Record number
(column 2)      Flight
(column 3)      Line
(column 4)      Fiducial
(column 5)      Easting (m)
(column 6)      Northing       (m)
(column 7)      Elevation      (m)
(column 8)      Laser altimeter        (m)
(column 9)      Transmitter loop terrain clearance    (m)
(column 10)     Transmitter loop pitch (degrees)
(column 11)     Transmitter loop roll  (degrees)
(column 12)     Supplied transmitter loop to receiver coil horizontal separation (DX)      (m)
(column 13)     Supplied transmitter loop to receiver coil vertical separation (DZ) (m)
(column 14)     Supplied receiver coil pitch  (degrees)
(column 15)     Supplied receiver coil roll   (degrees)
(column 16)     Maximum number of iterations
(column 17)     Minimum data objective function
(column 18)     Minimum data objective improvement
(column 19)     Damping factor (not used)
(column 20)     Damping reduction factor (not used)
(column 21)     Switch to use X component data        (0=fixed, 1=variable)
(column 22)     Switch to use Z component data        (0=fixed, 1=variable)
(column 23)     Switch to solve for layer thickness   (0=fixed, 1=variable)
(column 24)     Switch to solve for transmitter loop terrain clearance      (0=fixed,
1=variable)
(column 25)     Switch to solve for DX (0=fixed, 1=variable)
(column 26)     Switch to solve for DZ (0=fixed, 1=variable)
(column 27)     Switch to solve for receiver coil pitch      (0=fixed, 1=variable)
(column 28)     Switch to solve for receiver coil roll       (0=fixed, 1=variable)
(column 29)     Number of layers
(column 30)     Number of constraints
(column 31)     Supplied response for X window 1      (fT)
(column 32)     Supplied response for X window 2      (fT)
(column 33)     Supplied response for X window 3      (fT)
(column 34)     Supplied response for X window 4      (fT)
(column 35)     Supplied response for X window 5      (fT)
(column 36)     Supplied response for X window 6      (fT)
(column 37)     Supplied response for X window 7      (fT)
(column 38)     Supplied response for X window 8      (fT)
(column 39)     Supplied response for X window 9      (fT)
(column 40)     Supplied response for X window 10     (fT)
(column 41)     Supplied response for X window 11     (fT)
(column 42)     Supplied response for X window 12     (fT)
(column 43)     Supplied response for X window 13     (fT)
(column 44)     Supplied response for X window 14     (fT)
(column 45)     Supplied response for X window 15     (fT)
(column 46)     Supplied response for Z window 1      (fT)
(column 47)     Supplied response for Z window 2      (fT)
(column 48)     Supplied response for Z window 3      (fT)
(column 49)     Supplied response for Z window 4      (fT)
(column 50)     Supplied response for Z window 5      (fT)
(column 51)     Supplied response for Z window 6      (fT)
(column 52)     Supplied response for Z window 7      (fT)
(column 53)     Supplied response for Z window 8      (fT)
(column 54)     Supplied response for Z window 9      (fT)
(column 55)     Supplied response for Z window 10     (fT)
(column 56)     Supplied response for Z window 11     (fT)
(column 57)     Supplied response for Z window 12     (fT)
(column 58)     Supplied response for Z window 13     (fT)
(column 59)     Supplied response for Z window 14     (fT)
(column 60)     Supplied response for Z window 15     (fT)
(column 61)     Start and reference conductivity for layer 1 (S/m)
(column 62)     Start and reference conductivity for layer 2 (S/m)
(column 63)     Start and reference conductivity for layer 3 (S/m)
(column 64)     Start and reference conductivity for layer 4 (S/m)
(column 65)     Start and reference conductivity for layer 5 (S/m)
(column 66)     Start and reference conductivity for layer 6 (S/m)
(column 67)     Start and reference conductivity for layer 7 (S/m)
(column 68)     Start and reference conductivity for layer 8 (S/m)
(column 69)     Start and reference conductivity for layer 9 (S/m)
(column 70)     Start and reference conductivity for layer 10        (S/m)
(column 71)     Start and reference conductivity for layer 11        (S/m)
(column 72)     Start and reference conductivity for layer 12        (S/m)
(column 73)     Starting thickness for layer 1        (m)
(column 74)     Starting thickness for layer 2        (m)
(column 75)     Starting thickness for layer 3        (m)
(column 76)     Starting thickness for layer 4        (m)
(column 77)     Starting thickness for layer 5        (m)
(column 78)     Starting thickness for layer 6        (m)
(column 79)     Starting thickness for layer 7        (m)
(column 80)     Starting thickness for layer 8        (m)
(column 81)     Starting thickness for layer 9        (m)
(column 82)     Starting thickness for layer 10       (m)
```

```
(column 83)     Starting thickness for layer 11       (m)
(column 84)     Starting and reference value of DX    (m)
(column 85)     Starting and reference value of DZ    (m)
(column 86)     Starting and reference value of receiver coil pitch  (degrees)
(column 87)     Standard deviation for conductivity of layer 1       (log10(mS/m))
(column 88)     Standard deviation for conductivity of layer 2       (log10(mS/m))
(column 89)     Standard deviation for conductivity of layer 3       (log10(mS/m))
(column 90)     Standard deviation for conductivity of layer 4       (log10(mS/m))
(column 91)     Standard deviation for conductivity of layer 5       (log10(mS/m))
(column 92)     Standard deviation for conductivity of layer 6       (log10(mS/m))
(column 93)     Standard deviation for conductivity of layer 7       (log10(mS/m))
(column 94)     Standard deviation for conductivity of layer 8       (log10(mS/m))
(column 95)     Standard deviation for conductivity of layer 9       (log10(mS/m))
(column 96)     Standard deviation for conductivity of layer 10      (log10(mS/m))
(column 97)     Standard deviation for conductivity of layer 11      (log10(mS/m))
(column 98)     Standard deviation for conductivity of layer 12      (log10(mS/m))
(column 99)     Standard deviation for DX     (m)
(column 100)    Standard deviation for DZ     (m)
(column 101)    Standard deviation for receiver coil pitch   (degrees)
(column 102)    Data value for constraint 1   (log10(mS/m))
(column 103)    Data value for constraint 2   (log10(mS/m))
(column 104)    Data value for constraint 3   (log10(mS/m))
(column 105)    Data value for constraint 4   (log10(mS/m))
(column 106)    Data value for constraint 5   (log10(mS/m))
(column 107)    Data value for constraint 6   (log10(mS/m))
(column 108)    Data value for constraint 7   (log10(mS/m))
(column 109)    Data value for constraint 8   (log10(mS/m))
(column 110)    Data value for constraint 9   (log10(mS/m))
(column 111)    Data value for constraint 10  (log10(mS/m))
(column 112)    Standard deviation for constraint 1   (log10(mS/m))
(column 113)    Standard deviation for constraint 2   (log10(mS/m))
(column 114)    Standard deviation for constraint 3   (log10(mS/m))
(column 115)    Standard deviation for constraint 4   (log10(mS/m))
(column 116)    Standard deviation for constraint 5   (log10(mS/m))
(column 117)    Standard deviation for constraint 6   (log10(mS/m))
(column 118)    Standard deviation for constraint 7   (log10(mS/m))
(column 119)    Standard deviation for constraint 8   (log10(mS/m))
(column 120)    Standard deviation for constraint 9   (log10(mS/m))
(column 121)    Standard deviation for constraint 10  (log10(mS/m))
(column 122)    Constraint     1      coefficient for        parameter 1
(column 123)    Constraint     1      coefficient for        parameter 2
(column 124)    Constraint     1      coefficient for        parameter 3
(column 125)    Constraint     1      coefficient for        parameter 4
(column 126)    Constraint     1      coefficient for        parameter 5
(column 127)    Constraint     1      coefficient for        parameter 6
(column 128)    Constraint     1      coefficient for        parameter 7
(column 129)    Constraint     1      coefficient for        parameter 8
(column 130)    Constraint     1      coefficient for        parameter 9
(column 131)    Constraint     1      coefficient for        parameter 10
(column 132)    Constraint     1      coefficient for        parameter 11
(column 133)    Constraint     1      coefficient for        parameter 12
(column 134)    Constraint     1      coefficient for        parameter 13
(column 135)    Constraint     1      coefficient for        parameter 14
(column 136)    Constraint     1      coefficient for        parameter 15
(column 137)    Constraint     2      coefficient for        parameter 1
(column 138)    Constraint     2      coefficient for        parameter 2
(column 139)    Constraint     2      coefficient for        parameter 3
(column 140)    Constraint     2      coefficient for        parameter 4
(column 141)    Constraint     2      coefficient for        parameter 5
(column 142)    Constraint     2      coefficient for        parameter 6
(column 143)    Constraint     2      coefficient for        parameter 7
(column 144)    Constraint     2      coefficient for        parameter 8
(column 145)    Constraint     2      coefficient for        parameter 9
(column 146)    Constraint     2      coefficient for        parameter 10
(column 147)    Constraint     2      coefficient for        parameter 11
(column 148)    Constraint     2      coefficient for        parameter 12
(column 149)    Constraint     2      coefficient for        parameter 13
(column 150)    Constraint     2      coefficient for        parameter 14
(column 151)    Constraint     2      coefficient for        parameter 15
(column 152)    Constraint     3      coefficient for        parameter 1
(column 153)    Constraint     3      coefficient for        parameter 2
(column 154)    Constraint     3      coefficient for        parameter 3
(column 155)    Constraint     3      coefficient for        parameter 4
(column 156)    Constraint     3      coefficient for        parameter 5
(column 157)    Constraint     3      coefficient for        parameter 6
(column 158)    Constraint     3      coefficient for        parameter 7
(column 159)    Constraint     3      coefficient for        parameter 8
(column 160)    Constraint     3      coefficient for        parameter 9
(column 161)    Constraint     3      coefficient for        parameter 10
(column 162)    Constraint     3      coefficient for        parameter 11
(column 163)    Constraint     3      coefficient for        parameter 12
(column 164)    Constraint     3      coefficient for        parameter 13
(column 165)    Constraint     3      coefficient for        parameter 14
(column 166)    Constraint     3      coefficient for        parameter 15
(column 167)    Constraint     4      coefficient for        parameter 1
(column 168)    Constraint     4      coefficient for        parameter 2
(column 169)    Constraint     4      coefficient for        parameter 3
(column 170)    Constraint     4      coefficient for        parameter 4
(column 171)    Constraint     4      coefficient for        parameter 5
(column 172)    Constraint     4      coefficient for        parameter 6
```

(column 173)	Constraint	4	coefficient for	parameter 7
(column 174)	Constraint	4	coefficient for	parameter 8
(column 175)	Constraint	4	coefficient for	parameter 9
(column 176)	Constraint	4	coefficient for	parameter 10
(column 177)	Constraint	4	coefficient for	parameter 11
(column 178)	Constraint	4	coefficient for	parameter 12
(column 179)	Constraint	4	coefficient for	parameter 13
(column 180)	Constraint	4	coefficient for	parameter 14
(column 181)	Constraint	4	coefficient for	parameter 15
(column 182)	Constraint	5	coefficient for	parameter 1
(column 183)	Constraint	5	coefficient for	parameter 2
(column 184)	Constraint	5	coefficient for	parameter 3
(column 185)	Constraint	5	coefficient for	parameter 4
(column 186)	Constraint	5	coefficient for	parameter 5
(column 187)	Constraint	5	coefficient for	parameter 6
(column 188)	Constraint	5	coefficient for	parameter 7
(column 189)	Constraint	5	coefficient for	parameter 8
(column 190)	Constraint	5	coefficient for	parameter 9
(column 191)	Constraint	5	coefficient for	parameter 10
(column 192)	Constraint	5	coefficient for	parameter 11
(column 193)	Constraint	5	coefficient for	parameter 12
(column 194)	Constraint	5	coefficient for	parameter 13
(column 195)	Constraint	5	coefficient for	parameter 14
(column 196)	Constraint	5	coefficient for	parameter 15
(column 197)	Constraint	6	coefficient for	parameter 1
(column 198)	Constraint	6	coefficient for	parameter 2
(column 199)	Constraint	6	coefficient for	parameter 3
(column 200)	Constraint	6	coefficient for	parameter 4
(column 201)	Constraint	6	coefficient for	parameter 5
(column 202)	Constraint	6	coefficient for	parameter 6
(column 203)	Constraint	6	coefficient for	parameter 7
(column 204)	Constraint	6	coefficient for	parameter 8
(column 205)	Constraint	6	coefficient for	parameter 9
(column 206)	Constraint	6	coefficient for	parameter 10
(column 207)	Constraint	6	coefficient for	parameter 11
(column 208)	Constraint	6	coefficient for	parameter 12
(column 209)	Constraint	6	coefficient for	parameter 13
(column 210)	Constraint	6	coefficient for	parameter 14
(column 211)	Constraint	6	coefficient for	parameter 15
(column 212)	Constraint	7	coefficient for	parameter 1
(column 213)	Constraint	7	coefficient for	parameter 2
(column 214)	Constraint	7	coefficient for	parameter 3
(column 215)	Constraint	7	coefficient for	parameter 4
(column 216)	Constraint	7	coefficient for	parameter 5
(column 217)	Constraint	7	coefficient for	parameter 6
(column 218)	Constraint	7	coefficient for	parameter 7
(column 219)	Constraint	7	coefficient for	parameter 8
(column 220)	Constraint	7	coefficient for	parameter 9
(column 221)	Constraint	7	coefficient for	parameter 10
(column 222)	Constraint	7	coefficient for	parameter 11
(column 223)	Constraint	7	coefficient for	parameter 12
(column 224)	Constraint	7	coefficient for	parameter 13
(column 225)	Constraint	7	coefficient for	parameter 14
(column 226)	Constraint	7	coefficient for	parameter 15
(column 227)	Constraint	8	coefficient for	parameter 1
(column 228)	Constraint	8	coefficient for	parameter 2
(column 229)	Constraint	8	coefficient for	parameter 3
(column 230)	Constraint	8	coefficient for	parameter 4
(column 231)	Constraint	8	coefficient for	parameter 5
(column 232)	Constraint	8	coefficient for	parameter 6
(column 233)	Constraint	8	coefficient for	parameter 7
(column 234)	Constraint	8	coefficient for	parameter 8
(column 235)	Constraint	8	coefficient for	parameter 9
(column 236)	Constraint	8	coefficient for	parameter 10
(column 237)	Constraint	8	coefficient for	parameter 11
(column 238)	Constraint	8	coefficient for	parameter 12
(column 239)	Constraint	8	coefficient for	parameter 13
(column 240)	Constraint	8	coefficient for	parameter 14
(column 241)	Constraint	8	coefficient for	parameter 15
(column 242)	Constraint	9	coefficient for	parameter 1
(column 243)	Constraint	9	coefficient for	parameter 2
(column 244)	Constraint	9	coefficient for	parameter 3
(column 245)	Constraint	9	coefficient for	parameter 4
(column 246)	Constraint	9	coefficient for	parameter 5
(column 247)	Constraint	9	coefficient for	parameter 6
(column 248)	Constraint	9	coefficient for	parameter 7
(column 249)	Constraint	9	coefficient for	parameter 8
(column 250)	Constraint	9	coefficient for	parameter 9
(column 251)	Constraint	9	coefficient for	parameter 10
(column 252)	Constraint	9	coefficient for	parameter 11
(column 253)	Constraint	9	coefficient for	parameter 12
(column 254)	Constraint	9	coefficient for	parameter 13
(column 255)	Constraint	9	coefficient for	parameter 14
(column 256)	Constraint	9	coefficient for	parameter 15
(column 257)	Constraint	10	coefficient for	parameter 1
(column 258)	Constraint	10	coefficient for	parameter 2
(column 259)	Constraint	10	coefficient for	parameter 3
(column 260)	Constraint	10	coefficient for	parameter 4
(column 261)	Constraint	10	coefficient for	parameter 5
(column 262)	Constraint	10	coefficient for	parameter 6

(column 263)	Constraint	10	coefficient for	parameter 7
(column 264)	Constraint	10	coefficient for	parameter 8
(column 265)	Constraint	10	coefficient for	parameter 9
(column 266)	Constraint	10	coefficient for	parameter 10
(column 267)	Constraint	10	coefficient for	parameter 11
(column 268)	Constraint	10	coefficient for	parameter 12
(column 269)	Constraint	10	coefficient for	parameter 13
(column 270)	Constraint	10	coefficient for	parameter 14
(column 271)	Constraint	10	coefficient for	parameter 15

Undefined value	-9999
Horizontal datum	GDA94
Projection	MGA55
Vertical datum	AHD

Header for inversion output file

```
Header for file: Inversion_output_file_st_george_sub5.asc
(Inversion output file)

(column 1)      Record number
(column 2)      Flight
(column 3)      Line
(column 4)      Fiducial
(column 5)      Easting (m)
(column 6)      Northing       (m)
(column 7)      Elevation      (m)
(column 8)      Laser altimeter        (m)
(column 9)      Transmitter loop terrain clearance    (m)
(column 10)     Transmitter loop pitch (degrees)
(column 11)     Transmitter loop roll  (degrees)
(column 12)     Solved transmitter loop to receiver coil horizontal separation (DX) (m)
(column 13)     Solved transmitter loop to receiver coil vertical separation (DZ)   (m)
(column 14)     Solved receiver coil pitch    (degrees)
(column 15)     Receiver coil roll     (degrees)
(column 16)     Number of layers
(column 17)     Layer conductivity 1   (mS/m)
(column 18)     Layer conductivity 2   (mS/m)
(column 19)     Layer conductivity 3   (mS/m)
(column 20)     Layer conductivity 4   (mS/m)
(column 21)     Layer conductivity 5   (mS/m)
(column 22)     Layer conductivity 6   (mS/m)
(column 23)     Layer conductivity 7   (mS/m)
(column 24)     Layer conductivity 8   (mS/m)
(column 25)     Layer conductivity 9   (mS/m)
(column 26)     Layer conductivity 10  (mS/m)
(column 27)     Layer conductivity 11  (mS/m)
(column 28)     Layer conductivity 12  (mS/m)
(column 29)     Layer thickness 1      (m)
(column 30)     Layer thickness 2      (m)
(column 31)     Layer thickness 3      (m)
(column 32)     Layer thickness 4      (m)
(column 33)     Layer thickness 5      (m)
(column 34)     Layer thickness 6      (m)
(column 35)     Layer thickness 7      (m)
(column 36)     Layer thickness 8      (m)
(column 37)     Layer thickness 9      (m)
(column 38)     Layer thickness 10     (m)
(column 39)     Layer thickness 11     (m)
(column 40)     Data objective function
(column 41)     Parameter objective function
(column 42)     Number of iterations
(column 43)     Calculated response for X window 1    (fT)
(column 44)     Calculated response for X window 2    (fT)
(column 45)     Calculated response for X window 3    (fT)
(column 46)     Calculated response for X window 4    (fT)
(column 47)     Calculated response for X window 5    (fT)
(column 48)     Calculated response for X window 6    (fT)
(column 49)     Calculated response for X window 7    (fT)
(column 50)     Calculated response for X window 8    (fT)
(column 51)     Calculated response for X window 9    (fT)
(column 52)     Calculated response for X window 10   (fT)
(column 53)     Calculated response for X window 11   (fT)
(column 54)     Calculated response for X window 12   (fT)
(column 55)     Calculated response for X window 13   (fT)
(column 56)     Calculated response for X window 14   (fT)
(column 57)     Calculated response for X window 15   (fT)
(column 58)     Calculated response for Z window 1    (fT)
(column 59)     Calculated response for Z window 2    (fT)
(column 60)     Calculated response for Z window 3    (fT)
(column 61)     Calculated response for Z window 4    (fT)
(column 62)     Calculated response for Z window 5    (fT)
(column 63)     Calculated response for Z window 6    (fT)
(column 64)     Calculated response for Z window 7    (fT)
(column 65)     Calculated response for Z window 8    (fT)
(column 66)     Calculated response for Z window 9    (fT)
(column 67)     Calculated response for Z window 10   (fT)
(column 68)     Calculated response for Z window 11   (fT)
(column 69)     Calculated response for Z window 12   (fT)
(column 70)     Calculated response for Z window 13   (fT)
(column 71)     Calculated response for Z window 14   (fT)
(column 72)     Calculated response for Z window 15   (fT)
(column 73)     Calculated X primary field    (fT)
(column 74)     Calculated Z primary field    (fT)
(column 75)     Supplied DX    (m)
(column 76)     Supplied DZ    (m)
(column 77)     Supplied X primary field      (fT)
(column 78)     Supplied Z primary field      (fT)
(column 79)     Difference between supplied and calculated DX        (m)
(column 80)     Difference between supplied and calculated DZ        (m)
(column 81)     Difference between supplied and calculated X primary field  (fT)
(column 82)     Difference between supplied and calculated Z primary field  (fT)

Undefined value                      -9999
```

Horizontal datum	GDA94
Projection	MGA55
Vertical datum	AHD

Inversion control file

```
Header for file inversion_12_layer_control_file.pc

Control Begin

        Intrepid Dataset = c:\st_george\intrepid\NONHPRG_SUB5
        First Line = 1
        Last Line = 371
        Subsample = 1

        #Intrepid input fields
        Flight Field = flight
        Line Field =   LINE
        Fid Field =    FID
        Easting Field = easting
        Northing Field = northing
        Elevation Field = topography
        Altimeter Field = laser_altimeter
        TX loop pitch Field = TX_loop_pitch_raw
        TX loop roll Field = TX_loop_roll_raw

        #These geometry fields represent the geometry as quoted in the delivered dataset
        TX loop clearance Field = TX_loop_clearance_raw_laser_minus1
        TX RX DX Field = TX_RX_horz_separation_raw
        TX RX DZ Field = TX_RX_vert_separation_raw
        RX pitch Field = RX_pitch_raw
        RX roll Field = RX_roll_raw

        #These X and Z fields represent the ground response plus primary field
        #calculated from the delivered ground response and the quoted geometry
        X Component Field = raw_x_observed
        Z Component Field = raw_z_observed

        #Initial and resultant model fields
        Initial Model Field = lei_12_layer_initial
        Resultant Model Field = lei_12_layer_result
        X Component Forward Model Field = lei_12_layer_X_forwardmodel
        Z Component Forward Model Field = lei_12_layer_Z_forwardmodel

        #Conductivity standard deviation field
        Log10 Conductivity Stddev Field = lei_12_layer_conductivity_stddev

        #Constraint Data and Stddev Fields
        Constraint Data Field = constraintdata
        Constraint Data Stddev Field = constraintdata_stddev

        #Inversion Options
        Use X Component = Yes
        Use Z Component = Yes
        Solve Layer Thickness = No
        Solve TX_Height = No
        Solve TX_RX_DX = Yes
        Solve TX_RX_DZ = Yes
        Solve RX_Pitch = Yes
        Solve RX_Roll = No

        #Termination Conditions
        Maximum Iterations = 20
        Minimum Data Objective = 5.0
        Minimum Data Objective Improvement = 0.5 #In percent

        Layers = 12
        Windows = 15

        #Smoothness
        Constraints = 10
        #1 row for each constraint, 1 column for each parameter
        ConstraintCoefficients Begin
                                    -1, 2,-1, 0, 0, 0, 0, 0, 0, 0, 0, 0,0,0
                                     0,-1, 2,-1, 0, 0, 0, 0, 0, 0, 0, 0,0,0
                                     0, 0,-1, 2,-1, 0, 0, 0, 0, 0, 0, 0,0,0
                                     0, 0, 0,-1, 2,-1, 0, 0, 0, 0, 0, 0,0,0
                                     0, 0, 0, 0,-1, 2,-1, 0, 0, 0, 0, 0,0,0
                                     0, 0, 0, 0, 0,-1, 2,-1, 0, 0, 0, 0,0,0
                                     0, 0, 0, 0, 0, 0,-1, 2,-1, 0, 0, 0,0,0
                                     0, 0, 0, 0, 0, 0, 0,-1, 2,-1, 0, 0,0,0
                                     0, 0, 0, 0, 0, 0, 0, 0,-1, 2,-1, 0,0,0
                                     0, 0, 0, 0, 0, 0, 0, 0, 0,-1, 2,-1, 0,0,0
        ConstraintCoefficients End

        TX_Height Stddev = 2.0
        TX_RX_DX Stddev =  2.0
        TX_RX_DZ Stddev =  2.0
        RX_Pitch Stddev =  2.0
        RX_Roll Stddev =  2.0

Control End
```

Header for manually levelled, point located inversion model data

```
Header for file : st_george_sub5_LEI_lev.asc

(column 1) Flight
(column 2) Line
(column 3) Fiducial
(column 4) East (m)
(column 5) North (m)
(column 6) Surface elevation (m AHD)
(column 7) Number of layers
(column 8) Conductivity for layer 1 (mS/m)
(column 9) Conductivity for layer 2 (mS/m)
(column 10) Conductivity for layer 3 (mS/m)
(column 11) Conductivity for layer 4 (mS/m)
(column 12) Conductivity for layer 5 (mS/m)
(column 13) Conductivity for layer 6 (mS/m)
(column 14) Conductivity for layer 7 (mS/m)
(column 15) Conductivity for layer 8 (mS/m)
(column 16) Conductivity for layer 9 (mS/m)
(column 17) Conductivity for layer 10 (mS/m)
(column 18) Conductivity for layer 11 (mS/m)
(column 19) Conductivity for layer 12 (mS/m)
(column 20) Layer thickness for layer 1 (m)
(column 21) Layer thickness for layer 2 (m)
(column 22) Layer thickness for layer 3 (m)
(column 23) Layer thickness for layer 4 (m)
(column 24) Layer thickness for layer 5 (m)
(column 25) Layer thickness for layer 6 (m)
(column 26) Layer thickness for layer 7 (m)
(column 27) Layer thickness for layer 8 (m)
(column 28) Layer thickness for layer 9 (m)
(column 29) Layer thickness for layer 10 (m)
(column 30) Layer thickness for layer 11 (m)

Undefined value    : -9999
Horizontal datum   : GDA94
Projection         : MGA55
```

Header for manually levelled and micro-levelled, point located inversion model data

```
Header for file : st_george_sub5_LEI_mlev.asc

(column 1) Flight
(column 2) Line
(column 3) Fiducial
(column 4) East (m)
(column 5) North (m)
(column 6) Surface elevation (m AHD)
(column 7) Number of layers
(column 8) Conductivity for layer 1 (mS/m)
(column 9) Conductivity for layer 2 (mS/m)
(column 10) Conductivity for layer 3 (mS/m)
(column 11) Conductivity for layer 4 (mS/m)
(column 12) Conductivity for layer 5 (mS/m)
(column 13) Conductivity for layer 6 (mS/m)
(column 14) Conductivity for layer 7 (mS/m)
(column 15) Conductivity for layer 8 (mS/m)
(column 16) Conductivity for layer 9 (mS/m)
(column 17) Conductivity for layer 10 (mS/m)
(column 18) Conductivity for layer 11 (mS/m)
(column 19) Conductivity for layer 12 (mS/m)
(column 20) Layer thickness for layer 1 (m)
(column 21) Layer thickness for layer 2 (m)
(column 22) Layer thickness for layer 3 (m)
(column 23) Layer thickness for layer 4 (m)
(column 24) Layer thickness for layer 5 (m)
(column 25) Layer thickness for layer 6 (m)
(column 26) Layer thickness for layer 7 (m)
(column 27) Layer thickness for layer 8 (m)
(column 28) Layer thickness for layer 9 (m)
(column 29) Layer thickness for layer 10 (m)
(column 30) Layer thickness for layer 11 (m)

Undefined value    : -9999
Horizontal datum   : GDA94
Projection         : MGA55
```

Header for point located re-sampled conductivity data

```
Header for file : st_george_sub5_LEI_mlev_resampled_cond.asc

(column 1) Flight
(column 2) Line
(column 3) Fiducial
(column 4) East (m)
(column 5) North (m)
(column 6) Surface elevation (m AHD)
(column 7) Number of layers
(column 8) Conductivity for interval 1 (mS/m), 0 to -5 m
(column 9) Conductivity for interval 2 (mS/m), -5 to -10 m
(column 10) Conductivity for interval 3 (mS/m), -10 to -15 m
(column 11) Conductivity for interval 4 (mS/m), -15 to -20 m
(column 12) Conductivity for interval 5 (mS/m), -20 to -25 m
(column 13) Conductivity for interval 6 (mS/m), -25 to -30 m
(column 14) Conductivity for interval 7 (mS/m), -30 to -35 m
(column 15) Conductivity for interval 8 (mS/m), -35 to -40 m
(column 16) Conductivity for interval 9 (mS/m), -40 to -45 m
(column 17) Conductivity for interval 10 (mS/m), -45 to -50 m
(column 18) Conductivity for interval 11 (mS/m), -50 to -55 m
(column 19) Conductivity for interval 12 (mS/m), -55 to -60 m
(column 20) Conductivity for interval 13 (mS/m), -60 to -65 m
(column 21) Conductivity for interval 14 (mS/m), -65 to -70 m
(column 22) Conductivity for interval 15 (mS/m), -70 to -75 m
(column 23) Conductivity for interval 16 (mS/m), -75 to -80 m
(column 24) Conductivity for interval 17 (mS/m), -80 to -85 m
(column 25) Conductivity for interval 18 (mS/m), -85 to -90 m
(column 26) Conductivity for interval 19 (mS/m), -90 to -95 m
(column 27) Conductivity for interval 20 (mS/m), -95 to -100 m
(column 28) Conductivity for interval 21 (mS/m), -100 to -105 m
(column 29) Conductivity for interval 22 (mS/m), -105 to -110 m
(column 30) Conductivity for interval 23 (mS/m), -110 to -115 m
(column 31) Conductivity for interval 24 (mS/m), -115 to -120 m
(column 32) Conductivity for interval 25 (mS/m), -120 to -125 m
(column 33) Conductivity for interval 26 (mS/m), -125 to -130 m
(column 34) Conductivity for interval 27 (mS/m), -130 to -135 m
(column 35) Conductivity for interval 28 (mS/m), -135 to -140 m
(column 36) Conductivity for interval 29 (mS/m), -140 to -145 m
(column 37) Conductivity for interval 30 (mS/m), -145 to -150 m
(column 38) Conductivity for interval 31 (mS/m), -150 to -155 m
(column 39) Conductivity for interval 32 (mS/m), -155 to -160 m
(column 40) Conductivity for interval 33 (mS/m), -160 to -165 m
(column 41) Conductivity for interval 34 (mS/m), -165 to -170 m
(column 42) Conductivity for interval 35 (mS/m), -170 to -175 m
(column 43) Conductivity for interval 36 (mS/m), -175 to -180 m
(column 44) Conductivity for interval 37 (mS/m), -180 to -185 m
(column 45) Conductivity for interval 38 (mS/m), -185 to -190 m
(column 46) Conductivity for interval 39 (mS/m), -190 to -195 m
(column 47) Conductivity for interval 40 (mS/m), -195 to -200 m
(column 48) Conductivity for interval 41 (mS/m), -200 to -205 m
(column 49) Layer thickness for interval 1 (m), 0 to -5 m
(column 50) Layer thickness for interval 2 (m), -5 to -10 m
(column 51) Layer thickness for interval 3 (m), -10 to -15 m
(column 52) Layer thickness for interval 4 (m), -15 to -20 m
(column 53) Layer thickness for interval 5 (m), -20 to -25 m
(column 54) Layer thickness for interval 6 (m), -25 to -30 m
(column 55) Layer thickness for interval 7 (m), -30 to -35 m
(column 56) Layer thickness for interval 8 (m), -35 to -40 m
(column 57) Layer thickness for interval 9 (m), -40 to -45 m
(column 58) Layer thickness for interval 10 (m), -45 to -50 m
(column 59) Layer thickness for interval 11 (m), -50 to -55 m
(column 60) Layer thickness for interval 12 (m), -55 to -60 m
(column 61) Layer thickness for interval 13 (m), -60 to -65 m
(column 62) Layer thickness for interval 14 (m), -65 to -70 m
(column 63) Layer thickness for interval 15 (m), -70 to -75 m
(column 64) Layer thickness for interval 16 (m), -75 to -80 m
(column 65) Layer thickness for interval 17 (m), -80 to -85 m
(column 66) Layer thickness for interval 18 (m), -85 to -90 m
(column 67) Layer thickness for interval 19 (m), -90 to -95 m
(column 68) Layer thickness for interval 20 (m), -95 to -100 m
(column 69) Layer thickness for interval 21 (m), -100 to -105 m
(column 70) Layer thickness for interval 22 (m), -105 to -110 m
(column 71) Layer thickness for interval 23 (m), -110 to -115 m
(column 72) Layer thickness for interval 24 (m), -115 to -120 m
(column 73) Layer thickness for interval 25 (m), -120 to -125 m
(column 74) Layer thickness for interval 26 (m), -125 to -130 m
(column 75) Layer thickness for interval 27 (m), -130 to -135 m
```

(column 76) Layer thickness for interval 28 (m), -135 to -140 m
(column 77) Layer thickness for interval 29 (m), -140 to -145 m
(column 78) Layer thickness for interval 30 (m), -145 to -150 m
(column 79) Layer thickness for interval 31 (m), -150 to -155 m
(column 80) Layer thickness for interval 32 (m), -155 to -160 m
(column 81) Layer thickness for interval 33 (m), -160 to -165 m
(column 82) Layer thickness for interval 34 (m), -165 to -170 m
(column 83) Layer thickness for interval 35 (m), -170 to -175 m
(column 84) Layer thickness for interval 36 (m), -175 to -180 m
(column 85) Layer thickness for interval 37 (m), -180 to -185 m
(column 86) Layer thickness for interval 38 (m), -185 to -190 m
(column 87) Layer thickness for interval 39 (m), -190 to -195 m
(column 88) Layer thickness for interval 40 (m), -195 to -200 m

Undefined value : -9999
Horizontal datum : GDA94
Projection : MGA55

Header for point located re-sampled cumulative conductance data

```
Header for file : st_george_sub5_LEI_mlev_resampled_cum_cond.asc

(column 1) Flight
(column 2) Line
(column 3) Fiducial
(column 4) East (m)
(column 5) North (m)
(column 6) Surface elevation (m AHD)
(column 7) Number of layers
(column 8) Cumulative conductance to the base of interval 1 (S), 0 to -5 m
(column 9) Cumulative conductance to the base of interval 2 (S), -5 to -10 m
(column 10) Cumulative conductance to the base of interval 3 (S), -10 to -15 m
(column 11) Cumulative conductance to the base of interval 4 (S), -15 to -20 m
(column 12) Cumulative conductance to the base of interval 5 (S), -20 to -25 m
(column 13) Cumulative conductance to the base of interval 6 (S), -25 to -30 m
(column 14) Cumulative conductance to the base of interval 7 (S), -30 to -35 m
(column 15) Cumulative conductance to the base of interval 8 (S), -35 to -40 m
(column 16) Cumulative conductance to the base of interval 9 (S), -40 to -45 m
(column 17) Cumulative conductance to the base of interval 10 (S), -45 to -50 m
(column 18) Cumulative conductance to the base of interval 11 (S), -50 to -55 m
(column 19) Cumulative conductance to the base of interval 12 (S), -55 to -60 m
(column 20) Cumulative conductance to the base of interval 13 (S), -60 to -65 m
(column 21) Cumulative conductance to the base of interval 14 (S), -65 to -70 m
(column 22) Cumulative conductance to the base of interval 15 (S), -70 to -75 m
(column 23) Cumulative conductance to the base of interval 16 (S), -75 to -80 m
(column 24) Cumulative conductance to the base of interval 17 (S), -80 to -85 m
(column 25) Cumulative conductance to the base of interval 18 (S), -85 to -90 m
(column 26) Cumulative conductance to the base of interval 19 (S), -90 to -95 m
(column 27) Cumulative conductance to the base of interval 20 (S), -95 to -100 m
(column 28) Cumulative conductance to the base of interval 21 (S), -100 to -105 m
(column 29) Cumulative conductance to the base of interval 22 (S), -105 to -110 m
(column 30) Cumulative conductance to the base of interval 23 (S), -110 to -115 m
(column 31) Cumulative conductance to the base of interval 24 (S), -115 to -120 m
(column 32) Cumulative conductance to the base of interval 25 (S), -120 to -125 m
(column 33) Cumulative conductance to the base of interval 26 (S), -125 to -130 m
(column 34) Cumulative conductance to the base of interval 27 (S), -130 to -135 m
(column 35) Cumulative conductance to the base of interval 28 (S), -135 to -140 m
(column 36) Cumulative conductance to the base of interval 29 (S), -140 to -145 m
(column 37) Cumulative conductance to the base of interval 30 (S), -145 to -150 m
(column 38) Cumulative conductance to the base of interval 31 (S), -150 to -155 m
(column 39) Cumulative conductance to the base of interval 32 (S), -155 to -160 m
(column 40) Cumulative conductance to the base of interval 33 (S), -160 to -165 m
(column 41) Cumulative conductance to the base of interval 34 (S), -165 to -170 m
(column 42) Cumulative conductance to the base of interval 35 (S), -170 to -175 m
(column 43) Cumulative conductance to the base of interval 36 (S), -175 to -180 m
(column 44) Cumulative conductance to the base of interval 37 (S), -180 to -185 m
(column 45) Cumulative conductance to the base of interval 38 (S), -185 to -190 m
(column 46) Cumulative conductance to the base of interval 39 (S), -190 to -195 m
(column 47) Cumulative conductance to the base of interval 40 (S), -195 to -200 m
(column 48) Cumulative conductance to the base of interval 41 (S), -200 to -205 m
(column 49) Layer thickness for interval 1 (m), 0 to -5 m
(column 50) Layer thickness for interval 2 (m), -5 to -10 m
(column 51) Layer thickness for interval 3 (m), -10 to -15 m
(column 52) Layer thickness for interval 4 (m), -15 to -20 m
(column 53) Layer thickness for interval 5 (m), -20 to -25 m
(column 54) Layer thickness for interval 6 (m), -25 to -30 m
(column 55) Layer thickness for interval 7 (m), -30 to -35 m
(column 56) Layer thickness for interval 8 (m), -35 to -40 m
(column 57) Layer thickness for interval 9 (m), -40 to -45 m
(column 58) Layer thickness for interval 10 (m), -45 to -50 m
(column 59) Layer thickness for interval 11 (m), -50 to -55 m
(column 60) Layer thickness for interval 12 (m), -55 to -60 m
(column 61) Layer thickness for interval 13 (m), -60 to -65 m
(column 62) Layer thickness for interval 14 (m), -65 to -70 m
(column 63) Layer thickness for interval 15 (m), -70 to -75 m
(column 64) Layer thickness for interval 16 (m), -75 to -80 m
(column 65) Layer thickness for interval 17 (m), -80 to -85 m
(column 66) Layer thickness for interval 18 (m), -85 to -90 m
(column 67) Layer thickness for interval 19 (m), -90 to -95 m
(column 68) Layer thickness for interval 20 (m), -95 to -100 m
(column 69) Layer thickness for interval 21 (m), -100 to -105 m
(column 70) Layer thickness for interval 22 (m), -105 to -110 m
(column 71) Layer thickness for interval 23 (m), -110 to -115 m
(column 72) Layer thickness for interval 24 (m), -115 to -120 m
(column 73) Layer thickness for interval 25 (m), -120 to -125 m
(column 74) Layer thickness for interval 26 (m), -125 to -130 m
(column 75) Layer thickness for interval 27 (m), -130 to -135 m
```

(column 76) Layer thickness for interval 28 (m), -135 to -140 m
(column 77) Layer thickness for interval 29 (m), -140 to -145 m
(column 78) Layer thickness for interval 30 (m), -145 to -150 m
(column 79) Layer thickness for interval 31 (m), -150 to -155 m
(column 80) Layer thickness for interval 32 (m), -155 to -160 m
(column 81) Layer thickness for interval 33 (m), -160 to -165 m
(column 82) Layer thickness for interval 34 (m), -165 to -170 m
(column 83) Layer thickness for interval 35 (m), -170 to -175 m
(column 84) Layer thickness for interval 36 (m), -175 to -180 m
(column 85) Layer thickness for interval 37 (m), -180 to -185 m
(column 86) Layer thickness for interval 38 (m), -185 to -190 m
(column 87) Layer thickness for interval 39 (m), -190 to -195 m
(column 88) Layer thickness for interval 40 (m), -195 to -200 m

Undefined value : -9999
Horizontal datum : GDA94
Projection : MGA55

Appendix 2. Borehole metadata

Bore	East m	North m	Elevation m	Inclination degrees	Declination degrees	TD m	Top_Klgc m	Top_Klgc_F m	Cond_log_flag N/A	Elev_flag N/A	Elev_AEM m	Elev_9" m
24	605423	6904962	212.6	90	0	-9999	133	133	0	2	-9999.0	212.6
55	631313	6896595	206.5	90	0	-9999	-9997	125	0	1	206.5	207.9
64	596742	6858027	174.1	90	0	-9999	205	-9997	0	1	174.1	177.6
89	636782	6921611	223.4	90	0	-9999	-9997	144	0	2	-9999.0	223.4
106	674066	6880480	191.9	90	0	-9999	21	61	0	1	191.9	188.5
133	708235	6862365	221.6	90	0	-9999	55	79	0	1	221.6	215.7
147	603135	6894471	200.1	90	0	-9999	103	130	0	2	-9999.0	200.1
397	655693	6897814	199.3	90	0	-9999	14	63	0	1	199.3	196.2
2414	643838	6856222	183.1	90	0	-9999	36	-9998	0	1	183.1	184.3
4042	624376	6817329	164.8	90	0	-9999	19	88	0	1	164.8	168.6
4401	675590	6891565	197.1	90	0	-9999	53	-9998	0	1	197.1	194.2
4513	679019	6922931	248.5	90	0	-9999	1	44	0	2	-9999.0	248.5
4918	619948	6877230	191.6	90	0	-9999	-9997	92	0	1	191.6	190.6
4920	589131	6873966	187.1	90	0	-9999	54	102	0	2	-9999.0	187.1
4921	610168	6855419	175.8	90	0	-9999	179	-9998	0	1	175.8	177.0
5335	608015	6935283	231.7	90	0	-9999	45	84	0	2	-9999.0	231.7
5530	597923	6934670	229.3	90	0	-9999	110	-9998	0	2	-9999.0	229.3
6736	639790	6950238	235.2	90	0	-9999	70	70	0	2	-9999.0	235.2
8906	682053	6961375	232.4	90	0	-9999	-9998	43	0	2	-9999.0	232.4
9916	580495	6958193	242.4	90	0	-9999	8	8	0	2	-9999.0	242.4
9961	579386	6851704	166.3	90	0	-9999	-9996	-9997	0	2	-9999.0	166.3
11020	653209	6929241	218.3	90	0	-9999	-9999	-9997	0	1	218.3	216.9
12293	617352	6892390	199.3	90	0	-9999	-9996	-9997	0	1	199.3	200.8
12332	621216	6892811	202.3	90	0	-9999	-9997	-9997	0	1	202.3	203.4
12348	609122	6956805	259.5	90	0	-9999	85	106	0	2	-9999.0	259.5
12448	651023	6899676	203.8	90	0	-9999	15	82	0	1	203.8	206.7
12449	651004	6899573	204.0	90	0	-9999	-9997	20	0	1	204.0	206.5
12479	638391	6894519	199.4	90	0	-9999	-9997	-9997	0	1	199.4	198.2
12480	636647	6891370	197.9	90	0	-9999	-9996	-9997	0	1	197.9	198.2
12594	628972	6824998	168.7	90	0	-9999	23	-9997	0	1	168.7	165.3

Bore	East	North	Elevation	Inclination	Declination	TD	Top_Klgc	Top_Klgc_F	Cond_log_flag	Elev_flag	Elev_AEM	Elev_9"
	m	m	m	degrees	degrees	m	m	m	N/A	N/A	m	m
12662	597151	6871438	182.6	90	0	-9999	-9997	-9996	0	1	182.6	186.3
12663	593750	6868181	179.6	90	0	-9999	52	-9997	0	1	179.6	181.2
12678	636696	6870698	186.4	90	0	-9999	-9996	-9997	0	1	186.4	180.8
12679	638866	6876072	182.9	90	0	-9999	43	-9997	0	1	182.9	182.2
12690	633093	6871369	188.5	90	0	-9999	28	-9997	0	1	188.5	188.4
12708	632123	6847249	177.1	90	0	-9999	-9996	-9997	0	1	177.1	180.1
12709	634369	6847183	177.7	90	0	-9999	35	62	0	1	177.7	179.8
12710	632895	6852021	178.9	90	0	-9999	11	66	0	1	178.9	183.4
12726	594899	6864004	178.3	90	0	-9999	-9996	-9997	0	1	178.3	177.0
12752	580375	6861220	177.5	90	0	-9999	58	-9997	0	2	-9999.0	177.5
12754	598946	6864925	180.5	90	0	-9999	-9996	-9997	0	1	180.5	182.4
12757	583130	6863483	180.1	90	0	-9999	62	-9997	0	2	-9999.0	180.1
12758	583648	6862054	178.5	90	0	-9999	56	-9997	0	1	178.5	180.4
12871	626066	6901473	207.1	90	0	-9999	-9996	-9997	0	1	207.1	209.0
12878	619369	6883442	196.1	90	0	-9999	-9996	-9997	0	1	196.1	194.2
12932	611660	6817471	164.1	90	0	-9999	-9996	-9997	0	2	-9999.0	164.1
12954	600205	6869596	181.6	90	0	-9999	61	-9996	0	1	181.6	186.2
12980	639573	6874913	184.8	90	0	-9999	-9996	-9997	0	1	184.8	183.1
13092	657152	6897737	200.0	90	0	-9999	49	49	0	1	200.0	200.4
13331	607573	6865378	180.5	90	0	-9999	-9997	118	0	1	180.5	185.3
13464	648686	6898418	200.3	90	0	-9999	-9996	-9997	0	1	200.3	199.2
13470	665189	6871733	187.4	90	0	-9999	-9997	69	0	1	187.4	188.7
13613	641268	6897323	200.6	90	0	-9999	37	100	0	1	200.6	198.6
13614	637117	6877086	190.8	90	0	-9999	-9996	-9997	0	1	190.8	189.8
13638	632527	6867574	186.3	90	0	-9999	-9996	-9997	0	1	186.3	190.0
13639	640043	6878641	186.4	90	0	-9999	32	-9997	0	1	186.4	184.0
13700	637049	6874675	189.9	90	0	-9999	36	-9997	0	1	189.9	185.0
13701	634804	6853136	179.6	90	0	-9999	23	-9997	0	1	179.6	184.1
13702	639070	6849135	179.1	90	0	-9999	24	-9997	0	1	179.1	181.7
13703	656061	6848519	181.1	90	0	-9999	-9998	67	0	1	181.1	184.0
13760	649285	6898458	203.0	90	0	-9999	-9996	-9997	0	1	203.0	203.0
13814	656680	6925159	213.4	90	0	-9999	-9996	-9997	0	1	213.4	212.6
13820	647738	6815874	162.7	90	0	-9999	44	101	0	2	-9999.0	162.7
13865	639983	6878125	187.9	90	0	-9999	30	-9997	0	1	187.9	183.7

Bore	East	North	Elevation	Inclination	Declination	TD	Top_Klgc	Top_Klgc_F	Cond_log_flag	Elev_flag	Elev_AEM	Elev_9"
	m	m	m	degrees	degrees	m	m	m	N/A	N/A	m	m
14329	631896	6863307	184.2	90	0	-9999	-9996	-9997	0	1	184.2	188.1
14712	673224	6893043	198.1	90	0	-9999	17	81	0	1	198.1	196.6
14868	585994	6861416	176.4	90	0	-9999	-9996	-9997	0	1	176.4	178.1
15473	581354	6852199	172.5	90	0	-9999	-9997	94	0	2	-9999.0	172.5
15841	691685	6879911	193.4	90	0	-9999	-9996	-9997	0	1	193.4	193.1
16247	601654	6881595	189.3	90	0	-9999	-9996	-9997	0	1	189.3	189.8
16256	579953	6859547	173.9	90	0	-9999	-9996	-9997	0	1	173.9	177.0
16258	658885	6931766	216.9	90	0	-9999	-9996	-9997	0	1	216.9	215.8
16259	662082	6930713	214.0	90	0	-9999	-9996	-9997	0	1	214.0	213.7
16278	659464	6849442	182.5	90	0	-9999	43	93	0	1	182.5	181.4
16311	616842	6822707	167.2	90	0	-9999	-9996	-9997	0	1	167.2	164.2
16323	633160	6854568	179.4	90	0	-9999	46	70	0	1	179.4	183.4
16324	649261	6842841	178.0	90	0	-9999	-9996	-9997	0	1	178.0	179.3
17502	602735	6870342	183.0	90	0	-9999	-9996	-9997	0	1	183.0	187.7
17714	618276	6903963	211.4	90	0	-9999	-9996	-9997	0	2	-9999.0	211.4
17850	647595	6902068	204.1	90	0	-9999	11	53	0	1	204.1	202.9
18363	628528	6824723	168.3	90	0	-9999	-9996	-9997	0	1	168.3	165.0
24635	653531	6936539	222.7	90	0	-9999	-9996	-9997	0	1	222.7	222.9
24636	648247	6935003	230.2	90	0	-9999	-9996	-9997	0	2	-9999.0	230.2
36498	628281	6906029	210.3	90	0	-9999	-9996	-9997	0	1	210.3	212.2
38620	642130	6891981	196.8	90	0	-9999	-9996	-9997	0	1	196.8	195.6
43442	573782	6862486	177.4	90	0	-9999	-9999	-9999	0	2	-9999.0	177.4
43825	640537	6850839	180.1	90	0	-9999	-9996	-9997	0	1	180.1	182.5
49005	655822	6897470	199.8	90	0	-9999	-9996	-9997	0	1	199.8	197.5
49012	632098	6847708	177.5	90	0	-9999	-9998	-9998	0	1	177.5	180.6
49013	633692	6847805	177.8	90	0	-9999	-9998	-9998	0	1	177.8	180.0
49030	599273	6868975	179.3	90	0	-9999	-9996	-9997	0	1	179.3	183.1
49032	599655	6866366	181.0	90	0	-9999	-9996	-9997	0	1	181.0	184.0
49033	648740	6866188	186.7	90	0	-9999	-9996	-9997	0	1	186.7	187.4
49034	654773	6860282	185.2	90	0	-9999	42	77	0	1	185.2	184.9
49036	622840	6911679	219.5	90	0	-9999	68	-9997	0	2	-9999.0	219.5
49040	663294	6890796	196.0	90	0	-9999	3	43	0	1	196.0	195.1
49043	635587	6900809	204.6	90	0	-9999	84	-9997	0	1	204.6	202.2
49044	627640	6912341	215.7	90	0	-9999	97	-9996	0	2	-9999.0	215.7

Bore	East m	North m	Elevation m	Inclination degrees	Declination degrees	TD m	Top_Klgc m	Top_Klgc_F m	Cond_log_flag N/A	Elev_flag N/A	Elev_AEM m	Elev_9" m
49046	618801	6898326	206.9	90	0	-9999	78	-9996	0	1	206.9	207.0
49050	633457	6902106	205.6	90	0	-9999	-9996	-9997	0	1	205.6	206.2
49053	589140	6859348	175.7	90	0	-9999	-9996	-9997	0	1	175.7	177.8
49056	646463	6861273	185.8	90	0	-9999	-9996	-9997	0	1	185.8	187.2
49057	646111	6933337	223.7	90	0	-9999	9	68	0	2	-9999.0	223.7
49058	642870	6926713	219.7	90	0	-9999	-9997	-9997	0	1	219.7	224.7
49067	635808	6905039	207.0	90	0	-9999	-9999	-9999	0	1	207.0	205.1
49070	615045	6907314	213.9	90	0	-9999	-9996	-9997	0	2	-9999.0	213.9
49072	638178	6851258	179.6	90	0	-9999	-9996	-9997	0	1	179.6	182.4
49073	639526	6898259	201.4	90	0	-9999	-9999	-9999	0	1	201.4	200.2
49074	638940	6896336	199.6	90	0	-9999	38	82	0	1	199.6	199.3
49075	634769	6898072	202.7	90	0	-9999	53	71	0	1	202.7	204.2
49089	584475	6866477	182.0	90	0	-9999	75	132	0	2	-9999.0	182.0
49145	641584	6891211	196.4	90	0	-9999	-9996	-9997	0	1	196.4	193.6
49199	610947	6862388	176.3	90	0	-9999	-9997	-9996	0	1	176.3	181.0
49200	603162	6868280	182.5	90	0	-9999	87	-9997	0	1	182.5	186.0
49201	639228	6899079	202.6	90	0	-9999	-9996	-9997	0	1	202.6	198.1
49203	636385	6827013	170.7	90	0	-9999	9	52	0	1	170.7	164.7
49210	649321	6924251	217.2	90	0	-9999	-9996	-9997	0	1	217.2	215.4
49211	660002	6935509	217.8	90	0	-9999	-9997	111	0	1	217.8	217.6
49212	609505	6882661	194.0	90	0	-9999	194	194	0	1	194.0	195.4
49213	616741	6904607	212.0	90	0	-9999	94	-9997	0	2	-9999.0	212.0
49215	665244	6904691	202.6	90	0	-9999	1	79	0	1	202.6	201.4
49219	651308	6929500	220.1	90	0	-9999	-9996	-9997	0	1	220.1	217.7
49221	654396	6896182	199.9	90	0	-9999	14	-9997	0	1	199.9	197.7
49222	662358	6888651	195.0	90	0	-9999	21	66	0	1	195.0	193.8
49223	662358	6888651	195.0	90	0	-9999	-9996	-9997	0	1	195.0	193.8
49224	606920	6857682	175.8	90	0	-9999	-9996	-9997	0	1	175.8	178.9
49225	606372	6860237	176.8	90	0	-9999	-9996	-9997	0	1	176.8	181.9
49231	658514	6899707	201.7	90	0	-9999	12	-9996	0	1	201.7	197.0
49232	658395	6899643	201.5	90	0	-9999	12	-9996	0	1	201.5	196.7
49233	619897	6870010	185.6	90	0	-9999	110	110	0	1	185.6	186.9
49243	654592	6894143	197.3	90	0	-9999	24	-9997	0	1	197.3	193.2
49244	633801	6919396	217.6	90	0	-9999	-9996	-9996	0	2	-9999.0	217.6

Bore	East	North	Elevation	Inclination	Declination	TD	Top_Klgc	Top_Klgc_F	Cond_log_flag	Elev_flag	Elev_AEM	Elev_9"
	m	m	m	degrees	degrees	m	m	m	N/A	N/A	m	m
49250	656657	6893303	196.6	90	0	-9999	20	-9997	0	1	196.6	193.5
49252	653856	6896176	198.5	90	0	-9999	-9996	-9997	0	1	198.5	194.4
49253	639718	6900119	202.8	90	0	-9999	-9997	-9997	0	1	202.8	200.0
49254	639866	6901120	203.7	90	0	-9999	43	-9997	0	1	203.7	202.0
49255	639915	6901866	203.9	90	0	-9999	-9996	-9997	0	1	203.9	203.1
49263	639976	6900358	203.1	90	0	-9999	25	69	0	1	203.1	201.0
49266	654051	6896117	198.1	90	0	-9999	-9996	-9997	0	1	198.1	195.4
49274	648244	6901692	203.4	90	0	-9999	77	118	0	1	203.4	202.3
49275	648482	6861549	185.4	90	0	-9999	-9996	-9997	0	1	185.4	186.1
49276	648984	6862295	185.8	90	0	-9999	-9996	-9997	0	1	185.8	185.7
49286	679067	6853892	181.4	90	0	-9999	16	79	0	1	181.4	179.3
49287	654688	6894337	196.8	90	0	-9999	13	58	0	1	196.8	193.6
49296	598968	6880000	189.2	90	0	-9999	66	147	0	1	189.2	191.3
49298	668025	6882085	191.8	90	0	-9999	-9996	-9997	0	1	191.8	194.3
49299	632569	6901190	205.0	90	0	-9999	-9997	-9996	0	1	205.0	208.0
49300	653804	6895458	198.9	90	0	-9999	-9996	-9997	0	1	198.9	193.9
49301	644882	6862744	185.8	90	0	-9999	-9996	-9997	0	1	185.8	185.5
49302	653719	6895561	195.7	90	0	-9999	-9996	-9997	0	1	195.7	193.8
49303	669584	6888940	196.2	90	0	-9999	-9996	-9997	0	1	196.2	196.7
49304	670309	6888366	195.4	90	0	-9999	-9996	-9997	0	1	195.4	196.2
49305	670297	6888172	195.5	90	0	-9999	-9996	-9997	0	1	195.5	196.1
49306	669672	6888956	195.9	90	0	-9999	-9996	-9997	0	1	195.9	196.7
49307	660555	6896137	198.4	90	0	-9999	-9996	-9997	0	1	198.4	198.6
49308	660753	6896251	198.6	90	0	-9999	-9996	-9997	0	1	198.6	198.3
49309	669949	6880931	192.0	90	0	-9999	-9996	-9997	0	1	192.0	192.1
49310	669743	6881370	192.1	90	0	-9999	-9996	-9997	0	1	192.1	192.3
49311	654822	6894870	197.9	90	0	-9999	-9996	-9997	0	1	197.9	195.1
49312	672597	6886125	194.2	90	0	-9999	-9996	-9997	0	1	194.2	194.9
49313	639789	6892113	195.2	90	0	-9999	71	-9997	0	1	195.2	194.2
49314	659490	6901730	200.8	90	0	-9999	10	-9997	0	1	200.8	197.7
49315	632951	6910866	212.0	90	0	-9999	78	-9996	0	1	212.0	210.7
49316	635512	6899696	203.1	90	0	-9999	-9996	-9997	0	1	203.1	202.3
49332	647386	6928385	220.6	90	0	-9999	-9999	-9999	1	1	220.6	220.8
49343	590413	6934064	230.8	90	0	-9999	-9996	-9997	0	2	-9999.0	230.8

Bore	East	North	Elevation	Inclination	Declination	TD	Top_Klgc	Top_Klgc_F	Cond_log_flag	Elev_flag	Elev_AEM	Elev_9"
	m	m	m	degrees	degrees	m	m	m	N/A	N/A	m	m
49353	661362	6901138	201.5	90	0	-9999	12	65	0	1	201.5	199.1
49355	653211	6880280	193.3	90	0	-9999	-9996	-9997	0	1	193.3	192.4
49356	654448	6875973	190.3	90	0	-9999	-9996	-9997	0	1	190.3	191.5
49358	665853	6905506	204.5	90	0	-9999	21	-9996	1	1	204.5	200.5
49372	620423	6836938	171.2	90	0	-9999	-9997	110	0	1	171.2	171.0
49382	635527	6908667	209.0	90	0	-9999	-9997	-9996	0	1	209.0	207.7
49383	635534	6897163	201.4	90	0	-9999	-9996	-9997	0	1	201.4	202.1
49398	634673	6911784	211.4	90	0	-9999	-9996	-9997	0	1	211.4	211.0
49399	631532	6912410	213.1	90	0	-9999	-9996	-9997	0	1	213.1	212.1
49415	658039	6896733	199.6	90	0	-9999	-9996	-9997	0	1	199.6	200.6
49422	645936	6916651	212.7	90	0	-9999	-9997	95	0	1	212.7	214.6
49423	646110	6915738	212.9	90	0	-9999	-9996	-9997	0	1	212.9	212.1
49424	646282	6917386	213.6	90	0	-9999	-9996	-9997	0	1	213.6	214.3
49425	644828	6914714	213.1	90	0	-9999	-9996	-9997	0	1	213.1	215.0
49426	643489	6915270	213.3	90	0	-9999	-9996	-9997	0	1	213.3	214.6
49436	640001	6915056	214.5	90	0	-9999	-9996	-9997	0	1	214.5	215.0
49446	635865	6905482	207.1	90	0	-9999	-9996	-9997	0	1	207.1	205.7
49558	647381	6928384	220.6	90	0	-9999	-9997	134	0	1	220.6	220.8
49579	654766	6923703	212.4	90	0	-9999	-9997	102	0	1	212.4	207.5
49580	654710	6923661	212.4	90	0	-9999	-9997	103	0	1	212.4	207.7
49581	652431	6920845	213.8	90	0	-9999	-9997	75	0	1	213.8	213.9
49582	635397	6910003	210.3	90	0	-9999	-9996	-9997	0	1	210.3	209.8
49583	635809	6905040	207.0	90	0	-9999	-9996	-9997	0	1	207.0	205.1
49584	645817	6916686	212.6	90	0	-9999	-9997	94	1	1	212.6	214.9
49585	645825	6916651	212.4	90	0	-9999	-9997	94	0	1	212.4	214.8
49586	646481	6914961	212.2	90	0	-9999	-9996	69	1	1	212.2	212.8
49587	644604	6918531	213.9	90	0	-9999	-9997	116	1	1	213.9	215.3
49588	644500	6920515	215.6	90	0	-9999	-9996	-9997	0	1	215.6	217.7
49589	646158	6915993	212.7	90	0	-9999	-9999	-9999	1	1	212.7	212.6
49591	644919	6914740	212.8	90	0	-9999	-9997	-9996	0	1	212.8	214.9
49592	645265	6915196	213.0	90	0	-9999	-9997	-9996	1	1	213.0	214.0
49593	644939	6916651	214.2	90	0	-9999	-9997	110	0	1	214.2	213.8
49594	645558	6915657	212.9	90	0	-9999	-9997	-9996	1	1	212.9	212.6
49595	646151	6917921	213.9	90	0	-9999	-9999	-9999	1	1	213.9	214.5

Bore	East m	North m	Elevation m	Inclination degrees	Declination degrees	TD m	Top_Klgc m	Top_Klgc_F m	Cond_log_flag N/A	Elev_flag N/A	Elev_AEM m	Elev_9" m
49596	646240	6917422	213.5	90	0	-9999	-9997	-9996	0	1	213.5	214.4
49597	645582	6917767	213.3	90	0	-9999	-9997	115	1	1	213.3	214.9
49598	646881	6916881	213.6	90	0	-9999	-9997	93	1	1	213.6	212.9
49599	652464	6927539	216.5	90	0	-9999	-9997	123	0	1	216.5	214.7
49600	651498	6926331	217.2	90	0	-9999	-9997	-9997	0	1	217.2	219.8
49601	650809	6924857	216.7	90	0	-9999	-9997	131	0	1	216.7	217.4
49602	651803	6924313	215.1	90	0	-9999	-9996	-9997	1	1	215.1	214.7
49603	653068	6926026	216.7	90	0	-9999	-9996	-9997	1	1	216.7	213.8
49604	652164	6923720	214.2	90	0	-9999	-9996	-9997	0	1	214.2	213.4
49605	649239	6926028	217.9	90	0	-9999	-9997	124	1	1	217.9	219.9
49607	642844	6926616	219.8	90	0	-9999	-9996	-9997	1	1	219.8	224.6
49608	642855	6923533	218.6	90	0	-9999	-9997	127	0	1	218.6	222.7
49609	643688	6922379	219.4	90	0	-9999	-9997	129	1	1	219.4	220.7
49610	644151	6925586	218.3	90	0	-9999	-9997	130	1	1	218.3	221.3
49611	643713	6925668	218.0	90	0	-9999	-9997	135	0	1	218.0	222.3
49612	644189	6926518	219.0	90	0	-9999	-9997	136	1	1	219.0	223.3
49613	643788	6928913	220.3	90	0	-9999	134	134	1	2	-9999.0	220.3
49614	648165	6918359	214.5	90	0	-9999	-9996	-9997	1	1	214.5	213.4
49615	646118	6918391	213.6	90	0	-9999	-9999	-9999	1	1	213.6	214.7
101084	654610	6894092	197.4	90	0	-9999	-9996	-9997	0	1	197.4	193.2
41720021	695350	6873657	192.9	90	0	-9999	4	49	1	1	192.9	194.0
41720022	702933	6872775	193.0	90	0	-9999	2	-9996	1	1	193.0	192.8
41720048	694117	6890502	188.9	90	0	-9999	7	-9996	0	2	-9999.0	188.9
41720053	688587	6861986	200.7	90	0	-9999	2	-9996	1	1	200.7	195.2
41720058	679383	6864527	185.0	90	0	-9999	-9996	-9997	1	1	185.0	183.3
41720059	689099	6896516	202.2	90	0	-9999	67	94	1	2	-9999.0	202.2
41720060	677168	6883812	192.8	90	0	-9999	18	-9997	1	1	192.8	190.1
41720061	667578	6871745	188.6	90	0	-9999	-9996	-9997	1	1	188.6	191.4
41720062	680742	6844314	175.9	90	0	-9999	-9996	-9997	1	2	-9999.0	175.9
41720063	676127	6854728	181.6	90	0	-9999	28	96	1	1	181.6	179.1
41720064	667537	6831639	175.2	90	0	-9999	-9999	-9999	1	2	-9999.0	175.2
41720065	663370	6817321	169.5	90	0	-9999	33	-9996	0	2	-9999.0	169.5
41720067	701480	6870580	199.0	90	0	-9999	1	51	1	1	199.0	189.5
41720068	698276	6871342	191.9	90	0	-9999	10	39	1	1	191.9	188.1

Bore	East	North	Elevation	Inclination	Declination	TD	Top_Klgc	Top_Klgc_F	Cond_log_flag	Elev_flag	Elev_AEM	Elev_9"
	m	m	m	degrees	degrees	m	m	m	N/A	N/A	m	m
41720069	694395	6872270	194.6	90	0	-9999	10	45	1	1	194.6	195.7
42220023	664127	6890355	195.5	90	0	-9999	-9996	-9997	1	1	195.5	195.0
42220025	670495	6889773	195.2	90	0	-9999	-9996	-9997	0	1	195.2	196.9
42220026	660804	6887503	194.6	90	0	-9999	-9996	-9997	1	1	194.6	195.1
42220027	664308	6887635	195.0	90	0	-9999	-9996	-9997	0	1	195.0	195.5
42220029	669895	6886258	195.3	90	0	-9999	-9996	-9997	0	1	195.3	195.3
42220030	660681	6885592	193.6	90	0	-9999	22	-9997	1	1	193.6	195.0
42220031	663891	6885868	194.3	90	0	-9999	-9999	-9999	0	1	194.3	195.0
42220032	665985	6883738	192.5	90	0	-9999	-9996	-9997	1	1	192.5	195.1
42220033	669165	6881968	192.8	90	0	-9999	-9996	-9997	0	1	192.8	192.8
42220034	668962	6878540	193.0	90	0	-9999	-9996	-9997	0	1	193.0	192.5
42220053	672028	6890678	196.2	90	0	-9999	-9996	-9997	0	1	196.2	196.1
42220054	672046	6888573	194.9	90	0	-9999	-9996	-9997	1	1	194.9	195.4
42220055	670199	6884440	193.6	90	0	-9999	-9996	-9997	0	1	193.6	195.0
42220056	657839	6894914	198.6	90	0	-9999	-9996	-9997	1	1	198.6	200.4
42220057	655033	6895916	198.1	90	0	-9999	-9996	-9997	1	1	198.1	198.4
42220064	650869	6898755	202.9	90	0	-9999	21	-9997	0	1	202.9	205.5
42220065	634762	6902406	206.1	90	0	-9999	-9997	-9997	0	1	206.1	205.9
42220065	634752	6902397	206.1	90	0	-9999	-9999	-9999	0	1	206.1	205.9
42220066	634752	6902397	206.1	90	0	-9999	-9997	-9997	1	1	206.1	205.9
42220067	634752	6902397	206.1	90	0	-9999	-9996	-9997	0	1	206.1	205.9
42220068	636552	6914477	213.4	90	0	-9999	-9997	125	1	1	213.4	212.3
42220069	636567	6914419	213.4	90	0	-9999	-9997	-9997	1	1	213.4	212.3
42220070	636567	6914418	213.4	90	0	-9999	-9997	-9997	0	1	213.4	212.3
42220071	627332	6906221	212.2	90	0	-9999	-9997	153	1	1	212.2	211.3
42220072	650332	6888146	193.8	90	0	-9999	18	-9997	1	1	193.8	195.0
42220073	650333	6888129	193.8	90	0	-9999	-9997	-9997	1	1	193.8	195.0
42220074	643131	6894841	198.0	90	0	-9999	33	-9997	1	1	198.0	197.8
42220075	635078	6886235	194.3	90	0	-9999	-9996	-9997	1	1	194.3	195.6
42220076	624896	6879121	193.1	90	0	-9999	-9996	-9997	0	1	193.1	192.8
42220077	615306	6873083	186.1	90	0	-9999	-9997	115	1	1	186.1	185.0
42220078	615314	6873048	186.0	90	0	-9999	-9997	-9997	0	1	186.0	185.0
42220079	633520	6863321	185.2	90	0	-9999	23	-9997	1	1	185.2	182.9
42220080	608933	6906568	210.4	90	0	-9999	85	112	0	2	-9999.0	210.4

Bore	East	North	Elevation	Inclination	Declination	TD	Top_Klgc	Top_Klgc_F	Cond_log_flag	Elev_flag	Elev_AEM	Elev_9"
	m	m	m	degrees	degrees	m	m	m	N/A	N/A	m	m
42220081	608939	6906584	210.4	90	0	-9999	-9997	-9997	0	2	-9999.0	210.4
42220082	630711	6855339	179.1	90	0	-9999	-9996	-9997	1	1	179.1	185.9
42220083	627514	6847371	175.7	90	0	-9999	19	-9997	1	1	175.7	176.4
42220084	623628	6836648	171.9	90	0	-9999	25	-9997	1	1	171.9	170.6
42220085	617673	6835507	172.1	90	0	-9999	-9996	-9997	1	1	172.1	169.8
42220086	614801	6825992	166.9	90	0	-9999	38	-9997	1	1	166.9	166.6
42220087	607448	6844587	169.2	90	0	-9999	-9997	108	1	1	169.2	169.6
42220088	602044	6852156	171.5	90	0	-9999	-9997	122	0	1	171.5	174.5
42220089	602075	6852135	171.4	90	0	-9999	-9997	-9997	1	1	171.4	174.4
42220090	592688	6864548	178.8	90	0	-9999	-9997	165	1	1	178.8	179.6
42220091	582926	6876770	189.2	90	0	-9999	64	-9997	0	2	-9999.0	189.2
42220092	596580	6883965	194.5	90	0	-9999	84	109	0	2	-9999.0	194.5
42220093	611737	6894469	201.6	90	0	-9999	-9997	114	1	2	-9999.0	201.6
42220094	665720	6929866	209.8	90	0	-9999	-9997	103	0	1	209.8	208.4
42220096	668279	6960138	221.4	90	0	-9999	68	70	0	2	-9999.0	221.4
42220097	668280	6960131	221.4	90	0	-9999	-9997	-9997	0	2	-9999.0	221.4
42220132	590955	6851834	169.5	90	0	-9999	72	164	1	1	169.5	173.4
42220133	656770	6912799	208.5	90	0	-9999	4	51	1	1	208.5	207.8
42220134	656770	6912803	208.5	90	0	-9999	-9999	-9999	0	1	208.5	207.8
42220135	638567	6890409	196.2	90	0	-9999	72	110	1	1	196.2	196.4
42220136	630119	6872815	192.3	90	0	-9999	35	70	1	1	192.3	193.6
42220137	646587	6843306	178.6	90	0	-9999	9	52	1	1	178.6	181.3
42220138	614804	6825997	166.9	90	0	-9999	37	85	1	1	166.9	166.6
42220139	612025	6840280	170.2	90	0	-9999	63	98	1	1	170.2	172.3
42220140	643641	6831024	174.6	90	0	-9999	2	55	1	1	174.6	174.3
42220151	668935	6883775	193.5	90	0	-9999	83	89	1	1	193.5	194.6
42220152	668997	6883749	193.3	90	0	-9999	-9999	-9999	1	1	193.3	194.6
42220153	658585	6856670	184.1	90	0	-9999	-9996	-9997	0	1	184.1	183.8
42220154	658492	6856507	183.4	90	0	-9999	-9999	-9999	1	1	183.4	182.4
42220155	647708	6880443	189.0	90	0	-9999	-9999	-9999	1	1	189.0	185.6
42220156	656643	6878980	192.8	90	0	-9999	-9999	-9999	1	1	192.8	194.1
42220157	654190	6832748	174.1	90	0	-9999	-9999	-9999	1	1	174.1	177.1
42220158	640584	6852929	180.7	90	0	-9999	-9999	-9999	1	1	180.7	183.9
42220159	625382	6816284	166.0	90	0	-9999	-9999	-9999	1	1	166.0	169.1

Bore	East	North	Elevation	Inclination	Declination	TD	Top_Klgc	Top_Klgc_F	Cond_log_flag	Elev_flag	Elev_AEM	Elev_9"
	m	m	m	degrees	degrees	m	m	m	N/A	N/A	m	m
42220164	643737	6813486	158.8	90	0	-9999	34	-9996	0	2	-9999.0	158.8
42220165	601018	6814921	162.7	90	0	-9999	-9999	-9999	1	2	-9999.0	162.7
42220172	601711	6835260	166.2	90	0	-9999	-9999	-9999	1	1	166.2	166.1
42220175	585568	6830403	157.1	90	0	-9999	-9997	188	0	2	-9999.0	157.1
42220179	654161	6832748	174.2	90	0	-9999	-9999	-9999	0	1	174.2	177.1
42220180	640661	6853080	180.7	90	0	-9999	-9999	-9999	0	1	180.7	183.8
42220181	656430	6878855	192.9	90	0	-9999	-9999	-9999	0	1	192.9	194.2
42220197	574812	6868207	179.1	90	0	-9999	-9999	-9999	0	2	-9999.0	179.1
42220200	586462	6848585	169.8	90	0	-9999	-9999	-9999	1	2	-9999.0	169.8
42220203	571863	6866841	178.6	90	0	-9999	-9999	-9999	0	2	-9999.0	178.6
42240027	648636	6910381	211.4	90	0	-9999	-9997	-9997	0	1	211.4	213.4
42240028	647750	6913820	210.6	90	0	-9999	-9997	50	0	1	210.6	213.0
42240029	646920	6918338	214.2	90	0	-9999	-9997	121	1	1	214.2	213.9
42240030	646921	6918332	214.2	90	0	-9999	-9997	-9997	0	1	214.2	213.9
42240031	646919	6918336	214.2	90	0	-9999	-9997	-9997	0	1	214.2	213.9
42240032	648355	6923656	215.6	90	0	-9999	-9997	118	1	1	215.6	211.9
42240033	648363	6923647	215.7	90	0	-9999	-9997	-9997	0	1	215.7	211.9
42240034	644544	6928222	220.0	90	0	-9999	-9997	-9997	1	1	220.0	218.1
42240035	644563	6928240	219.7	90	0	-9999	-9997	-9997	0	1	219.7	217.9
42240036	644751	6941037	234.9	90	0	-9999	30	-9997	0	2	-9999.0	234.9
42240037	638811	6946890	237.5	90	0	-9999	-9996	-9997	0	2	-9999.0	237.5
42240038	632401	6954201	237.6	90	0	-9999	10	-9997	0	2	-9999.0	237.6
42240039	630516	6956265	247.3	90	0	-9999	12	-9997	0	2	-9999.0	247.3
42240040	620627	6957568	258.2	90	0	-9999	21	-9997	0	2	-9999.0	258.2
42240043	615726	6953901	253.9	90	0	-9999	22	-9997	0	2	-9999.0	253.9
42240044	617731	6944054	244.7	90	0	-9999	46	-9997	0	2	-9999.0	244.7
42240045	617731	6944054	244.7	90	0	-9999	-9997	-9997	0	2	-9999.0	244.7
42240046	628679	6923059	219.6	90	0	-9999	-9997	90	0	2	-9999.0	219.6
42240047	657162	6920952	210.2	90	0	-9999	-9996	-9997	1	1	210.2	209.1
42240048	652838	6923629	210.8	90	0	-9999	-9997	97	0	1	210.8	209.0
42240049	644569	6932179	220.7	90	0	-9999	-9997	123	0	2	-9999.0	220.7
42240063	652863	6923618	211.5	90	0	-9999	-9997	107	1	1	211.5	209.0
42250001	599648	6940642	235.6	90	0	-9999	-9997	-9997	0	2	-9999.0	235.6
42250002	599648	6940642	235.6	90	0	-9999	-9997	-9997	0	2	-9999.0	235.6

Bore	East m	North m	Elevation m	Inclination degrees	Declination degrees	TD m	Top_Klgc m	Top_Klgc_F m	Cond_log_flag N/A	Elev_flag N/A	Elev_AEM m	Elev_9" m
42250003	599648	6940642	235.6	90	0	-9999	-9997	-9997	0	2	-9999.0	235.6
42250004	587797	6931941	229.1	90	0	-9999	69	-9997	0	2	-9999.0	229.1
42250005	577779	6944692	231.6	90	0	-9999	-9997	-9997	0	2	-9999.0	231.6
42250006	588977	6963309	259.3	90	0	-9999	-9996	-9997	0	2	-9999.0	259.3
42250007	532958	6902350	183.1	90	0	-9999	-9997	-9997	0	2	-9999.0	183.1
42250008	598647	6904481	211.1	90	0	-9999	90	141	0	2	-9999.0	211.1
42250009	573109	6905771	195.8	90	0	-9999	55	-9997	0	2	-9999.0	195.8
42250010	597360	6968972	271.2	90	0	-9999	-9997	-9997	0	2	-9999.0	271.2
49426OBS13	643496	6915279	213.3	90	0	-9999	-9999	-9999	1	1	213.3	214.6
49588OBS15	644576	6920629	215.8	90	0	-9999	-9999	-9999	1	1	215.8	217.7
49591OBS12	644923	6914742	212.8	90	0	-9999	-9999	-9999	1	1	212.8	214.9
49596OBS16	646253	6917424	213.5	90	0	-9999	-9999	-9999	1	1	213.5	214.3
BRAESIDE	640065	6892556	196.0	90	0	-9999	-9999	-9999	1	1	196.0	193.5
CARAVANPAR	665673	6905123	204.9	90	0	-9999	-9999	-9999	1	1	204.9	200.8
DEEPWATER2	635395	6910014	210.3	90	0	-9999	-9999	-9999	1	1	210.3	209.8
DEEPWATER4	633878	6907494	209.3	90	0	-9999	-9999	-9999	1	1	209.3	209.4
DEEPWATER5	633870	6906204	208.9	90	0	-9999	-9999	-9999	1	1	208.9	208.6
KOOP#1	626641	6887041	199.1	90	0	-9999	-9999	-9999	0	1	199.1	201.9
KOOP#10	623683	6892182	202.5	90	0	-9999	-9999	-9999	0	1	202.5	200.9
KOOP#11	626385	6891598	202.3	90	0	-9999	-9999	-9999	1	1	202.3	204.0
KOOP#2	628798	6888575	200.7	90	0	-9999	-9999	-9999	0	1	200.7	202.3
KOOP#3	631601	6890873	203.1	90	0	-9999	-9999	-9999	0	1	203.1	204.5
KOOP#4	632518	6893203	204.6	90	0	-9999	-9999	-9999	1	1	204.6	203.0
KOOP#5	628175	6896496	204.7	90	0	-9999	-9999	-9999	0	1	204.7	205.1
KOOP#6	625441	6896419	203.7	90	0	-9999	-9999	-9999	0	1	203.7	205.4
KOOP#7	624287	6895922	203.7	90	0	-9999	-9999	-9999	0	1	203.7	204.0
KOOP#8	628289	6889219	199.3	90	0	-9999	-9999	-9999	0	1	199.3	202.6
KOOP#9	627549	6890145	202.2	90	0	-9999	-9999	-9999	1	1	202.2	203.9
LB01	656770	6912774	208.5	90	0	-9999	8	-9996	1	1	208.5	207.8
LB02	646920	6918327	214.1	90	0	-9999	-9997	-9996	1	1	214.1	213.9
LB03	634750	6902390	206.1	90	0	-9999	-9997	-9996	1	1	206.1	205.9
LB04	592790	6864078	177.3	90	0	-9999	-9997	-9996	1	1	177.3	180.7
LB05	667393	6878738	190.5	90	0	-9999	-9997	-9996	1	1	190.5	193.3
LB06	639267	6846769	178.1	90	0	-9999	6	-9996	1	1	178.1	185.0

Bore	East m	North m	Elevation m	Inclination degrees	Declination degrees	TD m	Top_Klgc m	Top_Klgc_F m	Cond_log_flag N/A	Elev_flag N/A	Elev_AEM m	Elev_9" m
LB07	635004	6886243	194.5	90	0	-9999	-9997	-9996	1	1	194.5	195.7
LB08	601580	6835063	166.2	90	0	-9999	-9997	-9996	1	1	166.2	166.1
LB09	669267	6855008	182.1	90	0	-9999	31	-9996	1	1	182.1	185.0
LB10	703154	6873502	193.2	90	0	-9999	2	-9997	1	1	193.2	193.2
LB11	661531	6911890	208.0	90	0	-9999	9	-9996	0	1	208.0	202.5
LB12	656763	6912792	208.5	90	0	-9999	4	-9996	0	1	208.5	207.8
LB13	659449	6912406	207.9	90	0	-9999	5	-9996	0	1	207.9	205.6
LB14	663813	6908825	204.6	90	0	-9999	-9996	-9997	0	1	204.6	201.0
LB15	655799	6899293	198.4	90	0	-9999	7	-9996	0	1	198.4	196.4
LB16	648868	6909988	212.1	90	0	-9999	4	-9996	0	1	212.1	213.5
LB17	647873	6912418	210.2	90	0	-9999	-9996	-9997	0	1	210.2	209.6
LB18	679453	6863440	185.4	90	0	-9999	7	-9996	0	1	185.4	181.8
LB19	681036	6862293	185.2	90	0	-9999	1	-9996	0	1	185.2	184.6
LB20	683186	6862106	193.1	90	0	-9999	1	-9996	0	1	193.1	188.2
LB21	685278	6861911	196.8	90	0	-9999	1	-9996	0	1	196.8	193.4
LB22	677655	6865825	185.4	90	0	-9999	21	-9996	0	1	185.4	182.0
LB23	643740	6858160	183.7	90	0	-9999	-9996	-9997	0	1	183.7	187.5
LB24	641440	6854863	182.3	90	0	-9999	-9996	-9997	0	1	182.3	183.7
LB25	640587	6852911	180.8	90	0	-9999	-9996	-9997	0	1	180.8	183.9
LB26	626137	6836279	172.7	90	0	-9999	14	-9996	0	1	172.7	169.1
LB27	622873	6836748	172.9	90	0	-9999	-9996	-9997	0	1	172.9	169.8
LB28	616857	6835884	171.4	90	0	-9999	-9996	-9997	0	1	171.4	169.5
LYOLLA1	701319	6877404	193.7	90	0	-9999	-9999	-9999	1	1	193.7	194.3
T-BARPARK	665438	6905060	193.7	90	0	-9999	-9999	-9999	1	1	193.7	194.3

TD = total depth
Top_Klgc = Top of Griman Creek Formation
Top_Klgc_F = Top of fresh Griman Creek Formation
Cond_log_flag = Flag for existence of conductivity log (1=exists)
Elev_flag = Flag for source of elevation data (1=AEM survey DEM, 2=AUSLIG 9 second DEM of Australia)
Elev_AEM = Elevation derived from AEM survey DEM
Elev_9” = Elevation derived from AUSLIG 9 second DEM of Australia

Horizontal datum: GDA94

Horizontal projection: MGA55
Vertical Datum: AHD

Undefined	-9999
Hole not logged (“unknown”)	-9998
Hole logged but horizon not present (“absent”)	-9997
Hole logged but horizon not present (“>”)	-9996

Lithological logging by Ben Maly and Jon Clarke.
Conductivity logging metadata from "bores.csv" (Author - Ross Brodie)
Table compiled by Richard Lane.

Appendix 3. Plots of borehole conductivity logs and mapped horizons

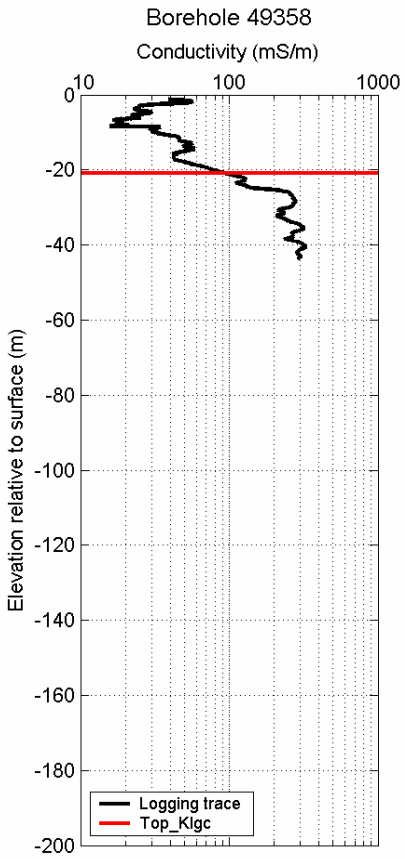
Borehole 49358
Conductivity (mS/m)
10
100
1000
0
-20
-40
-60
-80
-100
-120
-140
-160
-180
-200
Elevation relative to surface (m)
Logging trace
Top_Klgc

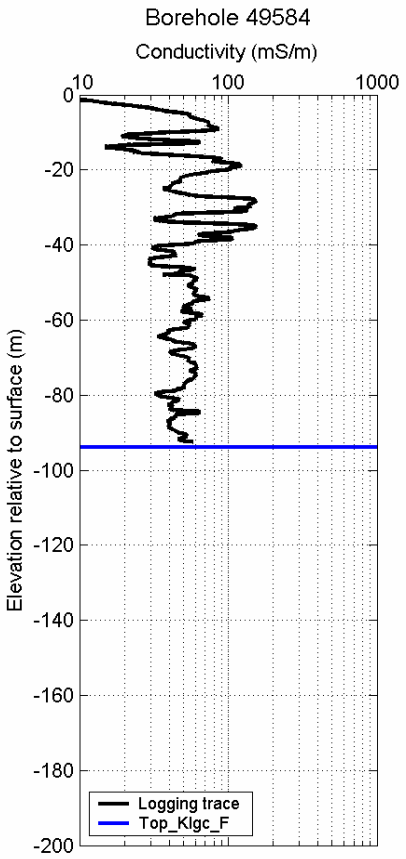
Borehole 49584
Conductivity (mS/m)
10
100
1000
0
-20
-40
-60
-80
-100
-120
-140
-160
-180
-200
Elevation relative to surface (m)
Logging trace
Top_Klgc_F

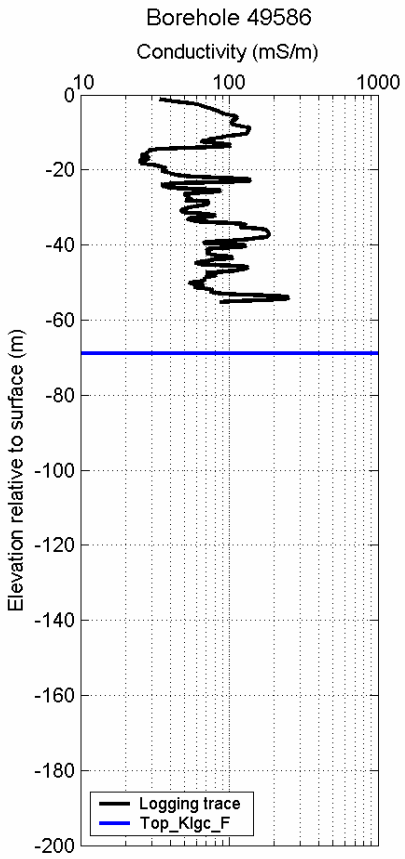
Borehole 49586
Conductivity (mS/m)
10
100
1000
0
-20
-40
-60
-80
-100
-120
-140
-160
-180
-200
Elevation relative to surface (m)
Logging trace
Top_Klgc_F

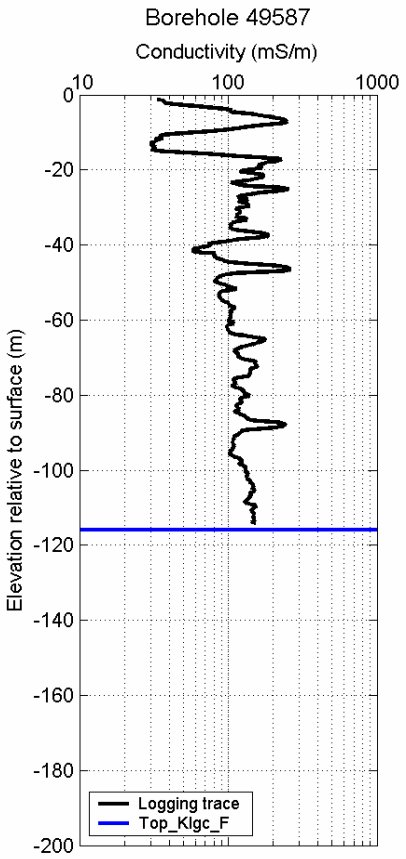
Borehole 49587
Conductivity (mS/m)
10
100
1000
0
-20
-40
-60
-80
-100
-120
-140
-160
-180
-200
Elevation relative to surface (m)
Logging trace
Top_Klgc_F

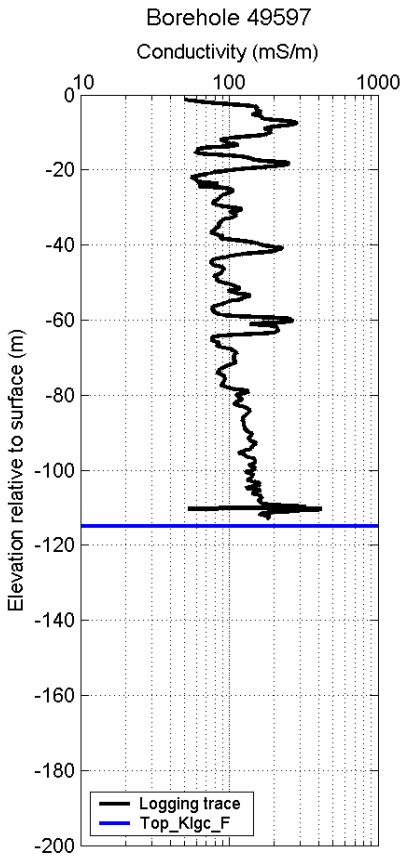
Borehole 49597
Conductivity (mS/m)
10
100
1000
0
-20
-40
-60
-80
-100
-120
-140
-160
-180
-200
Elevation relative to surface (m)
Logging trace
Top_Klgc_F

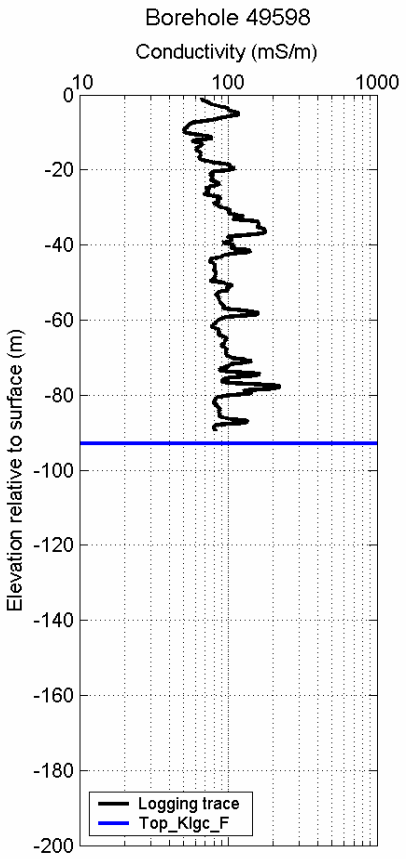
Borehole 49598
Conductivity (mS/m)
10
100
1000
0
-20
-40
-60
-80
-100
-120
-140
-160
-180
-200
Elevation relative to surface (m)
Logging trace
Top_Klgc_F

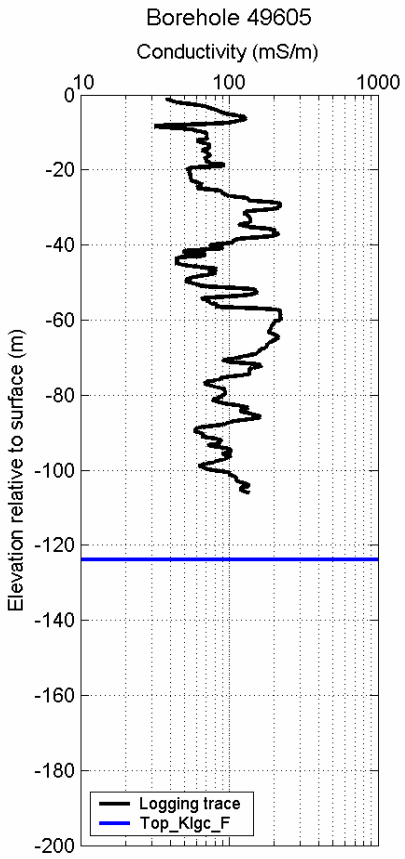
Borehole 49605
Conductivity (mS/m)
10
100
1000
0
-20
-40
-60
-80
-100
-120
-140
-160
-180
-200
Elevation relative to surface (m)
Logging trace
Top_Klgc_F

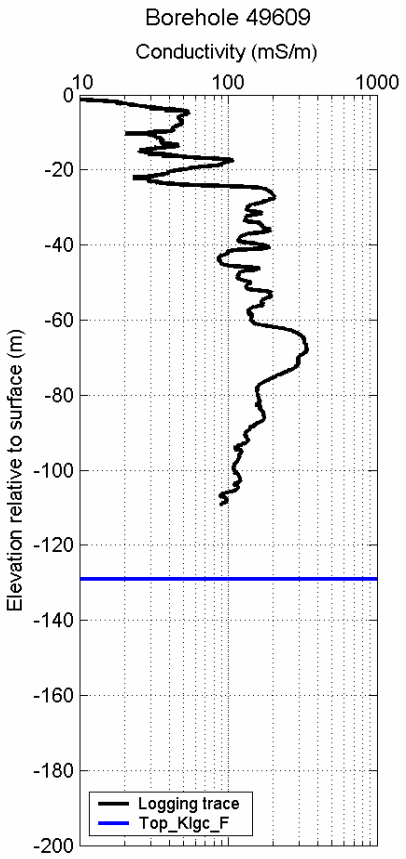
Borehole 49609
Conductivity (mS/m)
10
100
1000
0
-20
-40
-60
-80
-100
-120
-140
-160
-180
-200
Elevation relative to surface (m)
Logging trace
Top_Klgc_F

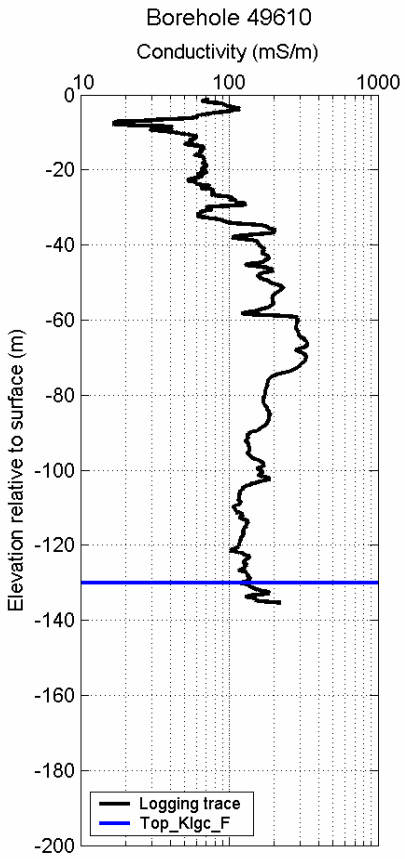
Borehole 49610
Conductivity (mS/m)
10
100
1000
0
-20
-40
-60
-80
-100
-120
-140
-160
-180
-200
Elevation relative to surface (m)
Logging trace
Top_Klgc_F

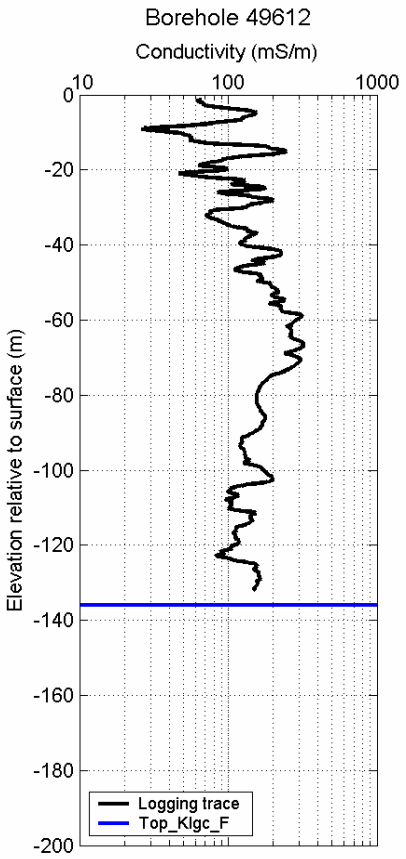
Borehole 49612
Conductivity (mS/m)
10
100
1000
0
-20
-40
-60
-80
-100
-120
-140
-160
-180
-200
Elevation relative to surface (m)
Logging trace
Top_Klgc_F

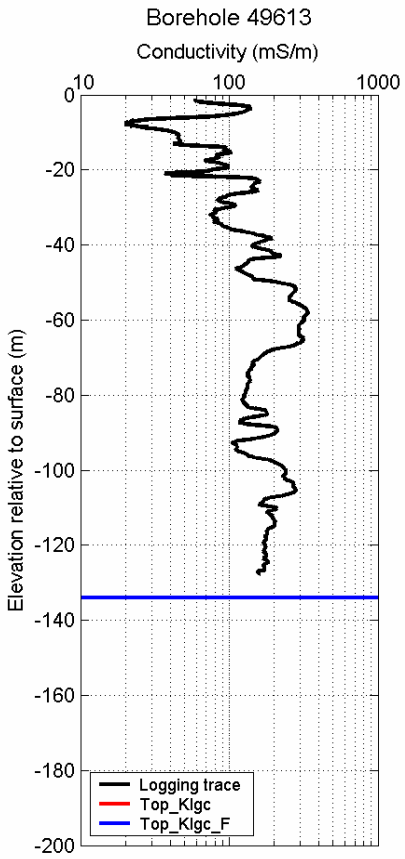
Borehole 49613
Conductivity (mS/m)
10
100
1000
0
-20
-40
-60
-80
-100
-120
-140
-160
-180
-200
Elevation relative to surface (m)
Logging trace
Top_Klgc
Top_Klgc_F

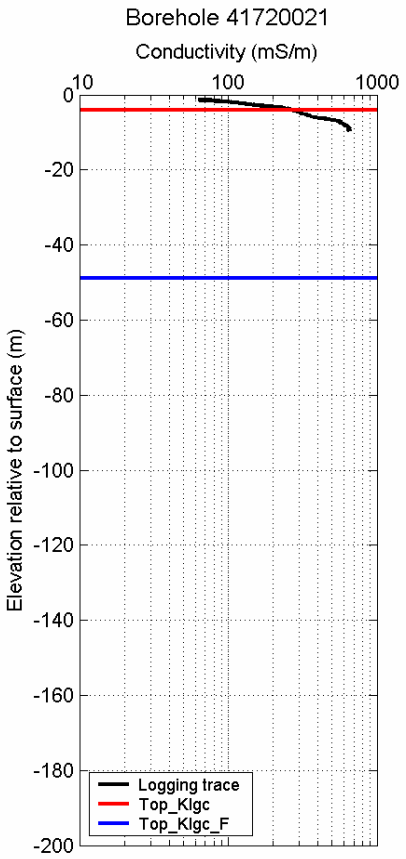
Borehole 41720021
Conductivity (mS/m)
10
100
1000
0
-20
-40
-60
-80
-100
-120
-140
-160
-180
-200
Elevation relative to surface (m)
Logging trace
Top_Klgc
Top_Klgc_F

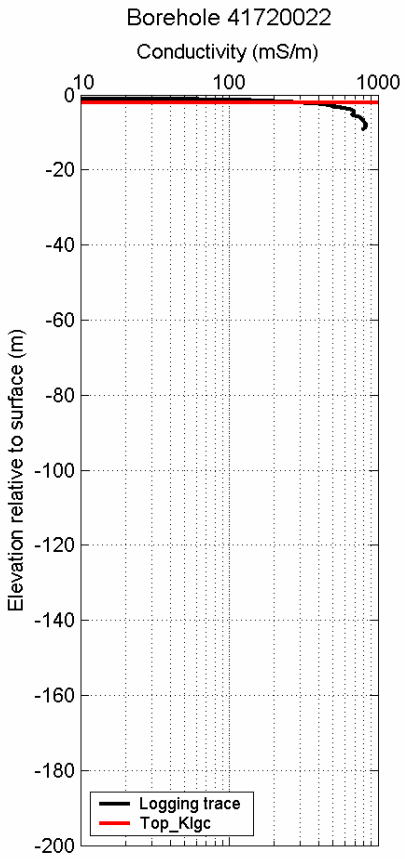
Borehole 41720022
Conductivity (mS/m)
10
100
1000
0
-20
-40
-60
-80
-100
-120
-140
-160
-180
-200
Elevation relative to surface (m)
Logging trace
Top_Klgc

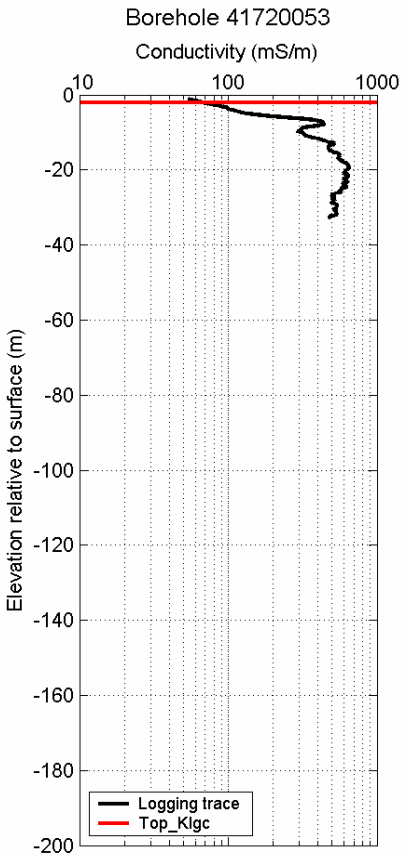
Borehole 41720053
Conductivity (mS/m)
10
100
1000
0
-20
-40
-60
-80
-100
-120
-140
-160
-180
-200
Elevation relative to surface (m)
Logging trace
Top_Klgc

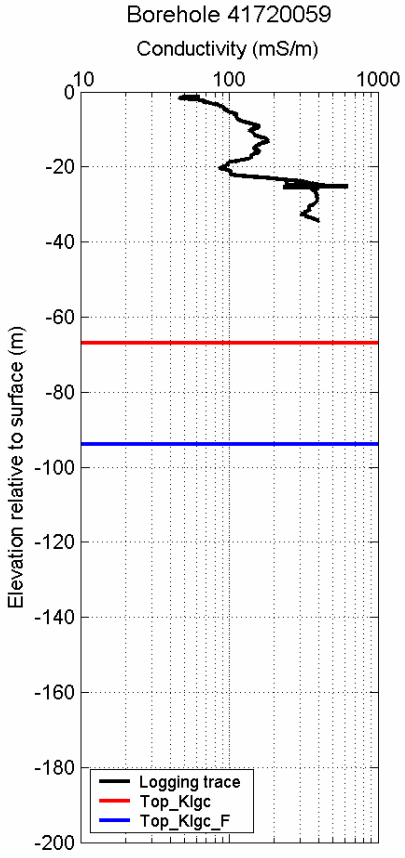
Borehole 41720059
Conductivity (mS/m)
10
100
1000
0
-20
-40
-60
-80
-100
-120
-140
-160
-180
-200
Elevation relative to surface (m)
Logging trace
Top_Klgc
Top_Klgc_F

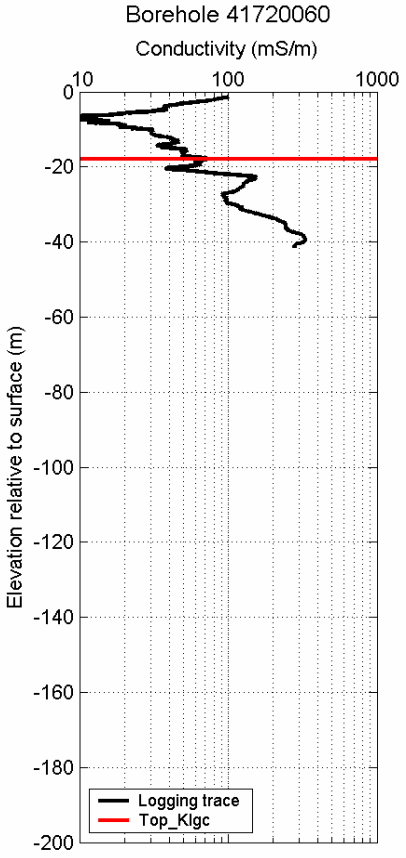
Borehole 41720060
Conductivity (mS/m)
10
100
1000
0
-20
-40
-60
-80
-100
-120
-140
-160
-180
-200
Elevation relative to surface (m)
Logging trace
Top_Klgc

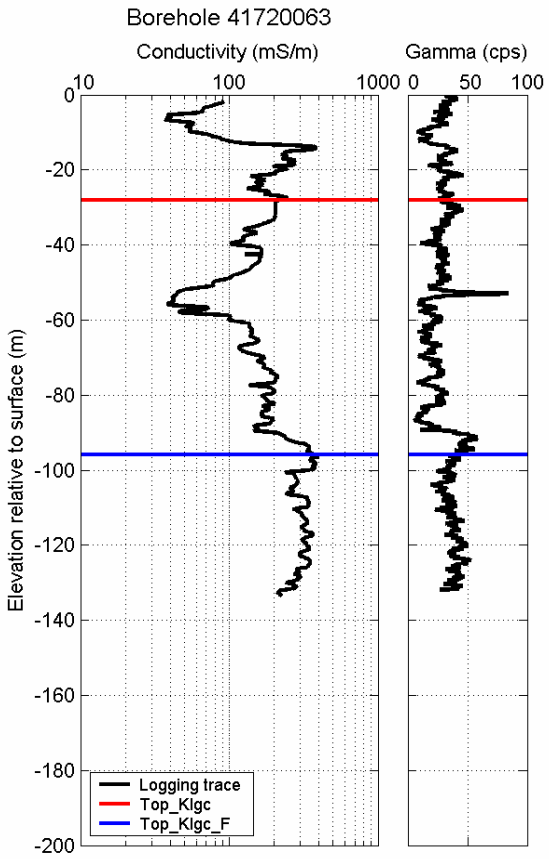
Borehole 41720063
Conductivity (mS/m)
Gamma (cps)
10
100
1000
0
50
100
0
-20
-40
-60
-80
-100
-120
-140
-160
-180
-200
Elevation relative to surface (m)
Logging trace
Top_Klgc
Top_Klgc_F

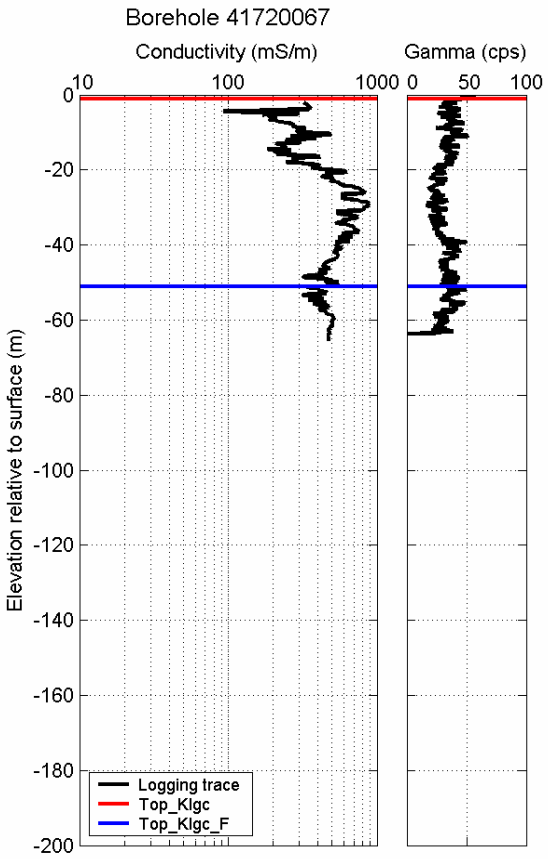
Borehole 41720067
Conductivity (mS/m)
Gamma (cps)
10
100
1000
0
50
100
0
-20
-40
-60
-80
-100
-120
-140
-160
-180
-200
Elevation relative to surface (m)
Logging trace
Top_Klgc
Top_Klgc_F

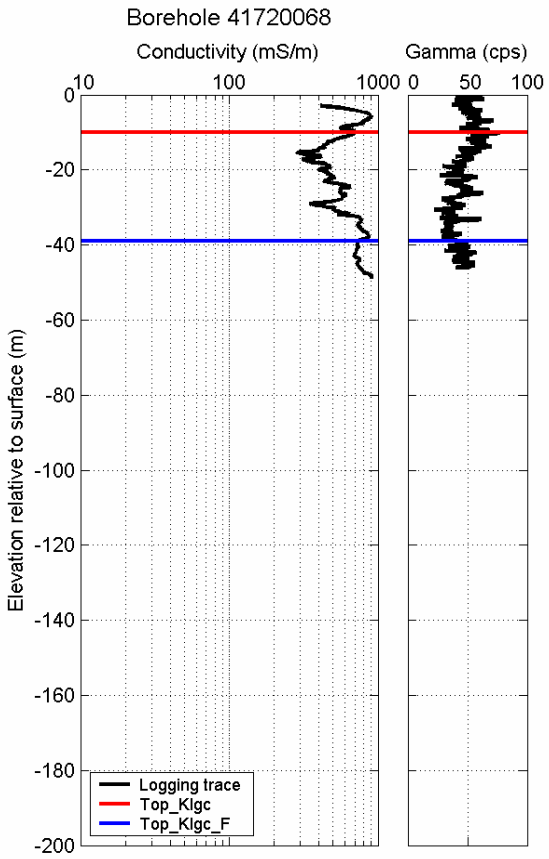
Borehole 41720068
Conductivity (mS/m)
Gamma (cps)
10
100
1000
0
50
100
0
-20
-40
-60
-80
-100
-120
-140
-160
-180
-200
Elevation relative to surface (m)
Logging trace
Top_Klgc
Top_Klgc_F

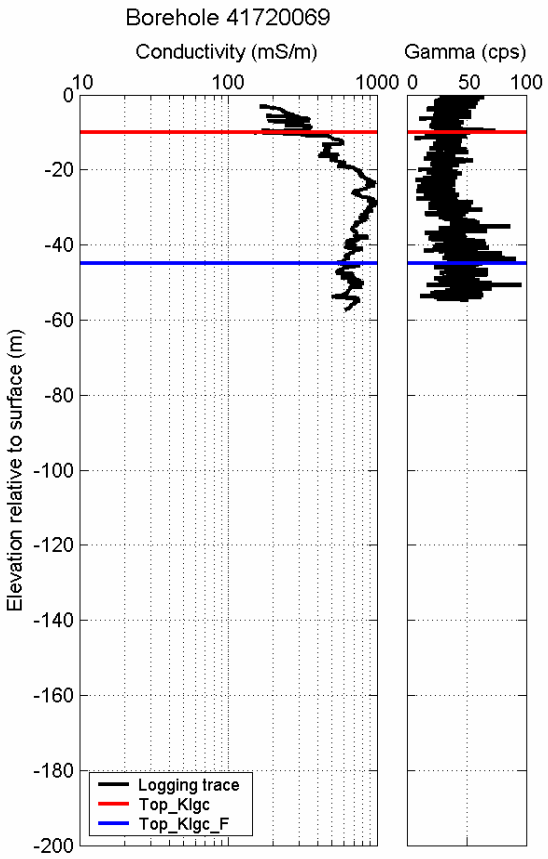
Borehole 41720069
Conductivity (mS/m)
Gamma (cps)
10
100
1000
0
50
100
0
-20
-40
-60
-80
-100
-120
-140
-160
-180
-200
Elevation relative to surface (m)
Logging trace
Top_Klgc
Top_Klgc_F

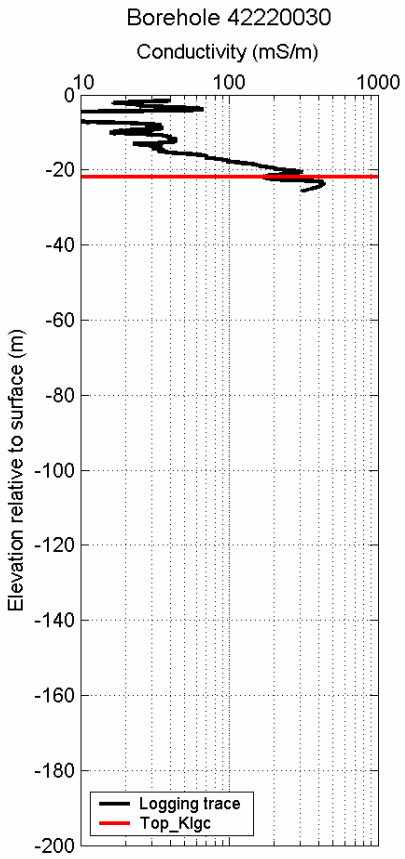
Borehole 42220030
Conductivity (mS/m)
10
100
1000
0
-20
-40
-60
-80
-100
-120
-140
-160
-180
-200
Elevation relative to surface (m)
Logging trace
Top_Klgc

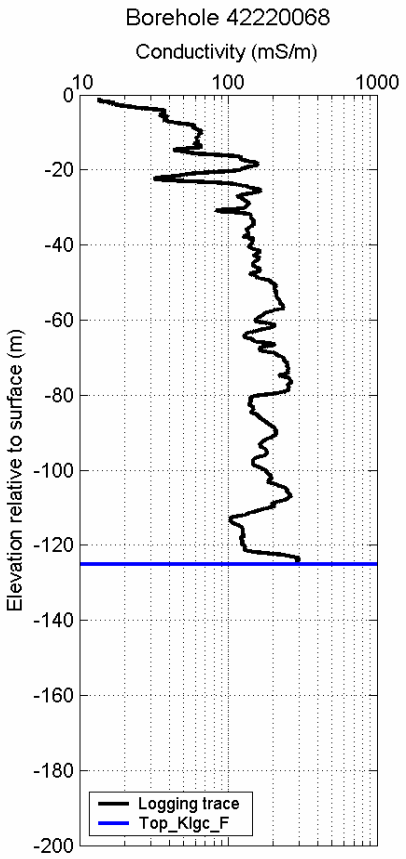
Borehole 42220068
Conductivity (mS/m)
10
100
1000
0
-20
-40
-60
-80
-100
-120
-140
-160
-180
-200
Elevation relative to surface (m)
Logging trace
Top_Klgc_F

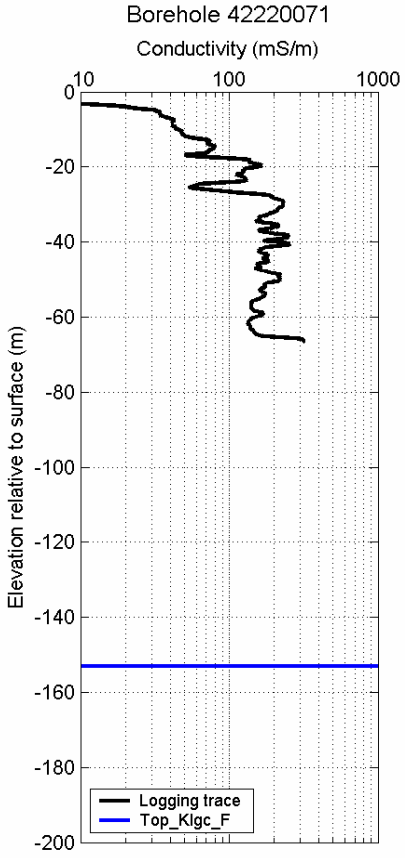
Borehole 42220071
Conductivity (mS/m)
10
100
1000
0
-20
-40
-60
-80
-100
-120
-140
-160
-180
-200
Elevation relative to surface (m)
Logging trace
Top_Klgc_F

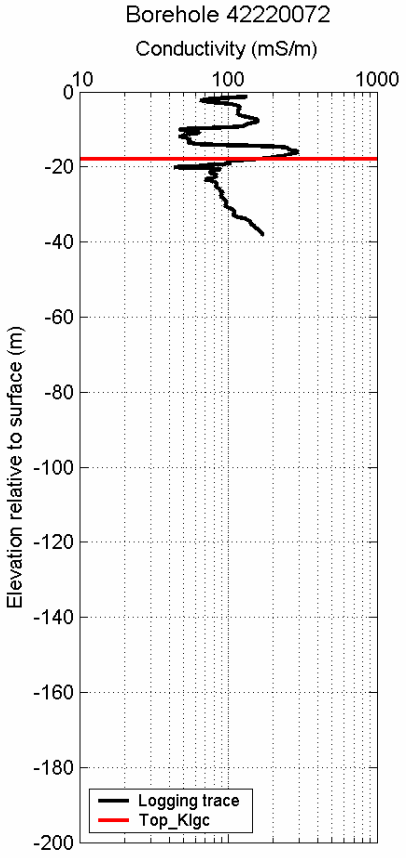
Borehole 42220072
Conductivity (mS/m)
10
100
1000
0
-20
-40
-60
-80
-100
-120
-140
-160
-180
-200
Elevation relative to surface (m)
Logging trace
Top_Klgc

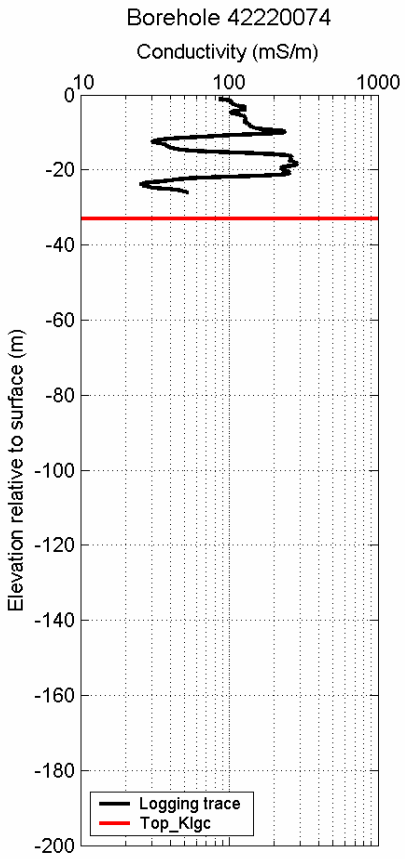
Borehole 42220074
Conductivity (mS/m)
10
100
1000
0
-20
-40
-60
-80
-100
-120
-140
-160
-180
-200
Elevation relative to surface (m)
Logging trace
Top_Klgc

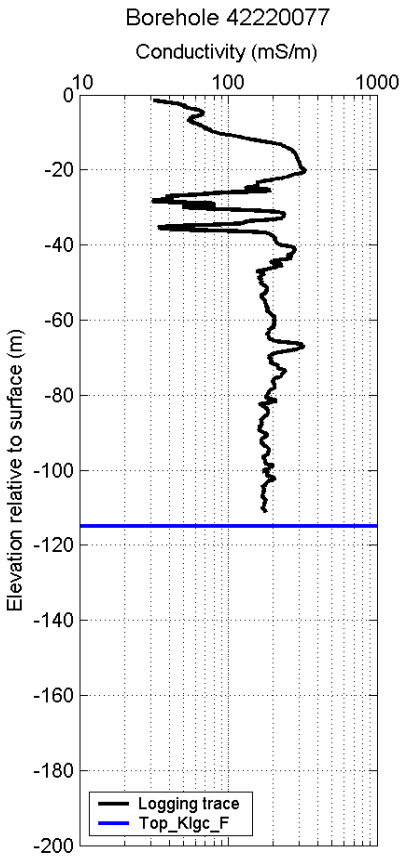
Borehole 42220077
Conductivity (mS/m)
10
100
1000
0
-20
-40
-60
-80
-100
-120
-140
-160
-180
-200
Elevation relative to surface (m)
Logging trace
Top_Klgc_F

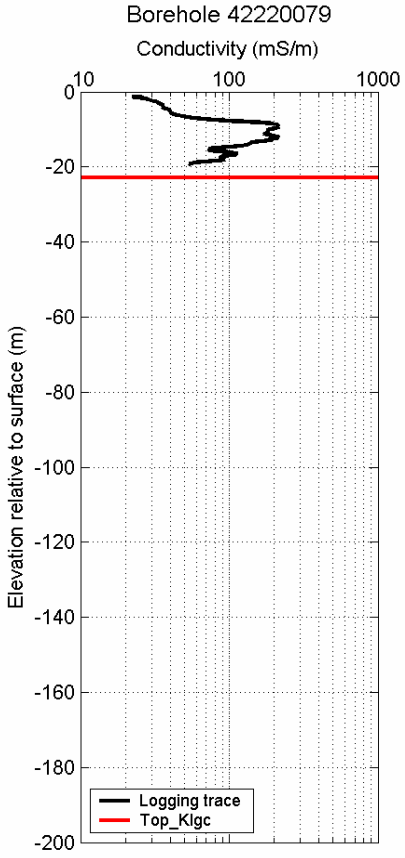
Borehole 42220079
Conductivity (mS/m)
10
100
1000
0
-20
-40
-60
-80
-100
-120
-140
-160
-180
-200
Elevation relative to surface (m)
Logging trace
Top_Klgc

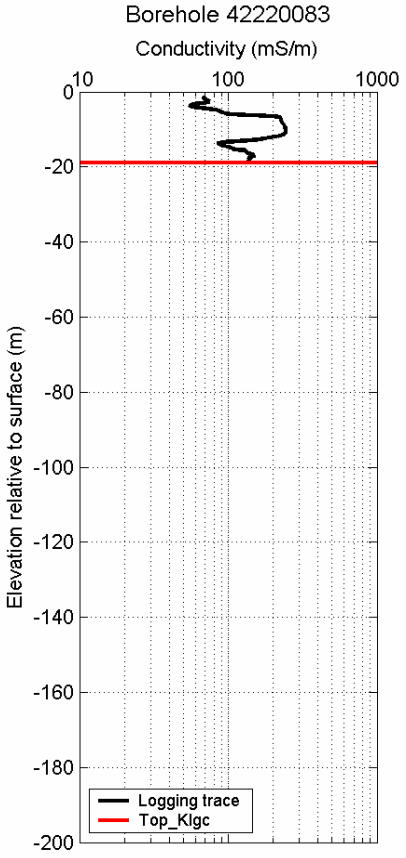
Borehole 42220083
Conductivity (mS/m)
10
100
1000
0
-20
-40
-60
-80
-100
-120
-140
-160
-180
-200
Elevation relative to surface (m)
Logging trace
Top_Klgc

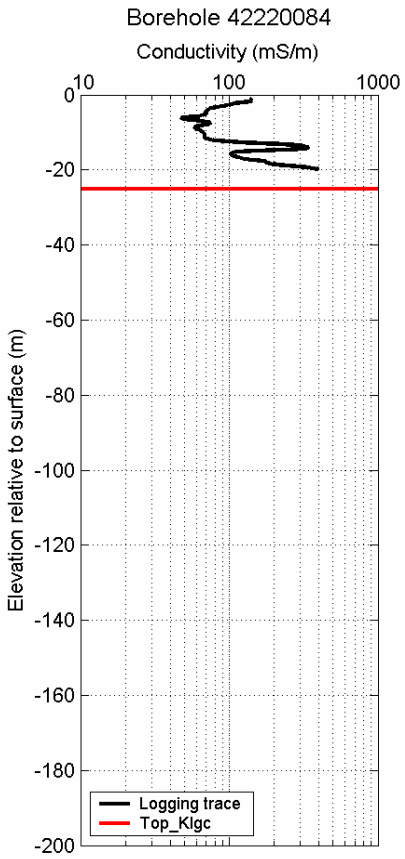
Borehole 42220084
Conductivity (mS/m)
10
100
1000
0
-20
-40
-60
-80
-100
-120
-140
-160
-180
-200
Elevation relative to surface (m)
Logging trace
Top_Klgc

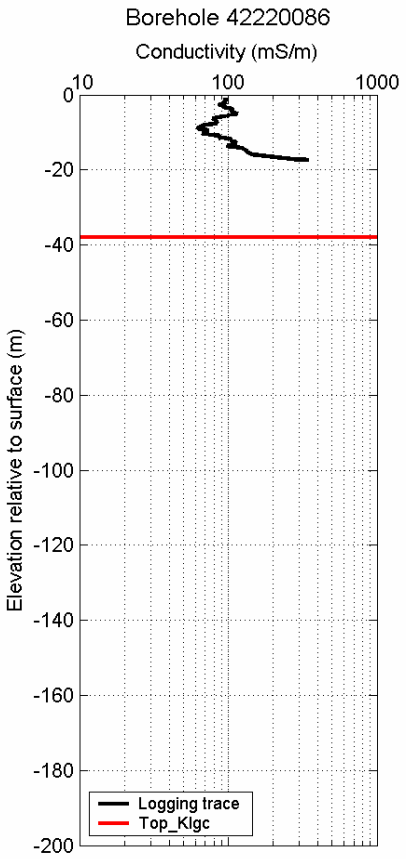
Borehole 42220086
Conductivity (mS/m)
10
100
1000
0
-20
-40
-60
-80
-100
-120
-140
-160
-180
-200
Elevation relative to surface (m)
Logging trace
Top_Klgc

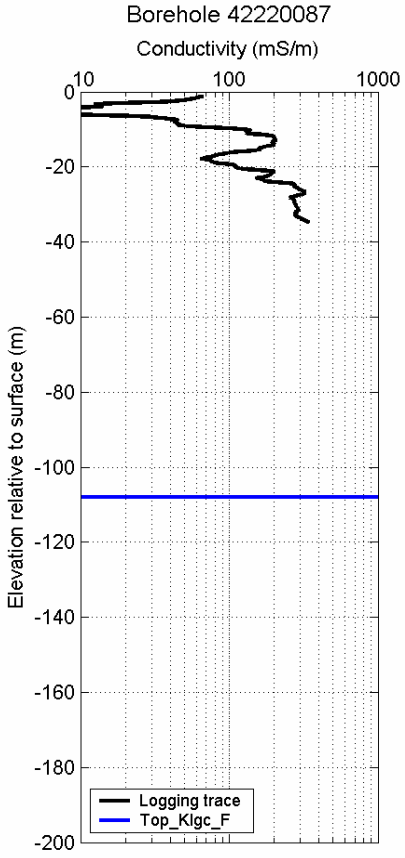
Borehole 42220087
Conductivity (mS/m)
10
100
1000
0
-20
-40
-60
-80
-100
-120
-140
-160
-180
-200
Elevation relative to surface (m)
Logging trace
Top_Klgc_F

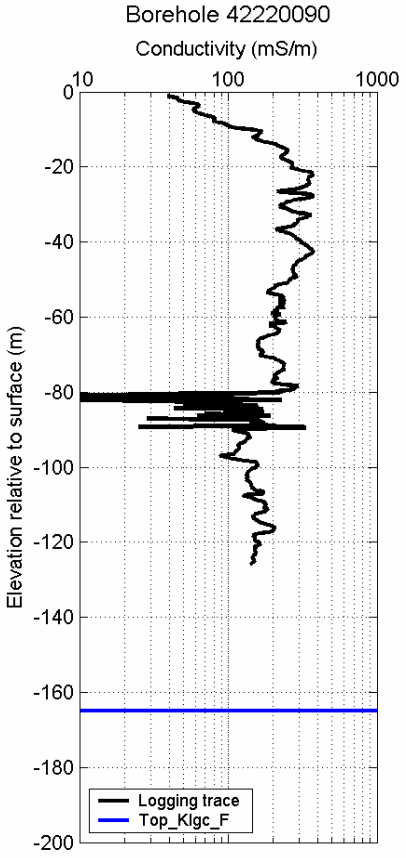
Borehole 42220090
Conductivity (mS/m)
10
100
1000
0
-20
-40
-60
-80
-100
-120
-140
-160
-180
-200
Elevation relative to surface (m)
Logging trace
Top_Klgc_F

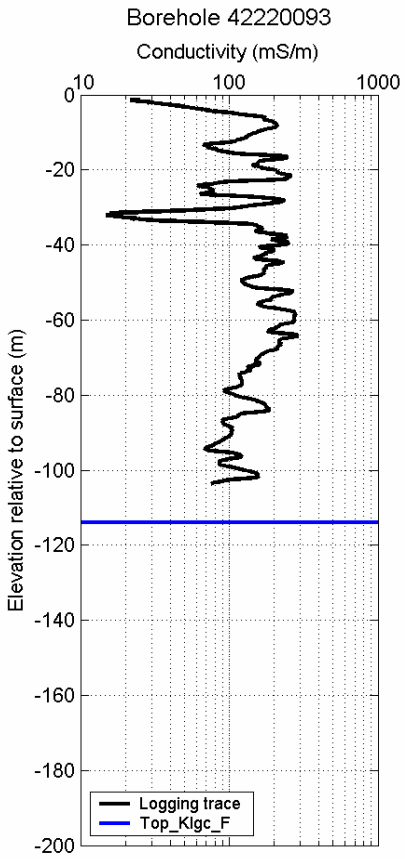
Borehole 42220093
Conductivity (mS/m)
10
100
1000
0
-20
-40
-60
-80
-100
-120
-140
-160
-180
-200
Elevation relative to surface (m)
Logging trace
Top_Klgc_F

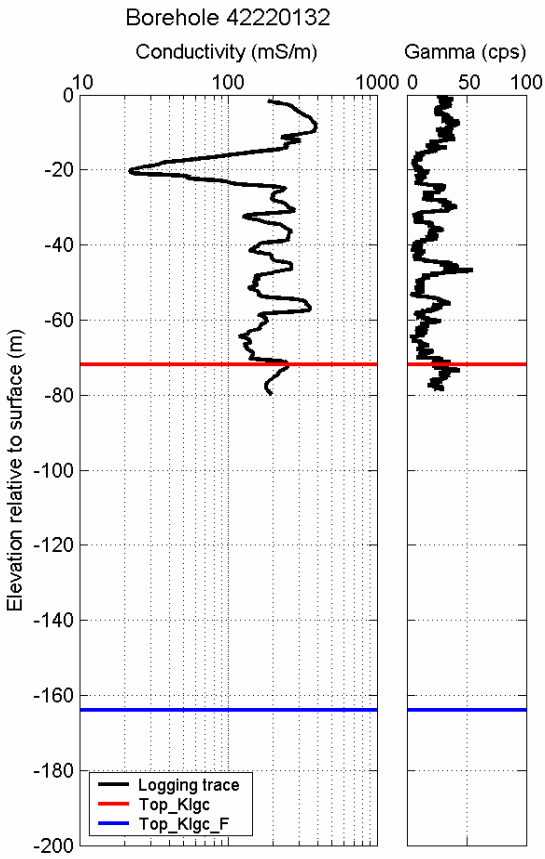
Borehole 42220132
Conductivity (mS/m)
Gamma (cps)
10
100
1000
0
50
100
0
-20
-40
-60
-80
-100
-120
-140
-160
-180
-200
Elevation relative to surface (m)
Logging trace
Top_Klgc
Top_Klgc_F

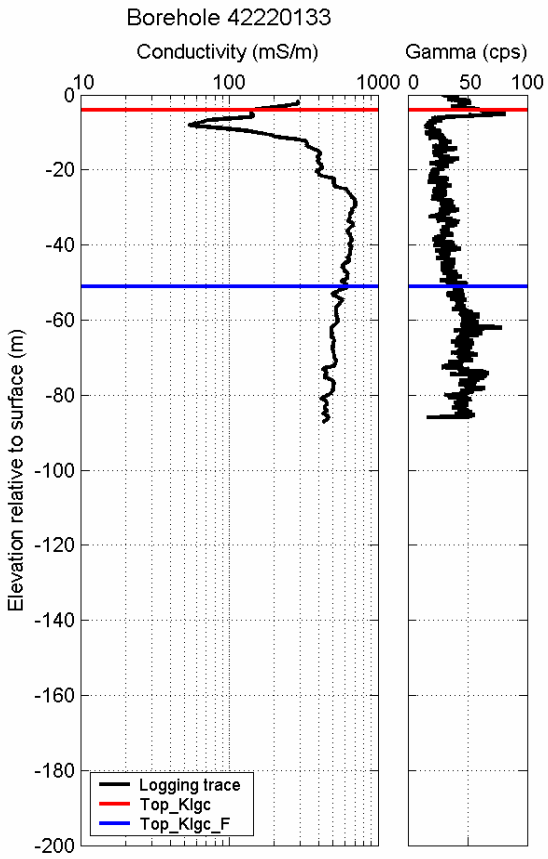
Borehole 42220133
Conductivity (mS/m)
Gamma (cps)
10
100
1000
0
50
100
0
-20
-40
-60
-80
-100
-120
-140
-160
-180
-200
Elevation relative to surface (m)
Logging trace
Top_Klgc
Top_Klgc_F

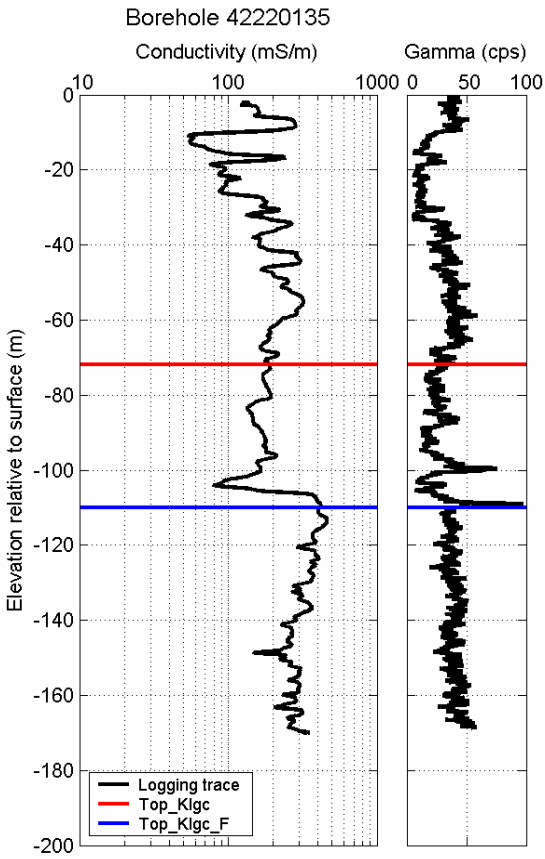
Borehole 42220135
Conductivity (mS/m)
Gamma (cps)
10
100
1000
0
50
100
0
-20
-40
-60
-80
-100
-120
-140
-160
-180
-200
Elevation relative to surface (m)
Logging trace
Top_Klgc
Top_Klgc_F

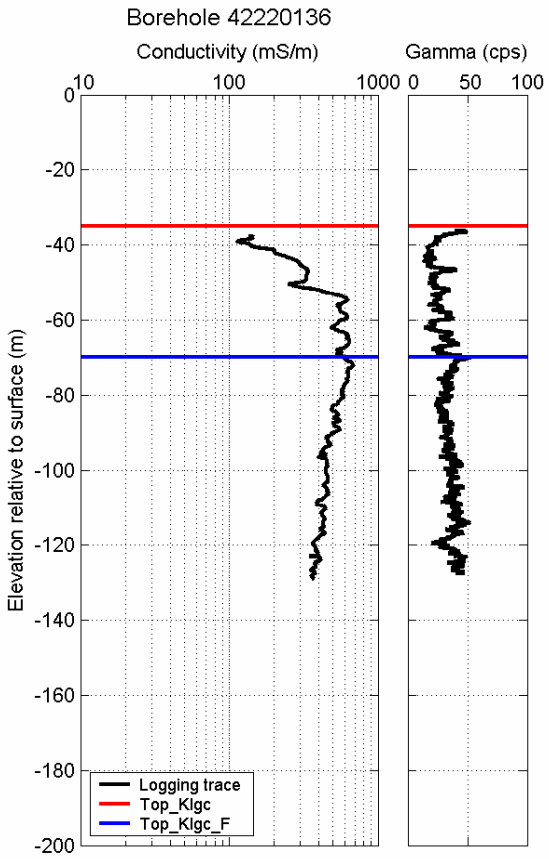
Borehole 42220136
Conductivity (mS/m)
Gamma (cps)
10
100
1000
0
50
100
0
-20
-40
-60
-80
-100
-120
-140
-160
-180
-200
Elevation relative to surface (m)
Logging trace
Top_Klgc
Top_Klgc_F

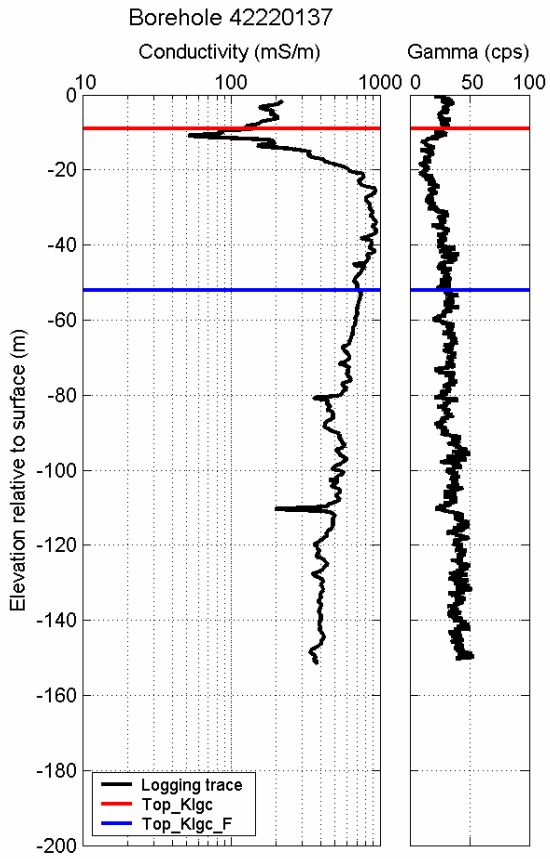
Borehole 42220137
Conductivity (mS/m)
Gamma (cps)
10
100
1000
0
50
100
0
-20
-40
-60
-80
-100
-120
-140
-160
-180
-200
Elevation relative to surface (m)
Logging trace
Top_Klgc
Top_Klgc_F

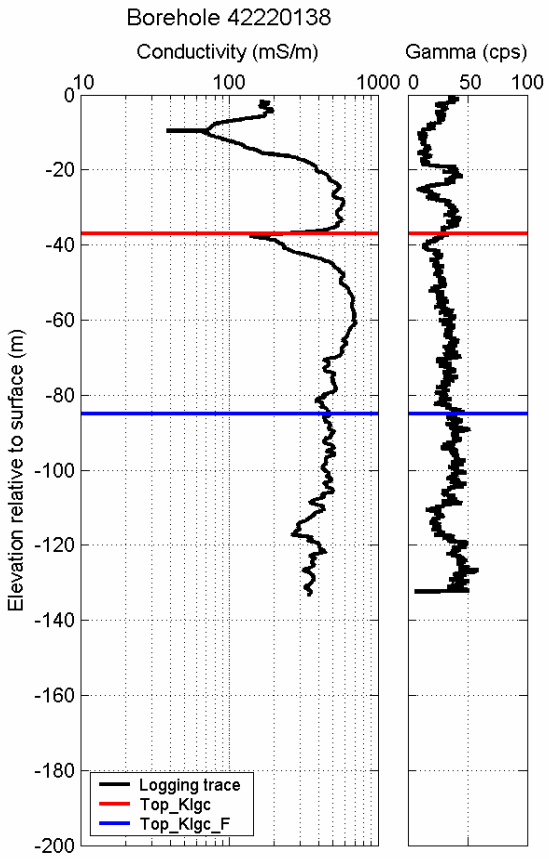
Borehole 42220138
Conductivity (mS/m)
Gamma (cps)
10
100
1000
0
50
100
0
-20
-40
-60
-80
-100
-120
-140
-160
-180
-200
Elevation relative to surface (m)
Logging trace
Top_Klgc
Top_Klgc_F

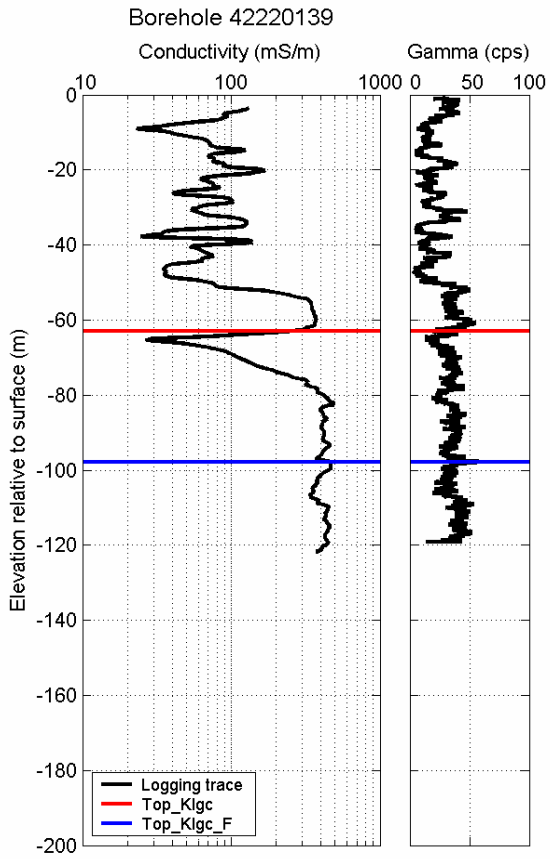
Borehole 42220139
Conductivity (mS/m)
Gamma (cps)
10
100
1000
0
50
100
0
-20
-40
-60
-80
-100
-120
-140
-160
-180
-200
Elevation relative to surface (m)
Logging trace
Top_Klgc
Top_Klgc_F

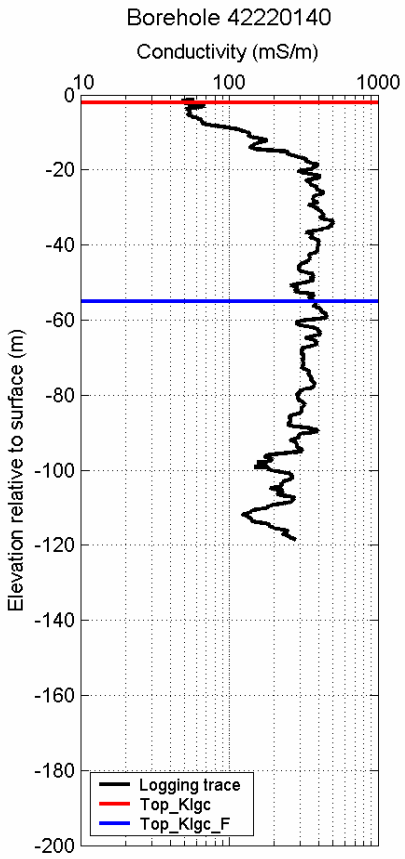
Borehole 42220140
Conductivity (mS/m)
10
100
1000
0
-20
-40
-60
-80
-100
-120
-140
-160
-180
-200
Elevation relative to surface (m)
Logging trace
Top_Klgc
Top_Klgc_F

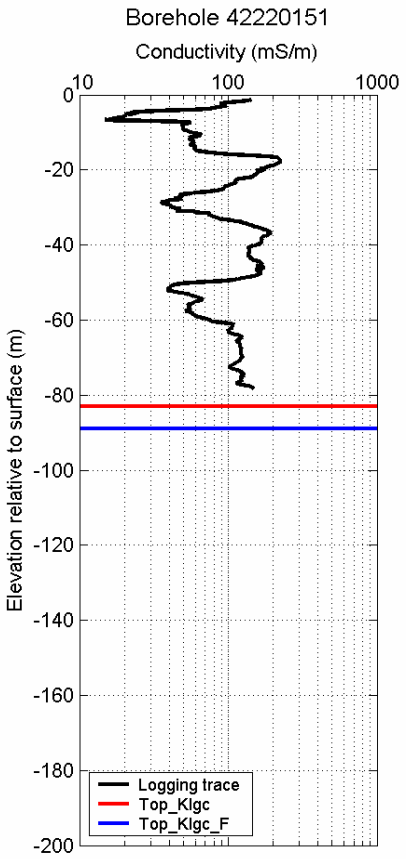
Borehole 42220151
Conductivity (mS/m)
10
100
1000
0
-20
-40
-60
-80
-100
-120
-140
-160
-180
-200
Elevation relative to surface (m)
Logging trace
Top_Klgc
Top_Klgc_F

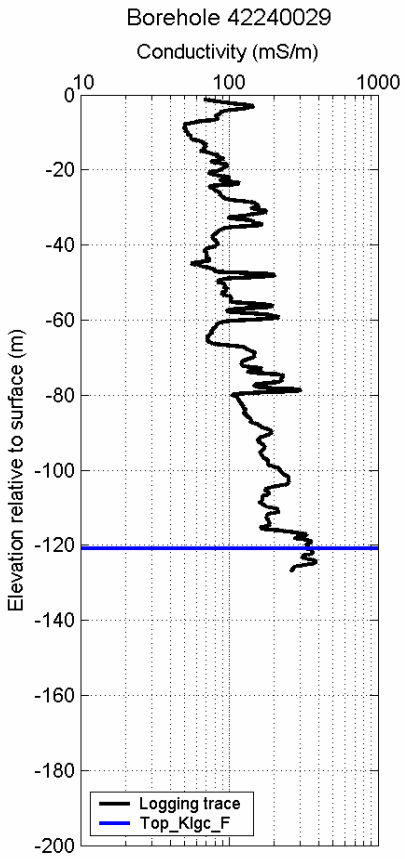
Borehole 42240029
Conductivity (mS/m)
10
100
1000
0
-20
-40
-60
-80
-100
-120
-140
-160
-180
-200
Elevation relative to surface (m)
Logging trace
Top_Klgc_F

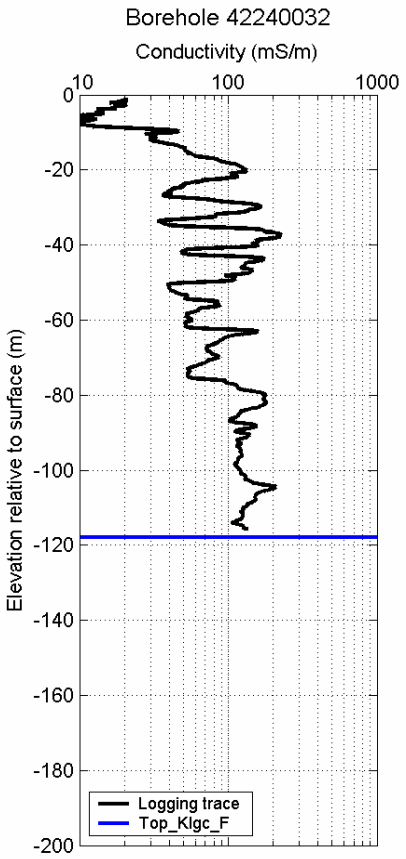
Borehole 42240032
Conductivity (mS/m)
10
100
1000
0
-20
-40
-60
-80
-100
-120
-140
-160
-180
-200
Elevation relative to surface (m)
Logging trace
Top_Klgc_F

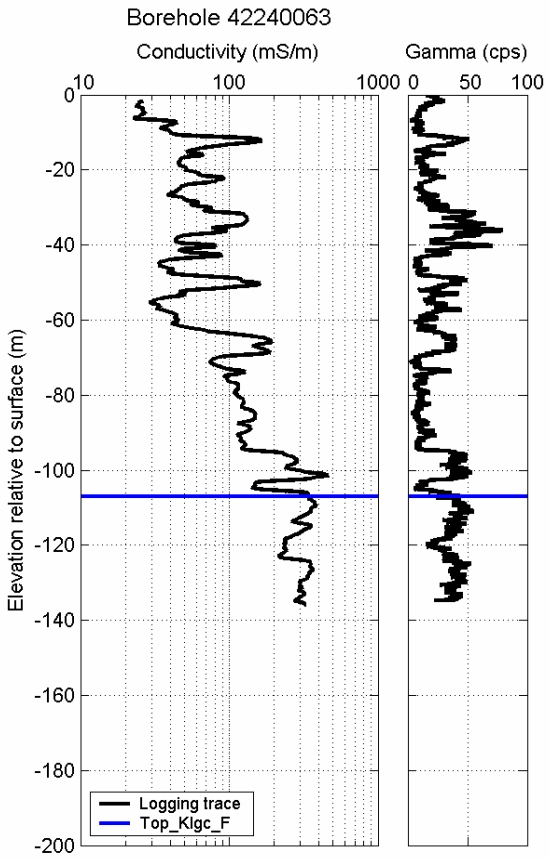
Borehole 42240063
Conductivity (mS/m)
Gamma (cps)
10
100
1000
0
50
100
0
-20
-40
-60
-80
-100
-120
-140
-160
-180
-200
Elevation relative to surface (m)
Logging trace
Top_Klgc_F

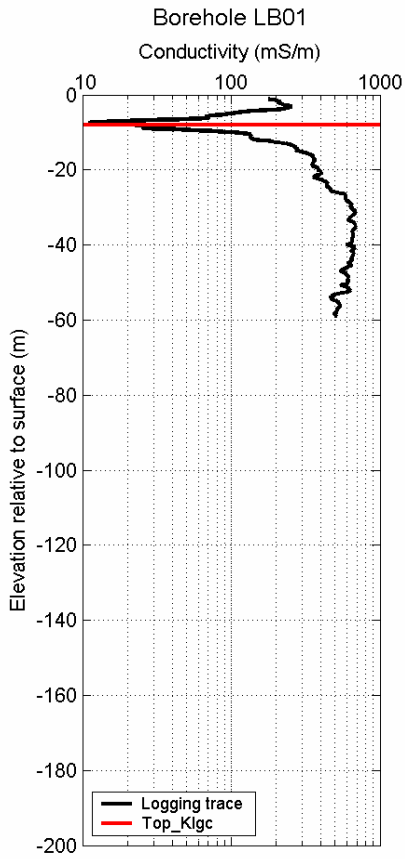
Borehole LB01
Conductivity (mS/m)
10
100
1000
0
-20
-40
-60
-80
-100
-120
-140
-160
-180
-200
Elevation relative to surface (m)
Logging trace
Top_Klgc

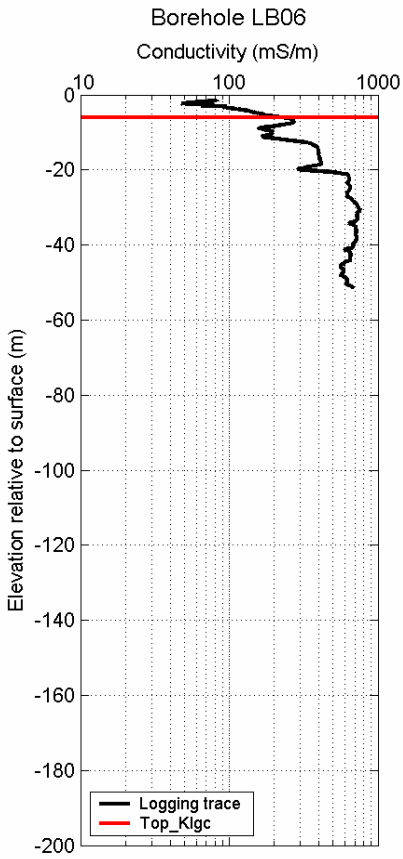
Borehole LB06
Conductivity (mS/m)
10
100
1000
0
-20
-40
-60
-80
-100
-120
-140
-160
-180
-200
Elevation relative to surface (m)
Logging trace
Top_Klgc

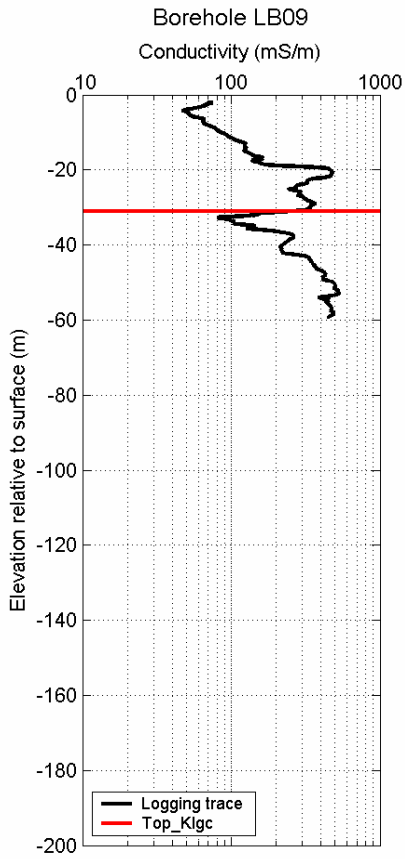
Borehole LB09
Conductivity (mS/m)
10
100
1000
0
-20
-40
-60
-80
-100
-120
-140
-160
-180
-200
Elevation relative to surface (m)
Logging trace
Top_Klgc

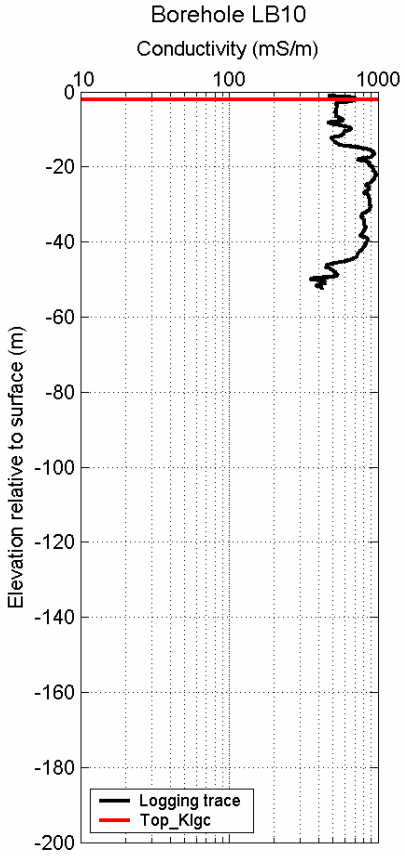
Borehole LB10
Conductivity (mS/m)
10
100
1000
0
-20
-40
-60
-80
-100
-120
-140
-160
-180
-200
Elevation relative to surface (m)
Logging trace
Top_Klgc

Appendix 4. Plots of borehole conductivity logs and inversion models

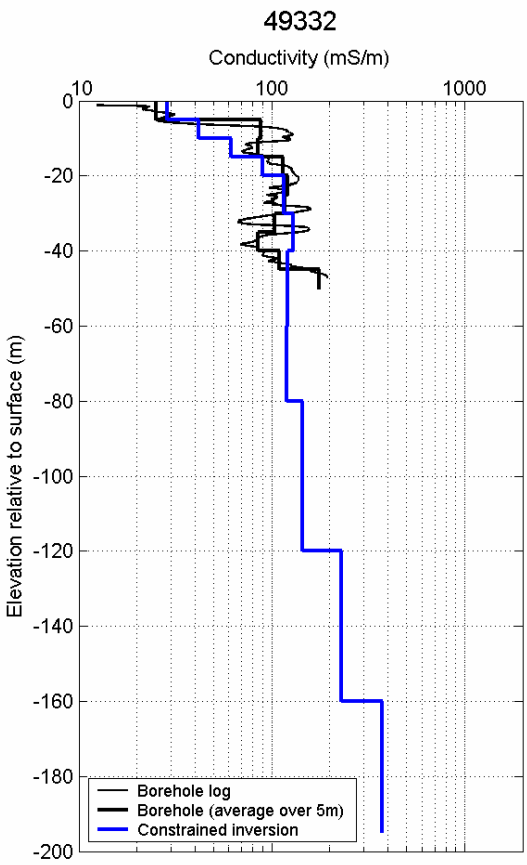
49332
Conductivity (mS/m)
10
100
1000
0
-20
-40
-60
-80
-100
-120
-140
-160
-180
-200
Elevation relative to surface (m)
Borehole log
Borehole (average over 5m)
Constrained inversion

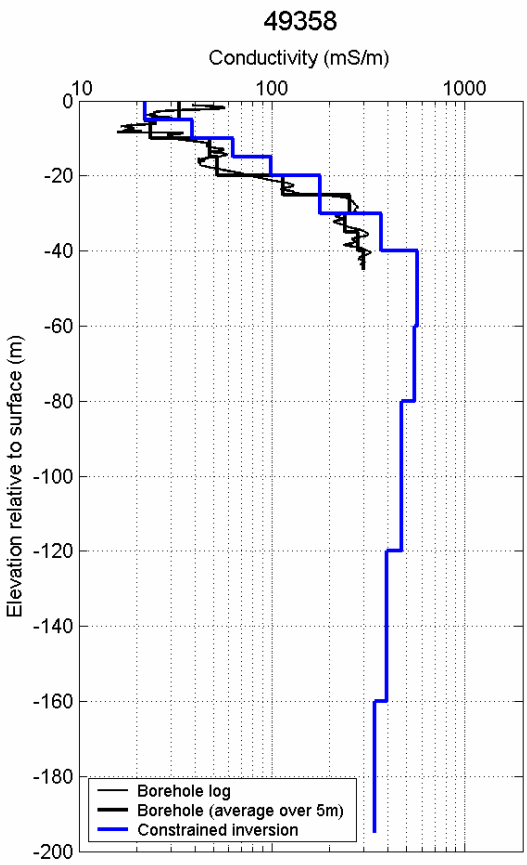
49358
Conductivity (mS/m)
10
100
1000
0
-20
-40
-60
-80
-100
-120
-140
-160
-180
-200
Elevation relative to surface (m)
Borehole log
Borehole (average over 5m)
Constrained inversion

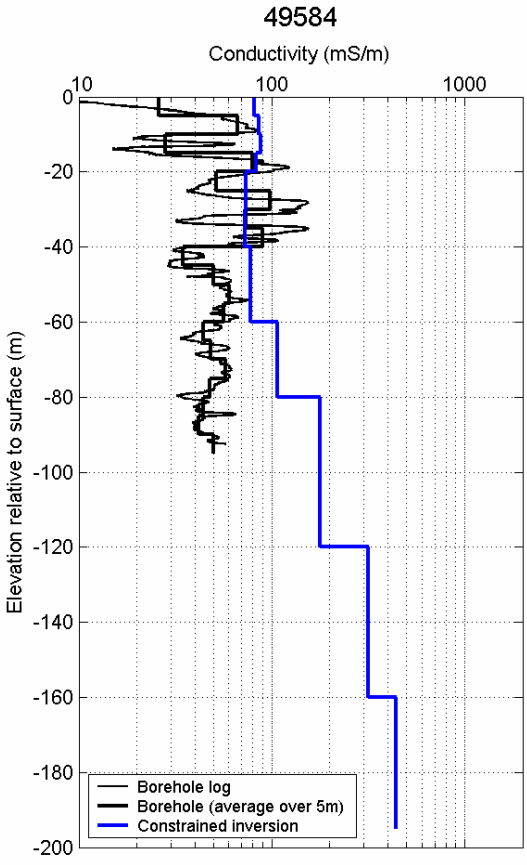
49584
Conductivity (mS/m)
10
100
1000
0
-20
-40
-60
-80
-100
-120
-140
-160
-180
-200
Elevation relative to surface (m)
Borehole log
Borehole (average over 5m)
Constrained inversion

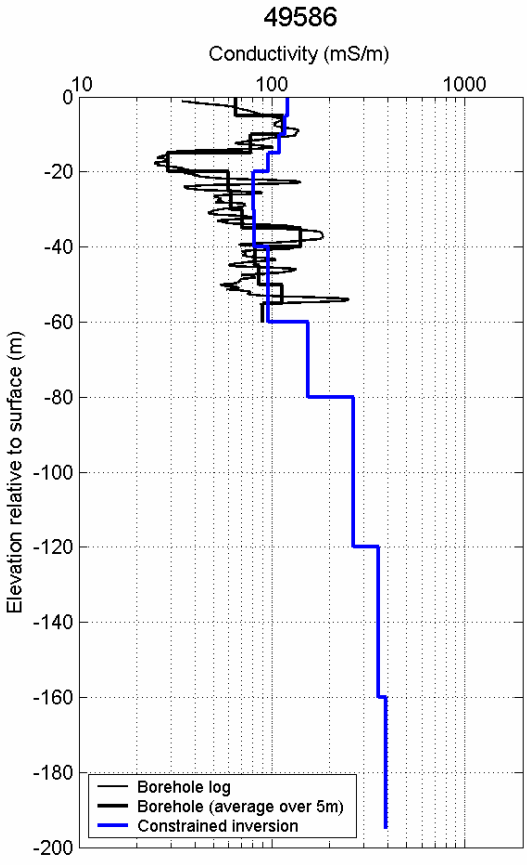
49586
Conductivity (mS/m)
10
100
1000
0
-20
-40
-60
-80
-100
-120
-140
-160
-180
-200
Elevation relative to surface (m)
Borehole log
Borehole (average over 5m)
Constrained inversion

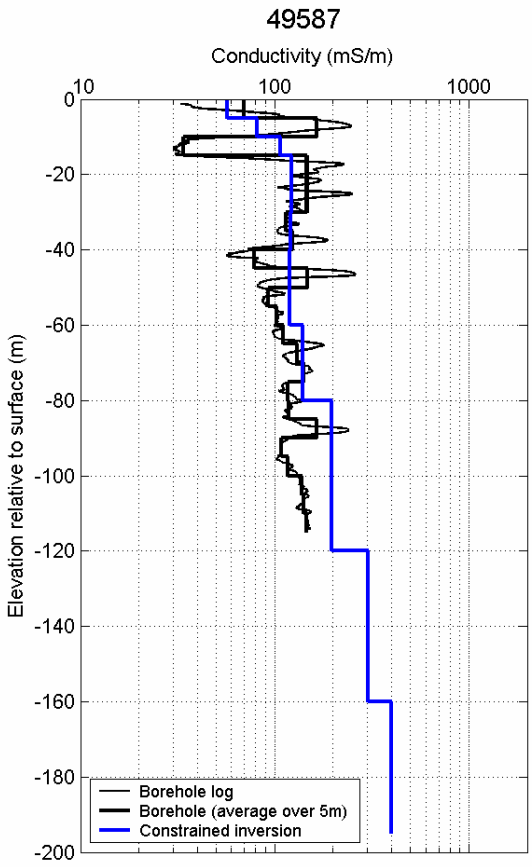
49587
Conductivity (mS/m)
10
100
1000
0
-20
-40
-60
-80
-100
-120
-140
-160
-180
-200
Elevation relative to surface (m)
Borehole log
Borehole (average over 5m)
Constrained inversion

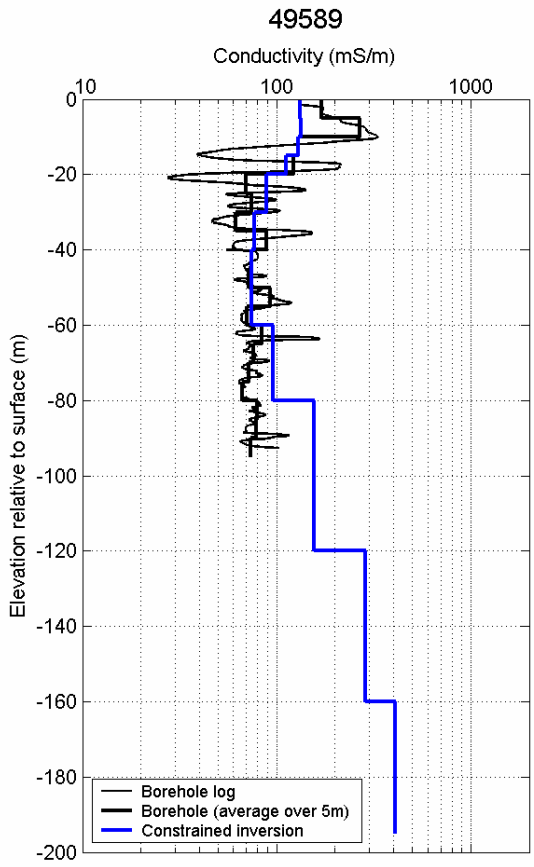
49589
Conductivity (mS/m)
10
100
1000
0
-20
-40
-60
-80
-100
-120
-140
-160
-180
-200
Elevation relative to surface (m)
Borehole log
Borehole (average over 5m)
Constrained inversion

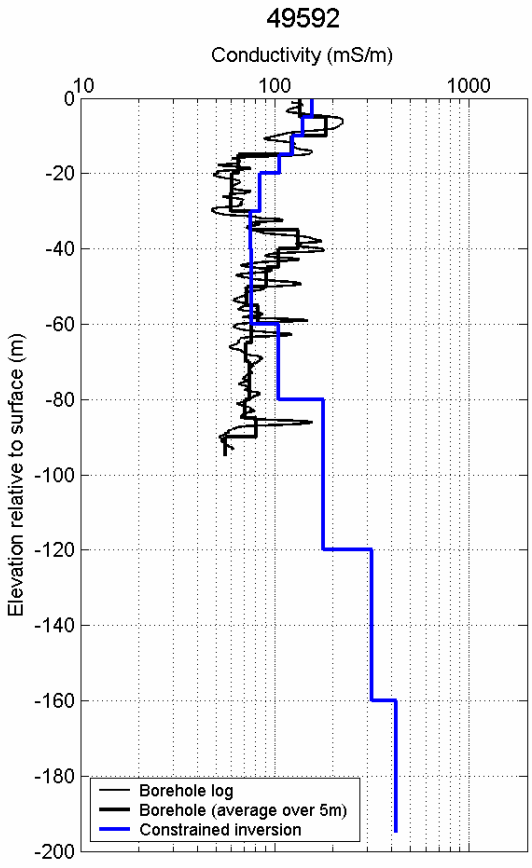
49592
Conductivity (mS/m)
10
100
1000
0
-20
-40
-60
-80
-100
-120
-140
-160
-180
-200
Elevation relative to surface (m)
Borehole log
Borehole (average over 5m)
Constrained inversion

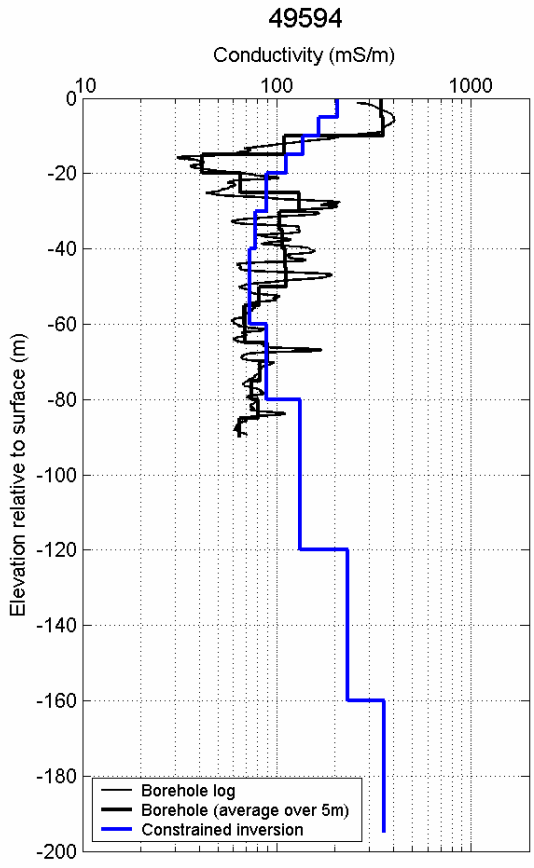
49594
Conductivity (mS/m)
10
100
1000
0
-20
-40
-60
-80
-100
-120
-140
-160
-180
-200
Elevation relative to surface (m)
Borehole log
Borehole (average over 5m)
Constrained inversion

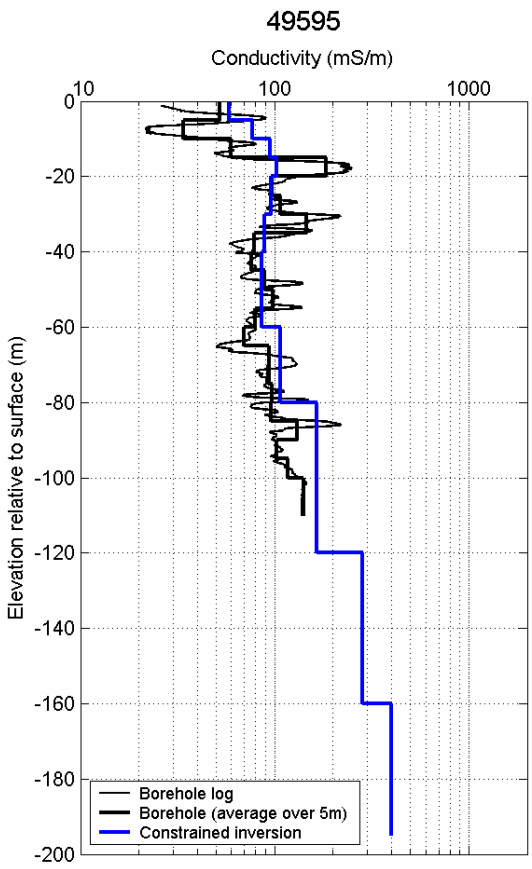
49595
Conductivity (mS/m)
10
100
1000
0
-20
-40
-60
-80
-100
-120
-140
-160
-180
-200
Elevation relative to surface (m)
Borehole log
Borehole (average over 5m)
Constrained inversion

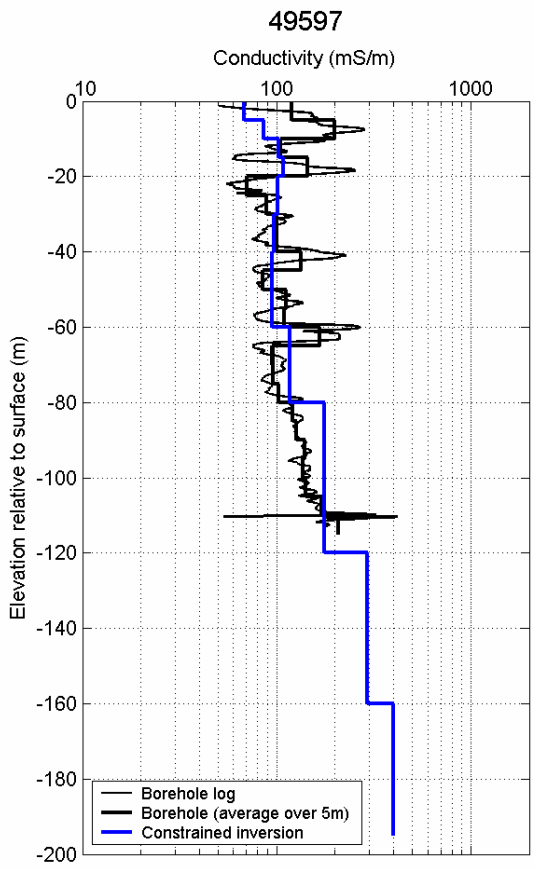
49597
Conductivity (mS/m)
10
100
1000
0
-20
-40
-60
-80
-100
-120
-140
-160
-180
-200
Elevation relative to surface (m)
Borehole log
Borehole (average over 5m)
Constrained inversion

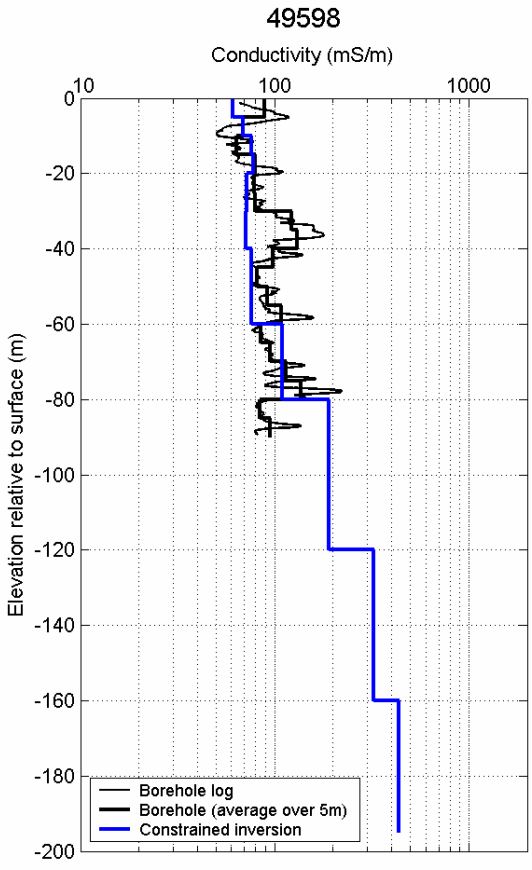
49598
Conductivity (mS/m)
10
100
1000
0
-20
-40
-60
-80
-100
-120
-140
-160
-180
-200
Elevation relative to surface (m)
Borehole log
Borehole (average over 5m)
Constrained inversion

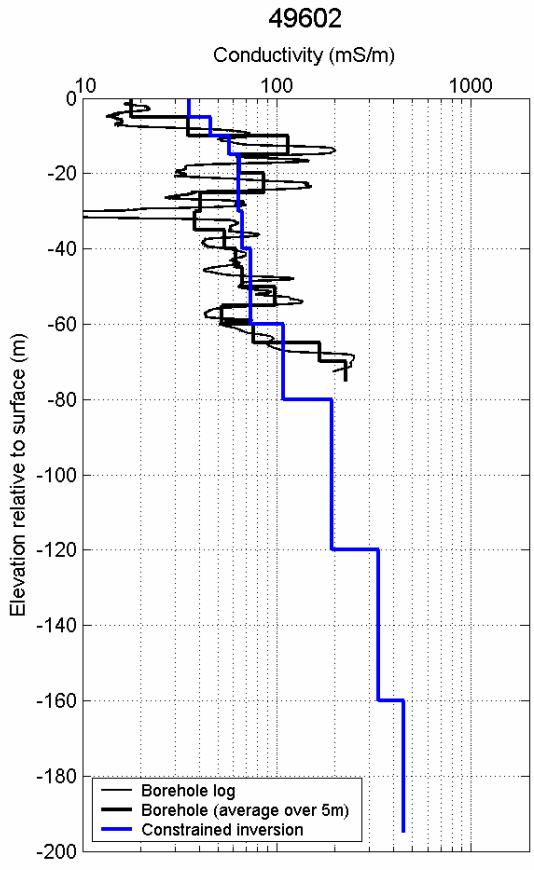
49602
Conductivity (mS/m)
10
100
1000
0
-20
-40
-60
-80
-100
-120
-140
-160
-180
-200
Elevation relative to surface (m)
Borehole log
Borehole (average over 5m)
Constrained inversion

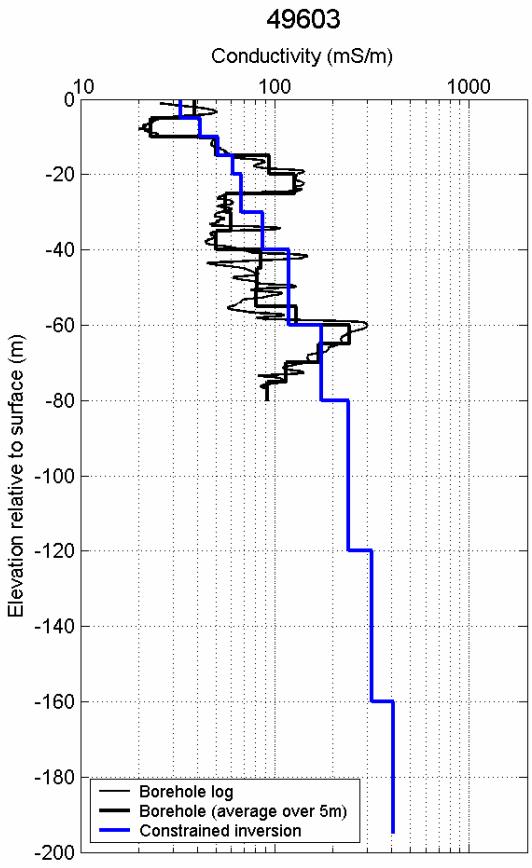
49603
Conductivity (mS/m)
10
100
1000
0
-20
-40
-60
-80
-100
-120
-140
-160
-180
-200
Elevation relative to surface (m)
Borehole log
Borehole (average over 5m)
Constrained inversion

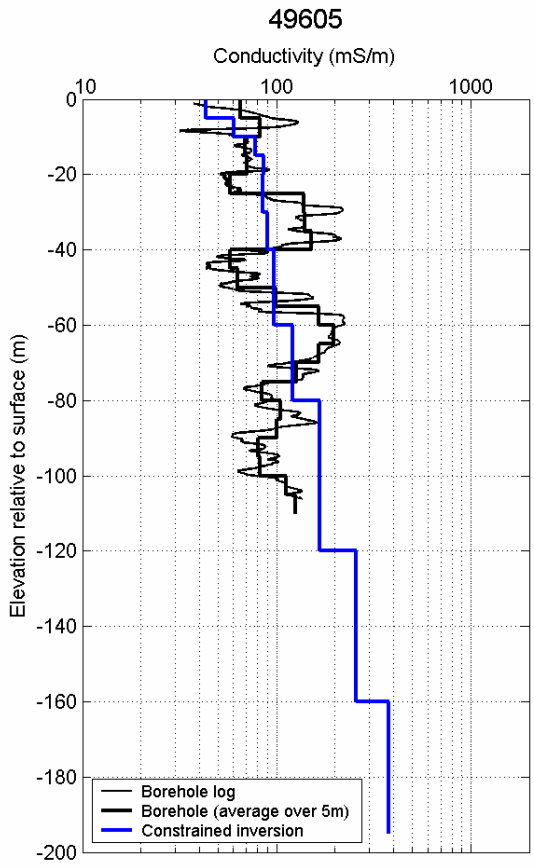
49605
Conductivity (mS/m)
10
100
1000
0
-20
-40
-60
-80
-100
-120
-140
-160
-180
-200
Elevation relative to surface (m)
Borehole log
Borehole (average over 5m)
Constrained inversion

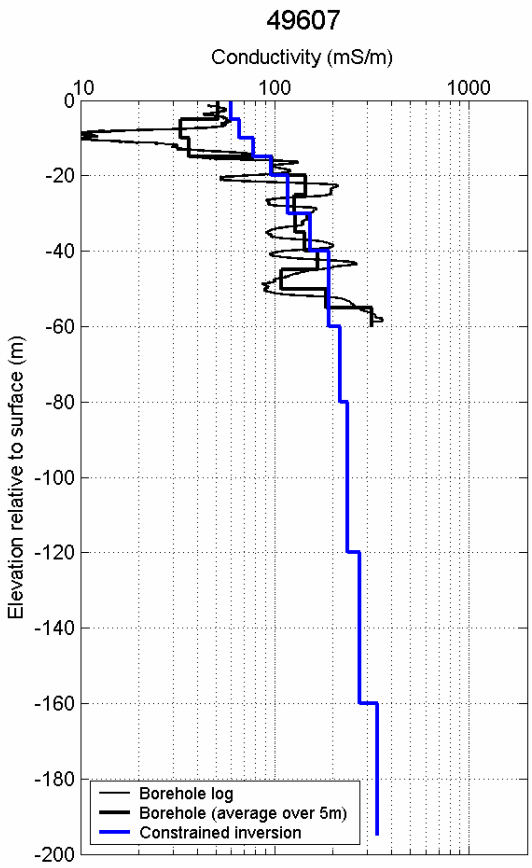
49607
Conductivity (mS/m)
10
100
1000
0
-20
-40
-60
-80
-100
-120
-140
-160
-180
-200
Elevation relative to surface (m)
Borehole log
Borehole (average over 5m)
Constrained inversion

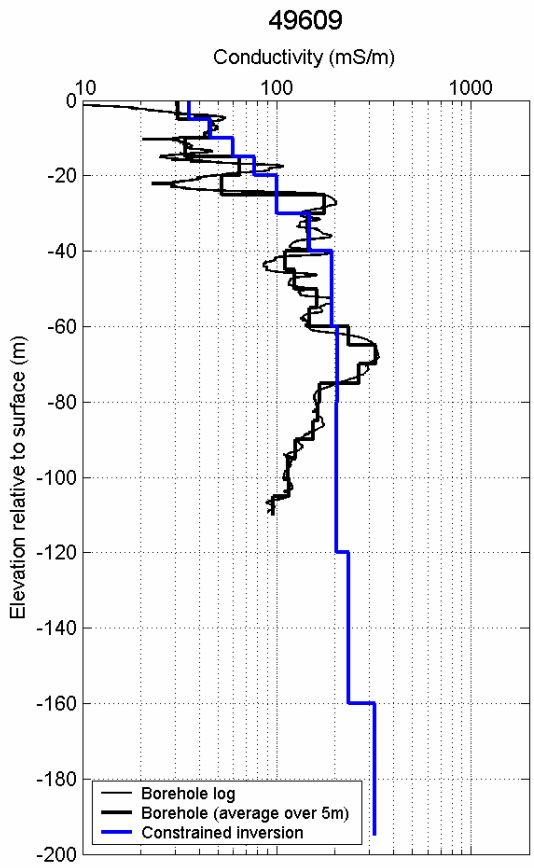
49609
Conductivity (mS/m)
10
100
1000
0
-20
-40
-60
-80
-100
-120
-140
-160
-180
-200
Elevation relative to surface (m)
Borehole log
Borehole (average over 5m)
Constrained inversion

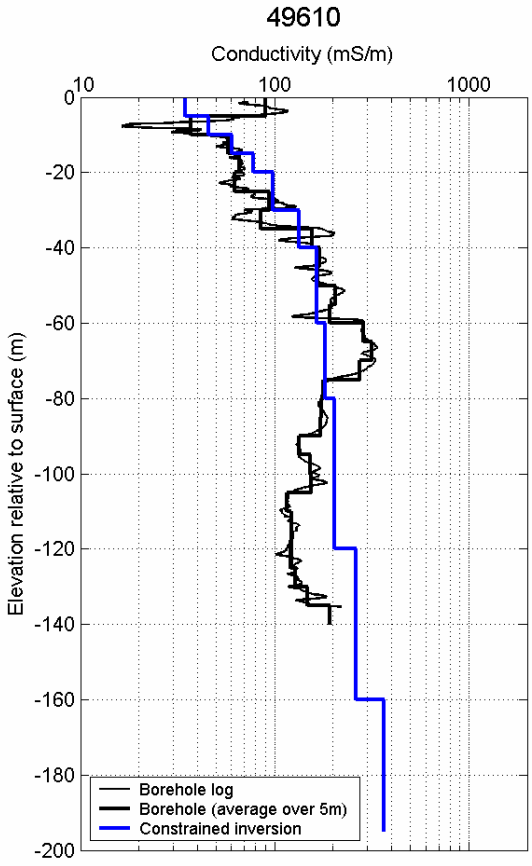
49610
Conductivity (mS/m)
10
100
1000
0
-20
-40
-60
-80
-100
-120
-140
-160
-180
-200
Elevation relative to surface (m)
Borehole log
Borehole (average over 5m)
Constrained inversion

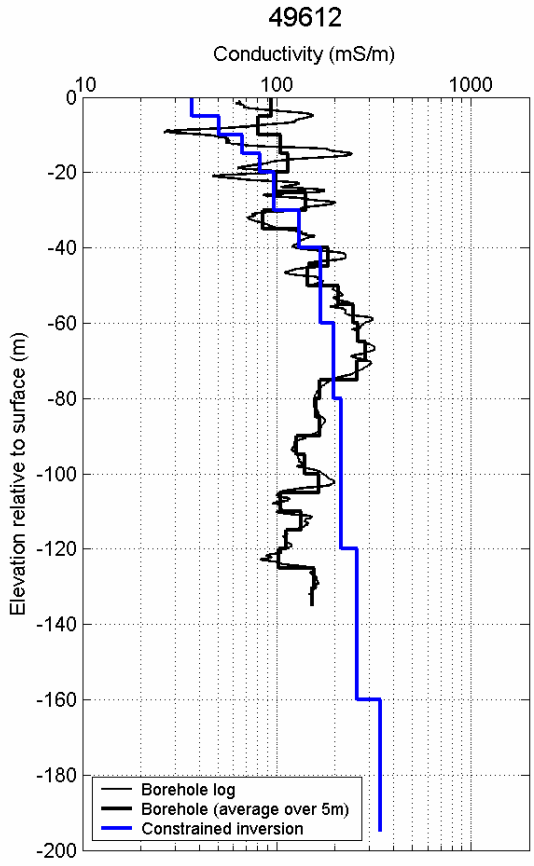
49612
Conductivity (mS/m)
10
100
1000
0
-20
-40
-60
-80
-100
-120
-140
-160
-180
-200
Elevation relative to surface (m)
Borehole log
Borehole (average over 5m)
Constrained inversion

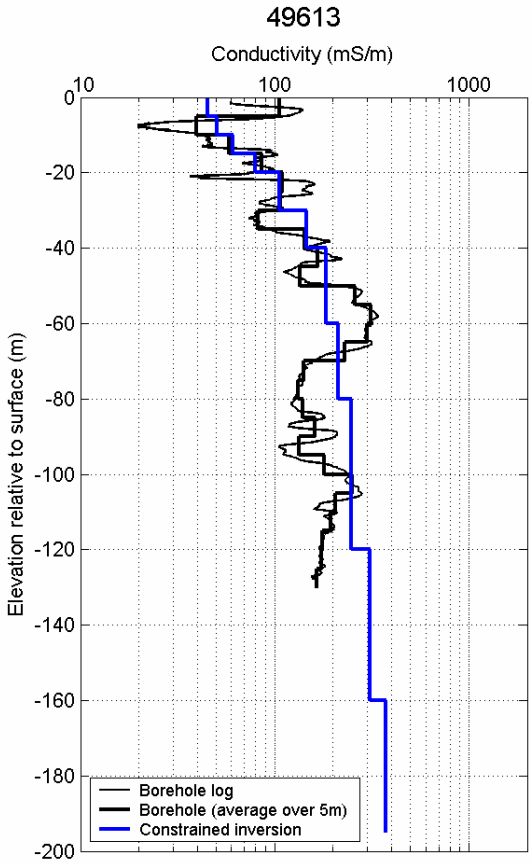
49613
Conductivity (mS/m)
10
100
1000
0
-20
-40
-60
-80
-100
-120
-140
-160
-180
-200
Elevation relative to surface (m)
Borehole log
Borehole (average over 5m)
Constrained inversion

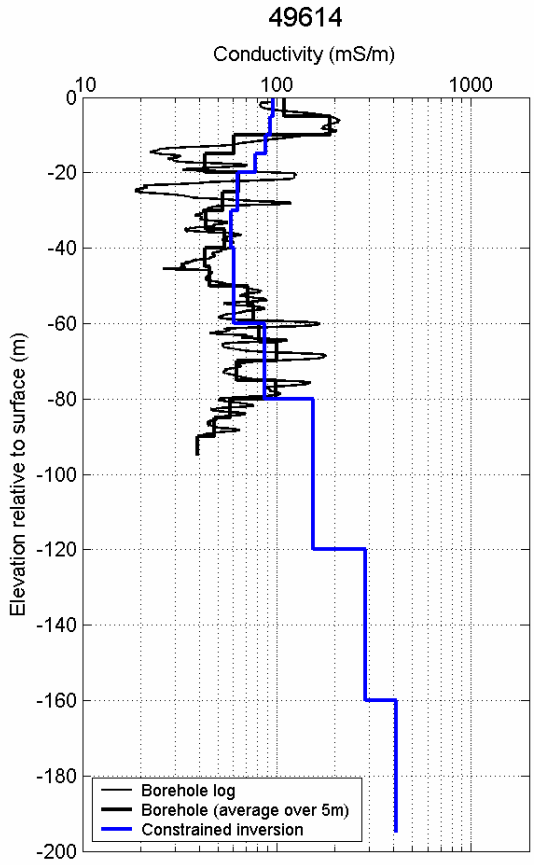
49614
Conductivity (mS/m)
10
100
1000
0
-20
-40
-60
-80
-100
-120
-140
-160
-180
-200
Elevation relative to surface (m)
Borehole log
Borehole (average over 5m)
Constrained inversion

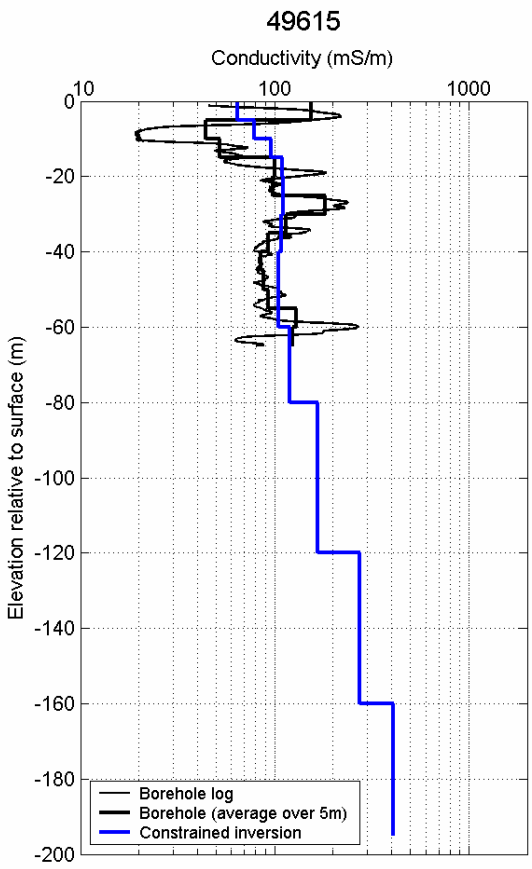
49615
Conductivity (mS/m)
10
100
1000
0
-20
-40
-60
-80
-100
-120
-140
-160
-180
-200
Elevation relative to surface (m)
Borehole log
Borehole (average over 5m)
Constrained inversion

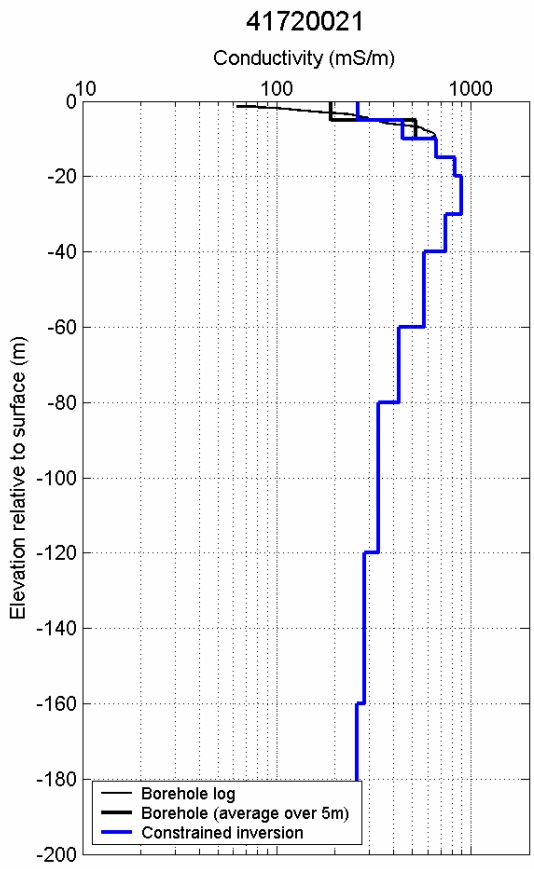
41720021
Conductivity (mS/m)
10
100
1000
0
-20
-40
-60
-80
-100
-120
-140
-160
-180
-200
Elevation relative to surface (m)
Borehole log
Borehole (average over 5m)
Constrained inversion

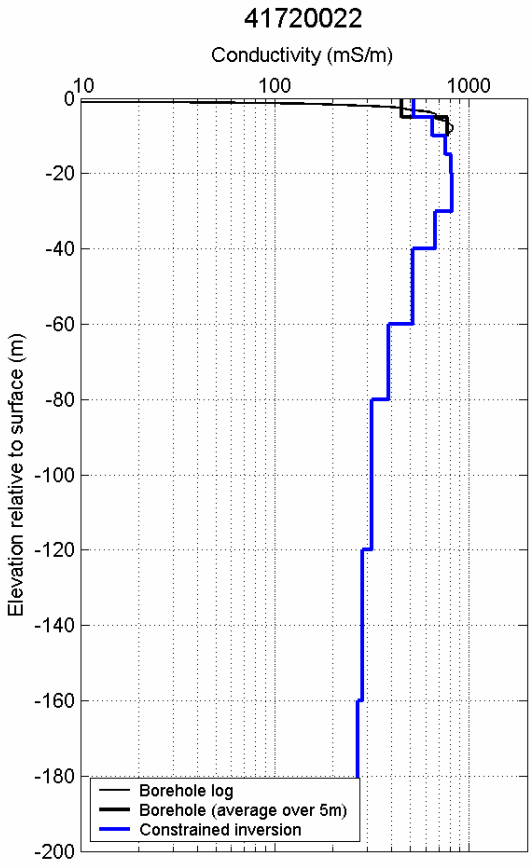
41720022
Conductivity (mS/m)
10
100
1000
0
-20
-40
-60
-80
-100
-120
-140
-160
-180
-200
Elevation relative to surface (m)
Borehole log
Borehole (average over 5m)
Constrained inversion

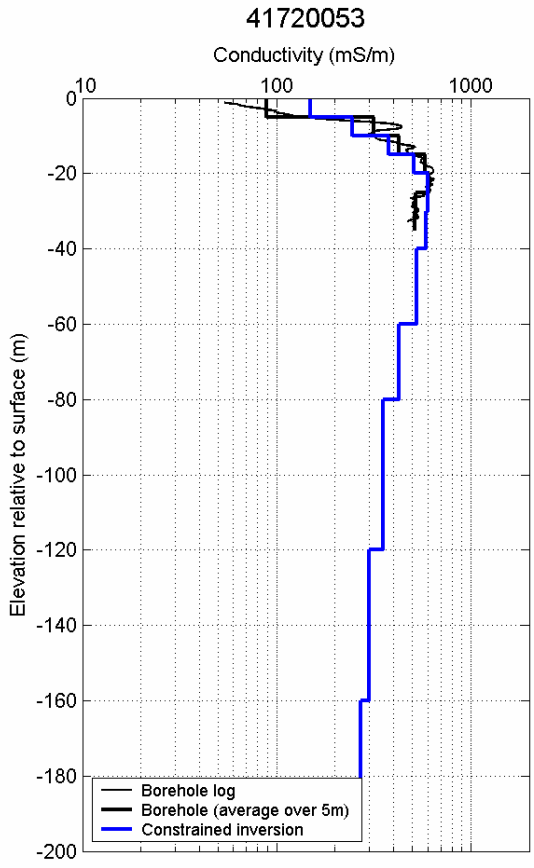
41720053
Conductivity (mS/m)
10
100
1000
0
-20
-40
-60
-80
-100
-120
-140
-160
-180
-200
Elevation relative to surface (m)
Borehole log
Borehole (average over 5m)
Constrained inversion

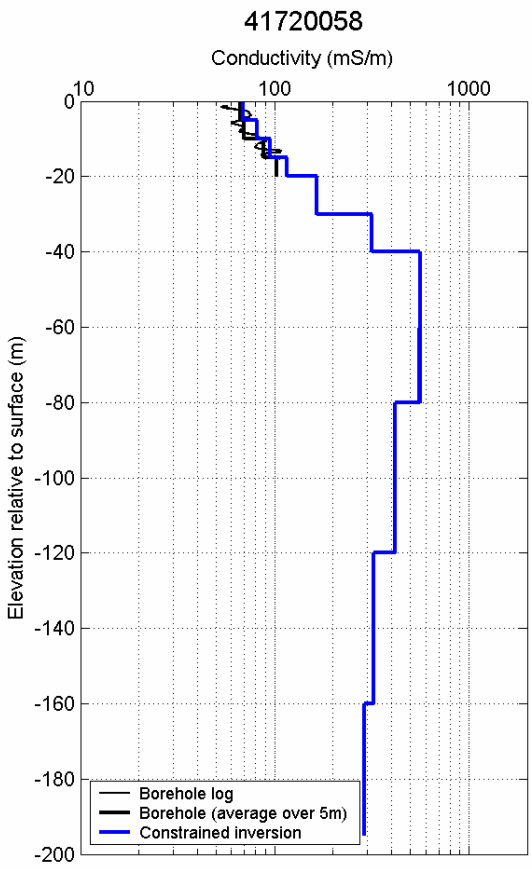
41720058
Conductivity (mS/m)
10
100
1000
0
-20
-40
-60
-80
-100
-120
-140
-160
-180
-200
Elevation relative to surface (m)
Borehole log
Borehole (average over 5m)
Constrained inversion

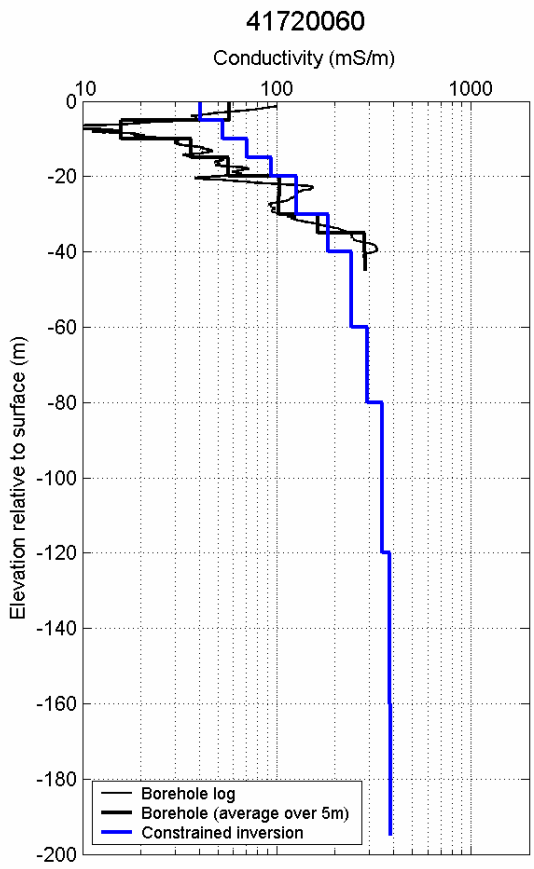
41720060
Conductivity (mS/m)
10
100
1000
0
-20
-40
-60
-80
-100
-120
-140
-160
-180
-200
Elevation relative to surface (m)
Borehole log
Borehole (average over 5m)
Constrained inversion

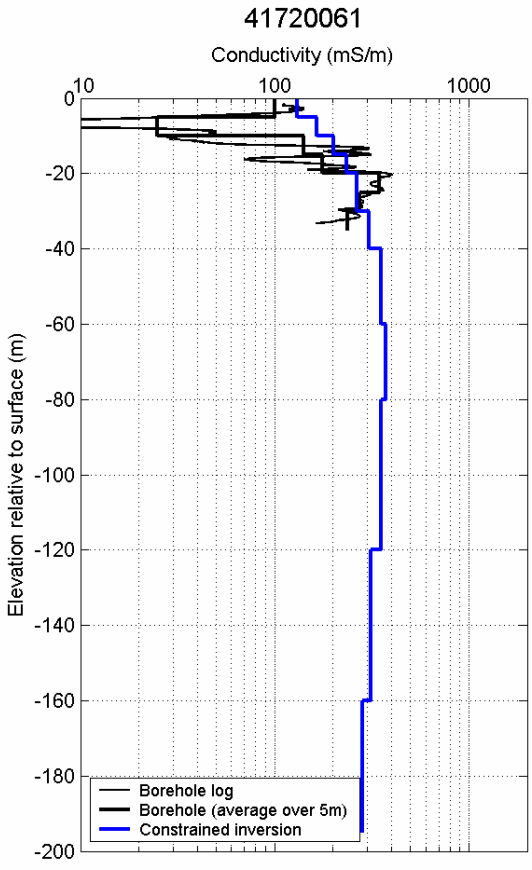
41720061
Conductivity (mS/m)
10
100
1000
0
-20
-40
-60
-80
-100
-120
-140
-160
-180
-200
Elevation relative to surface (m)
Borehole log
Borehole (average over 5m)
Constrained inversion

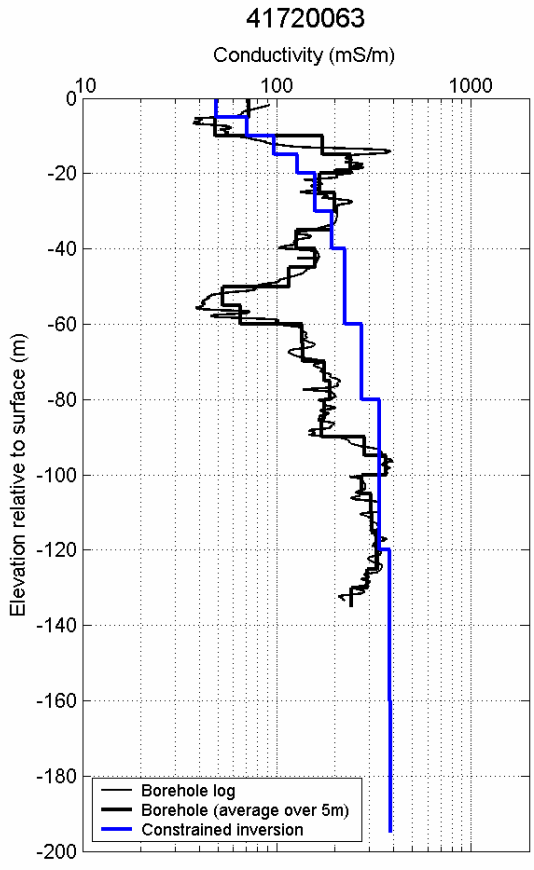
41720063
Conductivity (mS/m)
10
100
1000
0
-20
-40
-60
-80
-100
-120
-140
-160
-180
-200
Elevation relative to surface (m)
Borehole log
Borehole (average over 5m)
Constrained inversion

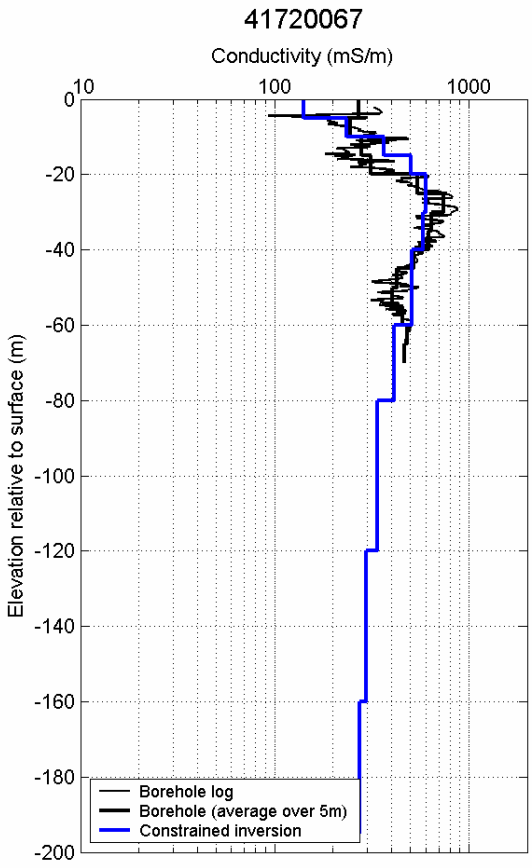
41720067
Conductivity (mS/m)
10
100
1000
0
-20
-40
-60
-80
-100
-120
-140
-160
-180
-200
Elevation relative to surface (m)
Borehole log
Borehole (average over 5m)
Constrained inversion

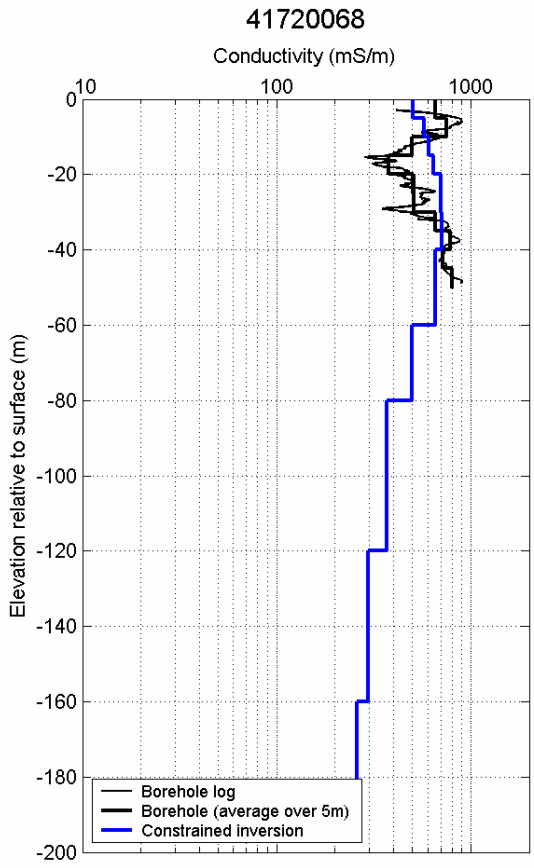
41720068
Conductivity (mS/m)
10
100
1000
0
-20
-40
-60
-80
-100
-120
-140
-160
-180
-200
Elevation relative to surface (m)
Borehole log
Borehole (average over 5m)
Constrained inversion

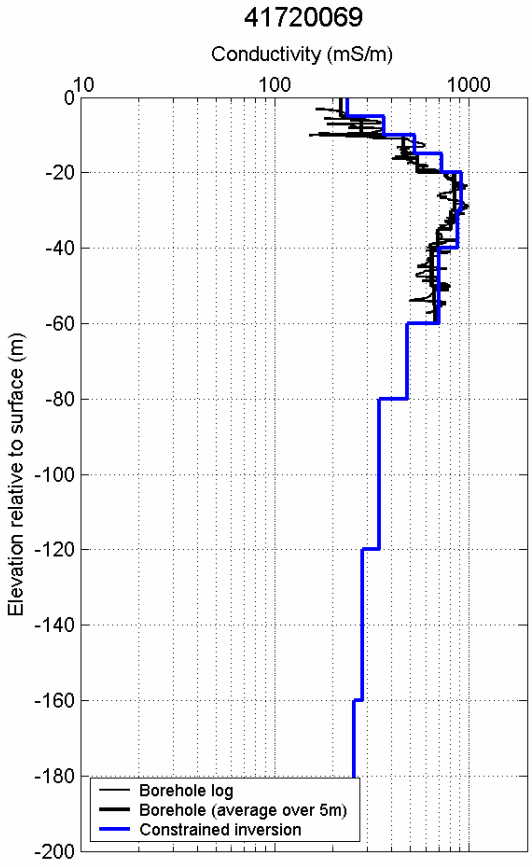
41720069
Conductivity (mS/m)
10
100
1000
0
-20
-40
-60
-80
-100
-120
-140
-160
-180
-200
Elevation relative to surface (m)
Borehole log
Borehole (average over 5m)
Constrained inversion

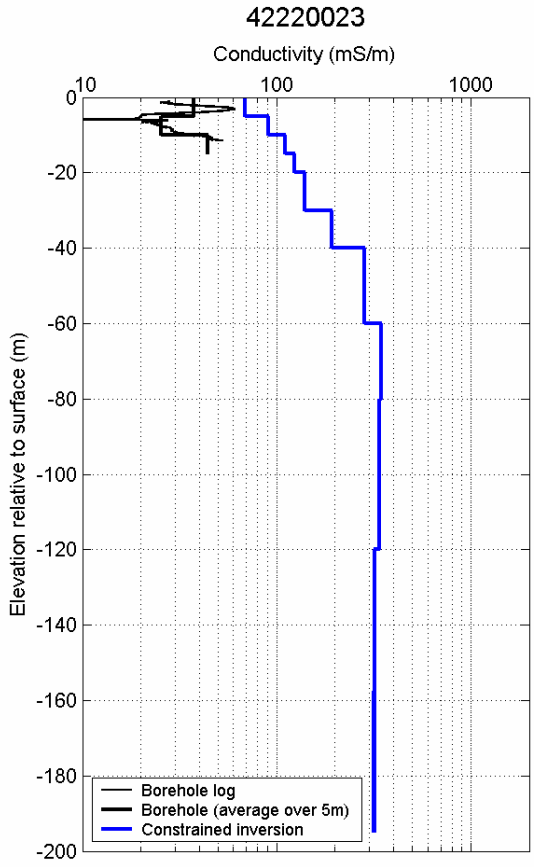
42220023
Conductivity (mS/m)
10
100
1000
0
-20
-40
-60
-80
-100
-120
-140
-160
-180
-200
Elevation relative to surface (m)
Borehole log
Borehole (average over 5m)
Constrained inversion

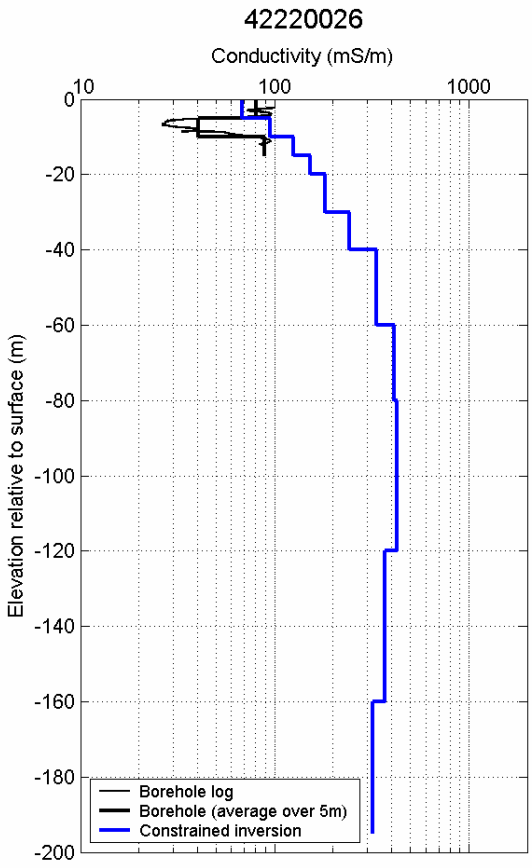
42220026
Conductivity (mS/m)
10
100
1000
0
-20
-40
-60
-80
-100
-120
-140
-160
-180
-200
Elevation relative to surface (m)
Borehole log
Borehole (average over 5m)
Constrained inversion

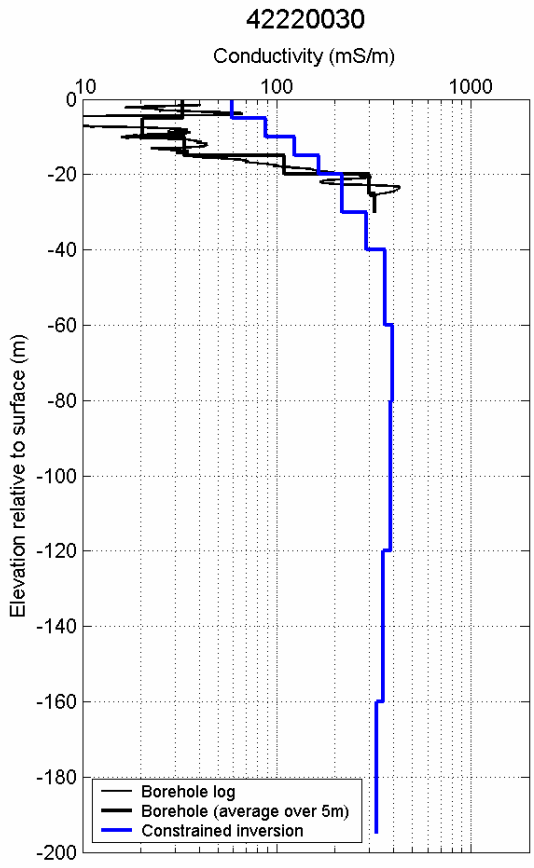
42220030
Conductivity (mS/m)
10
100
1000
0
-20
-40
-60
-80
-100
-120
-140
-160
-180
-200
Elevation relative to surface (m)
Borehole log
Borehole (average over 5m)
Constrained inversion

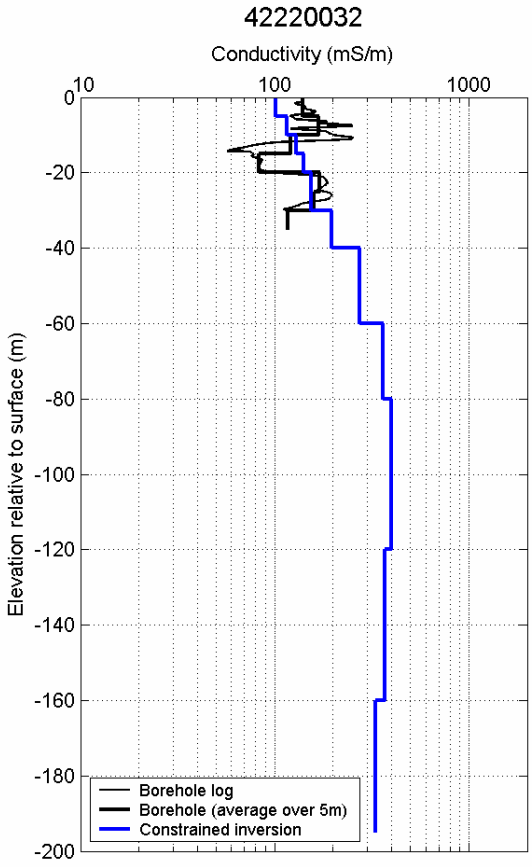
42220032
Conductivity (mS/m)
10
100
1000
0
-20
-40
-60
-80
-100
-120
-140
-160
-180
-200
Elevation relative to surface (m)
Borehole log
Borehole (average over 5m)
Constrained inversion

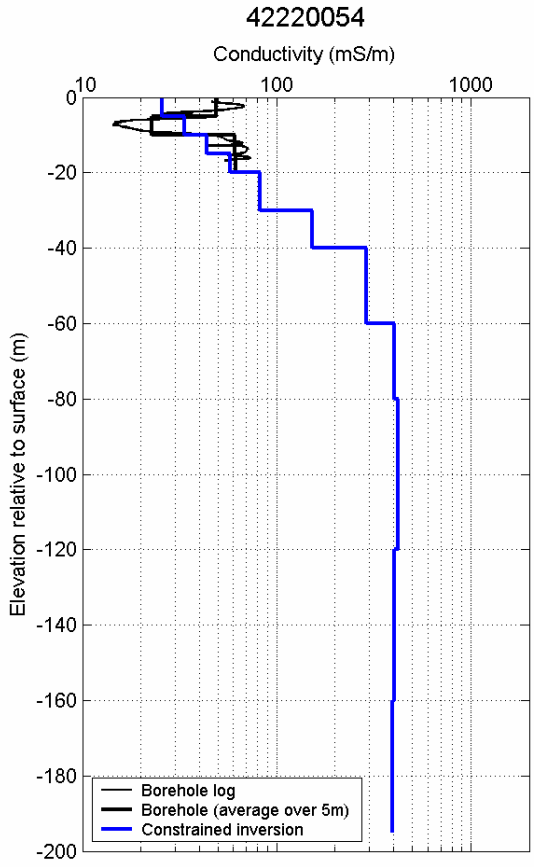
42220054
Conductivity (mS/m)
10
100
1000
0
-20
-40
-60
-80
-100
-120
-140
-160
-180
-200
Elevation relative to surface (m)
Borehole log
Borehole (average over 5m)
Constrained inversion

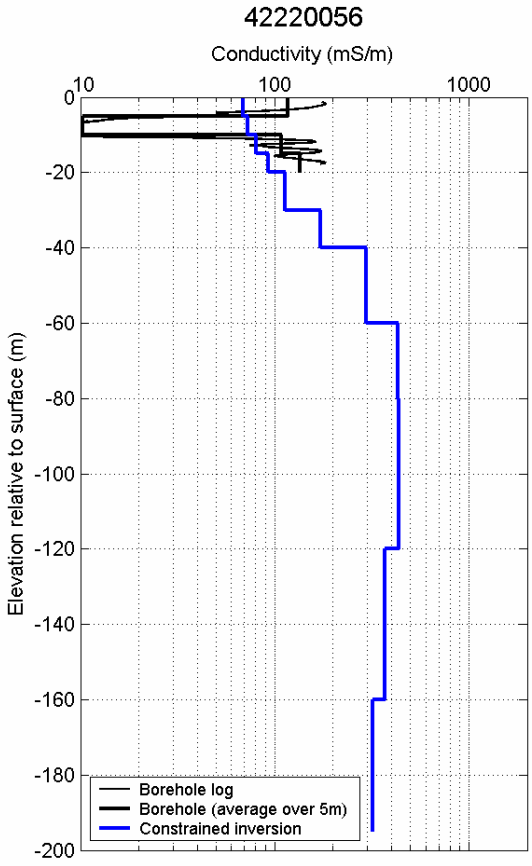
42220056
Conductivity (mS/m)
10
100
1000
0
-20
-40
-60
-80
-100
-120
-140
-160
-180
-200
Elevation relative to surface (m)
Borehole log
Borehole (average over 5m)
Constrained inversion

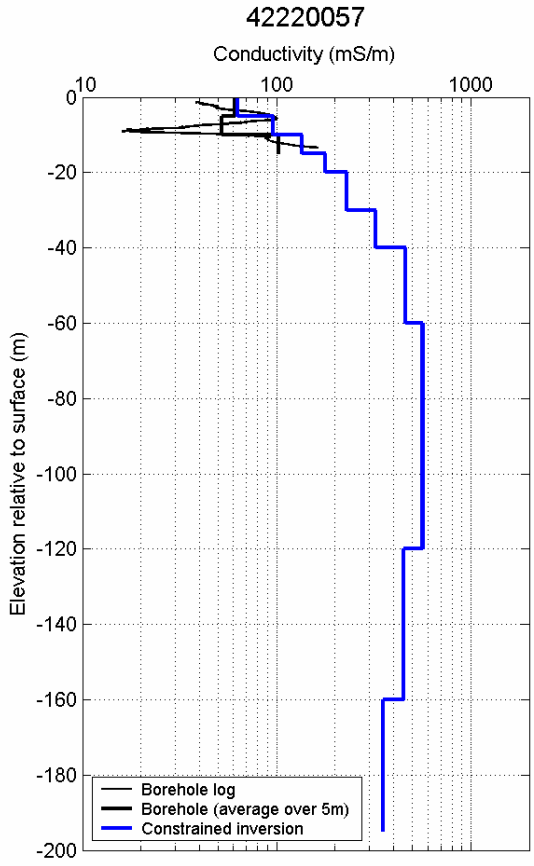
42220057
Conductivity (mS/m)
10
100
1000
0
-20
-40
-60
-80
-100
-120
-140
-160
-180
-200
Elevation relative to surface (m)
Borehole log
Borehole (average over 5m)
Constrained inversion

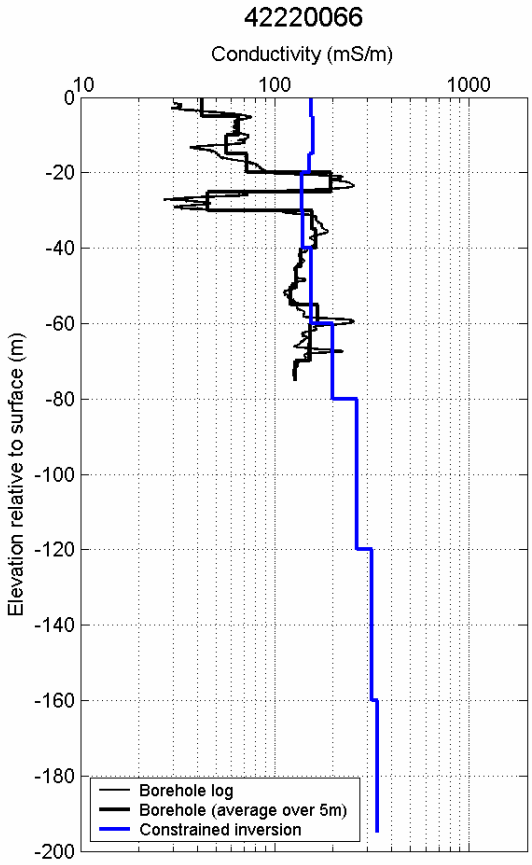
42220066
Conductivity (mS/m)
10
100
1000
0
-20
-40
-60
-80
-100
-120
-140
-160
-180
-200
Elevation relative to surface (m)
Borehole log
Borehole (average over 5m)
Constrained inversion

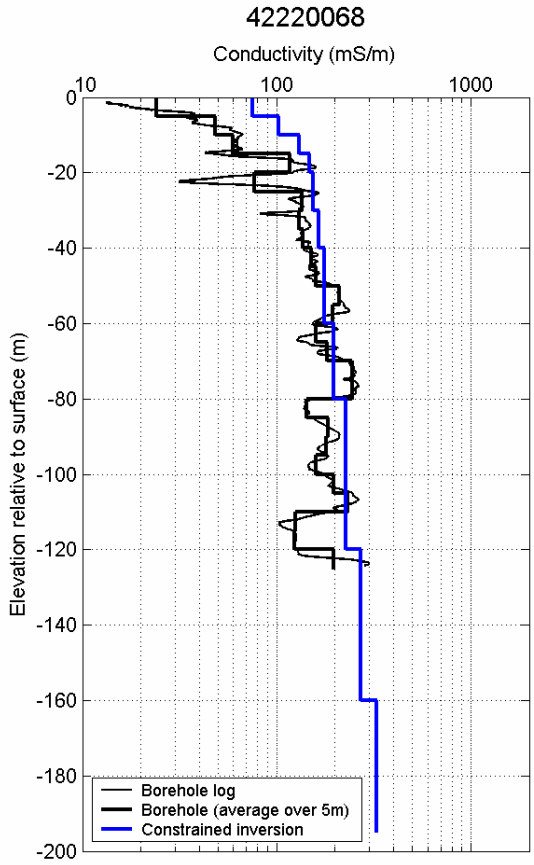
42220068
Conductivity (mS/m)
10
100
1000
0
-20
-40
-60
-80
-100
-120
-140
-160
-180
-200
Elevation relative to surface (m)
Borehole log
Borehole (average over 5m)
Constrained inversion

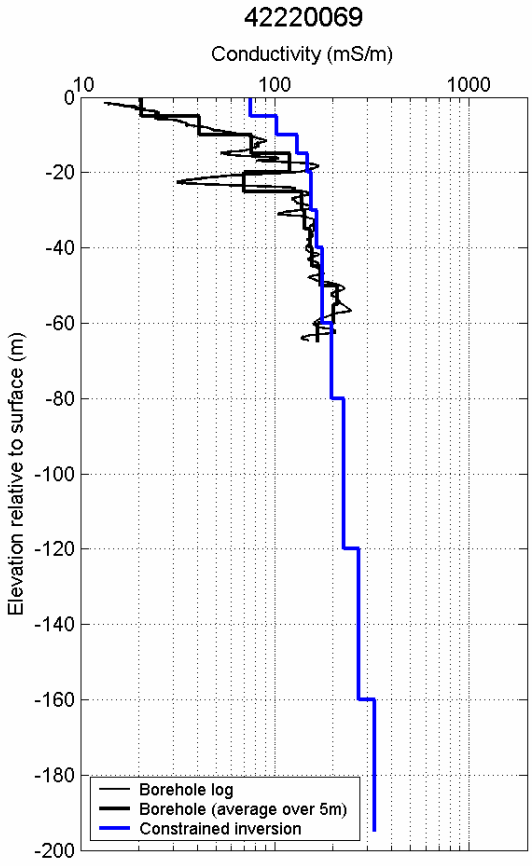
42220069
Conductivity (mS/m)
10
100
1000
0
-20
-40
-60
-80
-100
-120
-140
-160
-180
-200
Elevation relative to surface (m)
Borehole log
Borehole (average over 5m)
Constrained inversion

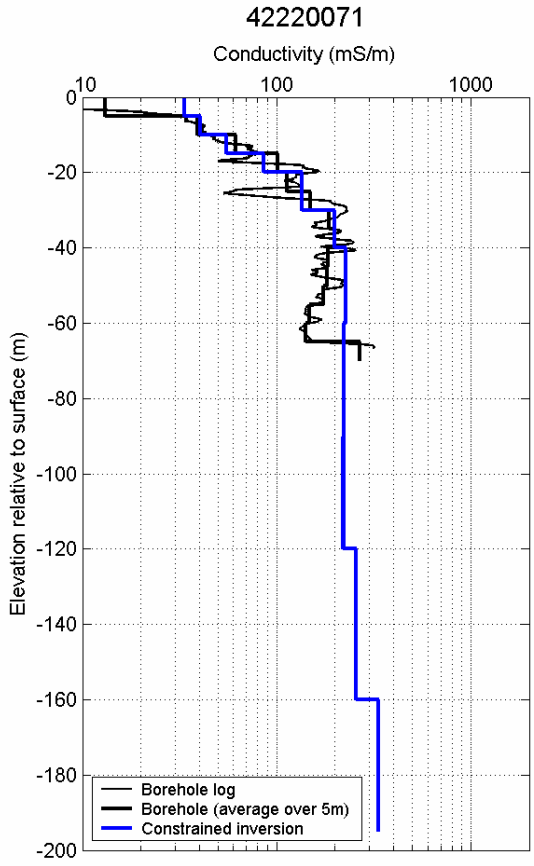
42220071
Conductivity (mS/m)
10
100
1000
0
-20
-40
-60
-80
-100
-120
-140
-160
-180
-200
Elevation relative to surface (m)
Borehole log
Borehole (average over 5m)
Constrained inversion

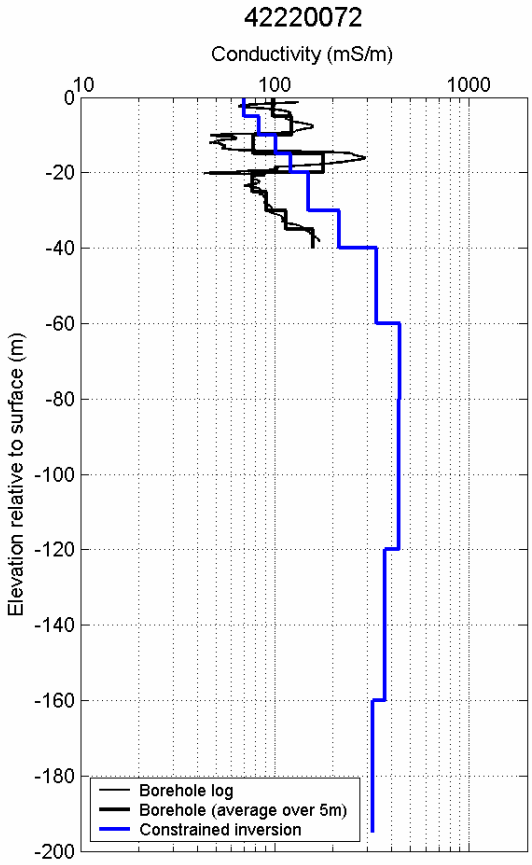
42220072
Conductivity (mS/m)
10
100
1000
0
-20
-40
-60
-80
-100
-120
-140
-160
-180
-200
Elevation relative to surface (m)
Borehole log
Borehole (average over 5m)
Constrained inversion

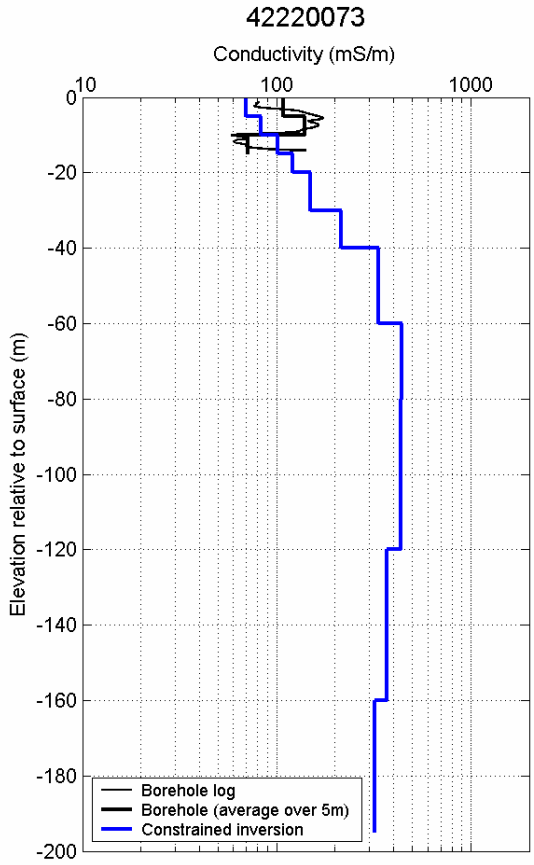
42220073
Conductivity (mS/m)
10
100
1000
0
-20
-40
-60
-80
-100
-120
-140
-160
-180
-200
Elevation relative to surface (m)
Borehole log
Borehole (average over 5m)
Constrained inversion

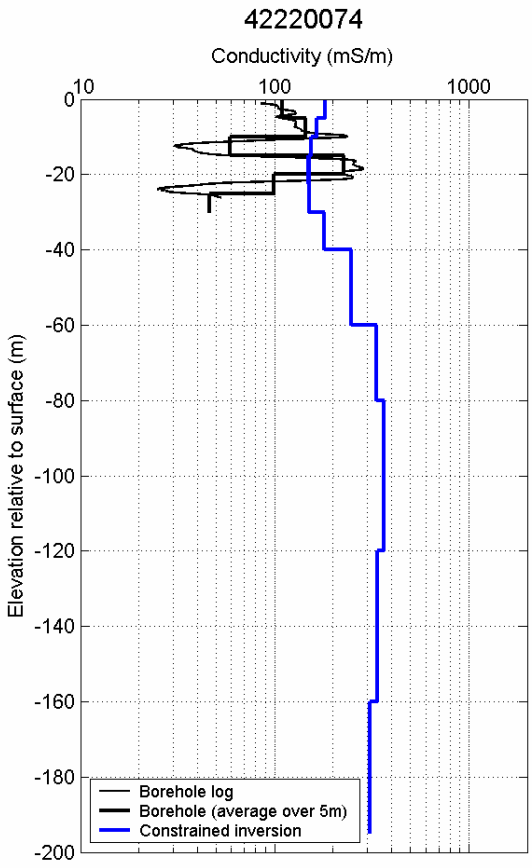
42220074
Conductivity (mS/m)
10
100
1000
0
-20
-40
-60
-80
-100
-120
-140
-160
-180
-200
Elevation relative to surface (m)
Borehole log
Borehole (average over 5m)
Constrained inversion

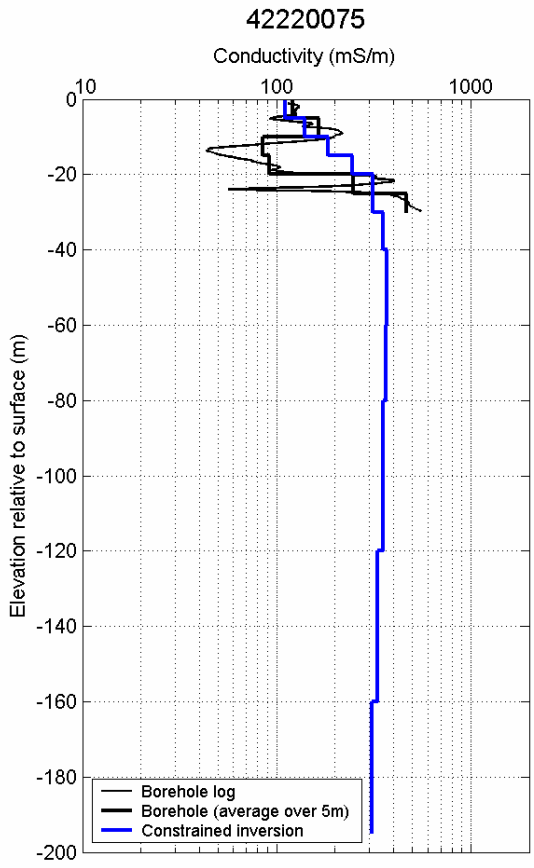
42220075
Conductivity (mS/m)
10
100
1000
0
-20
-40
-60
-80
-100
-120
-140
-160
-180
-200
Elevation relative to surface (m)
Borehole log
Borehole (average over 5m)
Constrained inversion

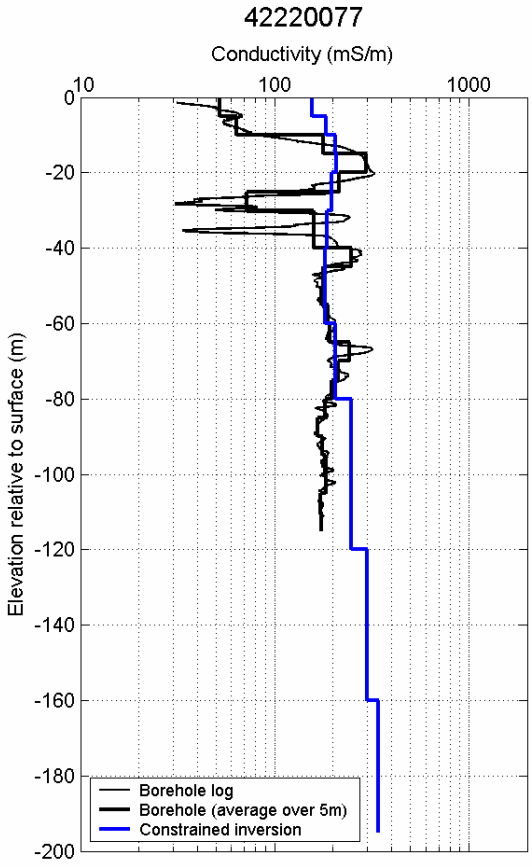
42220077
Conductivity (mS/m)
10
100
1000
0
-20
-40
-60
-80
-100
-120
-140
-160
-180
-200
Elevation relative to surface (m)
Borehole log
Borehole (average over 5m)
Constrained inversion

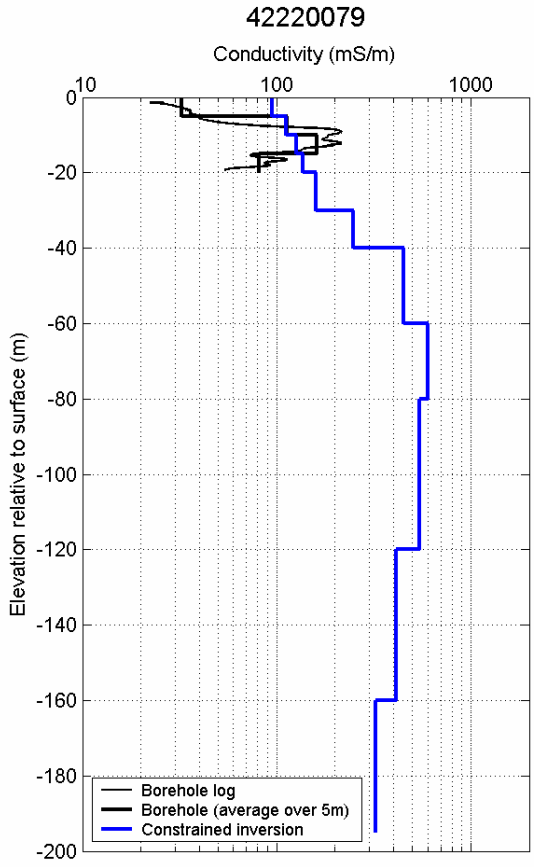
42220079
Conductivity (mS/m)
10
100
1000
0
-20
-40
-60
-80
-100
-120
-140
-160
-180
-200
Elevation relative to surface (m)
Borehole log
Borehole (average over 5m)
Constrained inversion

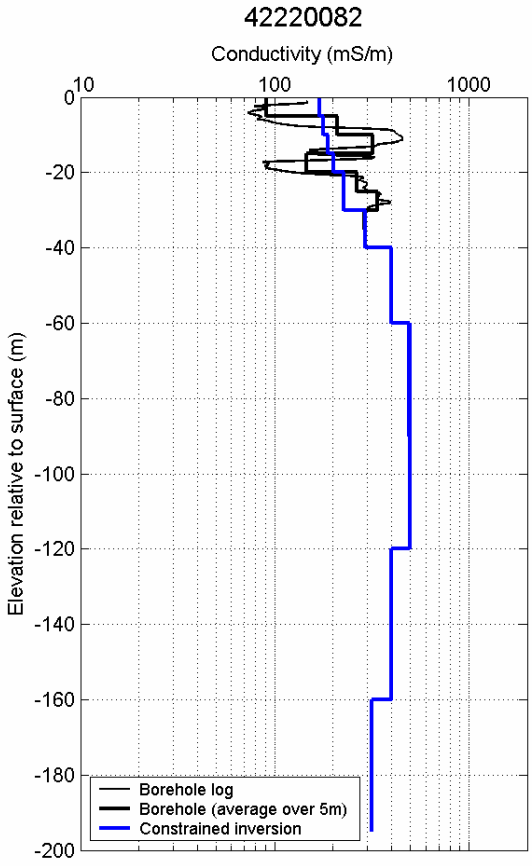
42220082
Conductivity (mS/m)
10
100
1000
0
-20
-40
-60
-80
-100
-120
-140
-160
-180
-200
Elevation relative to surface (m)
Borehole log
Borehole (average over 5m)
Constrained inversion

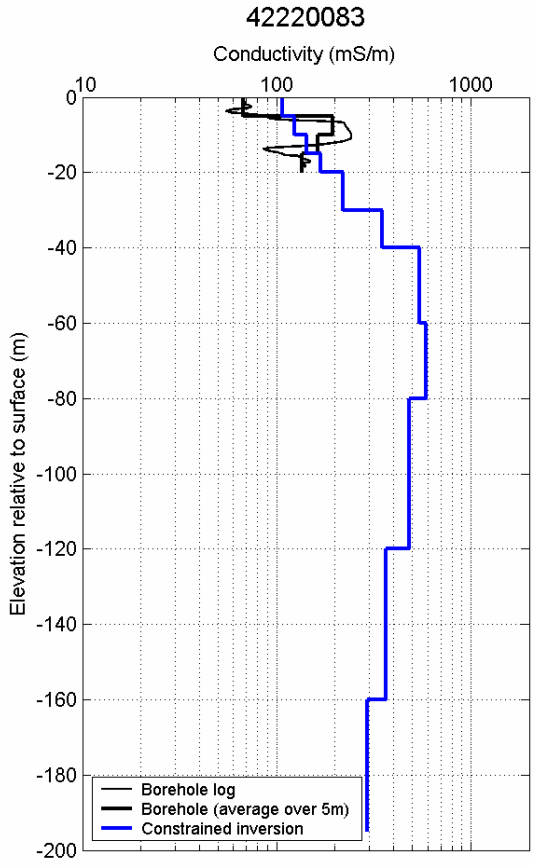
42220083
Conductivity (mS/m)
10
100
1000
0
-20
-40
-60
-80
-100
-120
-140
-160
-180
-200
Elevation relative to surface (m)
Borehole log
Borehole (average over 5m)
Constrained inversion

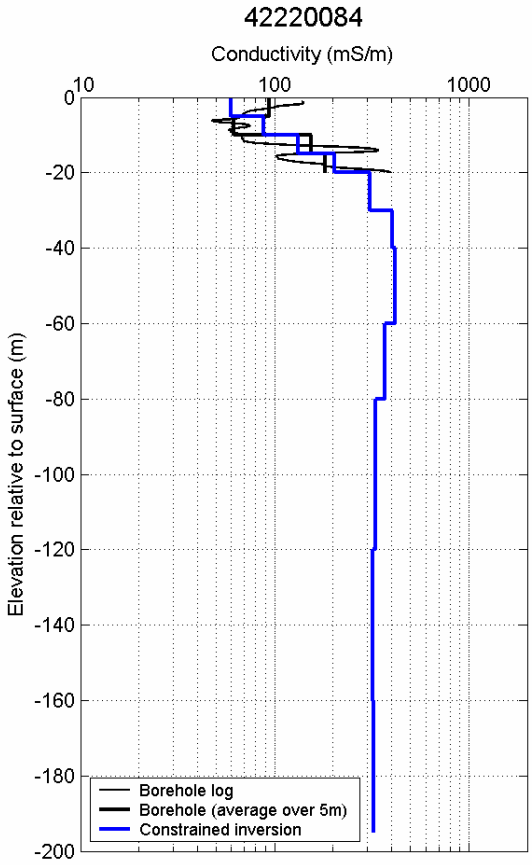
42220084
Conductivity (mS/m)
10
100
1000
0
-20
-40
-60
-80
-100
-120
-140
-160
-180
-200
Elevation relative to surface (m)
Borehole log
Borehole (average over 5m)
Constrained inversion

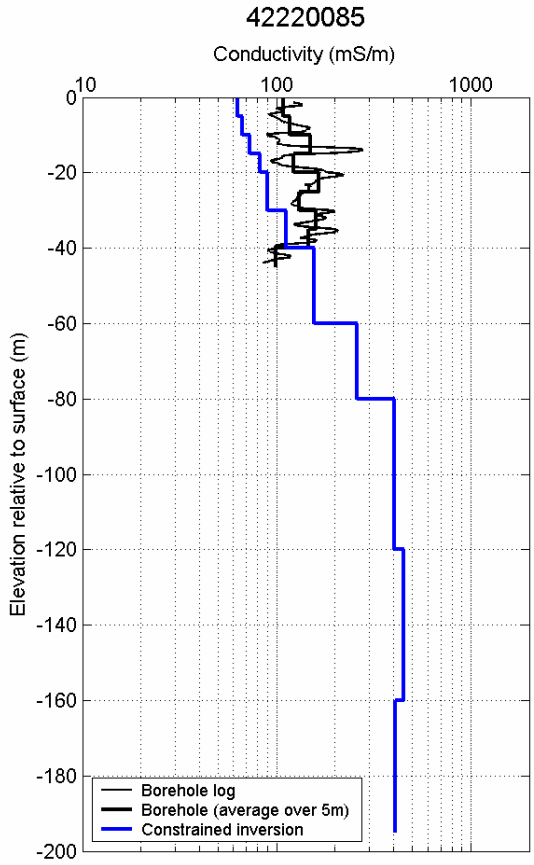
42220085
Conductivity (mS/m)
10
100
1000
0
-20
-40
-60
-80
-100
-120
-140
-160
-180
-200
Elevation relative to surface (m)
Borehole log
Borehole (average over 5m)
Constrained inversion

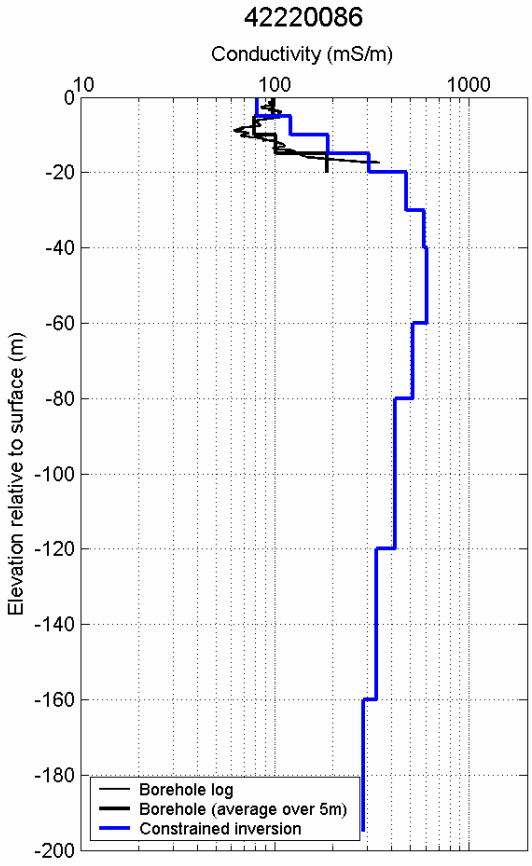
42220086
Conductivity (mS/m)
10
100
1000
0
-20
-40
-60
-80
-100
-120
-140
-160
-180
-200
Elevation relative to surface (m)
Borehole log
Borehole (average over 5m)
Constrained inversion

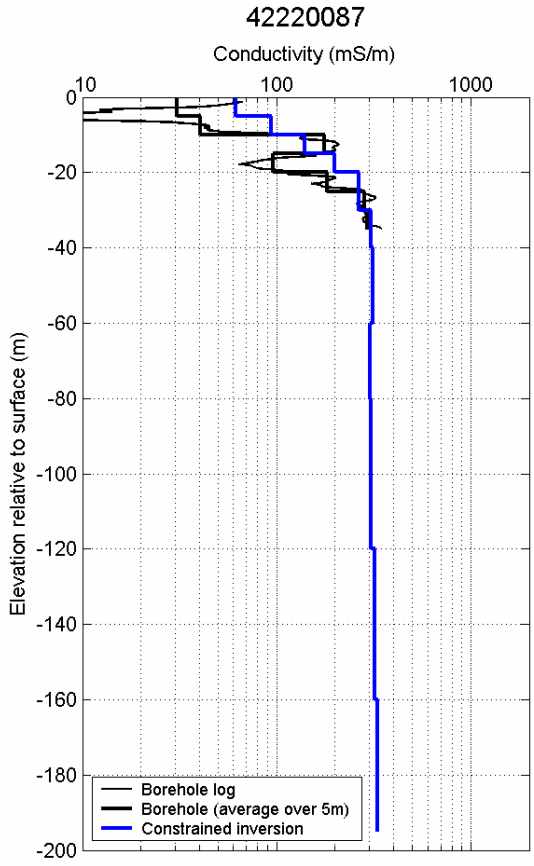
42220087
Conductivity (mS/m)
10
100
1000
0
-20
-40
-60
-80
-100
-120
-140
-160
-180
-200
Elevation relative to surface (m)
Borehole log
Borehole (average over 5m)
Constrained inversion

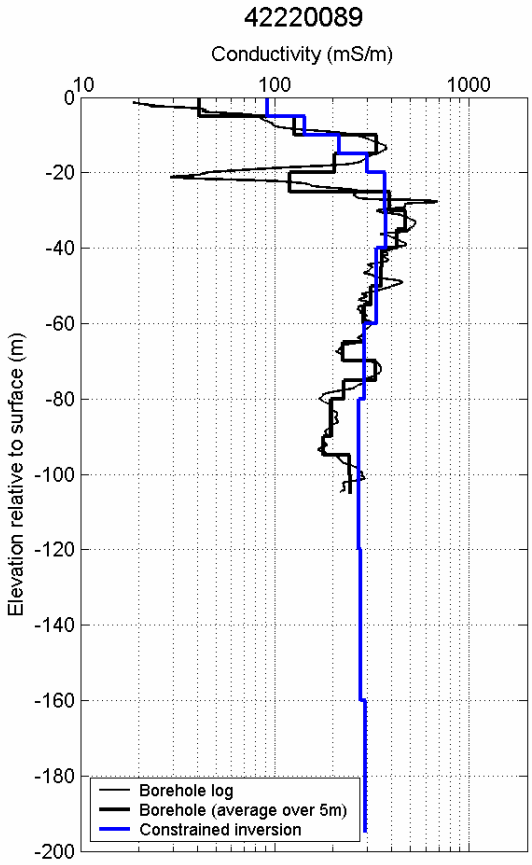
42220089
Conductivity (mS/m)
10
100
1000
0
-20
-40
-60
-80
-100
-120
-140
-160
-180
-200
Elevation relative to surface (m)
Borehole log
Borehole (average over 5m)
Constrained inversion

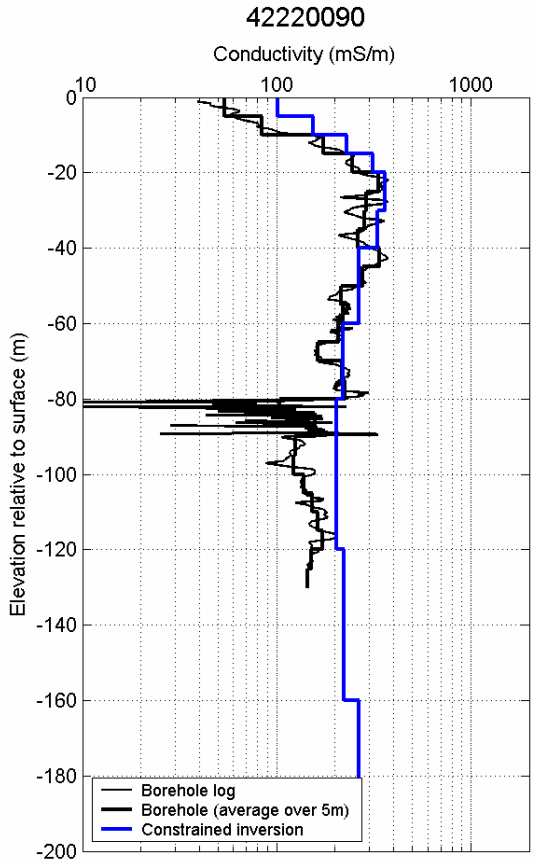
42220090
Conductivity (mS/m)
10
100
1000
0
-20
-40
-60
-80
-100
-120
-140
-160
-180
-200
Elevation relative to surface (m)
Borehole log
Borehole (average over 5m)
Constrained inversion

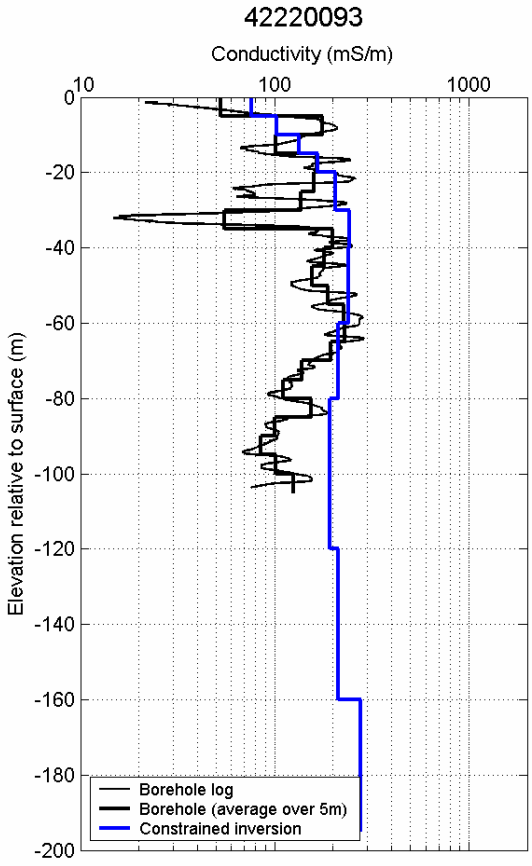
42220093
Conductivity (mS/m)
10
100
1000
0
-20
-40
-60
-80
-100
-120
-140
-160
-180
-200
Elevation relative to surface (m)
Borehole log
Borehole (average over 5m)
Constrained inversion

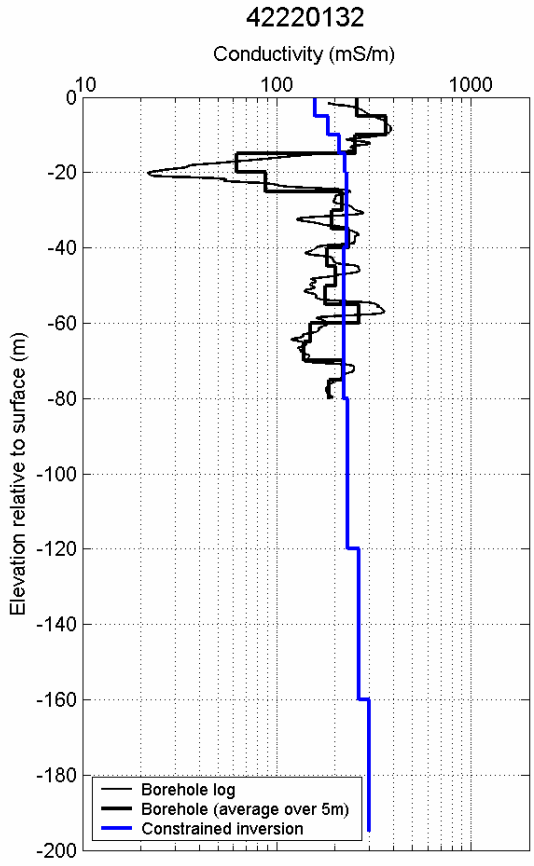
42220132
Conductivity (mS/m)
10
100
1000
0
-20
-40
-60
-80
-100
-120
-140
-160
-180
-200
Elevation relative to surface (m)
Borehole log
Borehole (average over 5m)
Constrained inversion

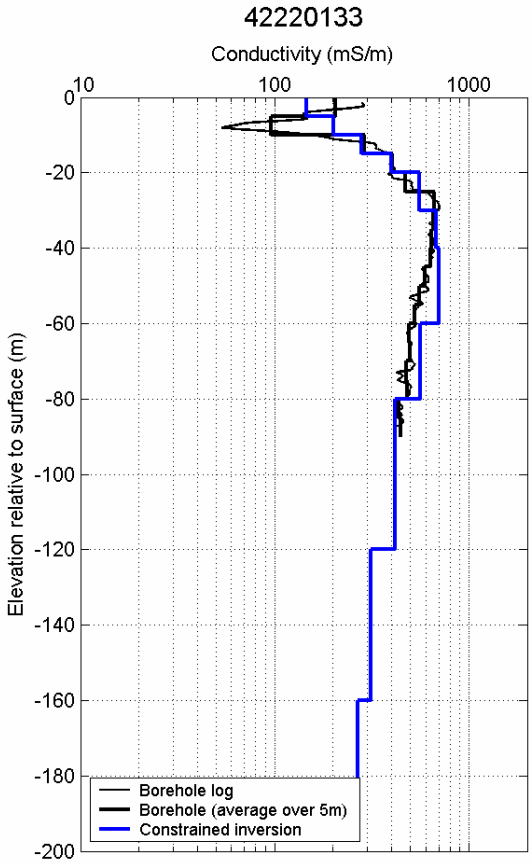
42220133
Conductivity (mS/m)
10
100
1000
0
-20
-40
-60
-80
-100
-120
-140
-160
-180
-200
Elevation relative to surface (m)
Borehole log
Borehole (average over 5m)
Constrained inversion

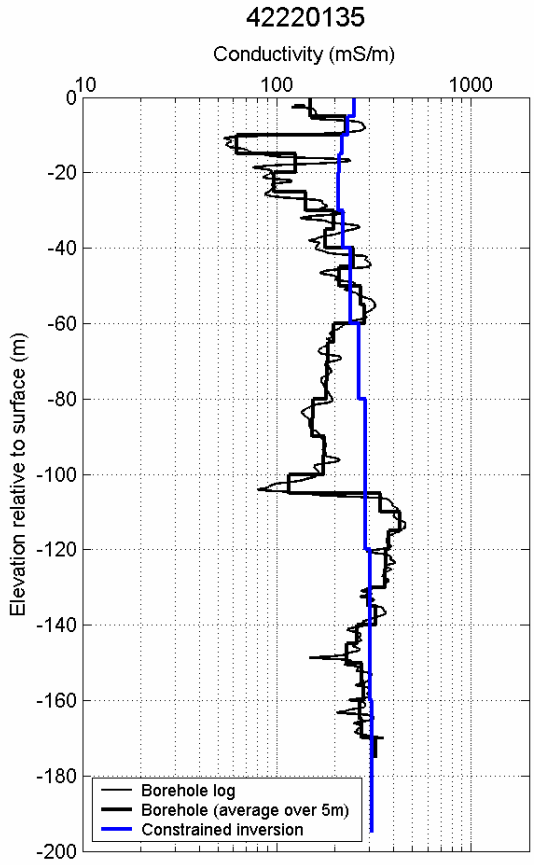
42220135
Conductivity (mS/m)
10
100
1000
0
-20
-40
-60
-80
-100
-120
-140
-160
-180
-200
Elevation relative to surface (m)
Borehole log
Borehole (average over 5m)
Constrained inversion

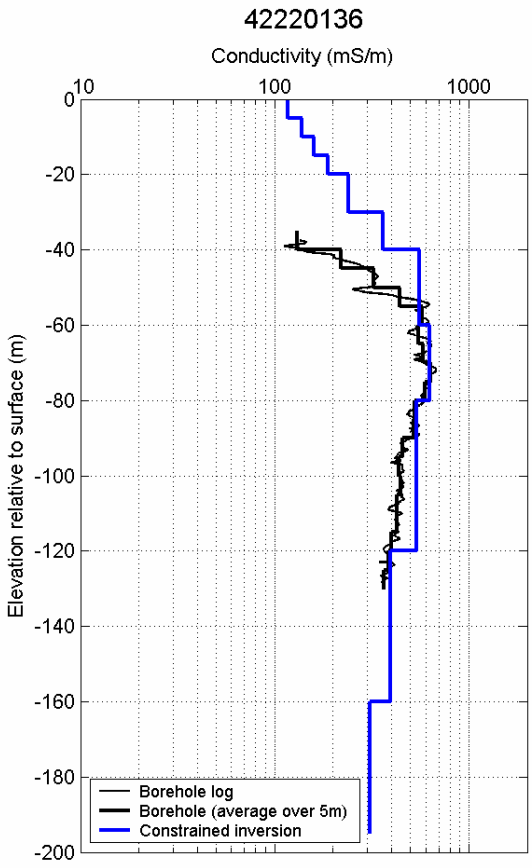
42220136
Conductivity (mS/m)
10
100
1000
0
-20
-40
-60
-80
-100
-120
-140
-160
-180
-200
Elevation relative to surface (m)
Borehole log
Borehole (average over 5m)
Constrained inversion

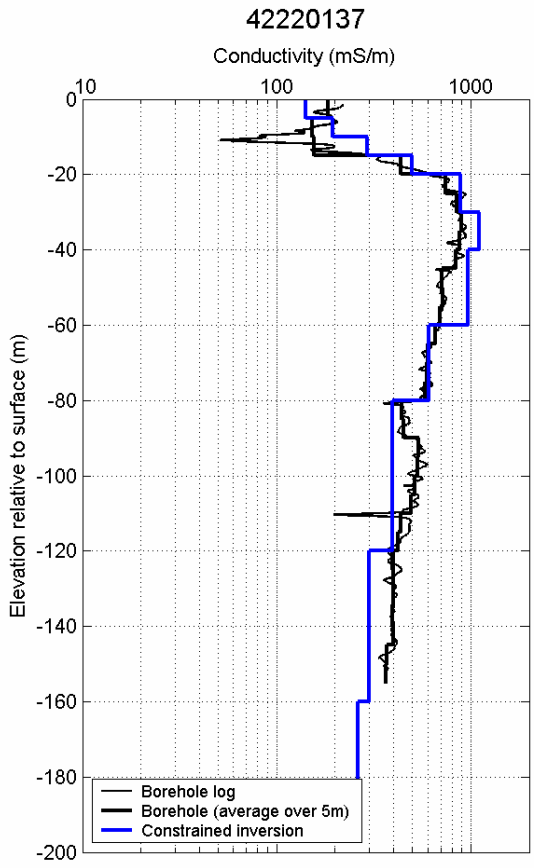
42220137
Conductivity (mS/m)
10
100
1000
0
-20
-40
-60
-80
-100
-120
-140
-160
-180
-200
Elevation relative to surface (m)
Borehole log
Borehole (average over 5m)
Constrained inversion

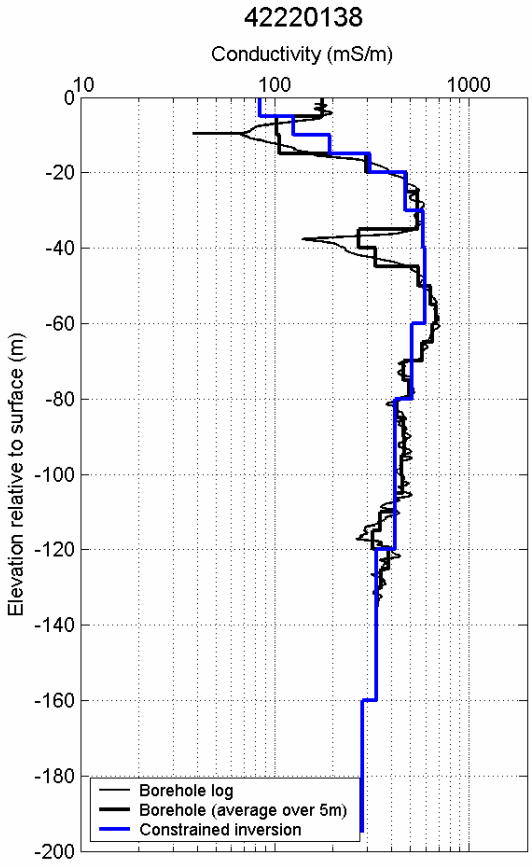
42220138
Conductivity (mS/m)
10
100
1000
0
-20
-40
-60
-80
-100
-120
-140
-160
-180
-200
Elevation relative to surface (m)
Borehole log
Borehole (average over 5m)
Constrained inversion

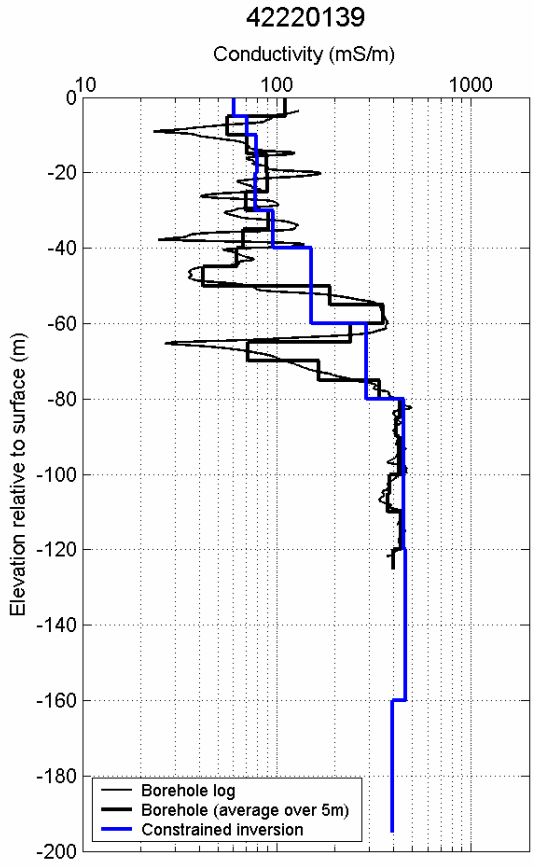
42220139
Conductivity (mS/m)
10
100
1000
0
-20
-40
-60
-80
-100
-120
-140
-160
-180
-200
Elevation relative to surface (m)
Borehole log
Borehole (average over 5m)
Constrained inversion

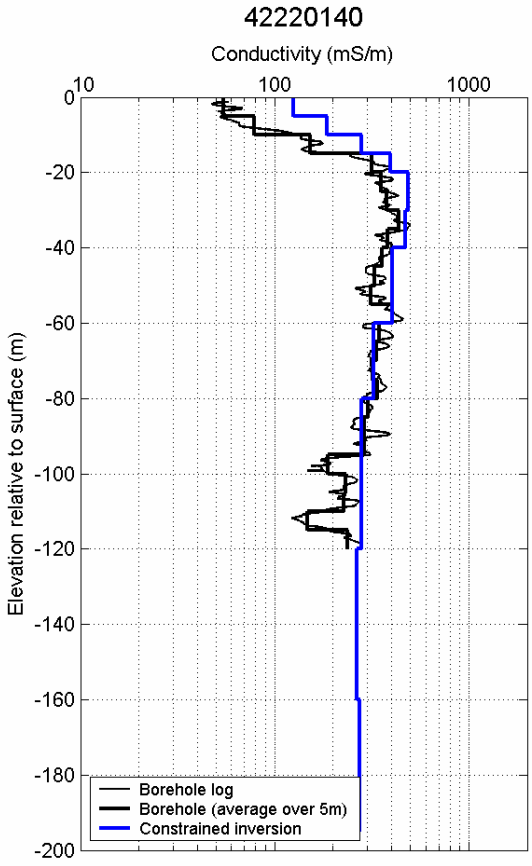
42220140
Conductivity (mS/m)
10
100
1000
0
-20
-40
-60
-80
-100
-120
-140
-160
-180
-200
Elevation relative to surface (m)
Borehole log
Borehole (average over 5m)
Constrained inversion

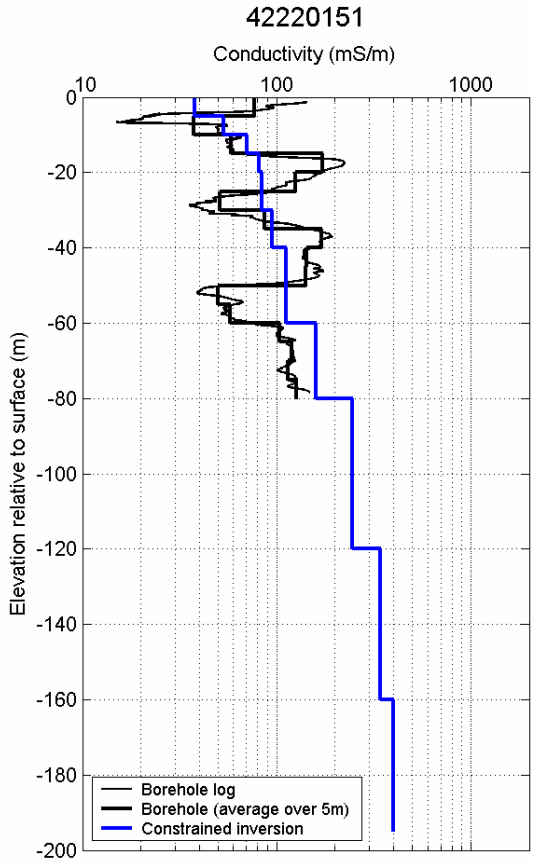
42220151
Conductivity (mS/m)
10
100
1000
0
-20
-40
-60
-80
-100
-120
-140
-160
-180
-200
Elevation relative to surface (m)
Borehole log
Borehole (average over 5m)
Constrained inversion

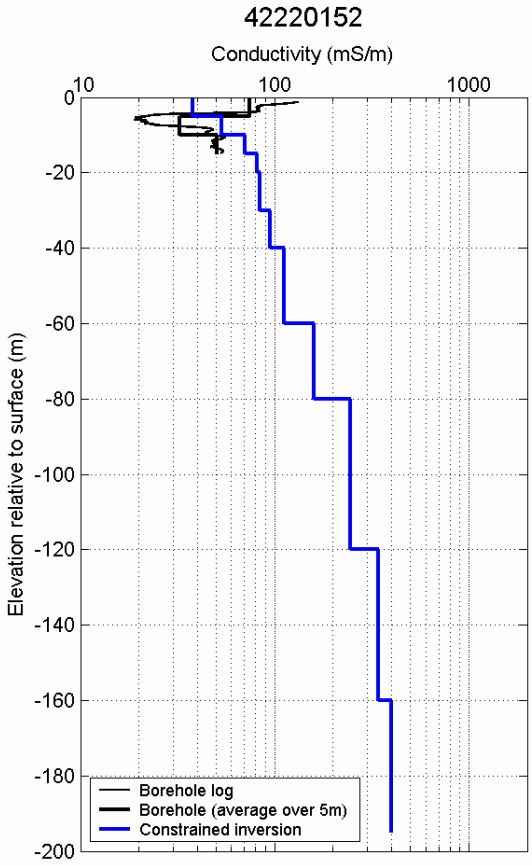
42220152
Conductivity (mS/m)
10
100
1000
0
-20
-40
-60
-80
-100
-120
-140
-160
-180
-200
Elevation relative to surface (m)
Borehole log
Borehole (average over 5m)
Constrained inversion

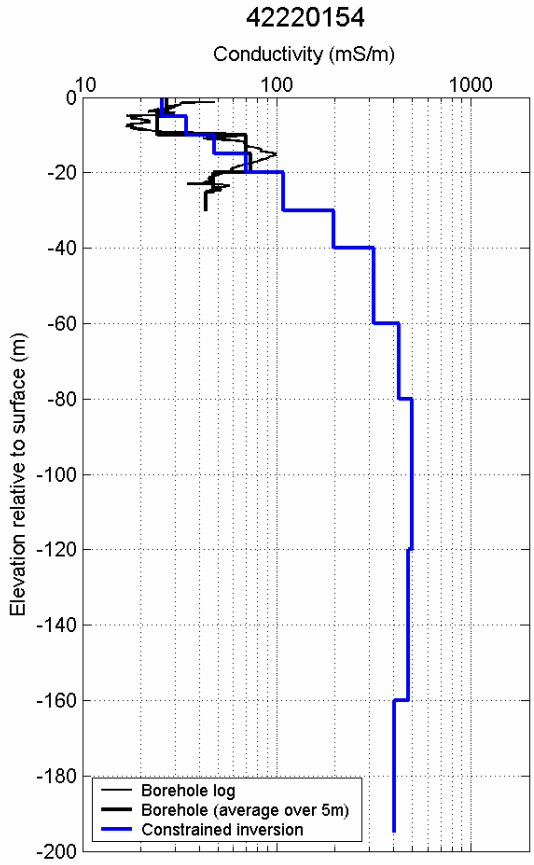
42220154
Conductivity (mS/m)
10
100
1000
0
-20
-40
-60
-80
-100
-120
-140
-160
-180
-200
Elevation relative to surface (m)
Borehole log
Borehole (average over 5m)
Constrained inversion

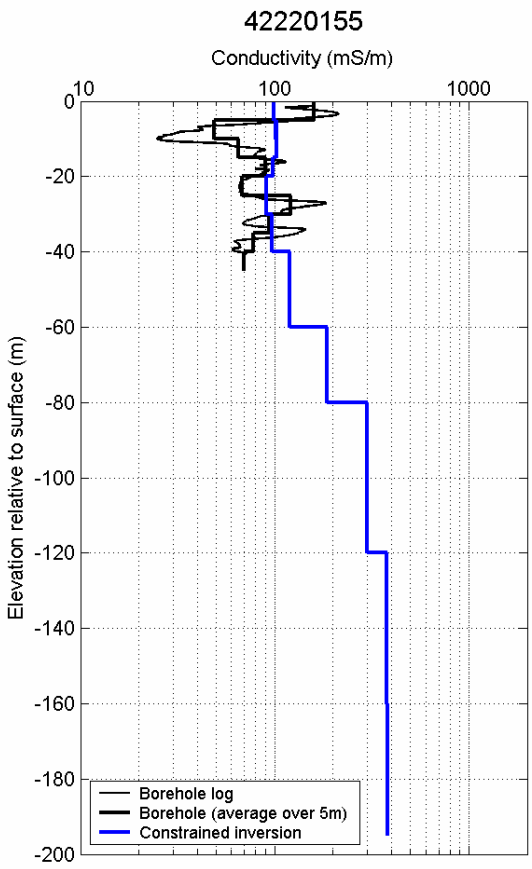
42220155
Conductivity (mS/m)
10
100
1000
0
-20
-40
-60
-80
-100
-120
-140
-160
-180
-200
Elevation relative to surface (m)
Borehole log
Borehole (average over 5m)
Constrained inversion

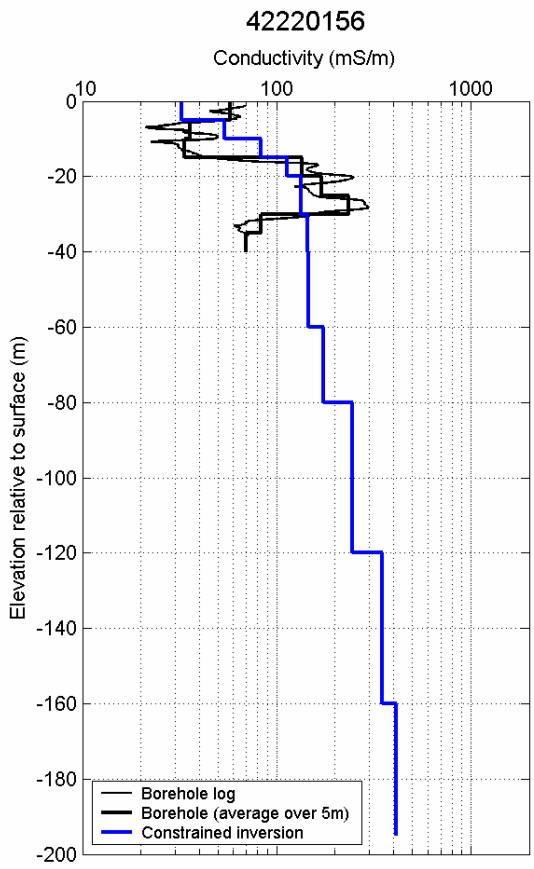
42220156
Conductivity (mS/m)
10
100
1000
0
-20
-40
-60
-80
-100
-120
-140
-160
-180
-200
Elevation relative to surface (m)
Borehole log
Borehole (average over 5m)
Constrained inversion

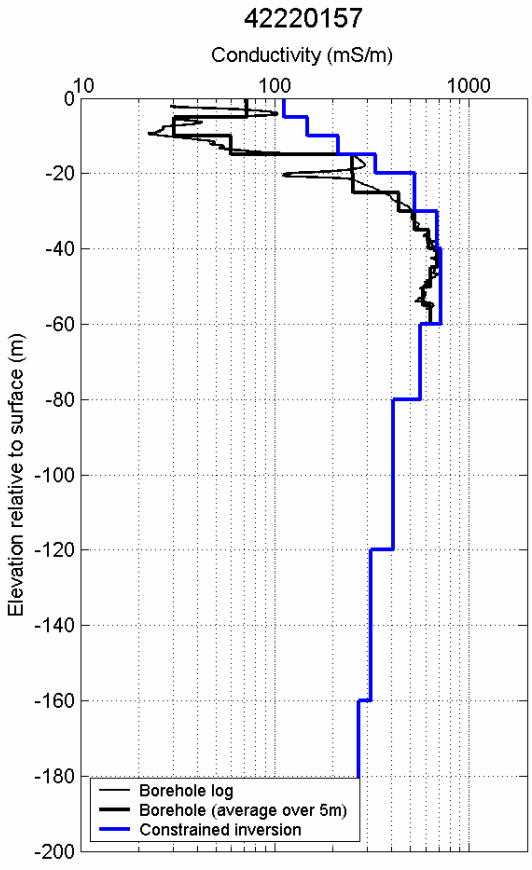
42220157
Conductivity (mS/m)
10
100
1000
0
-20
-40
-60
-80
-100
-120
-140
-160
-180
-200
Elevation relative to surface (m)
Borehole log
Borehole (average over 5m)
Constrained inversion

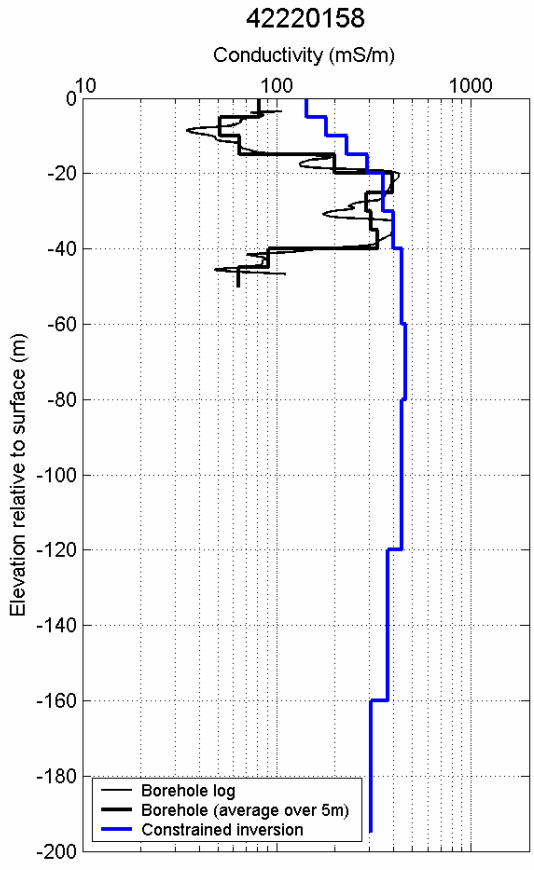
42220158
Conductivity (mS/m)
10
100
1000
0
-20
-40
-60
-80
-100
-120
-140
-160
-180
-200
Elevation relative to surface (m)
Borehole log
Borehole (average over 5m)
Constrained inversion

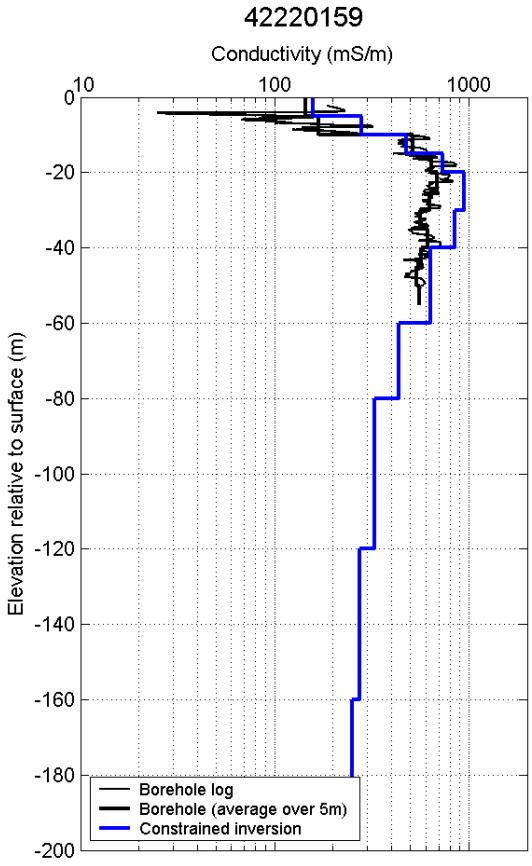
42220159
Conductivity (mS/m)
10
100
1000
0
-20
-40
-60
-80
-100
-120
-140
-160
-180
-200
Elevation relative to surface (m)
Borehole log
Borehole (average over 5m)
Constrained inversion

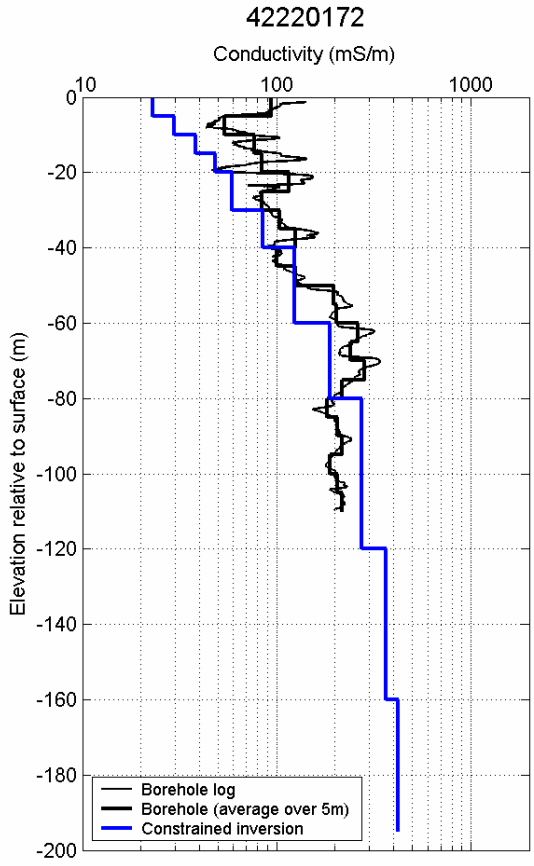
42220172
Conductivity (mS/m)
10
100
1000
0
-20
-40
-60
-80
-100
-120
-140
-160
-180
-200
Elevation relative to surface (m)
Borehole log
Borehole (average over 5m)
Constrained inversion

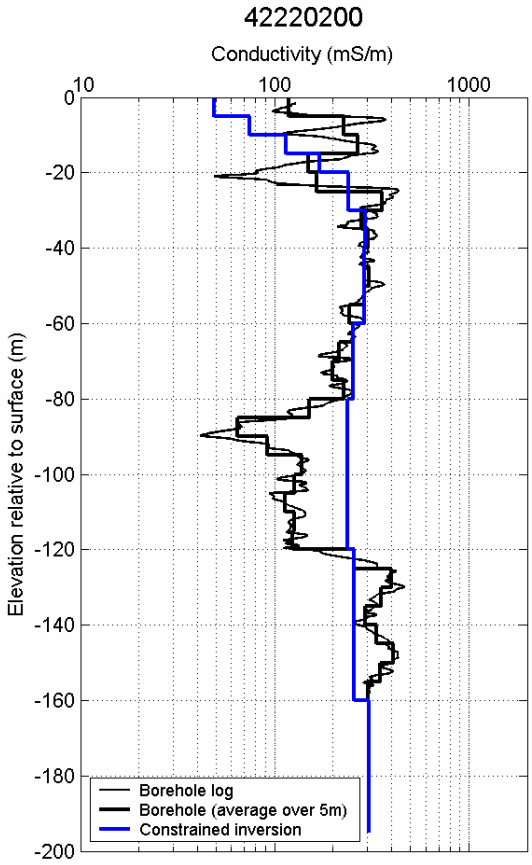
42220200
Conductivity (mS/m)
10
100
1000
0
-20
-40
-60
-80
-100
-120
-140
-160
-180
-200
Elevation relative to surface (m)
Borehole log
Borehole (average over 5m)
Constrained inversion

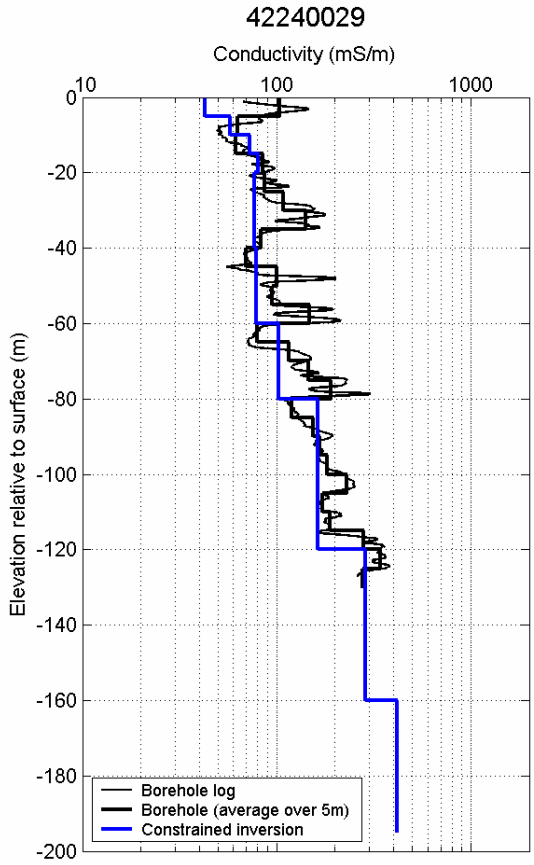
42240029
Conductivity (mS/m)
10
100
1000
0
-20
-40
-60
-80
-100
-120
-140
-160
-180
-200
Elevation relative to surface (m)
Borehole log
Borehole (average over 5m)
Constrained inversion

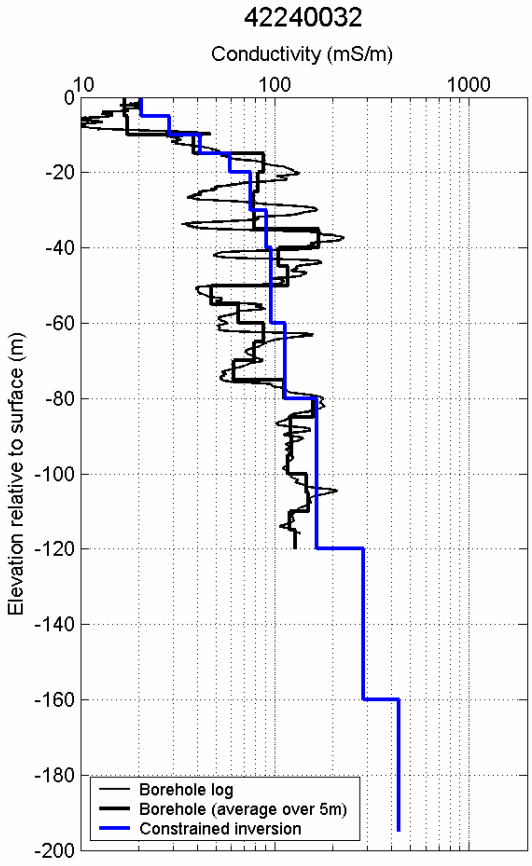
42240032
Conductivity (mS/m)
10
100
1000
0
-20
-40
-60
-80
-100
-120
-140
-160
-180
-200
Elevation relative to surface (m)
Borehole log
Borehole (average over 5m)
Constrained inversion

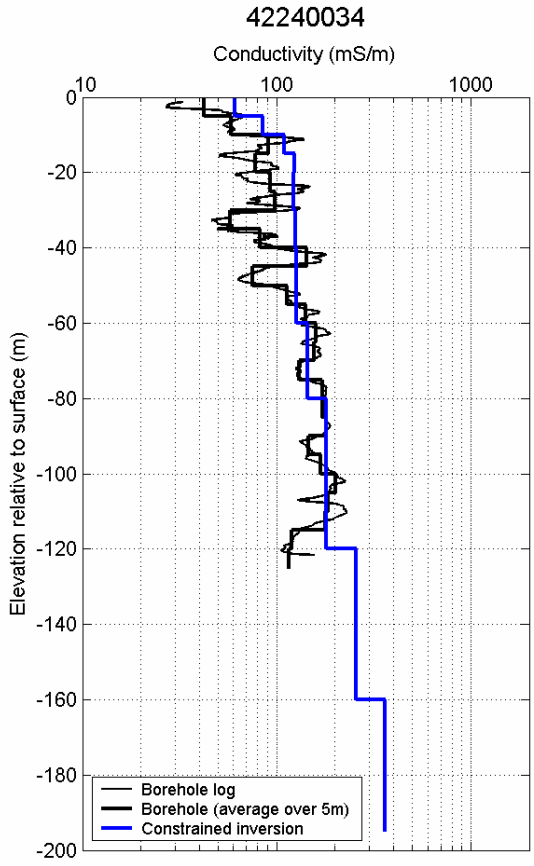
42240034
Conductivity (mS/m)
10
100
1000
0
-20
-40
-60
-80
-100
-120
-140
-160
-180
-200
Elevation relative to surface (m)
Borehole log
Borehole (average over 5m)
Constrained inversion

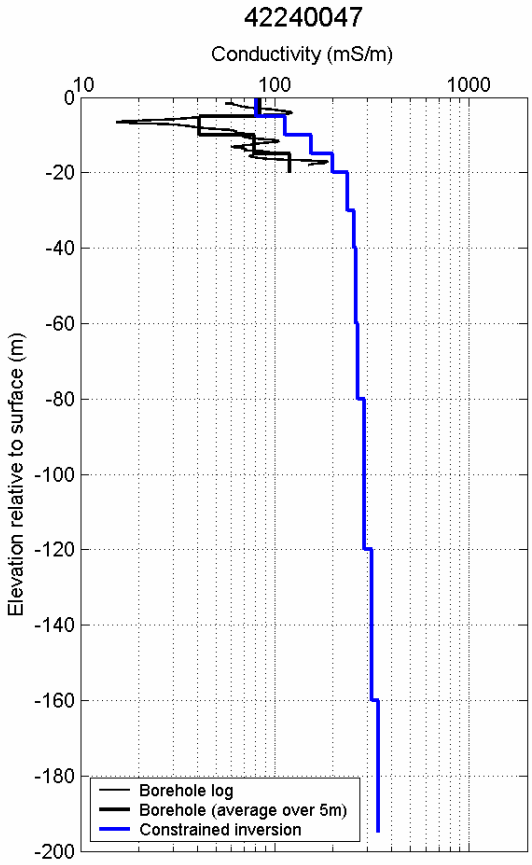
42240047
Conductivity (mS/m)
10
100
1000
0
-20
-40
-60
-80
-100
-120
-140
-160
-180
-200
Elevation relative to surface (m)
Borehole log
Borehole (average over 5m)
Constrained inversion

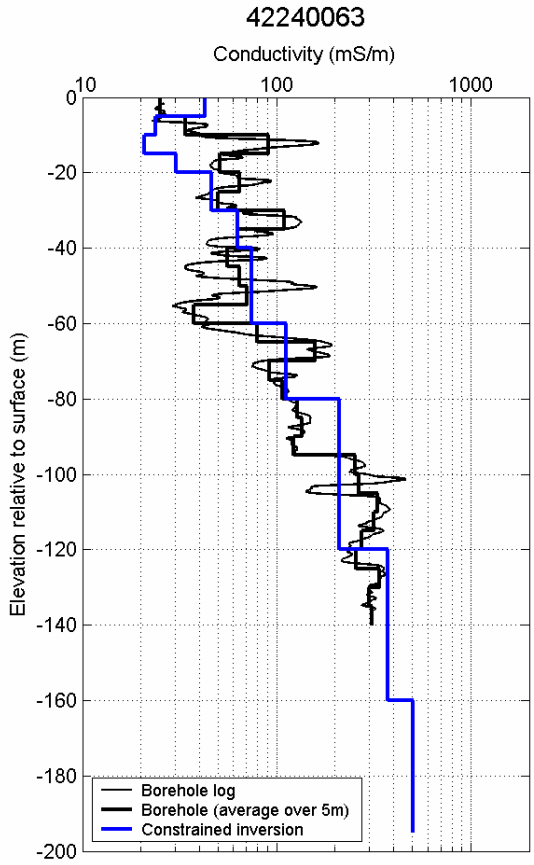
42240063
Conductivity (mS/m)
10
100
1000
0
-20
-40
-60
-80
-100
-120
-140
-160
-180
-200
Elevation relative to surface (m)
Borehole log
Borehole (average over 5m)
Constrained inversion

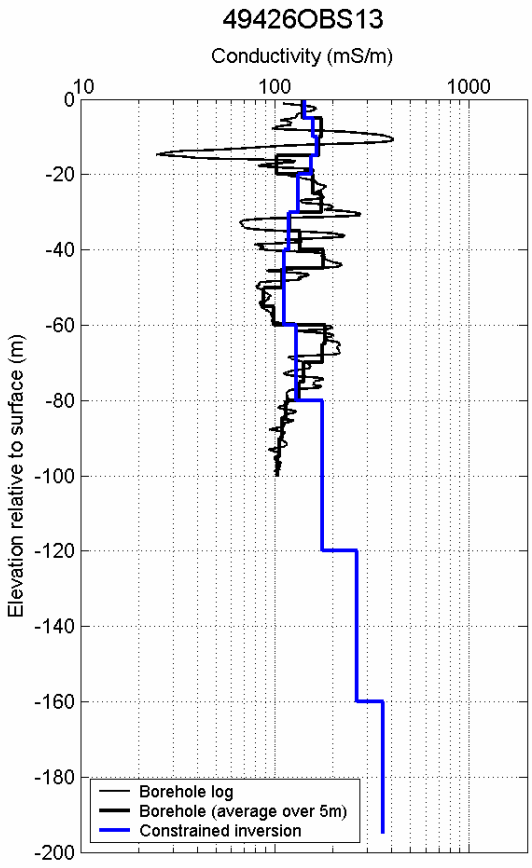
49426OBS13
Conductivity (mS/m)
10
100
1000
0
-20
-40
-60
-80
-100
-120
-140
-160
-180
-200
Elevation relative to surface (m)
Borehole log
Borehole (average over 5m)
Constrained inversion

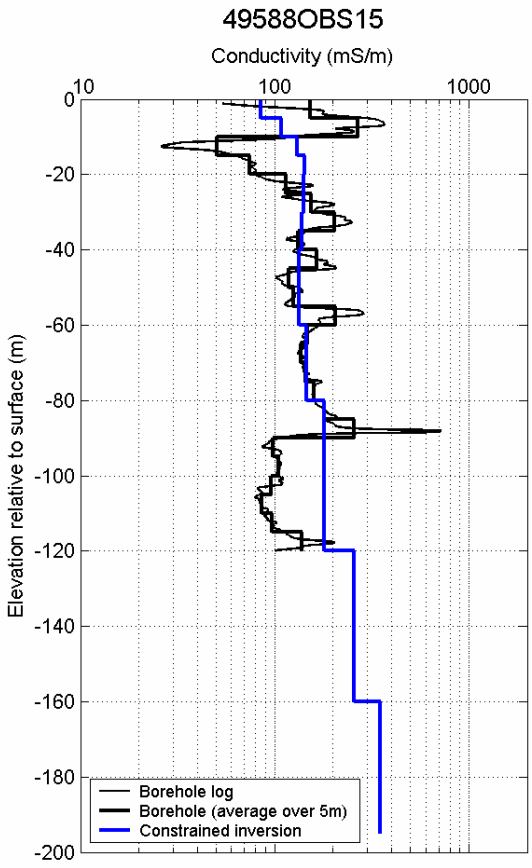
49588OBS15
Conductivity (mS/m)
10
100
1000
0
-20
-40
-60
-80
-100
-120
-140
-160
-180
-200
Elevation relative to surface (m)
Borehole log
Borehole (average over 5m)
Constrained inversion

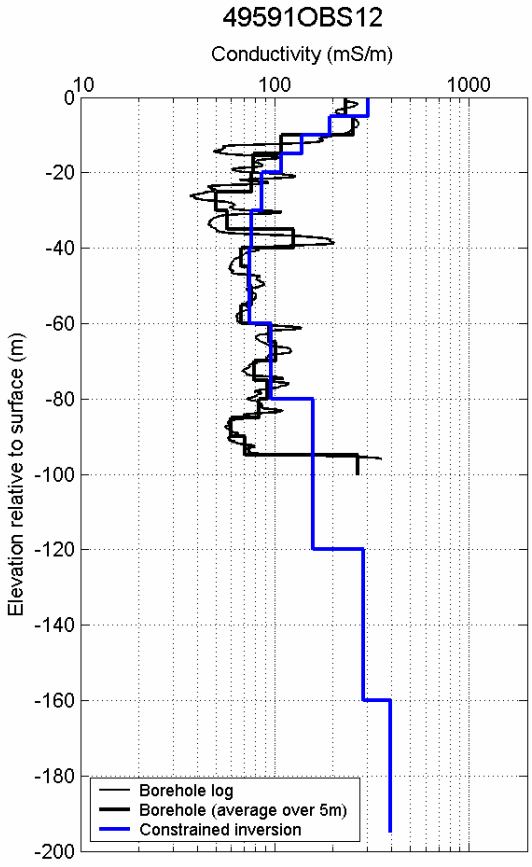
49591OBS12
Conductivity (mS/m)
10
100
1000
0
-20
-40
-60
-80
-100
-120
-140
-160
-180
-200
Elevation relative to surface (m)
Borehole log
Borehole (average over 5m)
Constrained inversion

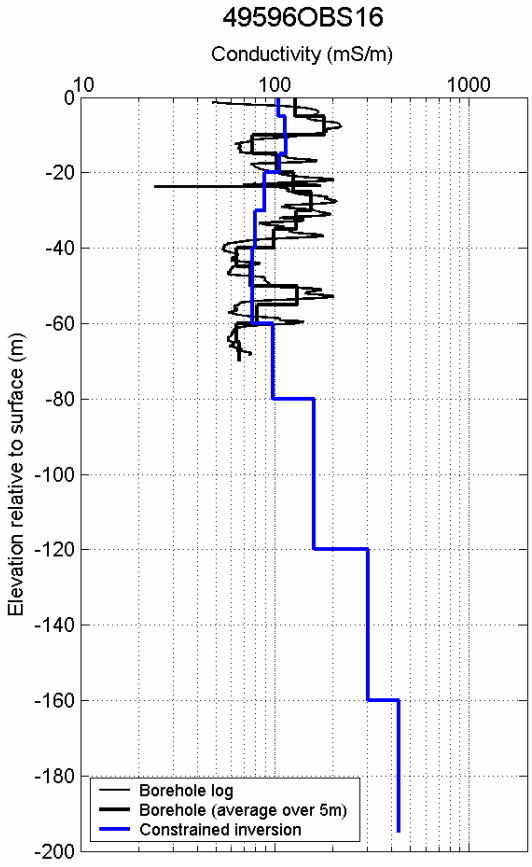
49596OBS16
Conductivity (mS/m)
10
100
1000
0
-20
-40
-60
-80
-100
-120
-140
-160
-180
-200
Elevation relative to surface (m)
Borehole log
Borehole (average over 5m)
Constrained inversion

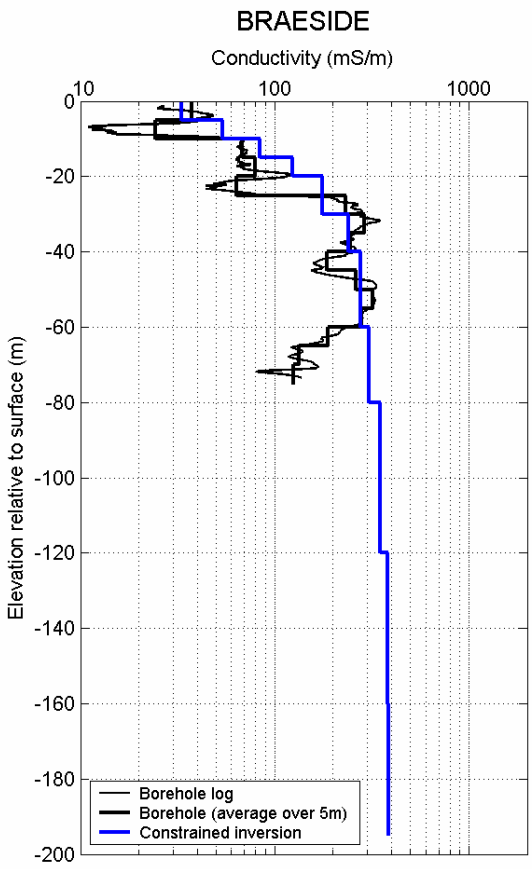
BRAESIDE
Conductivity (mS/m)
10
100
1000
0
-20
-40
-60
-80
-100
-120
-140
-160
-180
-200
Elevation relative to surface (m)
Borehole log
Borehole (average over 5m)
Constrained inversion

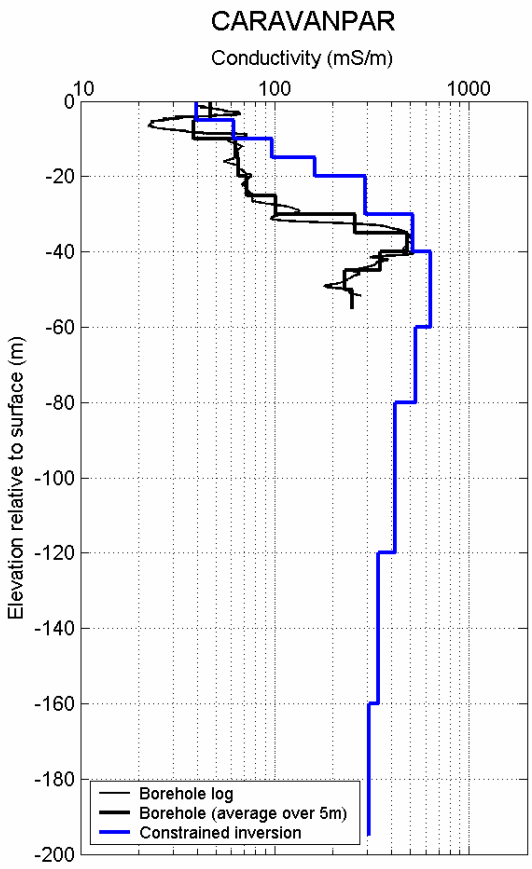
CARAVANPAR
Conductivity (mS/m)
10
100
1000
0
-20
-40
-60
-80
-100
-120
-140
-160
-180
-200
Elevation relative to surface (m)
Borehole log
Borehole (average over 5m)
Constrained inversion

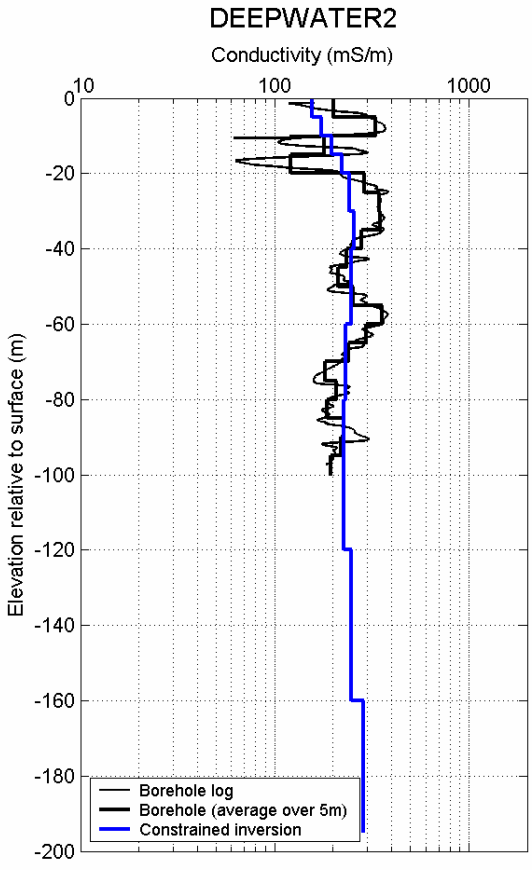
DEEPWATER2
Conductivity (mS/m)
10
100
1000
0
-20
-40
-60
-80
-100
-120
-140
-160
-180
-200
Elevation relative to surface (m)
Borehole log
Borehole (average over 5m)
Constrained inversion

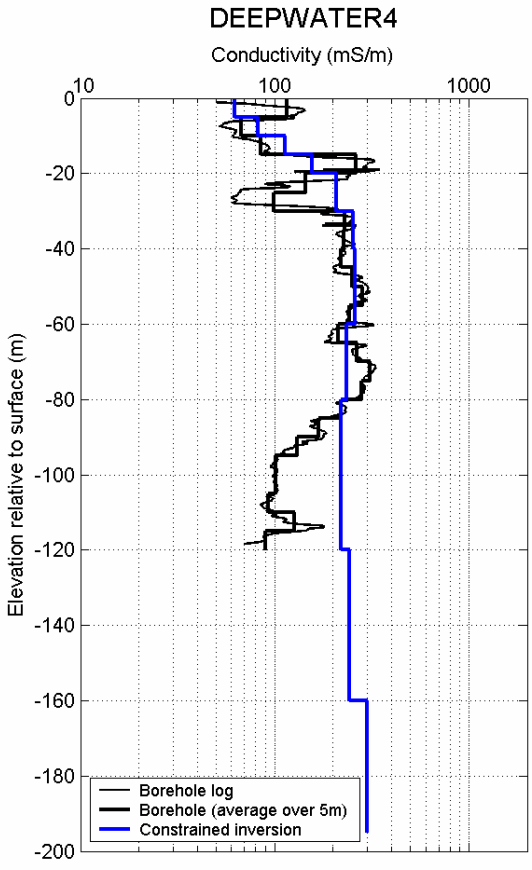
DEEPWATER4
Conductivity (mS/m)
10
100
1000
0
-20
-40
-60
-80
-100
-120
-140
-160
-180
-200
Elevation relative to surface (m)
Borehole log
Borehole (average over 5m)
Constrained inversion

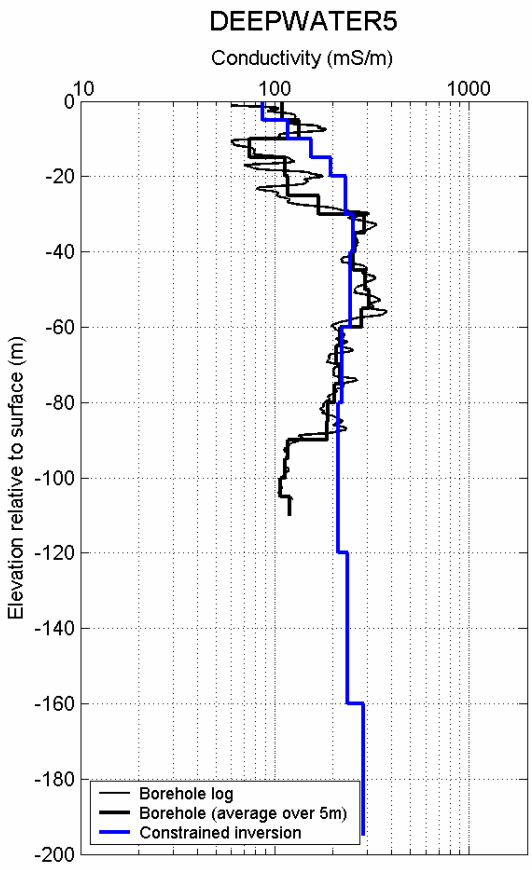
DEEPWATER5
Conductivity (mS/m)
10
100
1000
0
-20
-40
-60
-80
-100
-120
-140
-160
-180
-200
Elevation relative to surface (m)
Borehole log
Borehole (average over 5m)
Constrained inversion

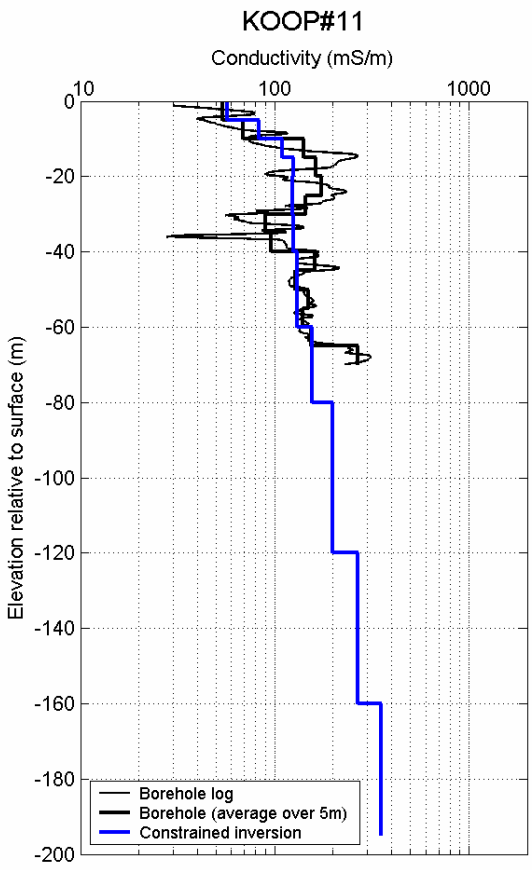
KOOP#11
Conductivity (mS/m)
10
100
1000
0
-20
-40
-60
-80
-100
-120
-140
-160
-180
-200
Elevation relative to surface (m)
Borehole log
Borehole (average over 5m)
Constrained inversion

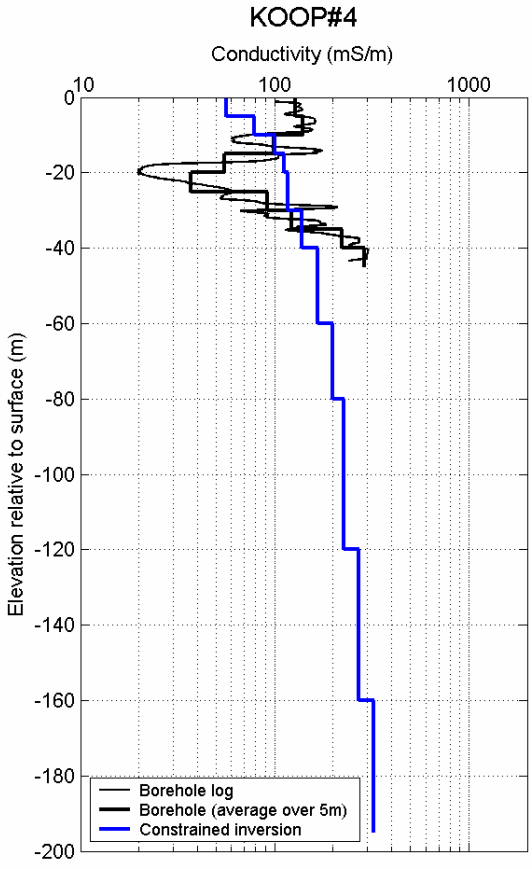
KOOP#4
Conductivity (mS/m)
10
100
1000
0
-20
-40
-60
-80
-100
-120
-140
-160
-180
-200
Elevation relative to surface (m)
Borehole log
Borehole (average over 5m)
Constrained inversion

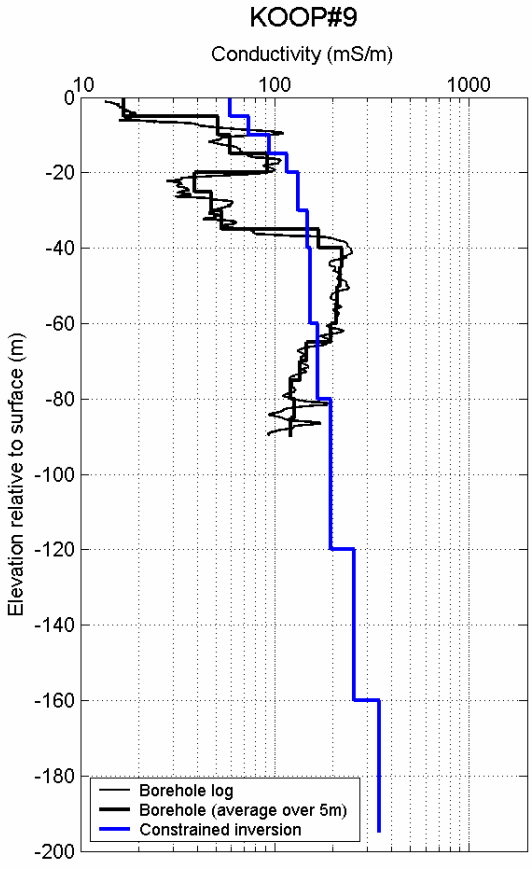
KOOP#9
Conductivity (mS/m)
10
100
1000
0
-20
-40
-60
-80
-100
-120
-140
-160
-180
-200
Elevation relative to surface (m)
Borehole log
Borehole (average over 5m)
Constrained inversion

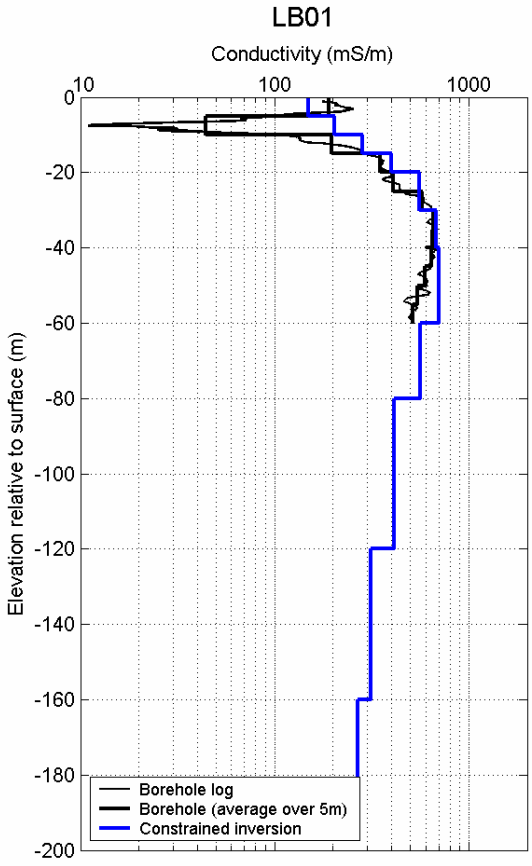
LB01
Conductivity (mS/m)
10
100
1000
0
-20
-40
-60
-80
-100
-120
-140
-160
-180
-200
Elevation relative to surface (m)
Borehole log
Borehole (average over 5m)
Constrained inversion

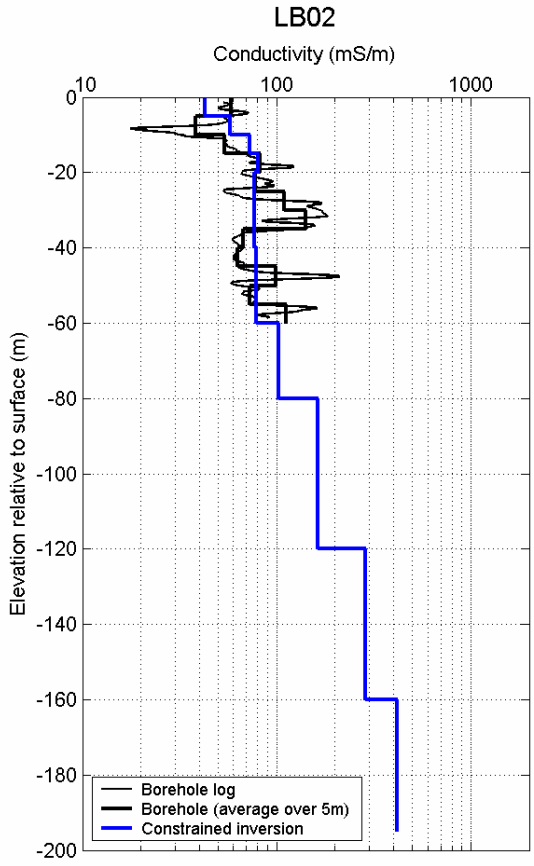
LB02
Conductivity (mS/m)
10
100
1000
0
-20
-40
-60
-80
-100
-120
-140
-160
-180
-200
Elevation relative to surface (m)
Borehole log
Borehole (average over 5m)
Constrained inversion

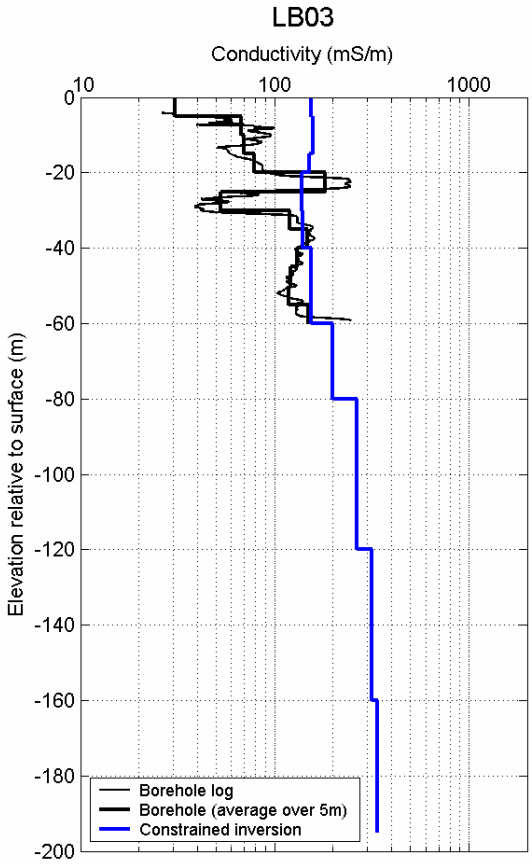
LB03
Conductivity (mS/m)
10
100
1000
0
-20
-40
-60
-80
-100
-120
-140
-160
-180
-200
Elevation relative to surface (m)
Borehole log
Borehole (average over 5m)
Constrained inversion

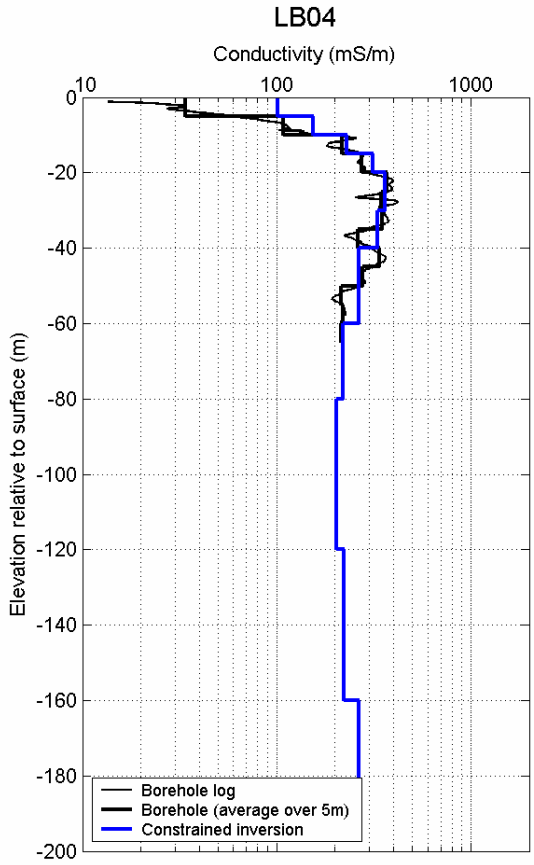
LB04
Conductivity (mS/m)
10
100
1000
0
-20
-40
-60
-80
-100
-120
-140
-160
-180
-200
Elevation relative to surface (m)
Borehole log
Borehole (average over 5m)
Constrained inversion

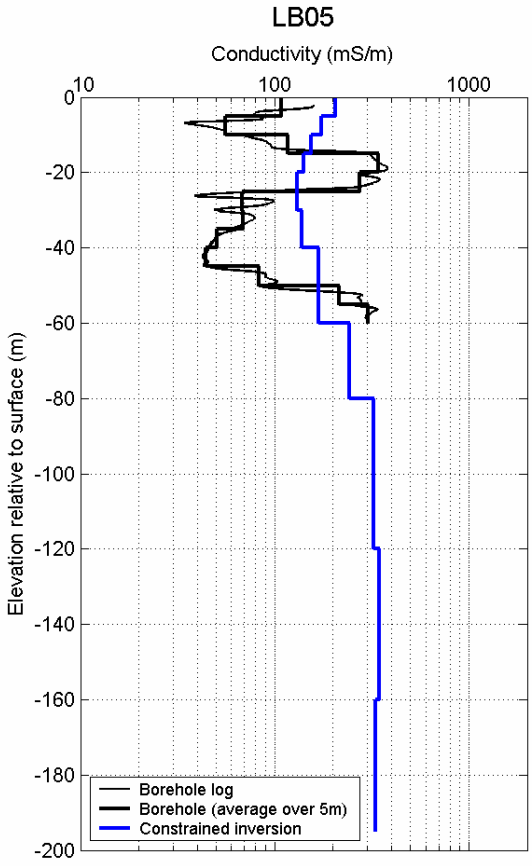
LB05
Conductivity (mS/m)
10
100
1000
0
-20
-40
-60
-80
-100
-120
-140
-160
-180
-200
Elevation relative to surface (m)
Borehole log
Borehole (average over 5m)
Constrained inversion

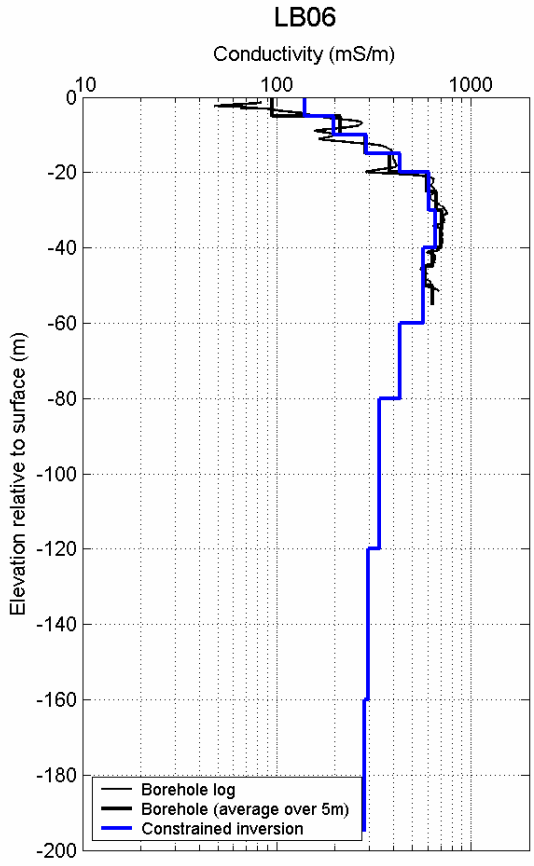
LB06
Conductivity (mS/m)
10
100
1000
0
-20
-40
-60
-80
-100
-120
-140
-160
-180
-200
Elevation relative to surface (m)
Borehole log
Borehole (average over 5m)
Constrained inversion

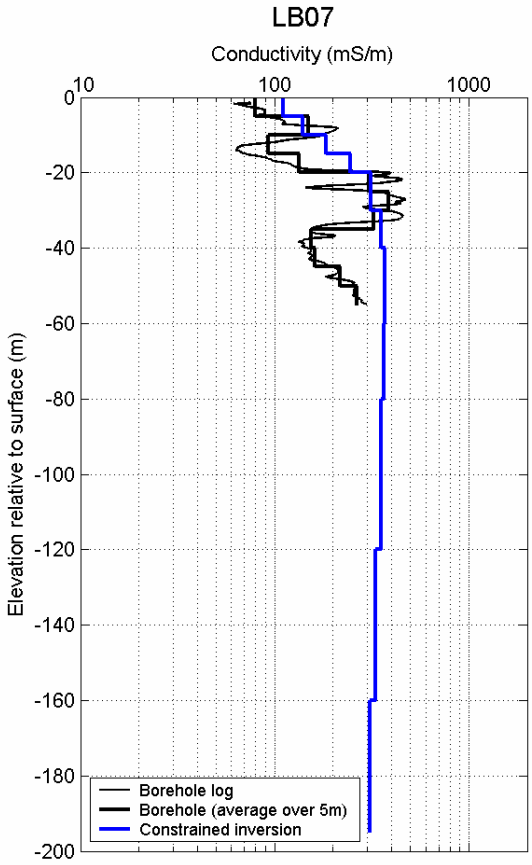
LB07
Conductivity (mS/m)
10
100
1000
0
-20
-40
-60
-80
-100
-120
-140
-160
-180
-200
Elevation relative to surface (m)
Borehole log
Borehole (average over 5m)
Constrained inversion

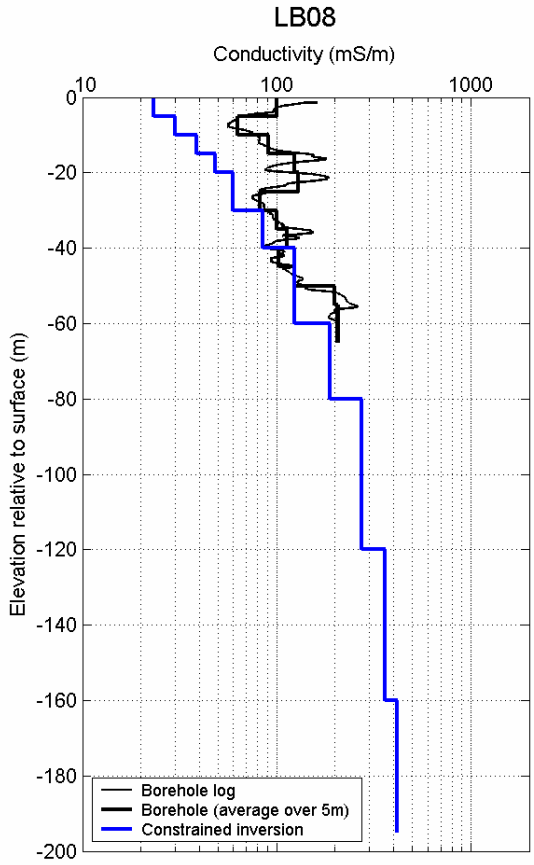
LB08
Conductivity (mS/m)
10
100
1000
0
-20
-40
-60
-80
-100
-120
-140
-160
-180
-200
Elevation relative to surface (m)
Borehole log
Borehole (average over 5m)
Constrained inversion

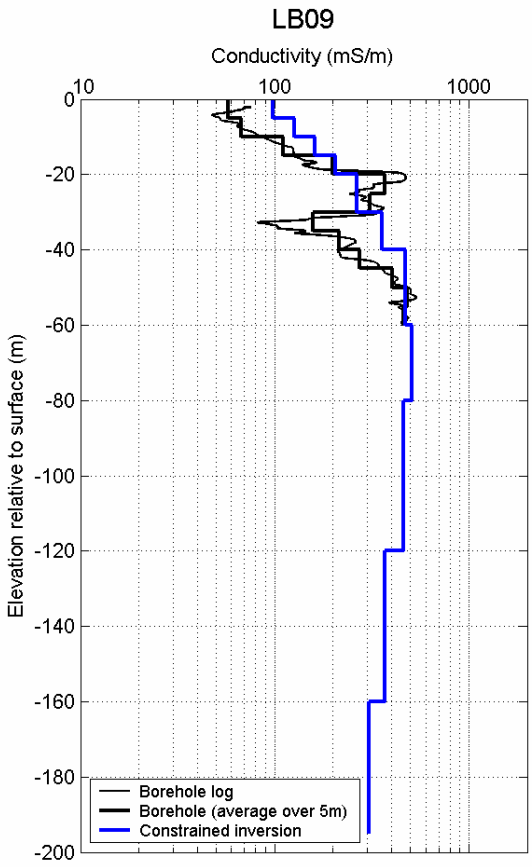
LB09
Conductivity (mS/m)
10
100
1000
0
-20
-40
-60
-80
-100
-120
-140
-160
-180
-200
Elevation relative to surface (m)
Borehole log
Borehole (average over 5m)
Constrained inversion

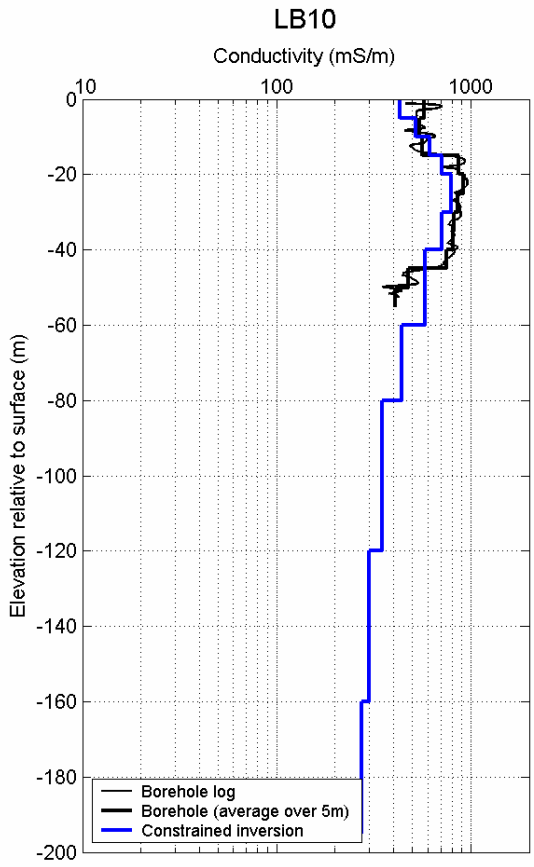
LB10
Conductivity (mS/m)
10
100
1000
0
-20
-40
-60
-80
-100
-120
-140
-160
-180
-200
Elevation relative to surface (m)
Borehole log
Borehole (average over 5m)
Constrained inversion

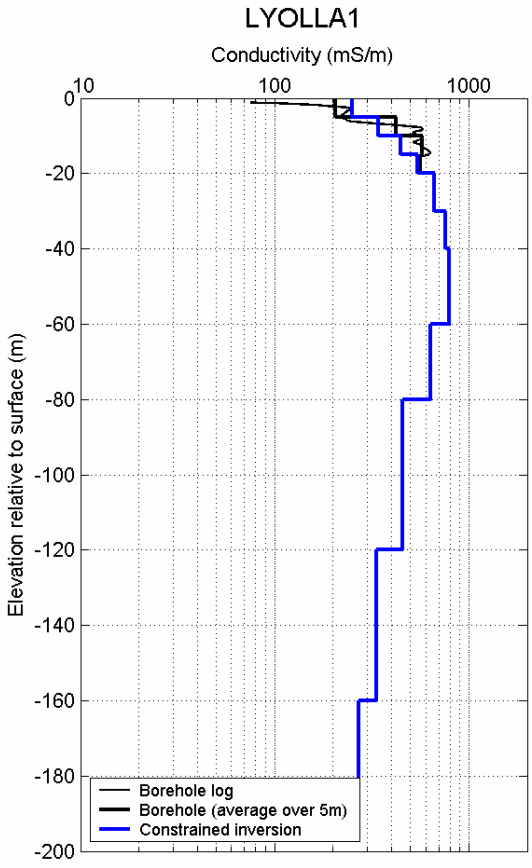
LYOLLA1
Conductivity (mS/m)
10
100
1000
0
-20
-40
-60
-80
-100
-120
-140
-160
-180
-200
Elevation relative to surface (m)
Borehole log
Borehole (average over 5m)
Constrained inversion

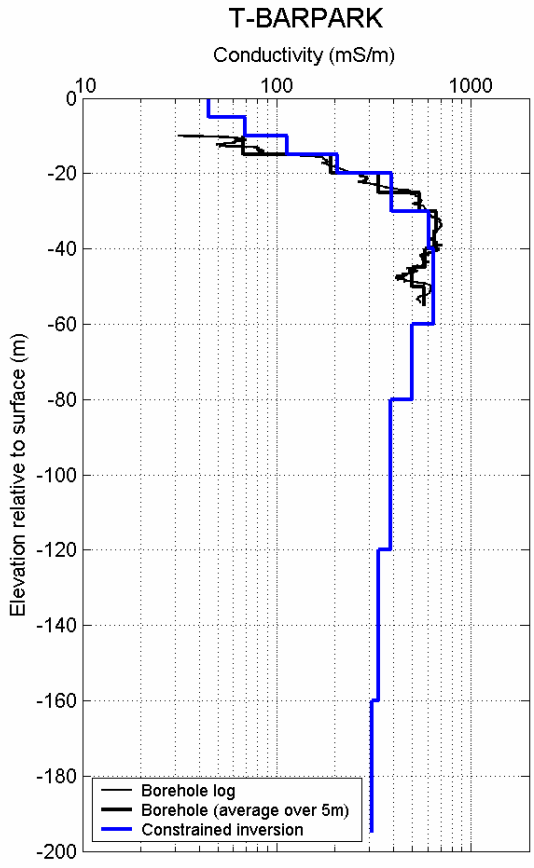
T-BARPARK
Conductivity (mS/m)
10
100
1000
0
-20
-40
-60
-80
-100
-120
-140
-160
-180
-200
Elevation relative to surface (m)
Borehole log
Borehole (average over 5m)
Constrained inversion

Appendix 5. Table of summary statistics for 5m depth increments

1	2	3	4	5	6	7	8	9	10	11	12	13
Top of interval m	Base of interval m	Minimum log10(mS/m)	Median log10(mS/m)	Maximum log10(mS/m)	Mean log10(mS/m)	Standard deviation log10(mS/m)	Number of observations N/A	Mean of misfit log10(mS/m)	Standard deviation of misfit log10(mS/m)	Correlation coefficient (R) N/A	Slope of regression line N/A	Intercept of regression line log10(mS/m)
0	-5	1.316	1.879	2.717	1.910	0.303	102	0.005	0.272	0.641	0.858	0.274
-5	-10	1.377	1.993	2.815	2.011	0.290	102	0.089	0.278	0.715	0.648	0.766
-10	-15	1.320	2.094	2.787	2.092	0.272	101	0.096	0.221	0.705	0.876	0.345
-15	-20	1.484	2.143	2.869	2.178	0.290	96	0.059	0.190	0.789	0.985	0.092
-20	-25	1.667	2.143	2.978	2.232	0.324	87	0.062	0.193	0.831	0.950	0.170
-25	-30	1.667	2.143	2.978	2.232	0.324	87	0.024	0.180	0.867	0.884	0.280
-30	-35	1.766	2.186	3.045	2.280	0.335	83	0.048	0.157	0.894	0.972	0.111
-35	-40	1.766	2.168	3.045	2.270	0.338	79	0.020	0.150	0.898	1.063	-0.121
-40	-45	1.782	2.245	2.987	2.299	0.324	77	0.067	0.166	0.877	0.948	0.183
-45	-50	1.782	2.245	2.987	2.297	0.330	72	0.070	0.157	0.885	1.010	0.047
-50	-55	1.782	2.245	2.987	2.287	0.327	69	0.026	0.139	0.906	1.046	-0.077
-55	-60	1.782	2.216	2.987	2.243	0.306	63	-0.013	0.151	0.883	0.965	0.065
-60	-65	1.939	2.284	2.801	2.266	0.217	54	0.033	0.126	0.886	0.789	0.503
-65	-70	1.939	2.284	2.801	2.268	0.224	50	0.032	0.158	0.795	0.833	0.406
-70	-75	1.939	2.284	2.801	2.266	0.223	46	0.049	0.137	0.847	0.848	0.386
-75	-80	1.939	2.276	2.801	2.265	0.226	43	0.051	0.114	0.892	0.885	0.305
-80	-85	2.123	2.310	2.731	2.347	0.143	40	0.164	0.142	0.857	0.540	1.168
-85	-90	2.123	2.310	2.731	2.347	0.143	40	0.165	0.171	0.806	0.477	1.306
-90	-95	2.191	2.316	2.731	2.350	0.137	36	0.201	0.163	0.867	0.473	1.334
-95	-100	2.199	2.331	2.731	2.366	0.137	32	0.125	0.134	0.801	0.573	1.082
-100	-105	2.211	2.332	2.731	2.376	0.139	29	0.110	0.133	0.767	0.605	1.004
-105	-110	2.211	2.332	2.731	2.377	0.142	27	0.108	0.145	0.770	0.568	1.088
-110	-115	2.211	2.349	2.731	2.393	0.148	22	0.094	0.141	0.763	0.614	0.982
-115	-120	2.211	2.356	2.731	2.406	0.154	19	0.100	0.156	0.738	0.586	1.055
-120	-125	2.346	2.476	2.665	2.486	0.087	15	0.107	0.169	0.676	0.298	1.777
-125	-130	2.346	2.479	2.598	2.481	0.077	12	0.064	0.159	0.560	0.258	1.858

1	2	3	4	5	6	7	8	9	10	11	12	13
Top of interval m	Base of interval m	Minimum log10(mS/m)	Median log10(mS/m)	Maximum log10(mS/m)	Mean log10(mS/m)	Standard deviation log10(mS/m)	Number of observations N/A	Mean of misfit log10(mS/m)	Standard deviation of misfit log10(mS/m)	Correlation coefficient (R) N/A	Slope of regression line N/A	Intercept of regression line log10(mS/m)
-130	-135	2.411	2.479	2.581	2.485	0.069	8	0.064	0.154	0.342	0.169	2.076
-135	-140	2.411	2.476	2.572	2.473	0.064	5	0.002	0.105	0.424	0.310	1.706
-140	-145	2.411	2.476	2.482	2.456	0.039	3	-0.056	0.109	-0.183	-0.091	2.685
-145	-150	2.411	2.476	2.482	2.456	0.039	3	-0.057	0.163	-0.685	-0.211	2.988
-150	-155	2.411	2.476	2.482	2.456	0.039	3	-0.059	0.093	-0.459	-0.352	3.342
-155	-160	2.411	2.446	2.482	2.446	0.050	2	-9999.000	-9999	-9999	-9999	-9999
-160	-165	2.491	2.491	2.491	2.491	0	1	-9999.000	-9999	-9999	-9999	-9999
-165	-170	2.491	2.491	2.491	2.491	0	1	-9999.000	-9999	-9999	-9999	-9999
-170	-175	2.491	2.491	2.491	2.491	0	1	-9999.000	-9999	-9999	-9999	-9999
-175	-180	-9999	-9999	-9999	-9999	-9999	0	-9999.000	-9999	-9999	-9999	-9999
-180	-185	-9999	-9999	-9999	-9999	-9999	0	-9999.000	-9999	-9999	-9999	-9999
-185	-190	-9999	-9999	-9999	-9999	-9999	0	-9999.000	-9999	-9999	-9999	-9999
-190	-195	-9999	-9999	-9999	-9999	-9999	0	-9999.000	-9999	-9999	-9999	-9999
-195	-200	-9999	-9999	-9999	-9999	-9999	0	-9999.000	-9999	-9999	-9999	-9999

Vertical datum : Ground level (up positive)
Undefined value : -9999

Statistics in columns 3 to 8 are based on an analysis of constrained inversion conductivity predictions for the closest observation to each of the boreholes for which there is a conductivity log.

The statistics in columns 9 to 13 are based on a comparison of borehole conductivity values with constrained inversion conductivity predictions for the closest observation to each of the boreholes.